Michal Tkac

Porosity Development in Composite Carbon Materials during Heat Treatment

Thesis for the degree of philosophiae doctor

Trondheim, April 2007

Norwegian University of
Science and Technology
Faculty of Natural Sciences and Technology
Department of Materials Science and Engineering

NTNU
Innovation and Creativity

NTNU
Norwegian University of Science and Technology

Thesis for the degree of philosophiae doctor

Faculty of Natural Sciences and Technology
Department of Materials Science and Engineering

ISBN 978-82-471-2212-9 (printed ver.)
ISBN 978-82-471-2226-6 (electronic ver.)
ISSN 1503-8181

Theses at NTNU, 2007:101

Printed by Tapir Uttrykk

This thesis has been submitted to

Department of Materials Science and Engineering

Norwegian University of Science and Technology

in partial fulfilment of the requirements for

the academic degree

Philosophiae doctor (PhD)

April 2007

ACKNOWLEDGEMENTS

The research was carried out between September 2003 and January 2007 at the Norwegian University of Science and Technology (NTNU), Department of Materials Science and Engineering. The financial support of this project has been provided by The Research Council of Norway and the Norwegian aluminium and ferro-alloy industries through the CarboMat program, and is gratefully acknowledged.

I would like to thank Professor Trygve Foosnæs as the main supervisor of my PhD study for engagement; fruitful discussions and his excellent guidance during the work. I especially thank him for his critical reading of the manuscript and king size dosage of enthusiasm that was very important for me. I also wish to express my gratitude to Professor Harald A. Øye as the co-supervisor of my PhD study for sharing valuable experience and discussions in the field of the anode process in aluminium electrolysis.

Thanks goes to Dr. Arne Petter Ratvik, research engineer Anne Støre and research scientist Stein Rørvik from SINTEF Materials and Chemistry for their support and guidance in the beginning of the experimental work. Especially I am grateful to Stein Rørvik for introduction to optical microscopy and image analysis and for sharing his experience as well as for fruitful discussions about achieved observations.

I am very thankful to Hydro Aluminium a.s Technical and Operational Support in Årdal for allowing me to perform part of my experimental work in their laboratory. I would like to express my thanks to all their employees for their cooperation and enthusiasm which I really enjoyed. Especially I would like to thank Dr. Hogne Linga and Dr. Lorentz Petter Lossius for their help with providing me with samples and measurements at their facilities.

My deep appreciation goes to all technical staff from Department of Materials Science and Engineering for their assistance with all kinds of practical matters related to the experimental work. I would like to express my happiness with the fact that I was a part of collective of PhD students within the CarboMat project where I felt very comfortable. Great people like Sten Yngve Larsen, Mohamed Othman Ibrahiem, Juraj Chmelar, Kristin Vasshaug, Lina Jonasson and Odd Einar Frosta enriched my open mindedness and were great company not only in the scientific field. It was also a pleasure to feel the “Czech-Slovak” home through my countrymen and colleagues Jana, Marian and Martin who were always a bottomless source of good fun and understanding.

Finally, I would like to thank my family for their support. I am grateful to my parents for their encouragement and to my girlfriend Magdalena for her patience through all of my stay in Norway. At last but not least I would like to express my gratitude to Associate Professor Jan Hives who was an important person for the start of my PhD studies.

Trondheim, March 2007
Michal Tkáč

TABLE OF CONTENT

ABSTRACT

The pilot scale anode production was done in order to verify the effects of production conditions on pore and structural development as well as some of the physico mechanical properties. The single source petrol coke and industrial paste were used for laboratory pilot scale anode production. Approximately 130 pilot scale anodes were produced during the work and more than 500 segments were analysed using computerized image analysis in order to determine the total porosity.

In **Chapter 4.1** the porosity of the single source petrol coke was determined. The coke was sieved into 6 different coke fractions and pore size distribution curves were obtained. There was observed a general increase of the porosity with increasing coarseness. The largest increase in porosity was found for fractions above 2.0 mm which was due to presence of the gas bubble pores and that were created as gas entrapment in green coke prior the calcination.

The effect of the heating rate on porosity development was studied in **Chapter 4.2**. Pilot scale anodes with identical granulometry (18 % pitch content) were produced from single source petrol coke using a sigma mixer. Correlation between the heating rate and the porosity development was found. A general increase of the total porosity with increasing heating rate was observed. All eight samples showed a similar pore distribution with maxima in porosity around 100 μm of pore radius. This may indicate the evolution of porosity due to volatiles escape. In addition a marked decrease of the baked density with increasing heating rate was observed, probably due to increased mass reduction with increasing volatiles evolution. Extra consumption of pitch due to coke crushing during mixing caused the formation of more voids in the anode paste.

In **Chapter 4.3** the effect of vacuum vibration and vibration time on porosity development was studied. A set of 20 pilot scale anodes with uniform composition were produced from industrial paste (blended coke) using different vibration times. Part of the formed blocks was vibrated under vacuum. During baking four heating rates were used in order to study the influence on porosity development. An increase in baked density was observed when vacuum vibroforming is used. During vacuum vibration the entrapped gas and light binder volatiles are released from the paste which enables the elimination of void formation. This mechanism is the most probable reason for improved aggregate packing and paste densification. Also a close correlation between the baked density and the specific electrical resistivity was found. The specific electrical resistivity decreases as the baked density of pilot scale anodes increases. Increase of the aggregate packing improved the coke grain bridging and influences the electrical contacts between particles.

The specific electrical resistivity seemed to be more dependent on heating rate than vibration time. As the heating rate during baking increased the specific electrical resistivity of the samples increased. When high heating rates were used, as in the case of 80 °C/h, the excessive volatiles evolution caused an increase of internal pressure in dense anodes. In extreme cases this may lead to crack formation that negatively affects specific electrical resistivity. Therefore slow heating rates for dense samples should be

applied to minimize the potential for an anode defects. Lower resistivity values were measured for the samples that were formed under a vacuum compared to those vibrated at atmospheric pressure.

For the total porosity, there was found a marked effect of the vacuum vibration that caused the porosity reduction for pores above 40 μm of pore radius regardless the heating rate. However, with increasing heating rate the benefit of the vacuum vibroforming on porosity development was reduced due to increased amount of the volatile (baking) pores.

Chapter 4.4 describes the effect of the three production variables; mixing time, vibration time and vibration energy on total porosity and various anode properties. A set of 21 pilot scale anodes were produced from industrial paste (blended coke) using the vacuum vibration (4 kPa) and the Eirich laboratory mixer (RV 08 W).

With increasing the mixing and vibration time higher densities were achieved. Most marked improvement was achieved for 1 minute mixing where further increase of vibration time resulted in improved densification. The highest green and baked densities were observed for anodes that were vibrated for 2 minutes with high energy input.

Reduction of total porosity values was observed with increasing of mixing time regardless of vibration time. With increasing mixing time the pitch spreads more uniformly above coke particles creating an even thin film which allows denser aggregate packing. Increase of vibration time caused the largest decrease of the total porosity values for short mixing times (1 and 3 minute mixed batches). Reduction of the total porosity value in the case of 6 minute mixing was not so evident which indicated that properly mixed paste (more continuous binder film) was less demanding on the vibroforming process duration.

The mechanical properties (YM and CCS) were found to be closely related to the densities in the green and baked state and thus also influenced by the mixing and vibration conditions. Increase of the mixing time caused improvement of both mechanical properties. The same effect was observed for vibration time. The largest increase of the YM and CCS was observed for 1 minute mixed samples when increasing the vibration time from 0.5 to 1 minute. On the other hand the strength properties for 6 minute batch seemed not to be influenced much with increasing vibration time.

Porosity and permeability were closely correlated. Samples with high porosity had also high permeability. Increasing mixing time gave moderate decrease of permeability. The largest decrease of permeability with vibration time was observed for 1 minute mixed samples when increasing the vibration from 0.5 to 1 minute. The same effect was observed in measurements of physical properties for pilot scale anodes (Chapter 4.4.7).

The low correlation between reactivity properties and total porosity was found. A possible reason may be that the total porosity determines the total amount of pores (open and closed pores together) in the sample while for the reactivity only the open pores and their connection are important. Another explanation could be that reactivity

against CO_2 and air are more influenced by the presence of the catalytic elements as V, Ni, Na or S than manufacturing parameters.

In **Chapter 4.5** a set of 24 pilot scale anodes were produced in order to determine the optimal operational conditions for the intensive Eirich mixer (RV 02/E) prior its use in the laboratory. The pilot scale anodes were produced using a pitch content ranging from 14 to 21 %, two mixing times (5 and 10 minutes) and three tip speeds (10, 12 and 14 m/s).

Optimum tip speed as well as mixing time was determined as those giving the highest values of the green density and the lowest open porosity values.

The open porosity decreased with increasing pitch content. Increase of the mixing time from 5 to 10 minutes caused reduction of the porosity primarily for 14 % pitch samples. The lowest open porosity for 14 % pitch anodes was achieved when 12 m/s rotor tip speed was used.

The green density increased with increasing pitch content. Samples with 19 % pitch and 10 minutes mixing time had the highest green densities. Green density increased as the rotor tip speed increased from 10 to 12 m/s. Further increase to 14 m/s caused decrease in green density regardless of the mixing times for 14 % pitch samples. Based on this, 12 m/s rotor tip speed was taken as the optimum for further pilot scale anode production.

In **Chapter 4.6** the effect of five variables (fines, pitch content, mixer type, mixing time and heating rate) on porosity and physico mechanical properties of pilot scale anodes was studied. Samples were produced from single source coke in half fractional, 5 - factorial experimental design. Half of the anodes were produced using an intensive mixer and other half with a sigma blade mixer.

As a response to these variables, green and baked densities, specific electrical resistivity, mechanical properties and porosity were measured. The strength of the effects was statistically evaluated using the Minitab software. The mixer type, pitch content and mixer pitch interaction were statistically the most significant factors influencing porosity, green and baked density as well as the specific electrical resistivity.

Intensive mixing was found more efficient and produced samples with higher green densities compared to sigma mixed samples. One of the benefits of intensive mixing is a better statistical distribution of grain sizes throughout the paste. Sigma mixing compared to high speed intensive mixing may have lower possibility of filling and impregnation of voids by capillary effects. In addition there was a significantly higher level of aggregate crushing.

The total porosity was influenced most by the three main effects: mixer type (C), pitch content (E) and heating rate (A). In general sigma mixed samples resulted in more porous anodes compared to intensive mixing. The 14 % pitch content intensive mixed

samples had larger porosity reduction compared to the sigma mixer. The sigma mixed samples had larger amount of the pores within the range of 100-10000 μm which indicate presence of large intergranular voids that were created due to poor and degradable mixing. The 19 % pitch intensive mixed samples had a dominant presence of the 100 μm pores in radius. This indicated over pitching of the anodes where the major porosity contributor was development of baking pores. The increase of the heating rate caused increase in porosity regardless of mixing type.

Mixer type, pitch content and heating rate had the strongest influence on permeability. Permeability for the sigma mixed samples passed through a minimum as the pitch content increases from 14 to 19 %. The medium pitch content (16.5 %) seemed to be optimal, where the coke crushing was compensated by the higher amount of pitch. Intensively mixed samples show increasing permeability as the pitch content increases from 14 % to 19 %. This increase of permeability was probably due to excessive development of volatile pores due to over-pitched anodes. This finding also correlated well with the total porosity values. There was a larger permeability increase when the heating rate 60 °C/h was used compared to slow baking at 10 °C/h. In the case of 10 °C/h heating rate, baking is slow and enables gradual volatile degassing of the sample without excessive development of baking pores and larger cracks. At a fast heating rate and dense anodes high internal pressure is built within the sample due to binder volatilisation. This pressure is released by escaping gases creating a porous system that is “frozen” during the following pitch solidification.

Mechanical properties (YM and CCS) were influenced by mixer type and pitch content. Mixer type affected proper aggregate distribution as well as pitch thickness film. As the pitch content increases, the amount of the binder coke increased which enables better bonding within coke aggregate and results in increased strength properties of produced anodes.

The image analysis of the green anodes presented in Chapter 4.6 was carried out in order to characterise the differences due to composition and variations in manufacturing conditions. The pitch thickness film increased with increasing pitch content. A thinner pitch film is developed when the intensive mixing technique is used. This observation supports the theory that during intensive mixing there is a uniform spread of the pitch over the coke particles which results in a thinner and more continuous binder film. Slow sigma mixing results in a thicker binder film. With increasing fineness of the dust fraction the pitch thickness layers become thinner.

The samples produced in Chapter 4.6 were pore classified. The central segments from the pilot scale anodes baked with 10 °C/h were picked. According to pore shape and size the pores were divided into three classes. Elongated and elliptic pores were attributed to the filler coke porosity. Irregular pores are found in the binder matrix and are created during anode production. These pores are associated with the mixing, forming or baking steps and are therefore specified as process pores.

Increased process porosity was observed for 14 % pitch content and sigma mixing. Larger presence of process pores above 300 μm indicated void formation due to poor

mixing. In addition there was an increase of porosity due to increased mixing time from 10 to 20 minutes which may refer to increased crushing with mixing time. The process porosity was far less for the intensively mixed samples. A slight porosity reduction was observed with increasing mixing time for intensively mixed samples. The samples with 19 % pitch had fewer voids even though the mixing was poor. Thus the largest process porosity development was due to an increased amount of baking pores.

The porosity in the coke filler represented by the elongated and elliptic pores had in general minor contribution to the total porosity compared to the process pores. This was expected as most of the coke pores are penetrated by the pitch during the mixing stage. However, some variations were observed that indicate improved particle penetration for intensive mixing. The intensive mixing caused an improved filling of the elongated and elliptic pores within the 10 - 60 μm range compared to the slow and more degradable sigma mixing.

In **Chapter 4.7** the effect of vacuum vibroforming on the porosity development was studied. Similar experimental design and same production routines were used as described in Chapter 4.6. The difference compared to the previous experimental design was that the anodes were produced with narrower pitch levels and heating rates using exclusively the intensive mixer. The green paste was formed on the vacuum vibration table under three mould pressure conditions, 4 kPa and 52 kPa with vacuum and 100 kPa (no vacuum).

Green and baked densities were affected by the pitch content, vibropressure and mixing time. Increase of both densities with increasing pitch content and mixing time was observed. Additional density increase was found when increasing the forming vacuum. Increase of the vacuum causes exhaust of the entrapped air as well as light binder volatiles.

Specific electrical resistivity decreased with increasing pitch content and increasing mixing time. Increase of the vibration vacuum resulted in additional resistivity reduction.

The total porosity was affected most by pitch content, vibropressure and mixing time. For samples with 14 % pitch content reduced porosity above 80 μm was observed when 4 kPa vacuum vibroforming was applied. Additional porosity reduction was achieved by increasing the mixing time from 5 to 10 minutes. Samples with atmospheric vibration showed increased porosity within the interval 100 - 10 000 μm which is related to poor aggregate packing. Increasing the pitch content to 16 % reduces the intergranular voids compared to 14 % pitch. The effect of vacuum vibroforming was significant from pore radius 40 μm. Increase of the heating rate from 5 to 20 °C/h showed increase in total porosity probably due to the evolution of the baking pores. The samples vibrated at atmospheric pressure showed larger porosity above 50 μm of pore radius which indicated increased presence of the forming process pores.

A good correlation was found between porosity and permeability. Samples with high permeability were those that had higher porosity and low pitch content (14 %). The

most significant interaction, pitch content by vibropressure, indicated a larger decrease of permeability for vacuum vibroformed 14 % pitch samples compared to those with 16 % pitch. There was a larger reduction of permeability for vacuum formed samples that were mixed for 10 minutes compared to those mixed for 5 minutes.

Cold compression strength and Young's modulus improved for anodes with increasing pitch content and mixing time. The vacuum vibrated samples showed the highest strength of all anodes. Increase of pitch content, mixing time and vibropressure caused increase of the Young's modulus. A correlation between porosity and mechanical properties was also found. With increasing porosity both mechanical properties deteriorates. The porosity that affects mechanical properties was probably due to increased amount of the process pores (forming, mixing and baking pores).

1 INTRODUCTION

1.1 Aluminium production

Aluminium is produced by the Hall-Héroult process. Liquid aluminium is produced by electrolytic reduction of alumina (Al_2O_3) dissolved in an electrolyte mainly containing cryolite (Na_3AlF_6) AlF_3 and CaF_2 at 960 °C. A schematic drawing of the main features of an alumina reduction cell is shown in Fig. 1.1-1.

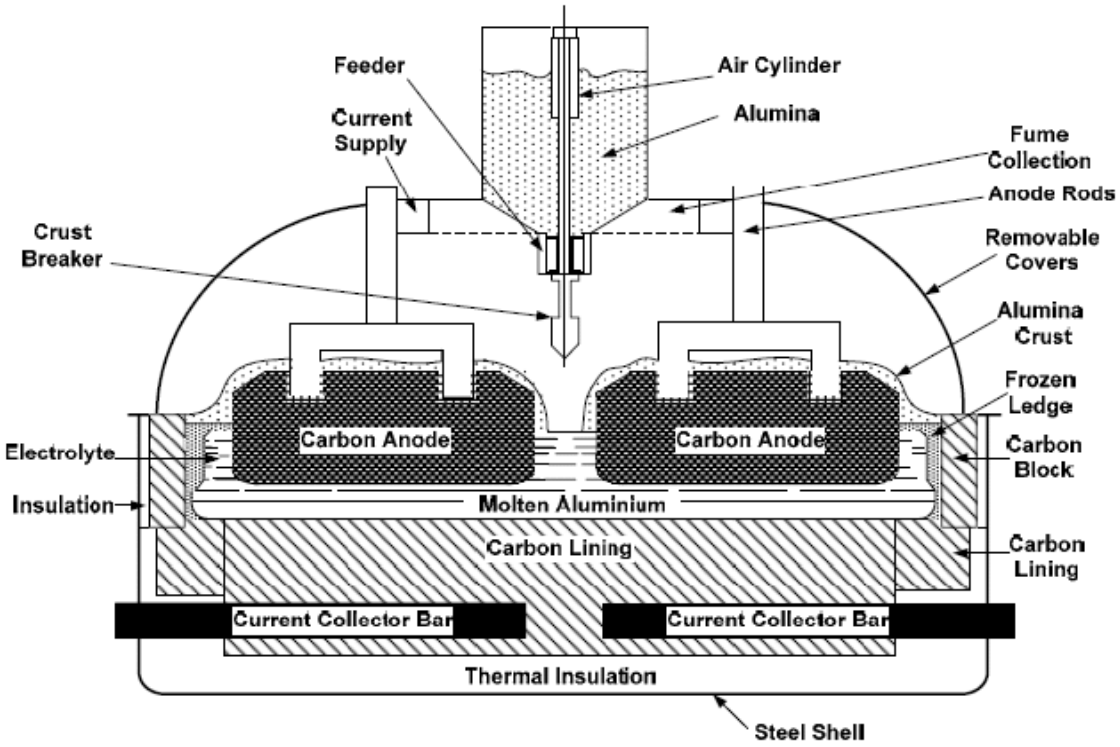

Fig. 1.1-1. Aluminium electrolysis cell with prebake anodes [1].

In the cell, oxygen from the alumina is discharged electrolytically at the anode as an intermediate product. However, the oxygen immediately reacts with the carbon anode and thus gradually consumes it by the formation of gaseous carbon dioxide (CO_2). The bath and liquid aluminium are contained in a carbon lining inside a steel shell with refractory and insulation materials. The aluminium is formed at the bath metal interface, which acts as the cathode. Thus, the overall chemical reaction can be written:

$$2Al_2O_3(diss) + 3C(s) \longrightarrow 4Al(l) + 3CO_2(g) \qquad \text{Eqn. 1}$$

A typical feature of the Hall-Héroult process is that the anodes are consumable. There are two basic anode designs, the prebaked anode and the Söderberg anode.

Prebaked anodes are moulded into blocks and baked in separate anode baking furnaces. An aluminium rod with iron studs is then cast into stub holes in the top of the anode

block in order to conduct the electric current to the anode when it has been positioned in the cell. The prebaked anodes give lower carbon consumption per ton aluminium compared to Söderberg anodes. However, prebake anodes have to be changed at regular intervals (20-30 days) when they are consumed, which is a major disturbance in the operation of the cell. The remains from the anodes are called butts, and are cleaned outside the cell in a separate cleaning station for recycling of the carbon and adhered bath. The cleaned butts are then crushed and used as addition to the raw materials in the manufacturing of new anodes.

In the Söderberg process anode paste is continuously supplied and baked, eliminating the costs of the anode forming, baking and butts treatment. The Söderberg anodes are manufactured from briquettes composed of petroleum coke and coal tar pitch. The pitch binder content is about 25 wt%, which is considerably higher than the amount used in prebaked anodes (13-15 %) to ensure sufficient flow of the carbon paste. Briquettes are placed on top of the Söderberg anode block, where they are softened by the heat generated from the cell. The paste passes downwards through a rectangular steel casing and is baked into a solid composite. One of the most problematic issues of Söderberg anodes is the environmental aspect. The high pitch content in the anode and the open top leads to release of potentially hazardous gaseous polycyclic aromatic hydrocarbons (PAH) during the process.

The anodes along with alumina represent two major raw materials costs. The net anode consumption for a modern prebake cell is around 400 kg C/ton Al, and the gross consumption, which also includes the mass of the butts, may lay between 500 to 550 kg C/ton Al. The theoretical consumption of the Hall-Héroult process is 334 kg C/ton Al (Fig. 1.1-2).

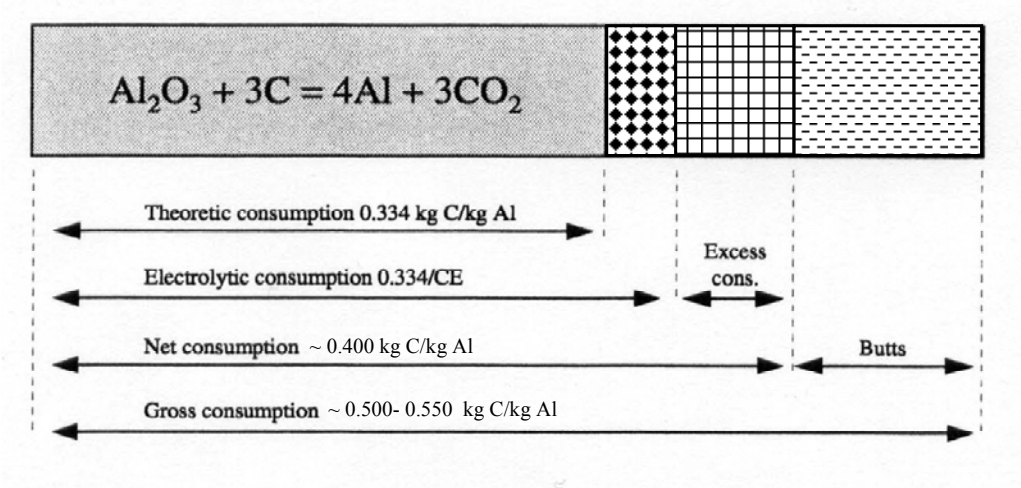

Fig. 1.1-2. Anode consumption in an electrolysis cell with prebaked anodes [2].

The main reasons for excess carbon consumption are:

- Carboxy reaction, also called the Boudoard reaction:
  $$1/2CO_2(g)+1/2C(s)=CO(g)$$ Eqn. 2
- Dusting, which is the mechanical release of carbon particles from the anode into the bath
- Airburn, air oxidation of the exposed parts of the anode:
  $$C(s)+O_2(g)=CO_2(g)$$ Eqn. 3
- Back reaction, the metal being re-oxidized to its oxide:
  $$3CO_2(g)+2Al(l)=3CO(g)+Al_2O_3(s)$$ Eqn. 4

Increasing carbon and energy costs are strong incentives for reducing unnecessary carbon consumption, and the monitoring of the anode consumption is an important criterion for determining the overall cell efficiency. It represents an area in which significant cost reductions may be made.

1.2 Aim of the work

Over last decades the situation in the crude oil market has changed significantly with effect on the petrol coke situation. Anode paste plants needs to deal with variation in coke quality which is not favourable for maintaining sustained anode quality. In addition there is a globally increasing demand for aluminium both through green field and brown field retrofit projects, and current increase. Accordingly, the demand for petrol coke already has outpaced the production of traditional, good quality petrol coke. Hence, lower quality cokes have to be used. Therefore there is an urgent need to optimize the anode production process so that lower quality cokes can be used without disturbing influence on the electrolysis process.

In the past much effort has been put into studying anode properties and performance with respect to petrol coke trace elements, for example the influence of the catalytic metal content on reactivity [3-5]. It has been indicated that porosity in coke and anode may be an important factor that influences the reactivity and the mechanical properties of the anode [6, 7]. However, little work has been done to clarify the porosity and its development as a consequence of the variation in anode manufacturing steps.

The aim of this work is to obtain fundamental knowledge of how the anode porosity is generated and how it influences important physical, mechanical and chemical properties. Laboratory pilot scale anode production was carried out in order to verify the importance of production steps during paste preparation. Two sources of paste were used; laboratory mixed paste from a single source petroleum coke and industrially mixed paste based on blended coke. The variations in mixing, vibroforming and baking conditions were studied with respect to porosity development in the anodes. From the literature survey, almost all authors report using a sigma blade mixer (or double Z-blade mixer) during pilot scale anode production. In this work two mixing techniques; sigma blade and high speed intensive mixing were used and their influence on the anode porosity and resulting anode properties were compared. In order to find the effect of vibration conditions on porosity, paste was shaped using different vibroforming times, energy inputs and vacuum conditions. During baking the effect of the heating rate and the soaking time was studied.

The porosity characterization in previous works was performed by Hg porosimetry while in this work image analysis is used. This fully automatic method was found to be capable to characterize macroporosity (from 10 μm to several mm) to describe its influence on baked density, specific electrical resistivity and mechanical properties. Anode properties were characterized by using standard quality test methods and ISO standards.

It is not anticipated that the results given in this thesis can be applied directly on an industrial scale; however it is believed that the work can serve as a guide for optimizing industrial anode production parameters. Part of the presented work has been published [8, 9].

1.3 Anode raw materials

Typical prebaked anodes for aluminium production consist of 65 % petroleum coke, 20 % anode butts and 15 % coal tar pitch. The costs of these raw materials amounts to approximately 50 % of the total anode production costs [10]. The consistency and quality of carbon products highly influences the operational regularity of the aluminium production. Anodes need to fulfil some important requirements: provide the means for electrical conductivity to the cell and to act as a reductant in the electrochemical process [11]. Other primary anode requirements are high chemical purity, high electrical conductivity, high mechanical strength and chemical homogeneity with low reactivity to CO_2 and air [12]. These factors are strongly influenced by the raw material quality. The petroleum coke has an inhomogeneous structure, depending on the precursor and production process. It is formed as a by-product of the petroleum refining process, where conditions are optimised towards the petrochemical industry's needs rather than the desired structural characteristics of the coke [11].

1.3.1 Petroleum coke

Anode grade petroleum coke is produced by a semi-continuous process called delayed coking. In this process the heated residue from fractionated crude oil is alternatively fed to one of two coking drums (485-515 °C, 0.4 MPa) for 16 to 24 h. After 24 hours the green coke is cut out by high pressure water jets (decoking). By regular feed of reduced bottom crude, the amount of hydrocarbon volatiles in delayed green coke normally averages 8 to 14 % from the bottom to the top of the drum [12]. While variability of the green coke quality to some extent is related to its height in the coke drum, the size distribution depends on the decoking method.

Delayed coking is applicable to a broad range of feedstocks, *i.e.*, shale oil, bituminous oil sand, naturally occurring solid hydrocarbons as well as for reduced bottom crude of varying aromacity and catalytically cracked oils [12]. Other parameters affecting quality are operating conditions like temperature, pressure, time and decoking characteristics.

1.3.1.1 Coke calcining

The raw or green coke produced by the delayed coking process is not suitable as a filler coke in electrodes. It has an amorphous, very weak structure with relatively high volatiles content, poor electrical conductivity and high reactivity [11]. As a consequence the green coke is heated (1250-1350 °C) prior to its use as filler, the process known as calcining. The calcining process is necessary to achieve the following properties prior to anode formulation, forming and baking [12]:

- Sufficient grain strength for handling and processing
- Minimum grain shrinkage
- Pore structure accessible to binder
- Sufficient thermal conductivity for effective indirect heating in the anode manufacturing process

Two major types of calciner units are presently used for cokes: the rotary kiln and the rotary hearth calciner. The rotary kiln is most widely used, due to its simple design and high throughput. In the rotary kiln the coke moves in a rotating slightly inclined refractory-lined steel tube (up to 90 m in length and 4.5 m in diameter). At the inlet the coke is heated by oil or gas. Additional heat is provided by burning of the volatile gases and carbon due to injection of air. This is sufficient to maintain the target temperature for 10 to 20 minutes.

In the rotary hearth calciner the coke is moved by rotating scrapes towards a central outlet inside a vertically mounted cylindrical reactor. Supplementary fuel and air are supplied through the top of the reactor. During normal operation the retention time for the coke in the hearth is approximately 1 hour. The quality of the resulting calcined coke is controlled by the chemical composition of the feedstock as well as the operational parameters during coking and calcining [10].

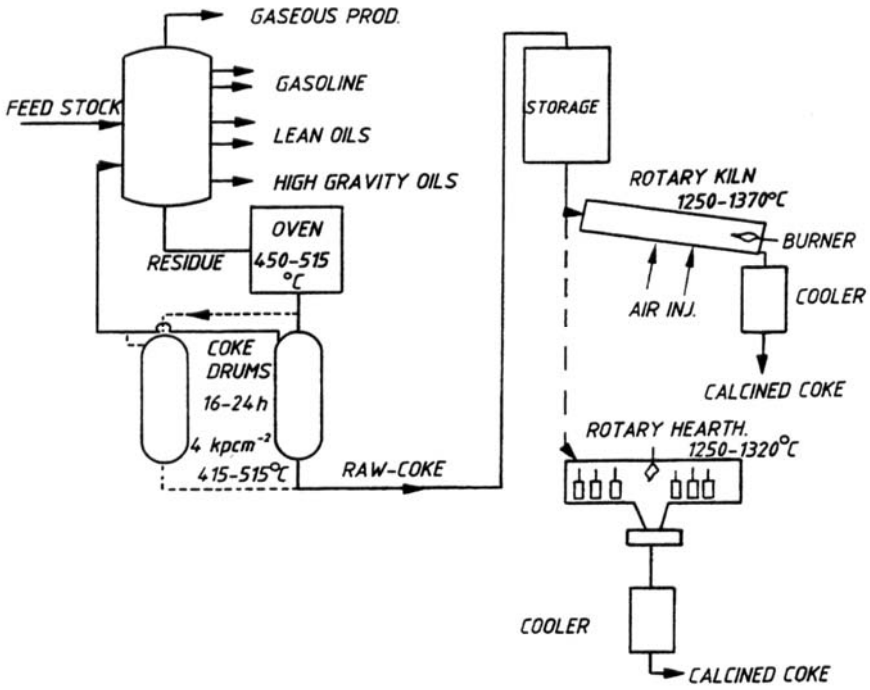

Fig. 1.3-1. Coke production by delayed coking and rotary kiln or hearth calcining [12].

1.3.2 Pitch

The binder used in production of prebaked anodes is usually coal tar pitch (although in some instances selected grades or mixtures of petroleum pitch and coal tar pitches are used) [5]. There are several functions of the binder pitch. During mixing the pitch coats the filler coke particles, penetrates the pores and voids between coke particles and thus plasticizes the originally dry aggregate, so it can be formed to bodies of required shape. During subsequent heat treatment, the pitch carbonizes and forms a coke that bridges the filler particles [11].

Pitch is an extremely complex mixture of numerous, essentially aromatic and heterocyclic compounds derived from pyrolysis of organic materials by tar distillation. Due to their high carbon content and polycyclic aromatic nature, pitches form isotropic or anisotropic cokes with relatively high yields upon thermal treatment [13].

The raw material for the production of coal-tar pitch, *i.e.,* crude coal-tar, is obtained as a by-product of metallurgical coke production [14]. Large-scale carbonisation of coal to produce blast-furnace coke is performed at temperatures between 1000 and 1200 °C and residence times of 14 to 20 hours. Besides coke as the main product (75 wt. % relative to feed coal) coke oven gas, water, benzene, ammonia and crude coal-tar are obtained. The tar yield amounts to approximately 3.5 wt % of the coal feed [14]. The hot gaseous products are quenched by flushing liquor. As the volatiles are cooled, about 75 % of the tar is condensed (called flushing liquor tar). The remaining tar is recovered by further cooling of the coke oven gas. The liquor and tar are then separated in the decanter. The decanted tar is then distilled in a refinery. The refining process includes denaturing of the crude tar, neutralization and vacuum rectification of the dewatered and neutralized tar. Coal-tar pitch is obtained as the distillation residue with 50-55 wt % yields, relative to the crude tar [14].

In the manufacturing of anodes, the balance between the aggregate coke and the binder coke properties in the final product is an exceedingly important key to product homogeneity [12]. Besides purity, strength and structure of the binder coke, several properties related to the anode manufacturing process itself have to be fulfilled by the binder pitch. The softness of pitches is usually classified into three groups by equiviscosity temperatures. Referring the temperature of softening to a viscosity of 950 Pa s, the three groups are [12]:

- Low melting pitch: 50-80 °C
- Medium melting pitch: 80-100 °C
- Hard pitch: > 100 °C

The high softening point pitches are of interest in the aluminium industry to fabricate anodes as it has high coke yield. The coke yield of the pitch indicates the amount of carbon generated when the pitch carbonizes. A typical value for a hard pitch is a coke yield round 60 %.

1.4 Industrial anode manufacturing

The anode manufacturing steps are shown schematically in Fig. 1.4-1. In these steps the aggregate filler is mixed with binder pitch to compose a paste formulation which is moulded prior to baking. Beyond these generalities each discipline has its distinct features related to product applications, available raw materials and process selections [12]. Each production step gives its contribution to the total porosity of the produced anode block. The essentials of carbon anode production can be summarised in the following steps:

- Paste production
  - Dry aggregate preparation by crushing, milling and sieving of anode butts and petroleum coke
  - Weighing of fractions
  - Mixing of the dry aggregate with pitch
- Paste compaction
- Anode baking

The principal goal of all processing stages is to produce homogeneous anodes that will meet the requirements concerning the performance in the electrolysis cell. As already outlined earlier by many authors [12, 15, 16] these requirements are summarized as follows:

- High resistance against attack of CO_2 and air
- Low specific electrical resistivity (< 65 μΩm)
- Moderately high thermal conductivity in order to decrease risk of air burn (< 6 W/mK)
- Mechanical properties
  - High crushing strength (> 35MPa)
  - High flexural strength (> 7MPa)
  - Adequate Young's modulus (< 10 000 MPa)
  - Low coefficient of linear thermal expansion (< $5 \cdot 10^{-6}$/K)

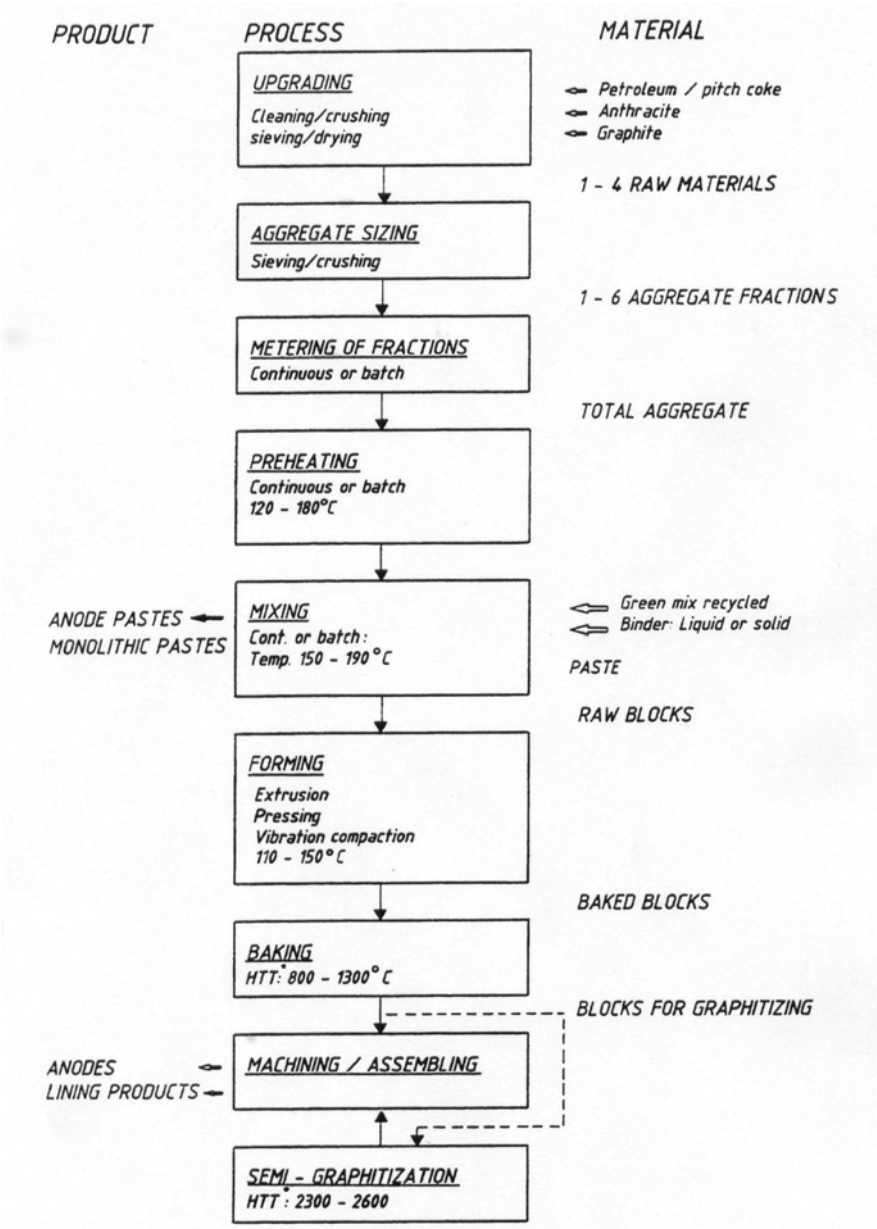

Fig. 1.4-1. Flow sheet of the carbon manufacturing of the Hall-Héroult process [12].

1.4.1 Paste production

1.4.1.1 Dry aggregate preparation

The first step of the paste production involves the crushing and screening of the petrol coke and butts. The filler aggregate of carbon products usually consists of a blend of 3 to 6 different particle size fractions in specific proportions according to the recipe. In a recipe, the particle size ranges from sub-micron diameters to about 20 mm. In order to achieve maximum packing density, fractions are portioned and weighted according to a defined recipe. In practice, deviations occur due to limitations in the crushing, grinding, sizing and weighing operations [11]. The applied aggregate sizing is also influenced by numerous factors, *i.e.,* coke porosity and strength, surface texture, manufacturing process limitations as well as the availability and price of the raw materials [12].

After weighing the coke fractions the dry aggregate is preheated and mixed with liquid pitch at a defined temperature. This process is important as it defines the paste mixing temperature at the inlet of the mixer. The preheater usually consists of 1 to 4 screws inside a shallow tube designed to maximize the heat transfer area. Thus a maximum aggregate temperature of 150 to 190 °C is easily reached within the 4 to 8 minutes of the aggregate residence time [12].

1.4.1.2 Mixing

Mixing is a key step in order to obtain a good anode product. During mixing the pitch must coat the particles uniformly creating a continuous film and penetrate accessible porosity [17]. Mixing of the aggregate and binder is performed at elevated temperatures (50 to 90 °C above the binder softening point) [12]. The amount of pitch used in preparing the prebake anode is between 14 to 18 % [18]. It varies with the composition of the aggregate fractions, the porosity and structure of the petroleum coke, and the chemical composition of the pitch. The amount of pitch is adjusted to give maximum density during the subsequent carbonization stage. Two different types of mixers are used:

A) Continuous mixer

The usual types of mixers consist of single or twin rotators inside a heated tube. Delta shaped blades fixed at certain angles along the rotor force the paste forward along a spiral path, where similar blades in the tube side maintain a counter pressure. By varying the speed of the rotator and chocking the outlet gate, the specific mixing energy is adjusted. The mixing capacity is altered by the feeding rate to the mixer. Current continuous mixing ko-kneader lines have rated capacities up to 30-45 t/h with mixing times from 4 to 6 minutes [12].

B) Batch mixer

The conventional concept of batch mixers includes a series of 2 to 4 tonnes charge sigma blade mixers for combining preheating/mixing. Present trends indicate preference on separate preheating systems combined with high speed mixers operated continuously

[19, 20]. For high speed mixers of modern design the specified mixing times are 2 to 10 minutes compared to 30 to 60 minutes in conventional batch mixers [12].

1.4.2 Paste compaction

Forming of the green paste into anode blocks can be carried out by either pressure moulding or vibratory compacting. Pressure moulding is usually carried out by using a double-acting press which applies pressure equally at the top and bottom of the anode. The paste is cooled down to 5 to 10 °C below the pitch softening point, weighed and then filled in the mould, where the mixture is compressed at approximately 35 MPa. The resulting density of the green anode typically is around 1.6 kg/m^3 [11].

Due to increasing anode dimensions, the technical importance of the vibratory compacting method has increased in the past 20 years [11]. Today most large size anodes are formed with this technique. After the mould is filled with the paste having a temperature of approximately 150 °C, the counterweight is placed on the top of it with a tight seal. In some cases a vacuum pump connected to the mould creates an underpressure of 0.1 to 0.3 bar. The vibration frequency ranges between 15 and 30 Hz. The counterweight exerts a pressure of 3 to 15 MPa. Usually the anode forming process is fully automated and several moulds can be operated simultaneously in alternate order. The formed green anode is cooled to ambient temperature, usually by dipping it into a water bath or by water spraying. The vacuum vibratory compacting method exhibits several advantages towards the regular high pressure moulding. The paste can be formed at higher temperature without creating problems caused by the evaporating gases. These gases are literally “shaken” out from the bulk [11]. The use of vacuum increases the viscosity of the binder; hence a higher forming temperature is possible. In addition, the vibration technique makes the anodes denser and it requires less capital investments than pressing [21].

1.4.3 Anode baking

Current large-scale anode baking furnace designs are all of the so-called ring furnace type, which essentially are high-temperature heat exchangers applying indirect heating by combustion of gases (natural gas, propane or gases from fired fossil fuel). Two distinctly different ring furnace concepts dominate the aluminium industry: The horizontal-flue or open-top furnace (Fig. 1.4-3, Fig. 1.4-4) and the vertical-flue or closed-top furnace (Fig. 1.4-5, Fig. 1.4-6). The anode blocks are placed in four to eight rectangular parallel pits in each heat-exchanger section. Granular coke is filled around the anodes to protect them against oxidation by the flue gases and to provide heat transfer from the flue walls to the blocks. The filling material is necessary as a support when anodes pass through the plastic state. Such a set of pits is referred to as a section chamber. The pits are enclosed in between flues and can hold anode block piles approximately 5 m long, 5 m high and 1 m wide. A complete furnace can include up to 70 sections or chambers in series, located in two parallel rows with crossover connections at each end, thus allowing the fire to progress perpetually. A ring contains up to four groups of sections with a fire, which are operated simultaneously. Fans located at the gas outlet provide a draft through the ring main surrounding the furnace.

Ambient air is thus pulled through the sections on cooling to recover heat before entering the peak fired and preheated sections. After passing through a certain number of sections, the flue gases are collected in the exhaust mainfold connecting each firing zone to the ring main. After a specified period the burners and the exhaust mainfold together with the air intake mainfold are shifted to the next section, in the direction of the flue gas flow. The anode temperature rises as the burners approach, and reaches its highest value when the burners are on top. The actual heat-up target is controlled by the applied draught and the actual combustion gas temperature in the fired sections. The flue walls are permeable for pitch fumes to pass from pit to flue where they are combusted. This has a significant impact on the flue gas temperature and thus on the anode temperature gradient.

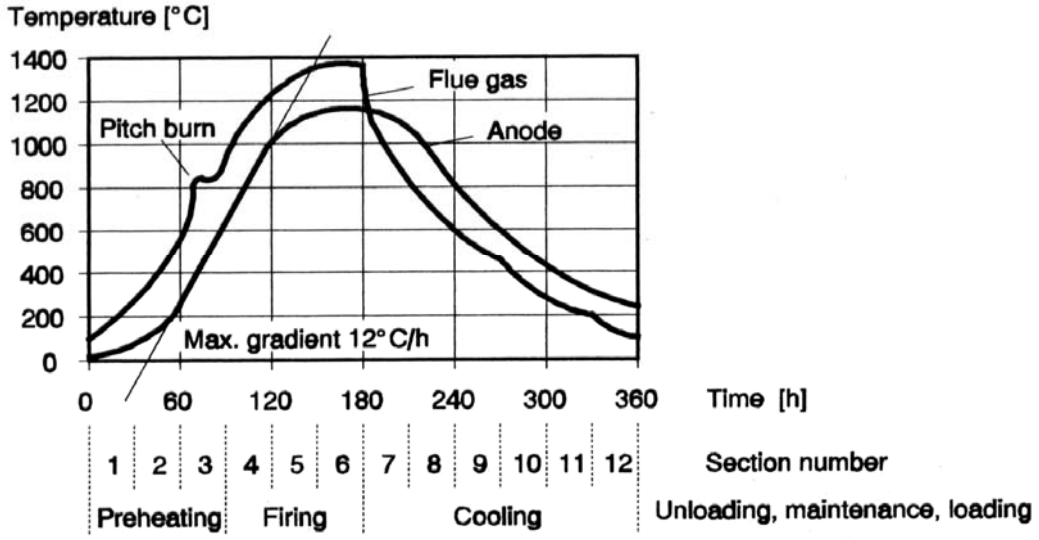

Fig. 1.4-2. Flue gas and anode temperature versus time during baking [11].

A computerized baking furnace process control system keeps the temperature increase under control. Due to release of light binder volatiles during heat up an internal pressure is built up in the anode. With a too high temperature gradient, this may cause crack propagation which influences the mechanical properties of the anode [22].

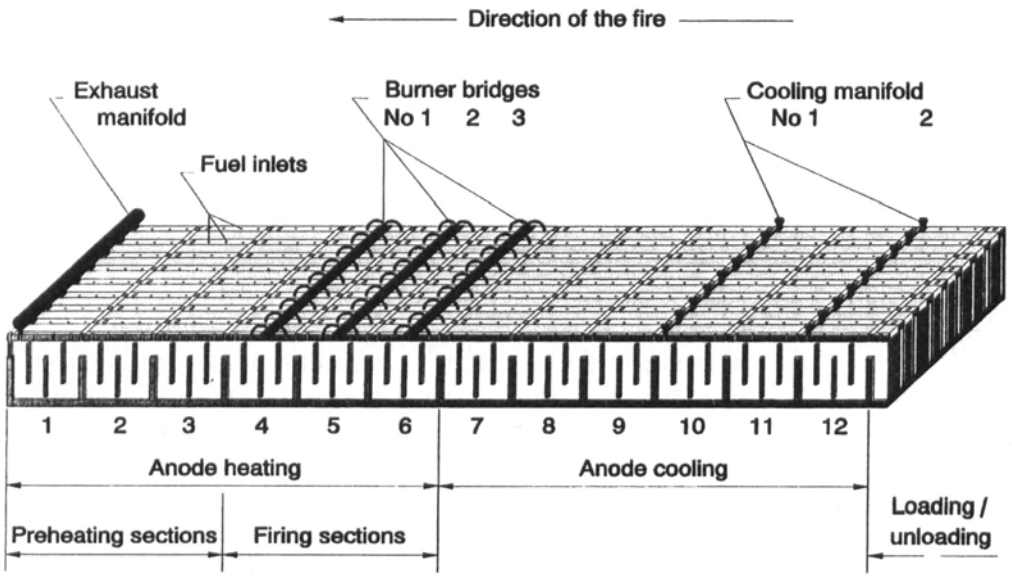

Fig. 1.4-3. Open top horizontal flue baking furnace [11].

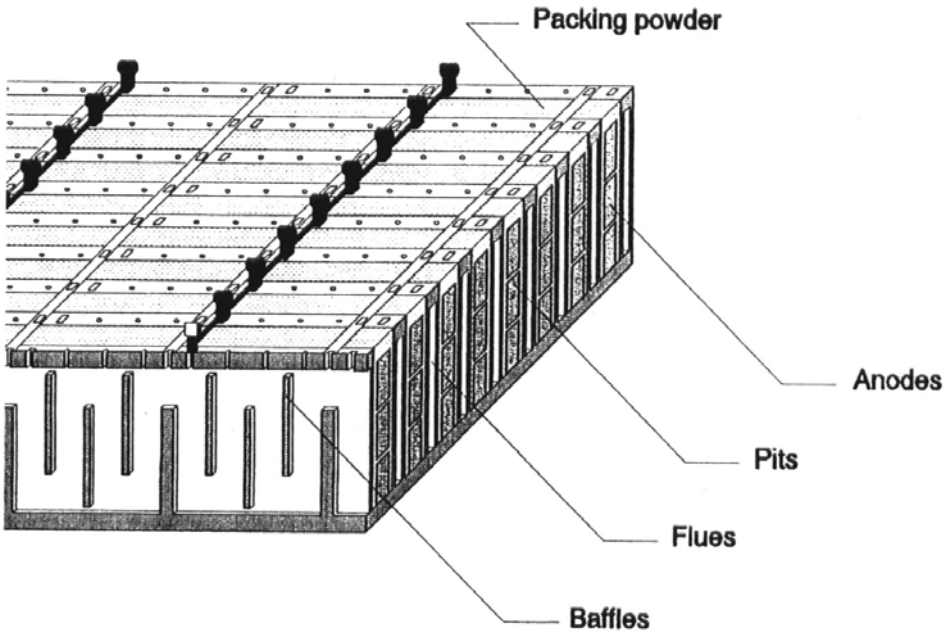

Fig. 1.4-4. Detail from open top horizontal flue baking furnace [11].

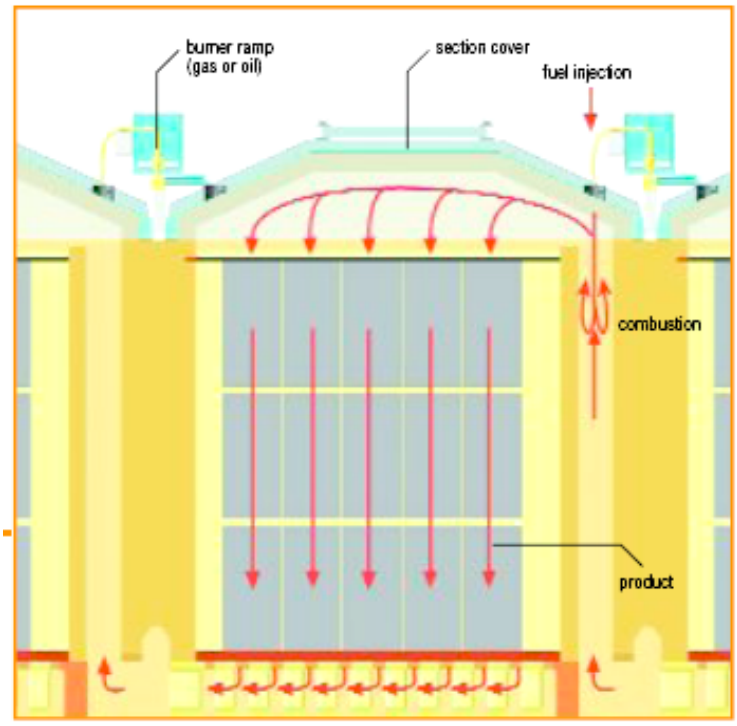

Fig. 1.4-5. Closed furnace type. Cross-section of one furnace chamber indicating the typical flue gas flow pattern [23].

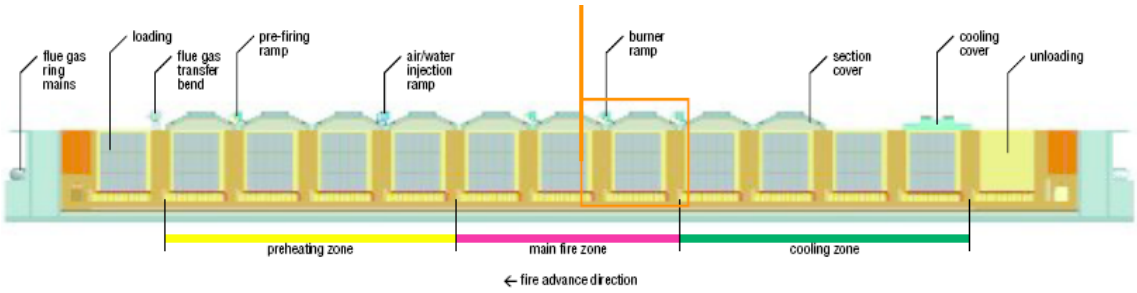

Fig. 1.4-6. Closed furnace type. Fire-group arrangement [23].

1.5 Influence of the anode manufacturing process parameters on the anode properties and porosity

1.5.1 Porosity in carbon

Carbon artefacts contain voids or pores which either result from the manufacturing process or are inherent in the chemical composition of the raw materials. A void is an empty space where a discontinuity of the solid material occurs [24]. A pore is a class of voids which is connected to the external surface of a solid and will allow the passage of fluids into, out of or through a material. Examples of different pore types are shown schematically in Fig. 1.5-1. Open pores are connected to the external surface which will allow the passage of the fluids into material. Transport pores will allow the passage of the fluids through the material. The closed and blind pores are not conducting the fluids. Thereby a distinction is made between open and closed pores.

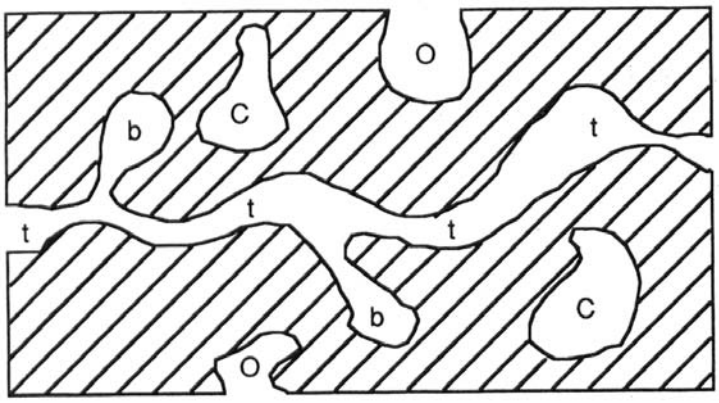

Fig. 1.5-1. Different types of porosity in a porous solid. O - open pores; C - closed pores; t - transport pores; b- blind pores.

Pores in carbons and graphites are classified by their size and shape. The pore size distribution extends from molecular dimensions to massive defects many centimetres in size in large carbon artefacts. A classification based upon pore size was proposed by the International Union of Pure and Applied Chemistry, IUPAC, [25], as follows:

- Micropores – width less than 2 nm
- Mesopores – width between 2 and 50 nm
- Macropores – width greater than 50 nm

This arbitrary classification is based upon the gas adsorption characteristics of porous solids, and was slightly modified for carbon anodes used in the aluminium production by Meier [11] as follows:

- Micropores – width less than 0.1 μm
- Mesopores – width between 0.1 and 10 μm
- Macropores – width greater than 10 μm

Rand, Hosty and West [26] characterized pores in carbon artefacts according their type:

- Pores within the filler phase
- Intergranular pores not completely filled by pitch due to inefficient mixing/infiltration or use of insufficient pitch
- Pores generated within the binder matrix phase during carbonization
- Interfacial pores, between binder and granular phase due to separation during processing (shrinkage)

Pores within coke grains are always present but further porosity develops if the granular material is heated during processing to a higher temperature than it previously has experienced. Open intra granular porosity may be partly filled by the binder phase during the mixing operation. This is determined by the wetting and flow characteristics of the pitch. However, the degree of penetration may be modified during subsequent processing because, as the pitch composition changes, so will its surface activity and rheology [26].

Pores within a binder phase arise due to volatile evolution during carbonization which causes volume shrinkage. The weight change of the carbon composites may be of the order of 50 % and is accompanied by a substantial increase in their true density [26].

Interfacial pores depend on adhesion between binder and filler phases and the extent to which this is maintained when the binder shrinks [26]. If adhesion is poor, the binder phase may separate from the aggregate grains during carbonization, opening up interfacial pores. However, if adhesion is maintained, the matrix mass pulls the grains together and overall shrinkage of the body (decrease in bulk volume) results. Whether this takes place or not will depend on the packing of the filler material. If the filler is efficiently packed, movement of grains relative to each other is allowed only if it leads to a volume expansion. Thus, control of porosity could be partly influenced by the interfacial interactions between constituent phases. Another aspect is important for the filler phase. If the packing is efficient and the intergranular space is filled with the binder phase prior to its carbonization, then it is difficult for the volatile matter to escape. Pressure of volatile matter builds up locally and creates „bubble-like" or so called gas entrapment pores in the carbonization region where the binder has high viscous fluidity. This causes a volume expansion of the anode, resulting in increasing porosity due to loss of volatiles and contraction of the binder during carbonization [26].

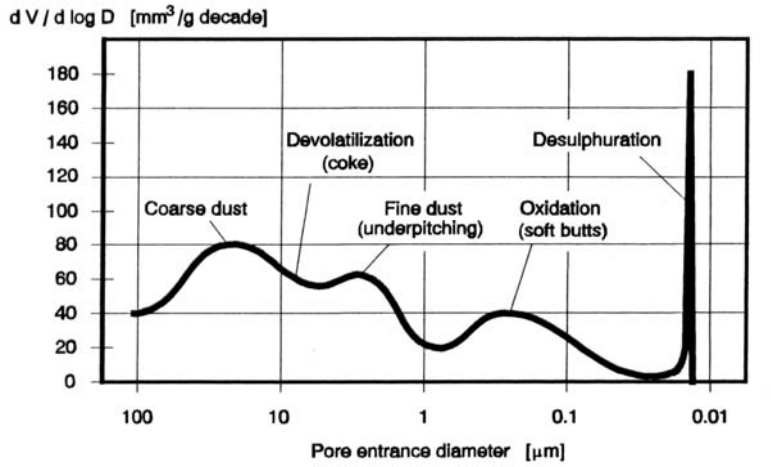

Fig. 1.5-2. Conceptional pore volume distribution of a carbon anode [11].

Fig. 1.5-2 shows a conceptional pore volume distribution diagram for carbon anodes including all different types of pores that may exist. The pore volume distribution diagram contains valuable information about the raw material and the manufacturing process which eventually influence the performance in the pots.

1.5.2 Coke porosity

Coke porosity is an important property of calcined coke. Porosity can be measured by a number of techniques: absorption of mercury, water, or other liquids, or by penetration of inert gases. Belitskus [27] proposed that the bulk density of coke can be used as a simple indicator of total coke porosity. This involves measuring the volume of a weighed, sized coke sample, usually after vibration to improve compaction. With closely sized fractions, bulk densities of calcined petroleum cokes tend to increase with decreasing particle size [28]. The cokes naturally contain pores and fissures of variety of sizes. As large pores are annihilated on particle size reduction, density increases. Jones and Hildebrandt [29] indicate that the porosity of the diameter range 1-10 µm is particularly significant for carbon anode consumption efficiency. However, quite satisfactory correlations have been made [30] between important anode properties and vibrated bulk density results, which give an indication of the total anode porosity.

The origin of coke porosity lies in the production steps and the calcination process [10]. The coke porosity depends mainly on the volatile matter of the green coke and on the heating rate during calcining. During calcining the coke shrinks about 10 - 22 % by volume [31, 32] and the volatile matter content is reduced to less than 0.5 %. The dimensional and structural changes are often connected with crack formation giving typical slit-like pores. In the manufacture of carbon anodes coke porosity adversely affects both the binder requirement and the apparent density. One of the principal factors controlling the pore structure and density of the coke is interaction between the degree of degasification and the degree of the coke contraction during calcination [32]. In the 1970's Alusuisse research [33] claimed that the following properties:

- Metal quality
- Anode consumption
- Energy consumption or current efficiency
- Pollution

can be explained by three basic parameters of the anodes: purity, structure and porosity. Open pores with more than 50 µm diameter influence the gas permeability [33]. The pore volume distribution in the range of 0.5 to 15 µm is of importance for the coke reactivity. In the case of pores with larger diameters, the specific surface is too small; in the case of smaller pores the diffusion coefficients decisive for the reaction are too small to influence the reactivity behaviour of the cokes. Typical coke pore volume distributions are shown graphically in Fig. 1.5-3.

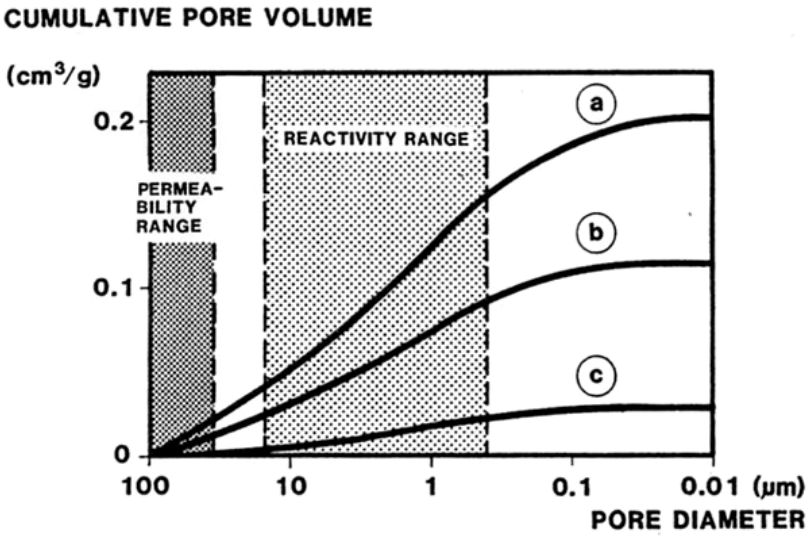

Fig. 1.5-3. Pore volume distribution as function of the pore diameter for different petroleum cokes. a – high porosity coke, b – typical petroleum coke, c – low porosity petroleum coke [10].

The pitch requirement is not only a function of the sizing or the surface area of the fines but also of the porosity. To illustrate the impact of coke porosity tests, Fischer and Perruchoud [34] examined 3 types of cokes using a plastograph mixer. Two calcining techniques; dynamic (industrial in rotary kiln) and static (laboratory calcining) were used. Microporosity of the paste was measured by Hg porosimetry and the total porosities and pore size distribution curves were measured. Details of the experimental setup are summarized in Table 1.5-I.

Table 1.5-I. Experimental data setup [34]. Pet coke D (dynamic) was calcined in a rotary kiln. Pet coke S (static) was calcined in a laboratory oven.

Type of coke	Calcined in	Micro porosity Hg (15 to 0.01 µm)	Bulk density (1 - 2 mm)
Pet coke D	Kiln at 100 °C/min	70 mm^3/g	0.84 kg/dm^3
Pet coke S	Furnace at 100 °C/h	40 mm^3/g	0.89 kg/dm^3
Pitch coke	Coke oven at 50 °C/h	20 mm^3/g	0.70 kg/dm^3

Not only the porosity of the materials is different but also their pore size distribution, as shown in Fig. 1.5-4. The typical peak of the dynamically calcined petroleum coke (D) at about 5 μm pore size disappeared for the petroleum coke statically calcined (S). Pitch coke prepared in coke ovens shows a very low microporosity but the presence of macropores larger than 100 μm and the lower bulk density value of the large (1-2 mm) grain fraction (Table 1.5-I).

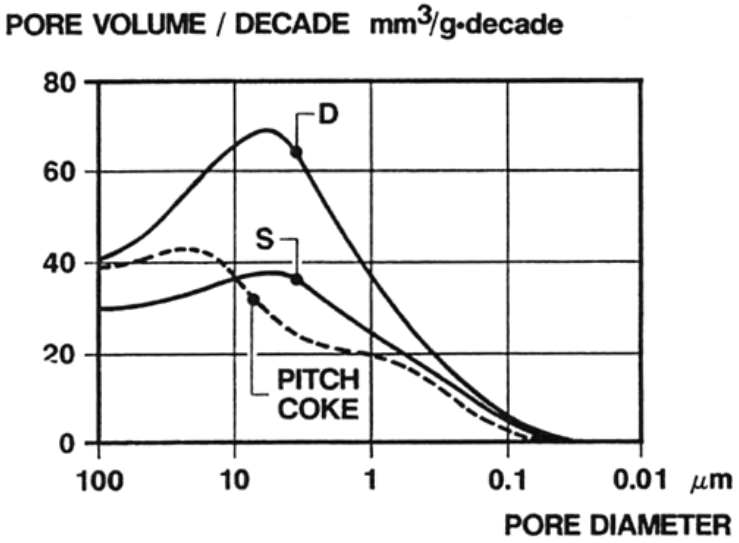

Fig. 1.5-4. Pore size distribution of petroleum cokes calcined dynamically (D) or statically- (S) and of a pitch coke prepared in a coke oven [34].

The coke porosity mostly depends on the volatile matter of the green coke and the heat-up rate during calcining. But also another phenomenon contributes to the coke porosity – coke desulphurization. Gehlbach and Grindstaff [35] performed a laboratory study of petroleum coke desulphurization. It was found that at a critical temperature T_c corresponding to the initial sulphur release, micropores with pore diameters smaller than 100 μm were formed. In a later study Samanos and Dreyer [36] pointed out that normally about 10 % of the sulphur content is released during the calcination process. As the calcination level increases the porosity increases due to thermal sulphur release. It first leads to prepuffing, *i.e.,* formation of closed pores without macroscopic expansion of coke grains and at higher temperature puffing with decrease in apparent density [36]. As has been well documented by Garbarino and Tonti [37] such sulphur evolution will result in higher porosity, lower coke density and declining anode properties. As will be shown later, (Chapter 1.5.4) such over-calcined cokes will also tend to desulphurize more easily during anode baking.

Kakuta and Tanaka [38] presented a new calcining technology to reduce the thermal expansion coefficient of the petrol coke. It was found that unique cracks developed during calcination were affected by the applied heating pattern. These microcracks absorb and relax the expansion of crystallites giving a reduction of the thermal expansion coefficient of the coke grains. Five different types of green coke were investigated. Calcining tests were conducted in two different ways, namely, the new (two-stage calcining) and traditional (one stage process in the calciner at a peak

temperature 1300-1400 °C). In the new calcining process green coke was initially calcined at a temperature between 600 to 900 °C, then cooled off and recalcined at a temperature of about 1300 to 1400 °C [38].

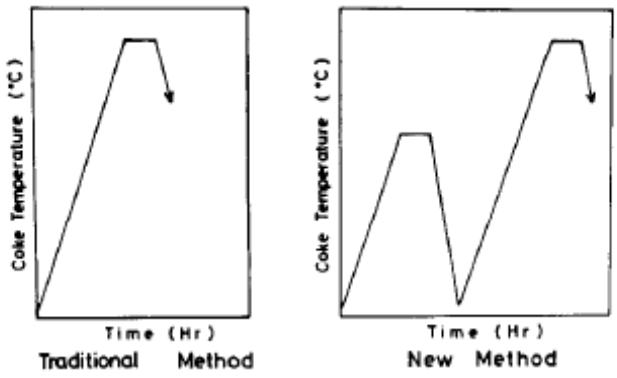

Fig. 1.5-5. Simplified calcination profile [38].

It was found that regardless of the green coke type, porosity is larger for the cokes calcined with the two-stage method compared to traditional method. Comparing the pore size distribution obtained by mercury porosimetry it was found the that new (two-stage) calcination method causes increased development of pores between 1 to 60 μm, regardless of the coke type. Development of these pores was found to contribute to reduction of the thermal expansion coefficient of the calcined coke by 16-20 % [38]. This pore size (microcracks) may affect the mechanical strength when processed into industrial anodes. However, no significant difference in strength was found for graphitized test pieces using the new and the traditional calcining method [38].

Letizia and Padeletti [39] investigated pore morphology (size distribution, axial ratio and number of pores) and pore microstructure of 21 petroleum coke samples by means of an optical semi automatic image analysis system. Two calcining techniques; dynamic (industrial) and static (lab calcining) were used. Part of the laboratory calcining was done in two steps in order to study the effect of a two-stage calcining process on the pore morphology of petroleum coke. It was observed that the industrial (dynamic) calcining process increases the total pore number, compared with the lab scale calcining process. The larger porosity from dynamic calcining results from a higher heating rate, which creates more swelling of the coke, as well as more extended cracks and pore formation. Independent of feedstock type or calcining process a larger number of long-shaped pores compared to round-shaped pores was observed, in any micropore range examined. The static two-stage calcining process carried out on cokes based on ethylene tar (ET) and a blend of thermal tar + decant oil (TT+DO) increases the ratio between the long-shaped pores and the round shaped pores, compared with the one-stage calcining process. On the other hand, the total coke porosity for the two types of feedstock develops in different ways:

- The blend TT+DO for the one stage calcined samples showed the highest total porosity. However, in the two-stage calcining process a readjustment of the pore shape takes place. The most notable changes happen in the range of pore area

20-30 μm^2, where the ratio long-shaped/round shaped pores increases, while the total pore number decreases.

- For the ET feedstock coke the two-stage calcining process increases the total porosity as well as the total pore number. Chiefly, the number of pores above 50 μm^2 increases. In the range of the area 10-30 μm^2 the one-stage calcined coke shows a larger pore number than the two-stage calcined [39]. This condition is the opposite of the situation described with TT+DO, but agrees well with the observations of Kakuta and Tanaka [38].

In the work of Medek and Weishauptova [40] Hg porosimetry was used to study the pore structure of needle coke and graphite electrodes, and the relation of the electrical resistivity, the bending and compressive strengths to the volume of meso- and macropores. With increasing porosity, the electrical resistivity of the electrode increased, and the strength decreased.

Yanko and Lazarev [41] observed similar trends for physico-chemical properties of electrode cokes. The cokes were calcined in an electrically heated vertical shaft furnace operating continuously. Three batches of pitch coke and one petroleum coke were examined. It was found that the electrical resistivity of the cokes decreases linearly with the calcining temperature. This was explained by increasing electrical conductivity due to free electrons in the carbon network. As the calcination temperature increases, crystallite ordering of the lattice is improved and the surface bonds are liberated by the removal of hydrogen and chemisorbed complexes. The overall result is reduced resistivity [41].

1.5.3 Influence of mixing and forming

Good mixing is an important objective to strive for to obtain good paste homogeneity and optimal characteristics of the anode. Improved mixing will reduce variations in anode properties, and may increase its service life in the potline [17]. To obtain a homogeneous paste, pitch and particles of various sizes must be distributed evenly and smaller particles fitted into voids between larger particles. If this does not happen, intra-particle porosity will increase, and the paste that enters the forming stage will be inhomogeneous and contain a higher amount of trapped air/volatiles. Both are not desirable in a green paste [42].

According to Foosnæs and Naterstad [12] the main events taking place during mixing are:

- Complete wetting of all grain surfaces by the binder
- Impregnation of grain pores and filling of voids larger than 6 μm by capillary effect and alternating static and dynamic pressure gradients imposed by mixer
- Statistical distribution of grain sizes throughout the paste

Clery [17] found that measuring the paste density by mercury porosimetry is a good indicator of the mixing efficiency. The maximum density of the paste was measured using a procedure similar to the mercury density test on coke. The maximum density is related to the coating degree of the coke particles. When the coke particle is properly

coated, the maximum density approximates to the mercury test density. When the coke particle is not properly coated, the maximum density approximates to the real density of the coke. It was also found that maximum density is affected by the raw materials, mixing energy (kWh/t), operating temperatures and grain size distribution of the mixture.

Stokka [42] measured the variations in intra-particle porosity and proposed this as a measure of the homogeneity of the green paste. Porosity in paste from different plants operating with different mixing systems was measured and used to indicate the efficiency of the mixing. The variations in paste porosity were studied as a function of pitch content, mixing time and temperature. It was suggested [42] that the pitch content reduces porosity in the paste both by increased penetration of pitch into coke pores and by filling of the inter-granular voids. If this was the case, the reduction in porosity would depend not only on the homogeneity of the mixed paste, but also on the degree of pitch penetration. But as shown by Vanvoren [43], an increase in pitch content at constant mixing temperature does not result in deeper penetration into the coke pores, but filling of the inter-granular voids. Thus for a given mixing temperature, the paste porosity at different pitch contents will only reflect variations in intra-particle porosity.

With increased mixing temperature more pitch is going into the coke pores as its viscosity is lower. More pitch into the coke pores should increase the porosity as less pitch is available to fill the voids between coke particles. Lower viscosity should also be expected to improve the distribution of the pitch and coke particles [42]. Thus for short mixing times the importance of viscosity was found important. Mixers with short retention time can improve paste homogeneity by increasing the mixing temperature. In the study of Stokka [42] the influence of the mixing technique was also reported. A more homogeneous and less porous paste was produced when changing the second ko-kneader in an industrial line to an intensive mixer.

A similar interesting study of a new process for anode preparation has been presented by Hohl and Bühler [20]. This process is based mainly on improved electric preheating of the aggregate and separate paste homogenizing and cooling in an intensive mixer and a mixing cooler. In order to compare the intensive mixing line to a conventional kneader line, one of the conventional kneader lines was shut down temporarily and replaced by the continuous intensive line whereas the other kneader line remained in operation unchanged. It was found that the new intensive continuous system produced anodes of similar quality compared to conventional anodes but at a 0.7 % (5 % relative) lower pitch content. Other advantages were better temperature control at the preheating and mixing stage and the possibility to use pitch types of higher softening point. In addition there is a considerable cut in cost due to reduced pitch consumption (pitch is two to three times more expensive than coke) [20].

Martirena [44] studied the effect of manufacturing parameters in the mixing and forming steps on the properties of carbon anodes using 4 cm diameter green samples. Dilatometric measurements during baking of the samples gave information on the mixing and forming temperatures and the degree of compaction. The heating rate from room temperature to 300 °C was critical for optimization of anode properties and

decreasing the risk of cracking, contrary to most of the published literature. The highest possible forming temperature (with respect to pitch softening point) gave dense anodes but the highest green density did not necessarily give satisfactory baked anodes. The expansion below 300 °C increased with increasing forming temperature. During forming the coke grains are aligned and bounded to each other. As the compaction efficiency increases, this linking mechanism replaces inter-granular voids and the macro porosity is reduced. Inside these voids there are air and pitch volatiles which should be expelled as completely as possible to reduce expansion during the first stage of baking (0-300 °C) when the remanent gases are released [44].

The effect of mixing variables and mould temperature was investigated by Belitskus [45] to determine effects of mixing time on the quality of pressed and vibrated prebaked bench scale anodes. Effects of coke and pitch preheating and mould temperatures were determined for anodes with the same pitch content. Aggregate preheating temperature had no apparent effect on anode properties or optimum mixing time. Thus, the only effect of preheating the aggregate is to shorten the mixing time in a commercial scale mixer with slower heat transfer. The mould temperature had a small effect on the anode properties. Decreasing mould temperature from 140 to 120 °C reduced green and baked apparent densities by 0.01 g/cm^3 and increased the electrical resistivity by 1 μΩm. An increase of green and baked apparent densities was observed for anodes with the same pitch level over the examined mixing time range. The electrical resistivity did not decrease over the entire mixing time range but was stable after 30 minutes. The electrical resistivity may be influenced by the relative amounts of binder coke formed in aggregate coke pores and bridging aggregate particles [45]. The amount of bridging coke may decrease with extended mixing, giving a higher density but poorer electrical contacts among particles. Thus it is possible to degrade anode properties by overmixing, which may result in less deep pitch penetration into coke pores during vibration of anodes [45].

The ability of the binder to wet the filler surface during the mixing process (*e.g.* < 160 °C in the case of carbon anodes) is critical to ensure good adhesion [46]. The wetting properties are dependent upon the filler and binder characteristics (*i.e.,* softening point, surface tension and viscosity of the binder; texture, granulometry and chemical and functional groups at the surface of the filler) [47].

Rocha et al. [48] studied the mechanisms of pitch/coke interactions at the mixing stage by spreading drop test, using a bed of calcined petroleum coke as a substrate. Three petroleum pitches and one coal-tar pitch were used. Low values of surface tension and viscosity are required for the pitch to spread and penetrate into the coke bed at temperatures below 160 °C. The pitch wetting behaviour was explained as the combination of two consecutive phenomena controlled by the surface tension (spreading) and viscosity (flowing). Thus, if the pitch surface tension is too high, the pitch does not spread, and does not flow through the coke bed, even when the viscosity is low. Conversely, if the pitch spreads but the viscosity is too high, wetting can not take place. The non-wetting behaviour observed in some petroleum pitches was ascribed to oxidation processes, as demonstrated by the fact that the non-wetting pitch behaviour can be improved by using an inert atmosphere and/or increasing the heating rate during

the spreading drop test. The wetting capacity of non-wetting pitches was easily reversed by blending them with wetting pitches (rich in sulphur containing compounds) and by addition of surface active agents contributing to reduction of the surface tension and viscosity of the non-wetting pitches [48].

Adams and Schobert [49] studied surface properties of the anode raw materials (coke and butts) and related them to pitch penetration behaviour. The extent of pitch penetration into coke and butts particles was evaluated by measuring the thickness of the pitch film that surrounds coarse filler particles of green mix from bench scale anodes. An image analysis technique was used for this measurement. Two mixes were produced, one mix contained butts particles as the coarse fraction, and the other mix contained petroleum coke as the coarse fraction. The granulometry was held constant for both mixtures. The results show that the average pitch film thickness for the mix containing butts filler is lower than the mix containing petroleum coke as the coarse filler. This behaviour was explained to be a result of the increased concentration of bath constituents found in butts, or as a result of the increased concentration of oxygen functional groups on the butts surface due to the anode exposure to air and CO_2 [49].

Belitskus et al. [50] and Proulx [51] independently observed that absence of butts particles in aggregate formulation increased the optimum pitch level by about 1 % relative to the level required with the butts content typically used in plants (18-20 % of butts).

As the binder content of prebaked anodes increases, physical properties of the anodes as baked density, electrical resistivity, air permeability pass through an optimum value [52-54]. Proulx [51] conducted experimental laboratory and plant work to define a binder control equation based on raw material properties. Optimum binder content was derived evaluating the physical properties of pilot scale anodes produced from various cokes and pitches. Based on the results, the binder control equation was defined and implemented for laboratory scale use.

In a study of Auguie, Oberlin and Hyvernat [55] the effect of mixing on mesophase layer coating on coke particles was studied. In the past pitches contained large amounts of mesophase spheres. These pitches were not suitable for preparing high quality anodes since the mesophase microstructure is partly destroyed by mixing. Various pitches were studied and also the interfaces between the filler and the binder, both in green and baked anodes. Characterization was carried out by high resolution electron microscopy. The data suggest that mixing destroys mesophase spheres. Wetting of coke by the mesophase rather than by the pitch is favoured; this is highly detrimental to anode quality. During anode baking, the destroyed mesophase partially recovers a local preferred orientation and shells of microporous carbon are formed around the coke grains, thus separating them from the binder lamellar particles. Presently the pitches with low mesophase content are exclusively used for the anode production.

1.5.4 Influence of baking

Baking represents by far the most expensive and critical step in the production of the anodes [56]. During the baking process the light components of the pitch binder evaporate and the heavier components carbonize, binding the petroleum coke grains together. Due to the release of light binder volatiles during the heating period, internal pressure is built up in the anode bulk. With a too high temperature increase, this may lead to crack formation and increased anode porosity [22, 57]. The standard deviation of the electrical resistivity and flexural strength increase because of micro crack formation [56]. The acceptable heating rate for the carbon anodes depends mainly on block dimensions, properties set by the paste plant processing steps and the actual temperature range.

Anode baking temperature is recognized as a critical factor in determining anode quality and performance [22]. Direct measurement of the baking temperature with thermocouples of the individual anodes inside a section is a laborious and costly method. Foosnæs et al. [58] presented a monitoring method based on the structural development (L_c) with temperature and time of a reference coke sample. In this way it is possible to establish a relation between the calcining level in the various anode positions of a furnace section by measuring the L_c of a reference sample following each anode. The L_c value corresponds to the average stack height of the graphitic layers (c direction) and indicates the degree of graphitization of the sample. By comparing this value with a calibration curve an "equivalent" baking temperature (°E) is obtained. The coke L_c method provides a reliable indication of the degree of anode heat treatment and is used in a number of smelters (ISO 17499). Most smelters also undertake routine anode core testing. A number of anode properties like thermal conductivity, the air and CO_2 reactivity, are known to be strongly influenced by the baking temperature. In the study of Foosnæs et al. [58] five anode quality parameters (CO_2 and air reactivity, CO_2 dusting, specific electrical resistivity and air permeability) were seen to be directly influenced by the baking level. For CO_2 reactivity a slight increase with equivalent temperature was observed that may indicate beginning post calcining of the coke aggregate at the highest equivalent temperatures. The CO_2 dusting was observed to increase at low equivalent temperatures. This has been observed also by other authors [59, 60] where anode consumption decreased with increasing baking level. Increased air reactivity was observed when the baking level exceeded the calcining level of the petrol coke [58]. This can be explained by the formation of microcracks and additional porosity which increases the surface accessible to air.

A low final baking temperature or too short soaking time leads to selective air and CO_2 reactivity of the anodes binder matrix in the electrolysis cell (
Fig. 1.5-6). A too high baking temperature creates air burn problems. Appropriate levels are in the range 1050 to 1200 °C [56] .

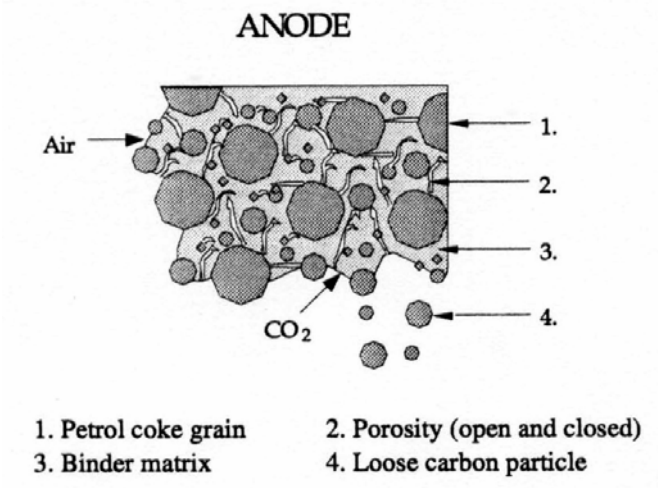

Fig. 1.5-6. Selective burning of anode [61].

Understanding the transitions in physico-chemical properties which take place during heat treatment of carbon blocks is important to the control of the baking process. Major transitions and critical temperature ranges during carbon baking are shown in Table 1.5-I.

Table 1.5-I. Physico-chemical transitions by heat treatment [12].

Temperature (°C)	***Physico- chemical changes***	***Major practical aspects***
0-200	Thermal expansion of pitch. Release of tensions caused by forming and cooling.	Reduced density. Slight release of aggregate interlocking.
150-350	Redistribution of pitch into voids by pitch expansion. Post impregnation of the coke aggregate.	Risk of stub hole slumping or damage. Permeability, mechanical strength and resistivity are affected.
350-450	Release of light binder volatiles.	Slight reduction in density of the aggregate packing.
450-600	Coking: Transition from plastic to solid matrix. Release of the major amount of non-coking volatiles.	Dilatometric tensions by thermal gradients causing expansion and contraction within the same block.
600-900	Post coking: Release of heavy cracked volatiles. Methane, hydrogen and annealing of tensions.	No particular effect within range of ordinary heating rates.
900-1200	Crystalline reorientation and growth of the binder coke and possibly of the lowest calcined aggregate coke.	Dilatometric tensions by contraction. Macro cracks may arise if the previous average calcining level for the coke exceeded (> 100 °C)

When the heating rate was too high, the volatiles release occurred suddenly causing an expansion of the specimen. If this expansion is too large it may induce formation of cracks and pores. The baking cycle of the laboratory samples was divided into three intervals according to observed dimensional changes [44]:

1. 0-300 °C – A considerable expansion was detected with a maximum around 200 °C. The height and the temperature at which it occurs decrease as the heating rate decreases. The reason for such behaviour was attributed to the release of frozen stresses (due to immediate cooling after forming) and/or occluded gases that were entrapped at the forming stage [44]. Some authors explain this behaviour as a consequence of volatiles evolution [62].
2. 300-600 °C – A fast heating rates below 300 °C causes larger expansion and permeability of the sample. Thus enough channels and transport pores inside the sample are generated for the pitch volatiles to escape above 300 °C without causing further expansion of the specimen. On the other hand, at low heating rates, the initial expansion from 0-300 °C is not so large, so the volatiles have to find their way out expanding the less permeable body [44].
3. 600-1000 °C – No dimensional change is observed whichever heating rate was considered [44].

Even if the baking of small samples is explained, the extrapolation of the results to full scale anodes baked in ring furnaces may not be straightforward. When a large anode is baked, several stages can be present simultaneously in the body; transition zones will appear where the different expansion or shrinkage mechanisms can interfere originating a kind of dislocation area. The pitch volatiles released from the block centre will have to travel through the porous structure of already calcined regions, where they have a chance to remain or to continue out to the surface. This depends on the open porosity and the temperature gradients [44].

The three analysis methods thermogravimetric analysis (TGA), gas chromatography (GC) and image analysis (IA) have been used to investigate the anode binder matrix [63]. The samples were made from commercial coal tar pitch that was crushed, sieved and mixed with the dust fraction of an industrial petroleum coke to an anode binder matrix with 40 wt% pitch level. The mixing was performed at room temperature in a Y-mixer. The preparation method was loose powder as mixed or hot pre-pressing at 1 bar at 185 °C for 20 seconds. The sample mass, heating rate, N_2 flow rate and sample pre-treatment were varied according to a fractional design shown in Table 1.5-II. The porosity of the matrix was measured by image analysis. The pores were measured from 5 μm and they were divided into three groups: small, medium (5-25 μm) or large (> 25 μm).

Table 1.5-II. Factorial experimental design [63].

Sample	***Mass (mg)***	***Heating rate (°C/min)***	***N_2 flow rate (ml/min)***	***Preparation method***
1-3	125	3.0	50	pre-pressing
2-6	200	3.0	50	loose powder
3-8	125	1.2	50	loose powder
4-2	200	1.2	50	pre-pressing
5-7	125	3.0	25	loose powder
6-1	200	3.0	25	pre-pressing
7-5	125	1.2	25	pre-pressing
8-4	200	1.2	25	loose powder

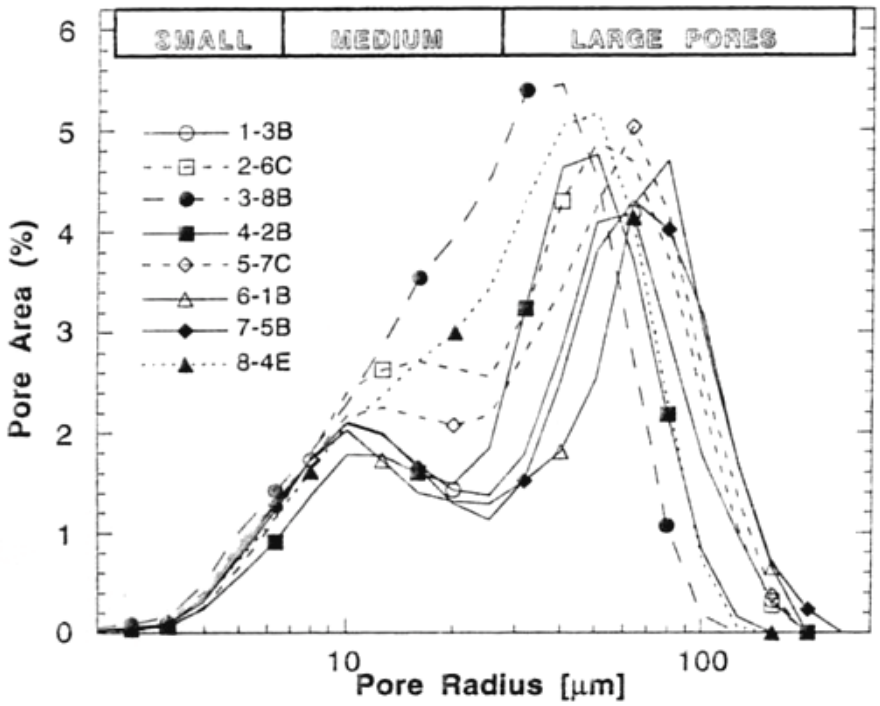

Fig. 1.5-7. Pore size distribution in an anode binder matrix. Full line = sample hot pre-pressed, filled symbol = slow heating (1.2 °C/min) [63].

Increase of the sample size increased the carbon yield during baking. Increasing the sample size increased the amount of the large pores, while the medium pores and the total porosity decreased. By increasing the heating rate the density increased by almost 10 %, which was considerable compared to the decrease in porosity. The cause of this was not explained. When increasing the N_2 flow rate the amount of medium pores increased, the large pores decreased and the total porosity was approximately unchanged. There were observed differences in porosity and shrinkage due to different pre-pressing (Fig. 1.5-7). Hot pre-pressing gave a baked binder matrix with almost no shrinkage due to better packing. It was proposed that pre-pressing changed the medium sized pores to small pores or prohibited the coalescence of pores. The reduction of medium porosity was the main factor for the decreased total porosity. The presence of

large pores due to gas entrapment was observed in all samples and was due to overpitched samples. Other pores found were medium entrapment pores and voids that were developed due to density decrease during carbonization [63].

Ehrburger, Sanseigne and Tahon [64] studied the change of the binder properties of a green body during baking with an attempt to determine the contribution of the pitch volatiles to porosity formation in carbon artefacts. The formation of porosity during heat treatment of an extruded mixture of coke particles (- 200 µm) and binder pitch was investigated using image analysis. Physico-chemical changes occurring in the pitch during pyrolysis were followed by measuring the glass transition temperature (T_g) in relation to the weight loss. The samples (Ø 25 mm, length 50 mm and 25.4 % pitch) were baked in N_2 flow using a thermogravimetric balance. The baking process was carried out using two different heating conditions. The first consisted of baking at a constant heating rate of 12 K/hour up to the final temperature which in all cases was 650 °C. In the second, the samples were heated at 12 K/hour until a pre-selected temperature was reached and thereafter treated isothermally for 60 hours. Afterwards, they were heated at 12 K/hour up to 650 °C (treatment with intermediate isothermal step). Typical views of the analysed areas are shown in Fig. 1.5-8.

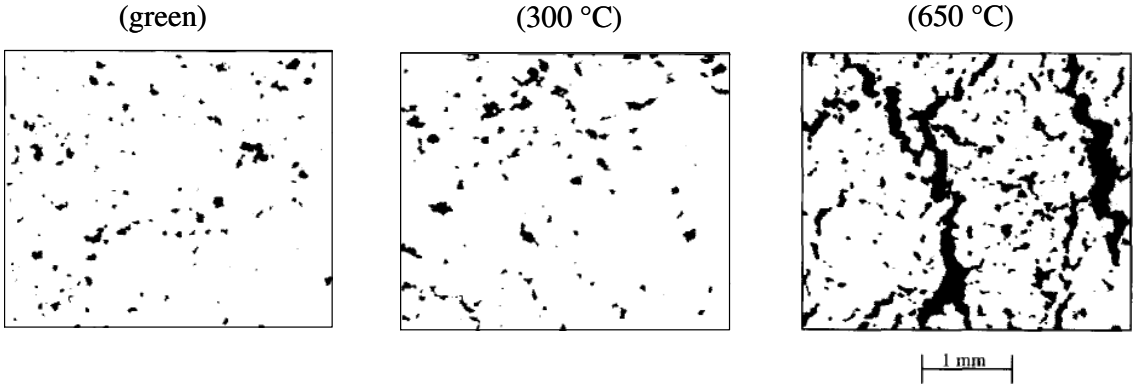

Fig. 1.5-8. Treatment at constant heating rate. Binarized views of studied cross sections of samples [64].

Important modifications are found in pore size shape after carbonization at 650 °C. Total porosity and number of pores per unit area are shown as functions of temperature in Table 1.5-III. A first increase in porosity is found between 100 and 200 °C. This was attributed to an expansion of pitch volume above its glass transition temperature and to the relaxation of stresses in the body after binder softening, since the weight loss in the same range of temperature is less than 1 % [64] (Fig. 1.5-9). The porosity remains nearly equal to 10 % between 200 and 375 °C. Thereafter, a marked increase is found between 385 and 400 °C and the porosity reaches a value close to 30 %. In the same temperature interval, the sample undergoes a weight loss equal to 10 % (Fig. 1.5-9). Up to 400 °C, the number of pores per unit area remains almost constant which suggests that the pore size increases between 375 and 385 °C [64].

Table 1.5-III. Porosity and number of pores in a sample heated with a linear heating rate 12 K/hour [64].

Temperature (°C)	***Porosity (%)***	***Number of pores (mm^{-2})***
Untreated (green)	4	5
200	11	7
250	10	7
300	12	6
350	11	5
375	7	3
385	26	7
400	32	6
650	24	10

A slight decrease of porosity was observed after treatment at 650 °C which probably corresponds to the shrinkage of the extruded sample. Meanwhile, the number of pores per unit area increased slightly which suggests that the porous texture of the sample undergoes a significant change during the transformation of pitch into semi-coke [64].

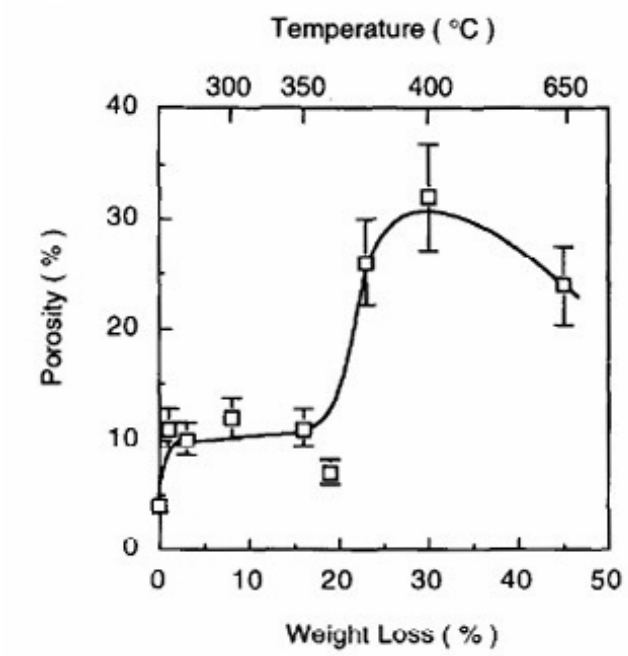

Fig. 1.5-9. Porosity as a function of weight loss during baking at 12 K/hour [64].

The change in the size and shape of pores during heat treatment was also investigated. Since various pore shapes can be found, the size of a pore is considered equal in a first approximation to the square root of its cross-section. In all cases, the most frequent pore size is in the range 100 to 200 μm. In the green sample, more than 95 % of the pores are smaller than 300 μm and slightly less than 90 % after heat treatment at 300 °C. In contrast, after carbonization at 650 °C, pores with sizes larger than 500 μm are present in the sample. The largest pores also tend to become more elongated. The formation of

porosity in the temperature range 300-400 °C is generally attributed to the departure of volatile compounds from the pitch, and the gradient in pitch composition may be expected from the external to the internal part of the shaped body. Observed difference in T_g between the outer and the inner parts of the sample indicated that the extend of pitch devolatilization differs quite significantly during heat treatment[64].

The selected temperatures of intermediate isothermal baking steps were 250, 300, 350, and 370 °C, respectively. The weight losses corresponding to the end of the isothermal plateau are shown in Table 1.5-IV. It was observed that weight losses at the end of the isothermal steps at 250 and 300 °C are similar to those baked at the constant heating rate to 350 (16 %) and 400 °C (30 %) respectively. These results suggest that the departure of low molecular mass compounds of the binder is more advanced in the isothermally treated sample although it has been exposed to a lower temperature than the other one [64].

The isothermal heating also has a significant effect on development of porosity in the sample after final baking at 650 °C as indicated in Table 1.5-IV.

Table 1.5-IV. Pitch weight loss an porosity in sample baked at intermediate isothermal step [64].

Temperature of isothermal treatment (°C)	***Pitch weight loss (%) at***		***Porosity at 650 °C (%)***
	end of plateau	***650 °C***	
250	14	40	7
300	30	47	9
350	42	47	8
370	42	44	18

In fact after an isothermal treatment in the temperature range 250-350 °C the porosity in the baked sample was similar to the one baked at a constant heating rate. When isothermal steps were performed at higher temperatures, the porosity increased again since the heating rate profile tends to become similar to those under constant heating rate conditions. Overview of an analysed cross section from the sample baked at isothermal step at 250 °C and final baking at temperature 650 °C is shown in Fig. 1.5-10.

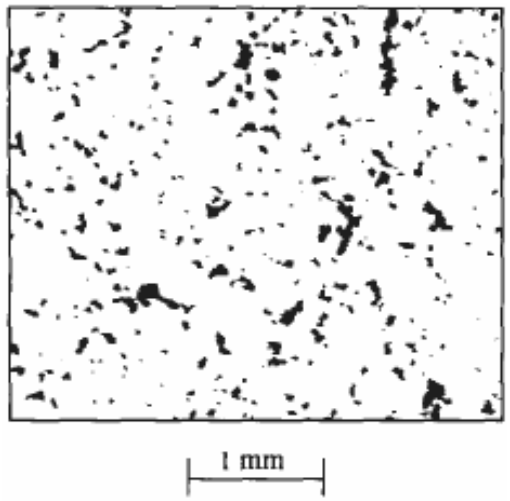

Fig. 1.5-10. Overview of sample baked at 650 °C with an isothermal step at 250 °C [64].

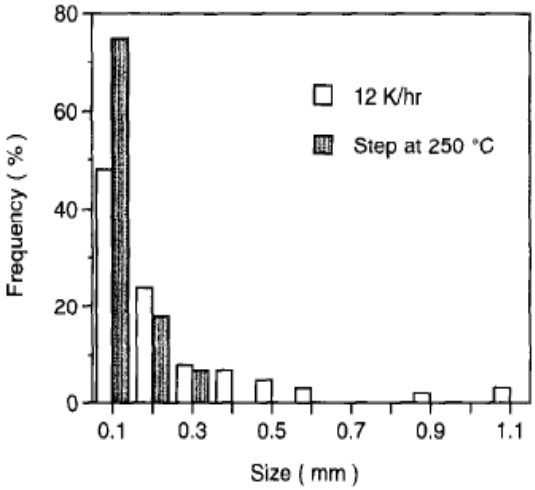

Fig. 1.5-11. Comparison of pore size distribution in samples baked at 650 °C in the constant heating condition and with an intermediate isothermal step at 250 °C [64].

It was found that pores are smaller and less elongated than after a constant heating rate to the same temperature, Fig. 1.5-8. Histograms of pore size corresponding to both types of baking are compared in Fig. 1.5-11. The difference in pore size is quite significant since all pores are smaller than 400 μm after isothermal treatment whereas in the other case their size can be much larger [64].

The formation of volatile compounds during pyrolysis of a binder pitch in a green body is a kinetically controlled process. In that respect, the porosity development depends basically on kinetic considerations, *i.e.,* the rate of formation of volatiles must be comparable to/or lower than the rate of their diffusion to the surface the green body [64]. Under sufficiently slow heating conditions, low molecular compounds essentially diffuse through the fluid pitch and evaporate at the external surface of the sample during baking [64]. As a result, no marked porosity is formed during baking. In contrast, a high heating rate allows low molecular mass compounds to accumulate inside the sample and the formation of a significant porosity is due to the evaporation inside the sample of these compounds [64]. The porosity formation due to pitch devolatilization takes place during a rather narrow temperature interval when the sample is heated at 12 K/hour. Only a small fraction of pores was formed when the sample was submitted to an intermediate isothermal step which allowed the departure of volatile compounds from the binder [64].

Another contributor to porosity development during anode baking can be desulphurization. Sulphur loss during the calcining of petroleum cokes and the subsequent impact on anode quality has been widely reported in the literature [35, 65-67]. Vogt and Ries [68] pointed out that calcined petroleum cokes that undergo further extensive heat treatment during anode baking, can lead to sulphur loss and porosity development. Although anodes are subjected to lower maximum temperatures during

baking than the petroleum coke during calcining, the exposure time in the baking operation is much longer. The combined effect of baking time and temperature (equivalent temperature) was examined and found to result in anode desulphurization leading to poorer anode quality [68]. The way in which the sulphur was lost affected the resulting porosity characteristics of the anode as well as the anodes physical, mechanical and chemical properties.

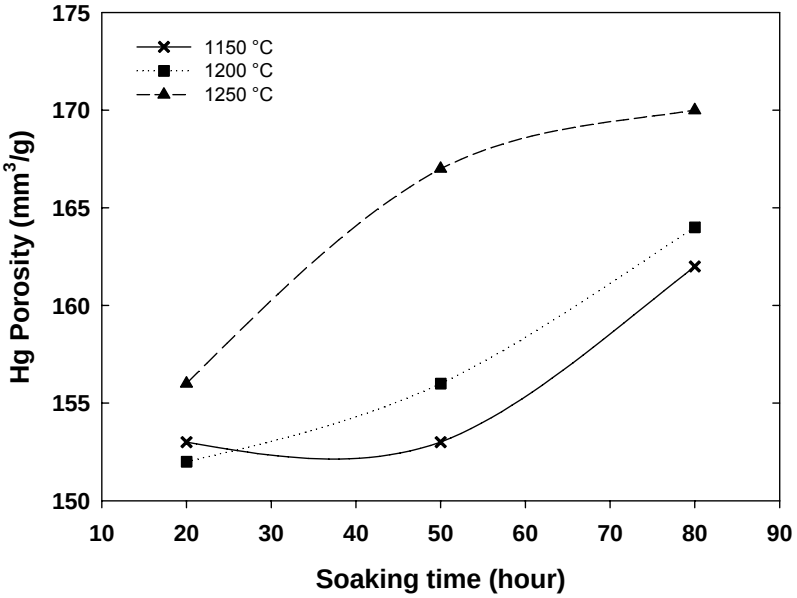

Fig. 1.5-12. Anode porosity, as determined by Hg porosimetry as a function of peak temperature and soaking time (Redrawn from Vogt and Ries [68]).

Fischer and Keller [22] have reported that anode desulphurization during baking, particularly with high sulphur content cokes, can dramatically impact the air reactivity due to increased anode porosity. This is also confirmed by a study of Samanos and Dreyer [36] where pilot scale anodes were made from cokes produced at different calcining conditions and different maximum baking temperatures of the anodes (920 °C to 1260 °C). Pilot scale anodes manufactured from highly calcined cokes resulted in less advantageous physical and mechanical properties. In particular:

- The specific electrical resistivity was higher with coke calcined at higher levels
- Flexural and compressive strength, as well as Young's modulus, were lower
- The calcining of cokes at high temperature leads to an additional demand in pitch (due to porosity increase) in order to reach the optimum baked apparent density. In any case, low calcined cokes produced anodes of higher baked density.

Above 1100 °C, larger sulphur release was observed for anodes made from high sulphur cokes. On the other hand, limited sulphur losses occurred for the low sulphur coke. For all cokes it was observed that the higher the coke was calcined, the earlier the sulphur escaped during baking. Thermal sulphur release seems to be a key phenomenon

affecting almost every anode characteristic including anode porosity [36]. It was stated that the optimum baking level, defined by the maximum temperature and minimum soaking time, should be chosen as close as possible to the level for which the desulphurization process starts to deteriorate the anode properties. A correct baking level is more important with high sulphur cokes than the level of coke calcination [36].

Xue, Aune and Øye [69] studied the influence of sulphur and AlF_3 addition in the pilot scale anodes on catalytic carbonization in order to facilitate the setting of baking parameters for a possible accelerated baking process. The sulphur in baked anodes has been found to reduce the CO_2 and air reactivity [60]. The coke yield of the pitch binder was found to increase with addition of sulphur powder and AlF_3 in pilot scale carbon anodes baked at 900 °C or 1060 °C. The AlF_3 additions result in lower porosity than the pure carbons (reference anodes with no addition of S and AlF_3). This was mostly due to a decrease of pores in the size range 60 to 180 μm (Fig. 1.5-13).

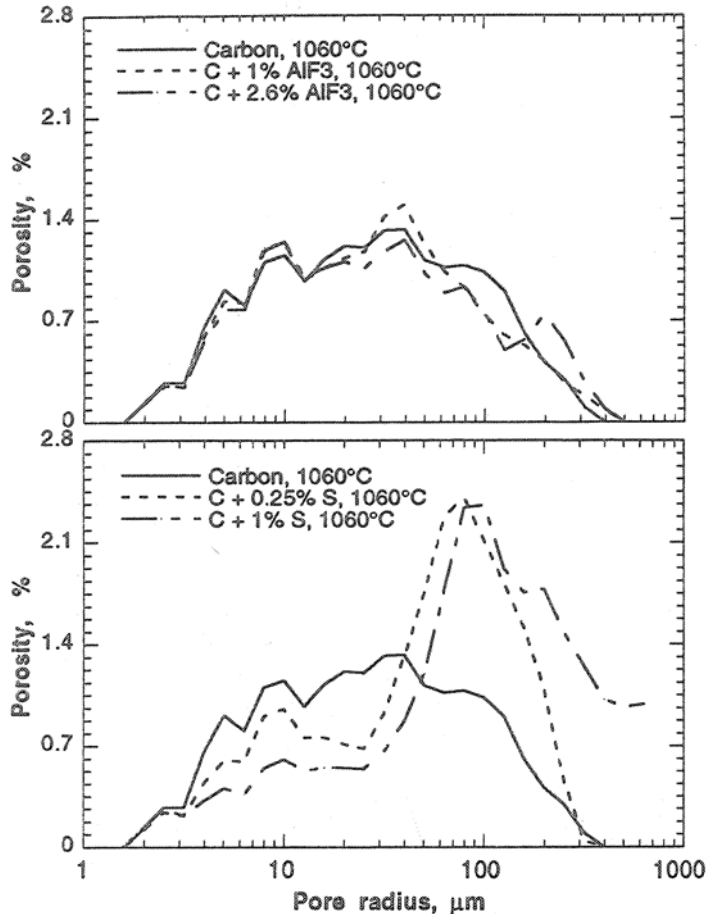

Fig. 1.5-13. Pore size distribution of the carbon anodes with various additions baked up to 1060 °C (Xue, Aune and Øye [69]).

The total porosity values for both 1 % and 2.6 % AlF_3 additions were similar, and also the fraction of large pores (> 180 μm) increases with 2.6 % AlF_3, suggesting that adding more AlF_3 would not yield further decrease in porosity. The added sulphur produces

more pores in the baked carbons. It was found that such increased porosity is due to an increase of larger (> 50 μm) pores (Fig. 1.5-13). It was also noted that the fraction of small pores (~ 50 μm) is less with the sulphur additions than with the pure carbons, probably as a result of a higher degree of carbonization [69]. However, more gaseous products can produce much larger pores, so that it can overtake the positive effect offered by the higher degree of carbonization. Reducing the sulphur addition to 0.25 %, the amount of larger pores (160 μm) decreases, as expected, but still not sufficient to have a resulting carbon structure like in the case of pure carbon anodes.

The trend of pore development versus baking temperature indicated that the majority of the pores are formed at a temperature below 550 °C, due to evolution of gaseous products. However, the AlF_3 addition reduced the number of pores with further increasing baking level, while sulphur addition did the opposite [69]. For this reason an alternative baking procedure was proposed: lower heating rate at stages involving volatiles evolution and higher rate at stages with increased degree of carbonization may improve the resulting carbon structures. Being aware of a predicted future shortage of low sulphur crude oil, the role of sulphur as an impurity should be viewed from both its negative and positive aspects [69].

In the previous work of Xue, Sørlie and Øye [70] it also was tried to reduce the baking temperature or time by accelerating the carbonization process with the addition of catalysts (S, $AlCl_3$, AlF_3) to green anode mixtures. It was found that the pyrolysis temperature for non-coking volatiles decreased with the catalyst content, and that the coke yield of the pitch binder increased.

1.6 Image analysis

1.6.1 Analytical methods for the anode porosity characterization

The traditional way to measure porosity in carbon materials is to use mercury porosimetry. With mercury porosimetry, the amount of liquid mercury (which does not wet carbon) penetrates the sample pores at increasing pressure. This method has several disadvantages. It cannot measure pores larger than 50 μm radius (because these are filled initially). It also assumes a non-intersecting cylindrical model [71] of the pore shape allowing calculation from the output pressure curve to a pore radius size distribution. The problem with using this method to measure pores in carbon is that the carbon pores are very irregularly and randomly shaped. They are also usually heavily interconnected with small cracks and smaller pores. A large pore with a small opening (crack) to the outside will appear as a large amount of smaller pores (at the size of the opening) when using mercury porosimetry [72].

The common way to characterize pores too large to be measured by mercury porosimetry is by using microscopy and image analysis [72]. This method can give an overview of the size distribution of the larger pores, fairly independent of the way they are connected. The image analysis software has a procedure for disconnecting connected pores. In addition to this, information can also be obtained on how the pores are arranged (connected vs. separated, clustered vs. distributed). Other advantages with image analysis include output of spreadsheet data for easy statistical treatment, and results that are independent of human evaluation. Disadvantages of the image analysis technique are that the smallest measurable pore size depends on the chosen magnification and the resolution of the image digitizing system (in our case a CCD video camera and movable stage). Image analysis also relies on the assumption that the analysed surface is statistically representative for the entire sample. Therefore analysis of as large areas as possible is desired. Another possible disadvantage with image analysis is that it is only capable of analyzing 2D sections, while the porosity is a 3D property. However, if the pores are randomly oriented, a 2D section will be statistically representative of the 3D structure [72].

True 3D information on porosity can be acquired through X-ray micro tomography and computer processing of the data. This method was used by Adams [73] to determine the density profile of carbon anodes through non-destructive analysis. X-ray computerized tomography (CT) is the method that can determine porosity and density of the materials and represent the information visually at high resolution. In X-ray CT operation the detectors collect data at different angles to make a 2D construction of the inner structural image. The third dimension of the images can be tuned by moving the position of the image slices (X-ray beam position emitted from the tube) and by moving the sample to another predetermined location by the computer controlled table. Fig. 1.6-1 shows 54 locations scanned, each with slice thickness of 2 mm, so that full coverage (enabling 2D or 3D reconstructions) could be achieved.

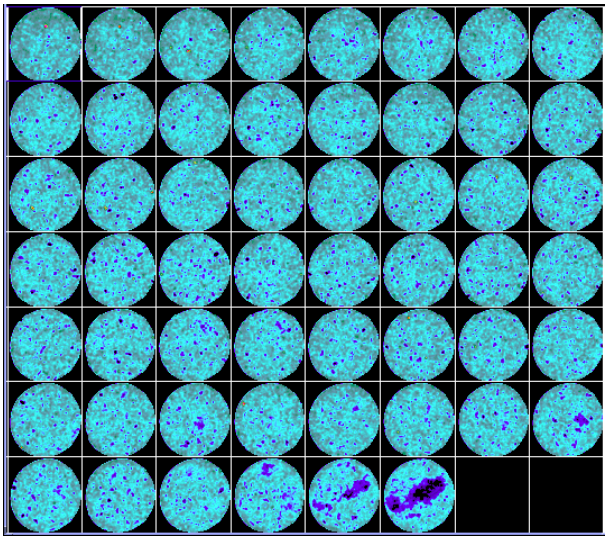

Fig. 1.6-1. X-ray images of a baked anode, Adams [73]. An anode sample of 50 mm in diameter was scanned at 54 locations each with a slice thickness of 2 mm.

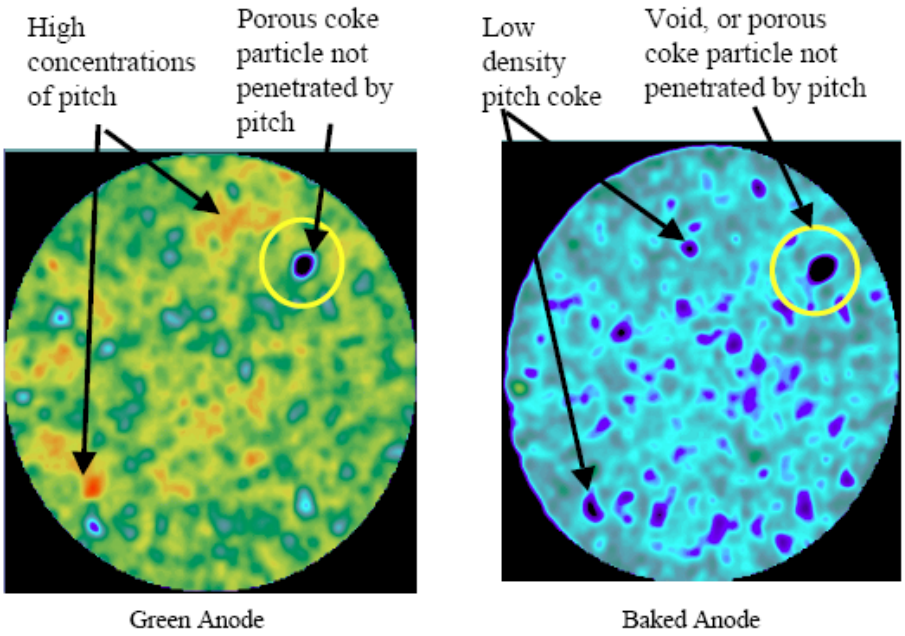

Fig. 1.6-2. Comparison of green and baked anode images at the centre of an anode [73]. Individual images from Fig. 1.6-1 in greater detail. At this level of detail, features such as voids or coke pores are apparent.

The advantage of scanning the object at regular intervals is that it enables the observation of the continuity of the structural features. The disadvantage of this technique is availability and it is useful only with very homogeneous materials where small volumes (e.g. a few mm^3) are representative of the entire sample [72].

1.6.2 Principle of the image analysis technique

A fully automatic method for image analysis of porosity in baked carbon anodes has been developed by Rørvik and Øye [72] and used for macro porosity characterization of the studied anodes. The method is based on optical microscopy and is capable of analysing large sample areas (several cm^2). It provides various statistics of pores in the range of 1 μm to 10 mm radius. The purpose of using image analysis in this work was to characterize macro-porosity of carbon anodes and to explain correlations with measured anode physical and chemical properties.

One major advantage of image analysis is that a pore model is not necessary to analyse and interpret the data. It must be remembered that all images are two-dimensional and to obtain three-dimensional structures the sample must be sectioned. This approach allows interconnections and blind/open macro pores to be recognized, which is not case for the majority of other techniques used to investigate porosity. Particular attention must be paid to sample preparation and a sufficient sample number must be analysed to give statistically representative results [71].

Prior to microscopy examination the samples require special preparation. Since the main interest in this work is to determine the porosity, the samples are impregnated with fluorescent epoxy resin [74]. The advantages with this technique is that the epoxy mix wets the carbon surface very well and there is practically no shrinkage or any heat development during curing that might affect the result. When the pores are filled with fluorescent resin they light up brightly when viewed in near ultraviolet light in the microscope. The hardness of the resin is also approximately the same as the carbon, thus avoiding problems with inhomogeneous abrasion during polishing. In the next step the samples need to be ground and polished to achieve a planar surface, ensuring that all points will be in focus at the same time.

A flat, polished carbon sample is then placed on a motorized stage with a computer programmable controller. This allows the sample to be moved systematically by the computer, so that a series of adjacent frames can be analysed. A grid of adjacent images, sufficiently large to cover most of the sample surface is captured by the camera (Fig. 1.6-3) and analysed by the image analysis program. The analysis program is a modified version of the public domain image analysis program NIH Image, developed by Wayne Rasband [75]. The image analysis program measures only pores entirely inside each frame, and suppresses measurement of the pores cut by the edge until the missing part of the pore is acquired in the next frame. When four frames are merged, the unanalysed parts are kept until the next four frames are finished. This process is recursive, so that an arbitrary number of levels can be analysed, thus allowing analysis of arbitrary large pores covering arbitrary large areas. This is the major strength of this image analysis method. The result is independent of the magnification and number of frames measured, since all pores on the entire surface are measured, and only once. The magnification determines the lower size limit of pores that can be measured.
Fig. 1.6-3 shows the recursive order of the frames that are captured and analysed. When e.g., frames 1-16 are analysed, these will make a rectangle containing the pores crossing the edges of the 1-4, 5-8, 9-12 and 13-16 sub-frames. This rectangle is therefore

processed after frame 16 is processed. Fig. 1.6-3 shows what the image analysis "sees" at each level.

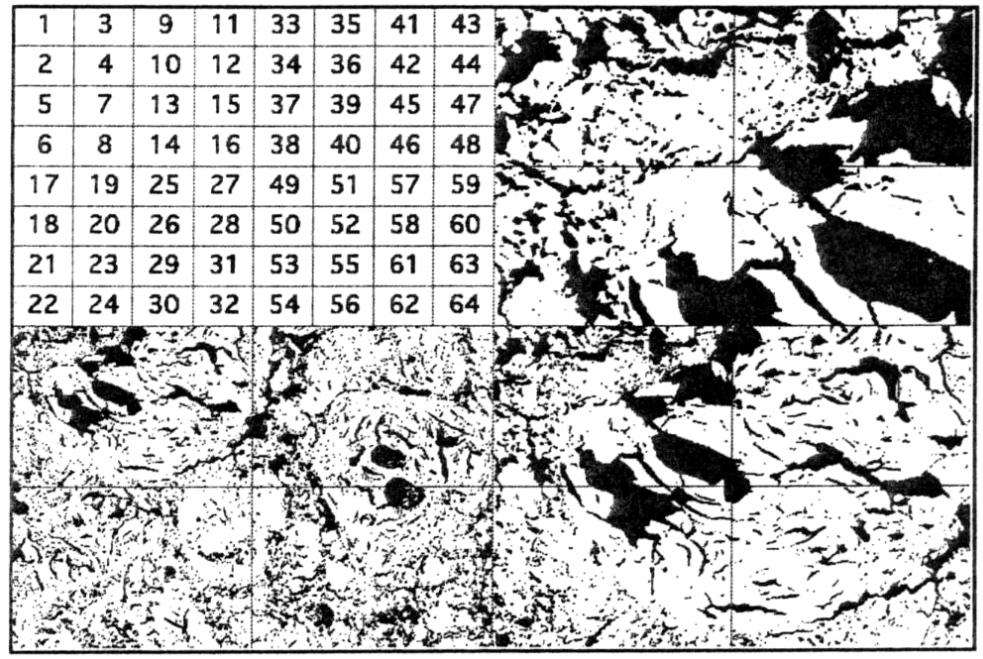

Fig. 1.6-3. The recursive order the frames acquired (clockwise) [72]: a) Frames 1-4 are merged, b) Frames 1-4, 5-8, 9-12 and 13-16 are merged, c) Frames 1-16, 17-32, 33-48 and 49-64 are merged.

The resulting data is merged using Microsoft Excel macros and presented using templates. The image analysis outputs the porosity values as the sum of the areas pores with a specified radius interval, as a percentage of the total analysed sample area. The sum of all porosity values is thus equivalent to the total porosity.

1.6.3 Pore classification

The technique of image analysis can be used also for classification of pores based on pore shape; particularly classification of calcination cracks and gas bubble pores in petroleum coke to distinguish the porosity due to the raw materials from the porosity that develops during production of the anode [76]. The main advantage of this method modification is that it can distinguish between coke pores and pores in the binder matrix. Binder matrix pores are the pores that come from the anode manufacturing process (mixing, forming or baking steps), and this is the only porosity that can be optimised by the anode plant.

There are two main areas of application of the anode porosity measurements: downstream, to study the anode structure and correlate it with the anode properties given by routine analysis such as density, reactivity, strength, electrical resistivity and thermal expansion. Upstream, to study the effect of production factors in the paste plant and the baking furnace on the anode porosity.

The diagram in Fig. 1.6-4 shows different classes of pores associated with certain production steps. Pores in coke have a different shape from pores in the binder matrix. Fig. 1.6-5 shows a part of a large coke grain. The pores consist of large rounded gas bubble pores (which were present in the green coke); thin elongated calcination cracks, and large cracks due to shrinkage. Fig. 1.6-6 shows a section of a prebaked anode. Pores are black and carbon is white. Several large coke grains are present, outlined manually. They cover several tens of percentage points of the total area. The pores from the mixing and baking process are outside the coke grains.

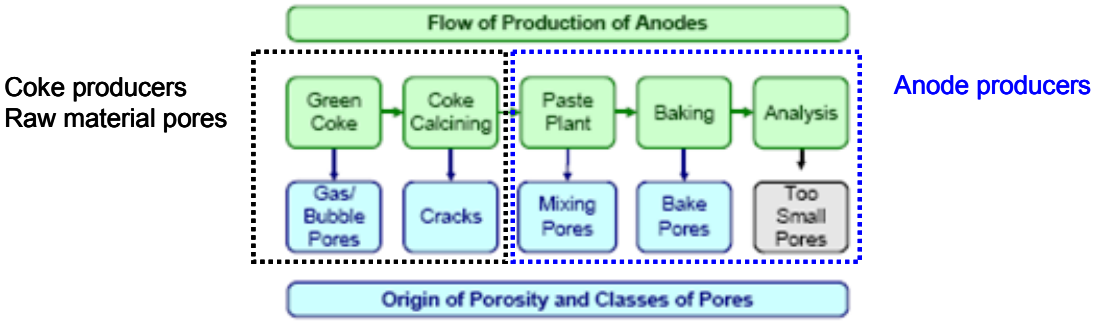

Fig. 1.6-4. The anode production steps and associated porosity, Rørvik, Lossius and Øye [76].

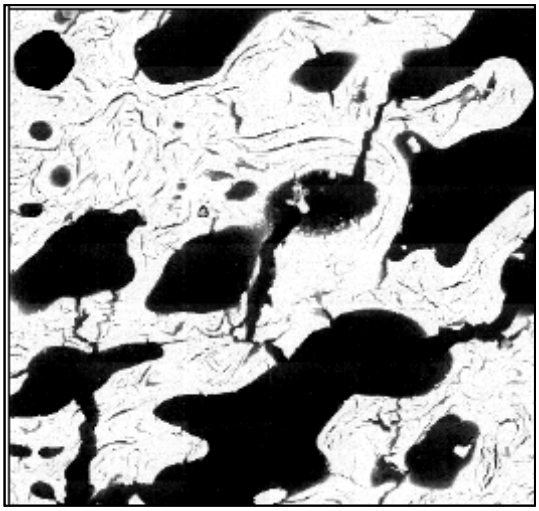

Fig. 1.6-5. Part of a large single coke grain [76].

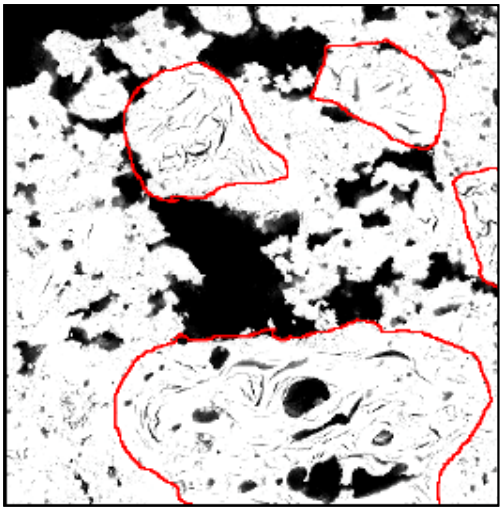

Fig. 1.6-6. Coke grains in prebake anode sample [76].

The most relevant parameters used in classifying pores are those related to deviation from a perfect circle; *i.e.,* pore roundness, and those related to the degree of pore edge roughness. The three main classification parameters were selected [76]:

1. Aspect ratio
2. Surface roughness
3. Degree of circularity

The aspect ratio is simply the ratio of the major/minor axis of an elliptical approximation of a pore. The surface roughness is defined as the number of pixels at the edge of a pore divided by the number of pixels at distance R from the edge, where R is the width of one pixel [76]. The degree of circularity was defined by an alternative measure called *Ellipse Coverage Ratio (ECR).*

$$EllipseCoverageRatio = \frac{intersected\ area\ of\ \ pore\ and\ its\ equivalent\ ellipse}{complete\ pore\ area}$$

This is measure of degree of ellipsity rather than circularity. It is simply the fraction of coverage between the pore and its equivalent ellipse (Fig. 1.6-7).

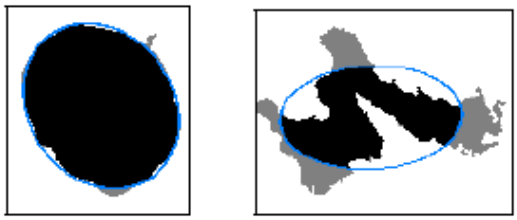

Fig. 1.6-7. A) Elliptical, ECR = 0.97, B), Irregular pore, ECR = 0.65.

It was decided to divide the pores into 5 different classes [76]:

1. Pores too small to be classified (light blue colour)
2. Elongated pores (coke calcination pores) (orange colour)
3. Round pores (coke gas bubble pores) (purple colour)
4. Irregular pores (binder pores due to imperfect mixing or baking pores) (green)
5. Edge pores (not counted) (blue colour)

In the image analysis program a procedure, which recognizes and colorizes all measured pores, according to the class number was implemented. An overview image showing all classified pore colours was merged into one image. Fig. 1.6-8 shows the capability of the pore classification to successfully distinguish between pores in coke and pores in the binder matrix, i.e., to distinguish pores due to production. The results are shown as multiple images according to pore classes.

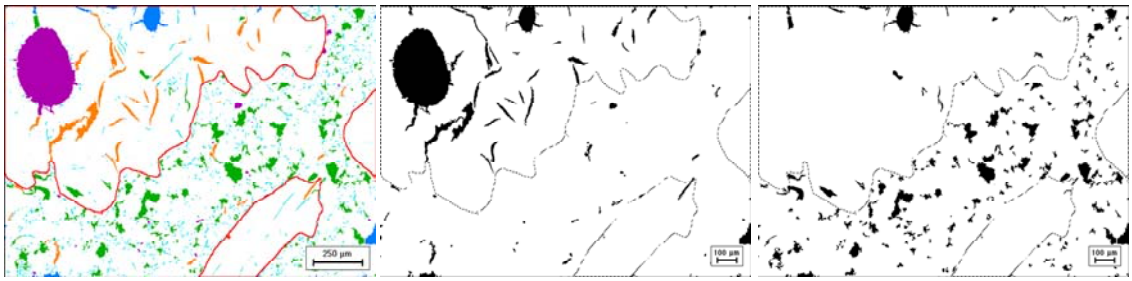

a) b) c)

Fig. 1.6-8. Multiple images of the pore type classification [76]
a) All pores are shown (classes 1, 2, 3, 4 and 5). Coke grain boundary is outlined with red colour.
b) Elongated and round pores that are already in the coke before anode production.
c) Irregular pores, mainly in the binder matrix due to the mixing or baking process.

The images in Fig. 1.6-8 illustrate how visual inspection alone can be of use; it is possible to guess the cause of high porosity from the shape and distribution of the pores. It can be determined if difference in porosity is related to the coke, binder or mixing pores.

2 RAW MATERIAL PROPERTIES

2.1 Petrol coke and pitch analysis

In the experimental work two types of petrol coke were used. For laboratory pilot anode production a single source petrol coke, SSA, was used. In another part of the experimental work pilot scale anodes were produced from industrial paste which was prepared in a paste plant from a coke blend. The investigated cokes were received with physical and chemical characterisation given in Table 2.1-I. The analysis was performed by the coke suppliers and the laboratory at Hydro Aluminium Årdal.

Table 2.1-I. Physical and chemical properties of the investigated cokes. SSA- single source A coke [77], Blend- blended coke [78, 79].

Properties	***Method***	***Unit***	***SSA***	***Blend***
Moisture	DIN 51904	wt%	0.05	0.02
Ash	ISO 8005	wt%	0.16	0.09
Sulphur	ISO 12980	%	1.18	2.01
V	ISO N 837	ppm	147	250
Si	ISO N 837	ppm	63	150
Fe	ISO N 837	ppm	105	200
Ca	ISO N 837	ppm	110	80
Ni	ISO N 837	ppm	82	150
Na	ISO N 837	ppm	55	60
Real density	ISO 8004	g/cm^3	2.07	2.08
Spec. el. resistivity	ISO 10143	μΩm	490	500
Air reactivity	Hydro method	mg/cm^2h	79.7	96.6
CO_2 reactivity	Hydro method	mg/cm^2h	24.5	11.0
Grain stability	ISO 10142	%	87	74
Porosity	Image analysis NTNU method	%	16.8	20.5

The two cokes differ in sulphur content where the blended coke has 2.01 % comparing to 1.18 % for the single source coke. There is also a difference in the grain stability where the SSA coke is mechanically stronger than the blended coke. Porosity was analysed on a 0.5 to 1 mm coke fraction [74, 80]. The porosity is larger for the blended coke which correlates well with the higher sulphur content. The blended coke has also higher content of catalytic elements (V, Ni, and Fe) and thus higher air reactivity. The specific electrical resistivities of two coke types are almost the same.

Table 2.1-II shows physical and chemical properties of pitch used in the experimental work.

Table 2.1-II. Physical and chemical properties of the applied pitch [81].

Analysis	***Unit***	***Analytical result***
Softening point	ºC	120.4
Insoluble in Quinoline	%	6.0
Density at 25 ºC	g/ml	1.309
Coking value	%	58.6
Ash	%	0.14
Zn	ppm	174
Pb	ppm	126
Fe	ppm	77
Ca	ppm	37
Na	ppm	155
S	%	0.48
Si	ppm	88

3 PILOT SCALE ANODE PRODUCTION AND EXPERIMENTAL PROCEDURES

The pilot scale anode production consisted of the four main production steps; aggregate preparation, mixing, forming and baking. The effects of variation in the production steps and their influence on the total porosity development as well as the physico-mechanical and chemical anode properties were studied.

3.1 Aggregate preparation

A defined recipe was used for all pilot scale laboratory produced anodes from SSA coke. The appropriate amounts of fractions and coal tar pitch were blended according to a typical industrial recipe that was recalculated for 4.9 kg of paste. The blocks were produced with three different fines fractions (dust fineness) and six different pitch contents that were used during the entire laboratory work. Dust fractions according to sieve analyses are marked as high (94 % < 63 μm), medium (63 % < 63 μm) and low fines (45 % < 63 μm). Thus low fines refer to the coarsest dust fraction and a high fines corresponds to the finest dust fraction.

In addition, particle size distributions of the dust fractions were measured by the particle size analyser Fine Particle Analyser 2001L (FPA). The particle analyser uses the computer vision technology, to image free falling particles with video camera and transfers the images to a computer for measurements. Particle size distribution curves of the three levels of fines are shown in Fig. 3.1-1 and Fig. 3.1-2. Table 3.1-I shows all the paste compositions used in the laboratory production.

Table 3.1-I. Composition of the paste.

	Pitch (wt %)	*14*	*15*	*16*	*16.5*	*19*	*21*
	Pitch (g)	686	735	784	808,5	931	1029
Fraction size	Weight (%)/(g)						
14-5.6 mm	17.2	725	716	708	704	683	666
5.6-2.0 mm	23.7	999	987	975	970	941	917
2.0-0 mm	34	1433	1416	1399	1391	1349	1316
Fines	25.1	1058	1045	1033	1027	996	972
Sum	100	4900	4900	4900	4900	4900	4900

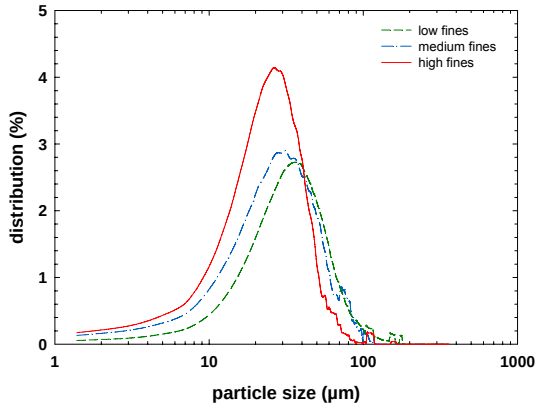

Fig. 3.1-1. Particle size distribution curves of the fines used in pilot scale production.

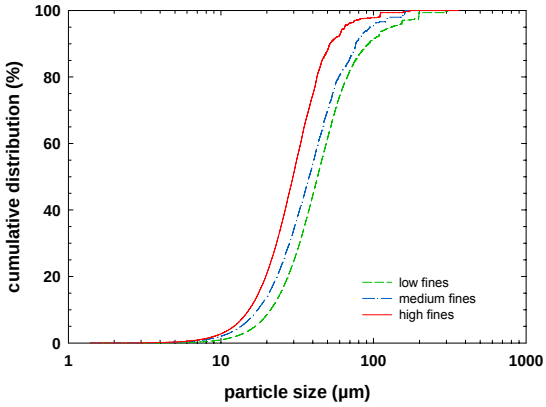

Fig. 3.1-2. Cumulative particle size distribution of the fines used in pilot scale production.

There is some minor incoherence in the distribution curves, mostly in large particle measurements around 100 µm. This could be due to measurement errors when larger clusters were formed during light projection which gives a false signal about particle size. However, there was not achieved exactly the same distribution for - 63 µm particles as in the case of sieve analysis [80], qualitative composition of the fines was confirmed by this alternative method.

3.2 Mixing

For pilot scale anode production two mixer types were used. The prepared coke fractions were preheated in a heating cabinet and then blended in the sigma and intensive mixers, respectively. In both cases the aggregate was preheated overnight at 170 °C to ensure constant temperature before the coal tar pitch was added. Mixing times were set for both mixer types individually (Chapter 4.5.), [82]. As shown later, the influence of mixer type and mixing time was found to be important parameters for analysed properties of pilot scale anodes.

3.2.1 Sigma mixer

In part of the experimental work a batch double blade Sigma mixer was used. The sigma mixer falls in the class of medium intensity mixer [83]. The mixer consists of two horizontal mixing blades revolving in the rectangular oil heated trough. The trough is curved at the bottom to form two half cylinders or saddles. The two blades are driven by gears and sweep the entire area of each half cylinder during each revolution. The blades revolve against each other by unequal speeds and mix by imparting both a transverse and a lateral motion in the charge. The sigma mixer has a good mixing action, readily discharges materials which do not stick to the blades, and is relatively easy to clean when sticky materials are processed.

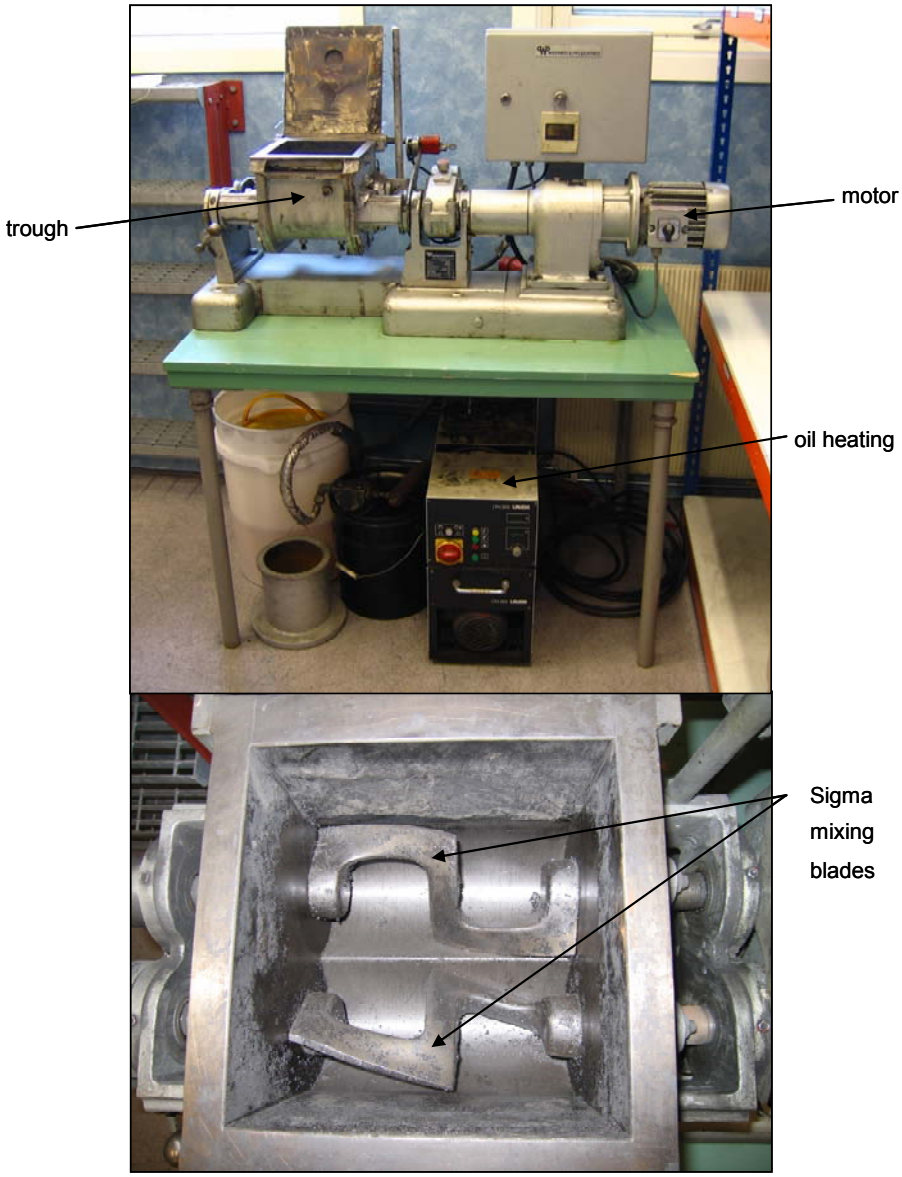

Fig. 3.2-1. Sigma blade mixer (Werner & Pfleiderer LUK 5.0 K2). Lower picture shows detail of trough with mixing blades.

3.2.2 Eirich mixer

An intensive Eirich mixer RV 02/E (Fig. 3.2-2) was used in the second part of the experimental work. The Eirich mixer's operational tools consist of the rotating mixing pan, an eccentrically arranged mixing tool and a scraper tool. The mixer was in addition equipped with a frequency controller (FC) Commander SE (size 2), that enables step less rotor tip speed control. An optimal tip speed 12 m/s (1218 rpm) was found (Chapter 4.5). The typical filling weight is in the range 4.8 to 5 kg of carbon paste. The rotating mixing pan is heated with a hot air blower LEISTER, (3100 W, 350 l/min.) up to 180 - 190 °C. Applied mixing times were 5, 7.5 and 10 minutes.

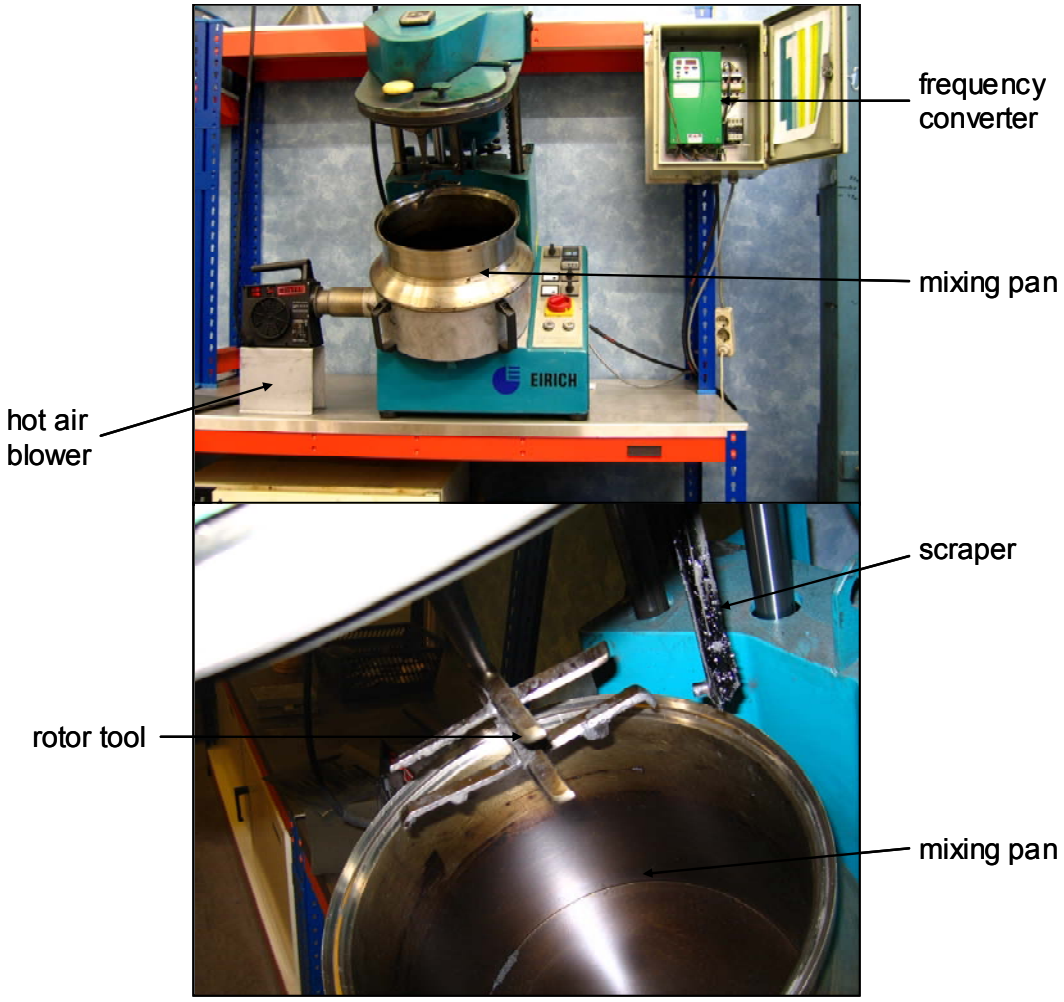

Fig. 3.2-2. Intensive Eirich mixer. Lower picture shows the rotating pan and detail of the mixing tool and scraper.

3.3 Forming

Anode forming was carried out in a pilot scale vibration compactor built at NTNU [84]. The compactor operates with an optimal load of 320 kg placed on top of the piston and an amplitude in the range of 0.8 to 1.2 mm [84]. The vibration frequency can be controlled from 0 to 50 Hz with a frequency inverter. The maximum mass of the sample is 5 kg.

The cylindrical mould has an internal diameter of 160 mm and can be heated to 165 °C. The vibrating compactor is also equipped with several sensors. Thus the vibrocompaction process can later be analysed. All data are logged to a PC with a sampling frequency of 1000 readings per second. The control program was written in the graphical language Lab View 6.1 [85] and controlled the duration and frequency of the compaction. The height of the anode sample was continuously monitored by a laser distance meter.

The following procedure was used for production of vibration compacted green anodes. The interior of the heated mould was sprayed with a silicone oil based lubricant in order to reduce friction and sticking as well as to improve the sample discharge. The mould was filled with paste and the temperature of the paste was measured through the paste volume. The compacting piston was lowered and allowed to rest freely on the paste. The forming parameters were launched from the PC, which then starts the vibration forming. Following paste compaction, the piston was raised and the formed block was pressed out from the mould. The green anode was allowed to cool in air before further measurements and experiments were performed.

Fig. 3.3-1 shows an image of the vibrating compactor. The load can be regulated by adding or reducing the quantity of the steel plates placed on the top. The lifting mechanism can be safely operated by a hand held remote control. The mould temperature is controlled by a transformer.

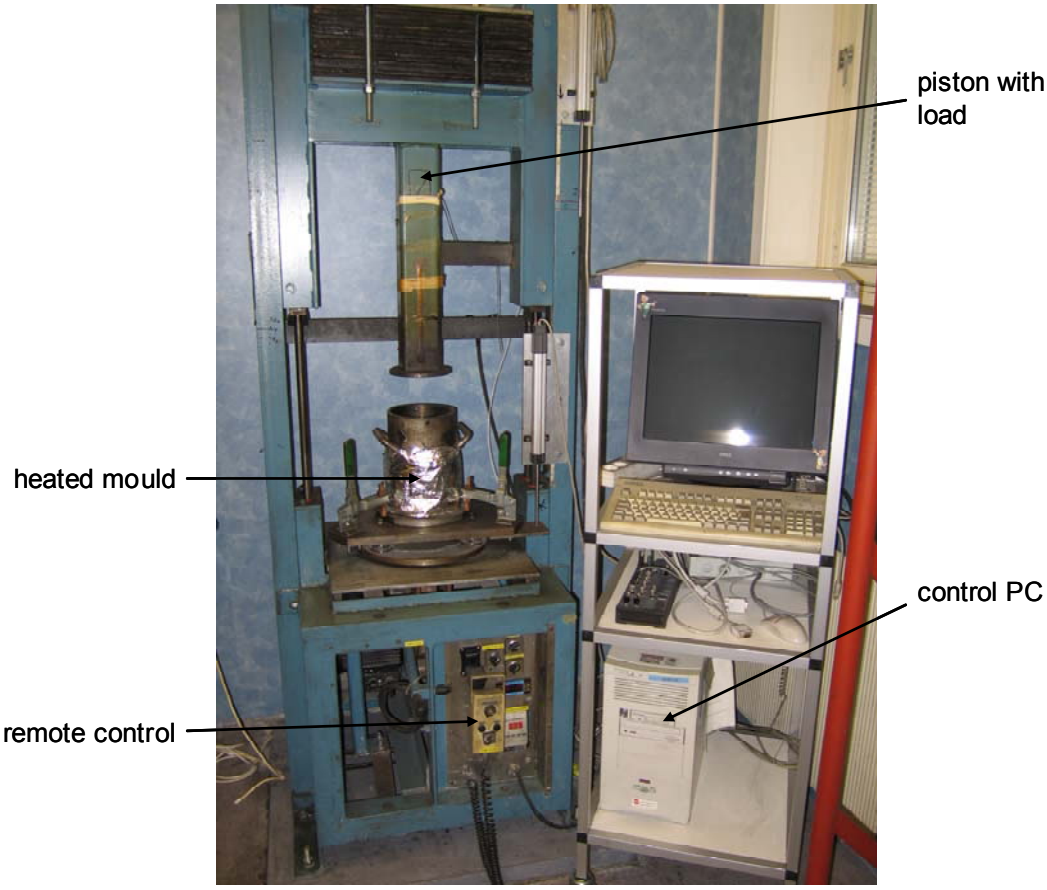

Fig. 3.3-1. Picture of the vibration compactor.

3.4 Baking

The green anodes were baked in an electrically heated oven (Nabertherm N 150/H) shown in Fig. 3.4-2. The anodes were heated to 550 °C with different heating rates ranging from 5 °C/h to 80 °C/h (Fig. 3.4-1). After reaching 550 °C a uniform heating rate of 100 °C/h was used for all samples. The soaking temperature was between 1100 and 1150 °C and soaking times of 5 and 8 hours were used. The dimensions of the oven

allowed baking of four green anodes simultaneously. They were placed two by two in steel containers and packed with coke. The packing coke had a particle size from 5 to 15 mm. The containers were stacked one on another and placed in the centre of the oven.

For some of the measurements a reference coke was used for determination of the mean crystallite size (L_c) according to ASTM D 5187-91 to verify even baking level for the pilot anodes.

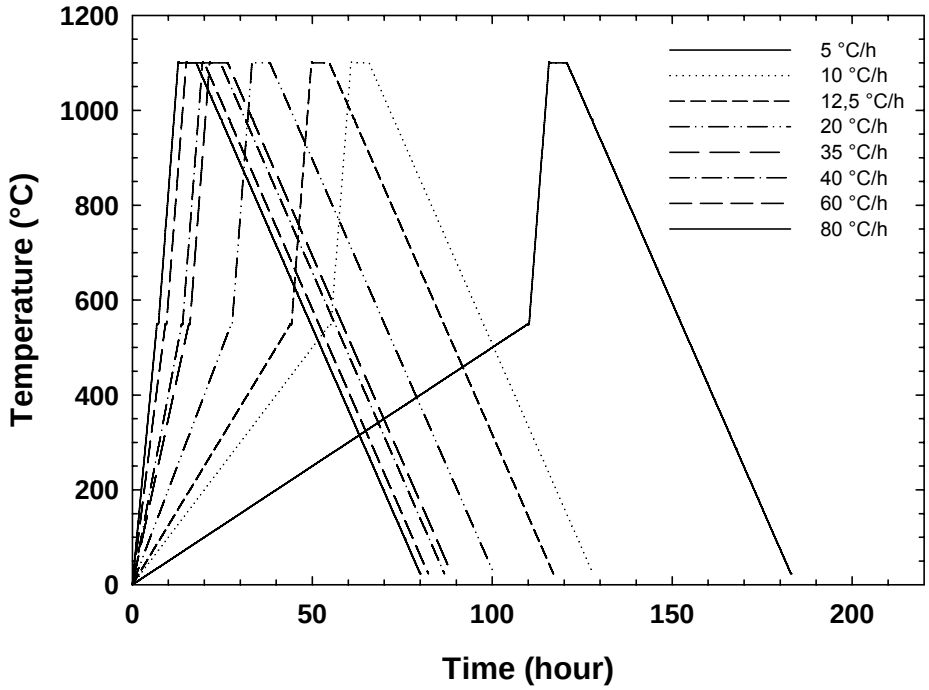

Fig. 3.4-1. Schematic plot for baking curves with different heating rates up to 550 °C.

Fig. 3.4-2. Electrically heated oven (Nabertherm N 150/H) and steel container used for the baking of green anodes.

3.5 Optical microscopy and image analysis

The hardware setup for the porosity measurements is shown in Fig. 3.5-2. Samples were examined by using an inverted reflected light metallurgical microscope (Leica/Reichert MeF3A), equipped with a motorised XY-stage and Z-focus controller. The stage movement and focus is controlled directly by the computer image analysis software. Digital images were acquired using an electronic 3-chip CCD video camera (Sony DCX 950P) with analogue RGB output and a frame-grabber card.

Prior to microscopy examination the samples required special preparation steps. An Ø 50 mm core was drilled from each baked anode and sliced into segments according to Fig. 3.5-3. Each segment and its top cutting surface were impregnated with fluorescent resin under vacuum. Epofix two-component epoxy (Bisphenol-A-(epichlorhydrin) and Oxirane, mono [(C12-C14-alkyloxyl) methyl] derivates) with Epodye green fluorescent dye (Struers, Denmark) was used. Using a fluorescent resin gave a good contrast between the pores and the bulk phase using near ultraviolet light. After the epoxy was cured segments were ground and polished in several steps using a combination of the SiC papers and diamond abrasives. The grinding and polishing were performed on a RotoPol-31 unit supplied by Struers. A force of 50 N per Ø 50 mm sample was applied and the rotation speed was 300 RPM. SiC papers of sizes 80, 120 and 220 grit were used and continuously wetted by water. The grinding was finished just after all excess resin was removed down to the carbon surface. Next, the samples were polished on polishing discs sprayed by diamond spray and continuously wetted by ethanol. The samples were polished in three consecutive steps using 9, 6 and 3 μm polishing discs with 40 N force per sample and 3 minutes polishing time. The final polishing step was performed using a cloth disc of 1 μm with reduced force 20 N per sample.

With sufficient storage space, images of the series of samples are acquired and analysed. At magnification 40x which was mostly used in this work, 16x24 = 384 frames are required to cover a Ø 50 mm sample (16 cm^2), and takes about half an hour to acquire and analyse. In Fig. 3.5-1 an overview of the analysed area for one segment is shown together with the frame partition.

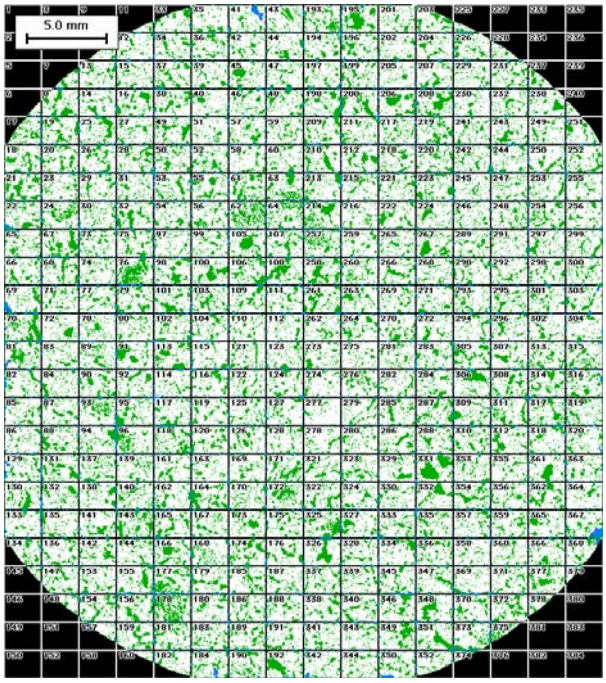

Fig. 3.5-1. Overview of an analysed area of one Ø 50 mm segment.

The total porosity of the pilot scale anode was determined from the average porosity of four segments. Thus with four Ø 50 mm segments, the total analysed area for one pilot scale anode is 64 cm^2.

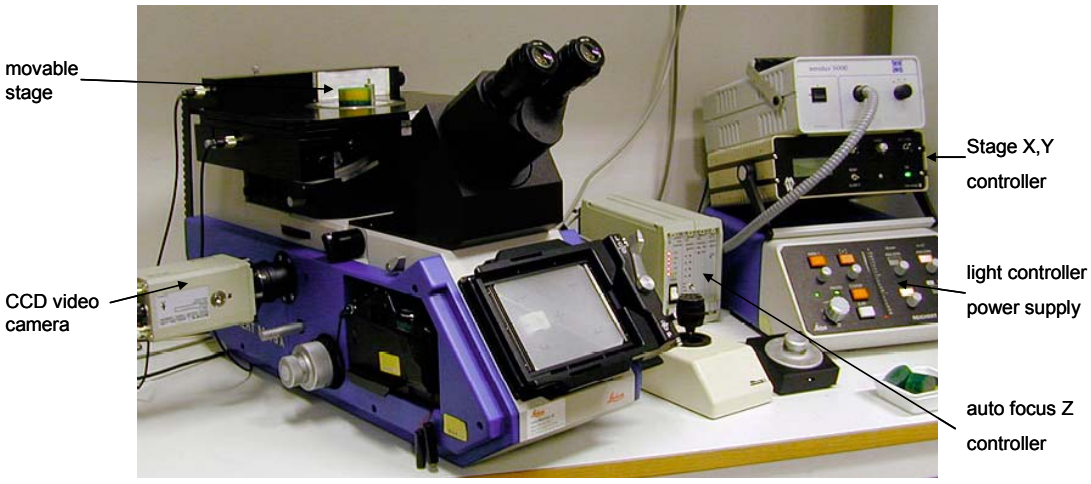

Fig. 3.5-2. Hardware setup used for optical microscopy and image analysis.

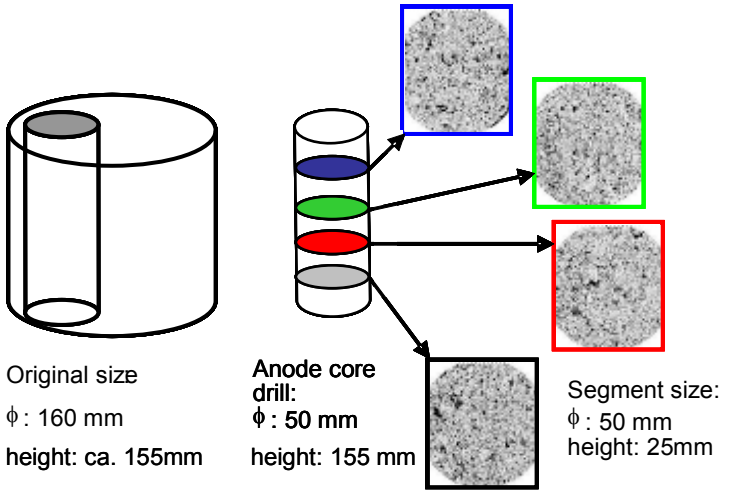

Fig. 3.5-3. Scheme of sample preparation.

3.6 Characterisation of green and baked density of the anodes

Two methods for green and baked density determination were used. Measurement of apparent density and open porosity using a hydrostatic method according to ISO 12985-2 was used for density determination of ca 5 kg anode blocks. The apparent density of a material is defined as the ratio of its dry mass to its volume (Eqn. 5). The volume was determined by measurement of the Archimedes's force applied to the sample saturated with water after boiling. The open porosity was simply measured by calculating the ratio of the mass of water, which has penetrated into sample after boiling, to the mass of the displaced water measured with the hydrostatic balance in Fig. 3.6-1 (Eqn. 6).

$$\rho_a = \frac{m_1}{m_3 - m_2} \times \rho_w \qquad \text{Eqn. 5}$$

$$\varepsilon_w = \frac{m_3 - m_1}{m_3 - m_2} \times 100 \qquad \text{Eqn. 6}$$

Where:

ρ_a is the apparent density
ε_w is the open porosity accessible by the water, expressed as a percentage by mass
m_1 is the dry mass
m_2 is the immersed mass
m_3 is the mass after saturation by boiling
ρ_w is the density of water at the actual temperature

Fig. 3.6-1. Hydrostatic balance used for density measurements.

In some cases determination of apparent density was done according to ISO 12985-1. These measurements were performed on core drills of 50 mm diameter and 120 mm length. The geometry of the observed specimen was measured with a digital calliper and its mass was used for apparent density calculation (Eqn. 7).

$$\rho_a = \frac{m_1}{V} \qquad \text{Eqn. 7}$$

Where:

m_1 is the dry mass
V is the calculated volume

Both methods showed good agreement.

3.7 Specific electrical resistivity

The specific electrical resistivity is important to determine of the anode quality. The specific electrical resistivity provides an indication of the structural condition through the current conducting properties of the anode. For example, high porosity and low baking level results in increased specific electrical resistivity. Large standard deviations may indicate irregularities during the paste production or baking. The presence of hairline cracks dramatically increases the specific electrical resistivity.

The specific electrical resistivity is determined by measuring the voltage drop over a cylindrical sample at a constant current.

$$\rho = \frac{U_{ab} \cdot A}{L \cdot I} \qquad \text{Eqn. 8}$$

Where:

ρ is the specific electrical resistivity
U_{ab} is voltage drop over the measured sample
A is the cross section in m^2
L is the distance between potential contacts in m
I is the electrical current through the sample

Core samples of 50 mm diameter and length 120 mm were measured 8 times (4 times around the sample periphery with 90 ° shifts and then one more measurement when the sample was rotated axially). Average resistivity values were obtained from an average of 8 measurements.

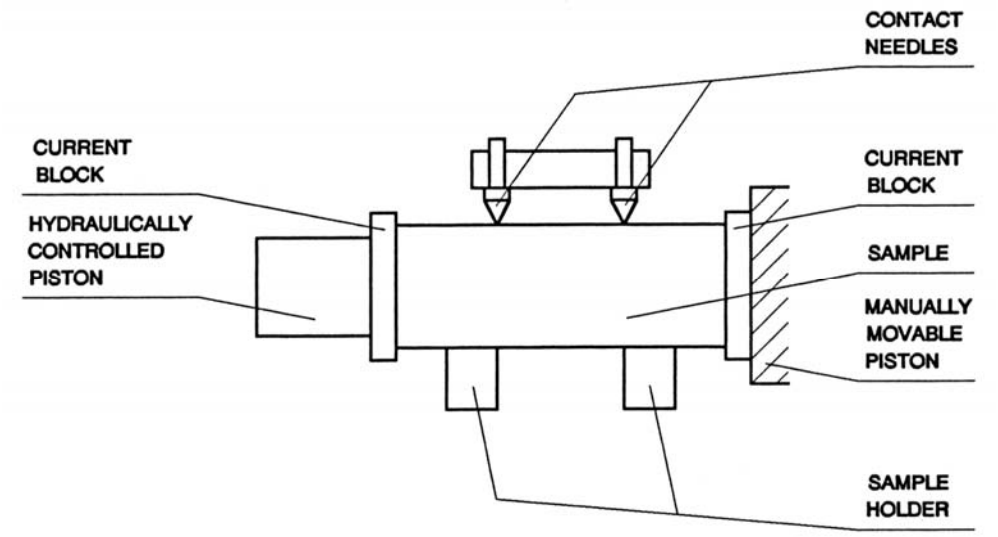

Fig. 3.7-1. Schematic view of the test arrangement for the determination of the specific electrical resistivity [86].

In the experimental work two parallel measurement methods for the specific electrical resistivity (SER) were used, the RDC-150 method and also by the Hydro Aluminium method according to ISO 11713. A very good consistency between the two methods was observed.

3.8 Air and CO_2 reactivities

The air and CO_2 reactivities of the anode samples were determined by thermogravimetry using the Hydro Aluminium method which is modification of the ISO 12989-2 and ISO 12988-2. The apparatus consists of a gold coated fused silica tube furnace and sample holder which is connected to the balance. A sketch of the furnace is given in Fig. 3.8-1. Carbon samples with length 50 and diameter 20 mm were subjected to air and CO_2 gas flows at 525 °C (air) or 960 °C (CO_2), respectively. In both measurements, the samples were preheated for 60 minutes before the reaction gas was introduced. The reaction time was 180 minutes. Reactivity is defined as the specific

weight loss with regard to the apparent surface area of the sample and time at constant reaction rate.

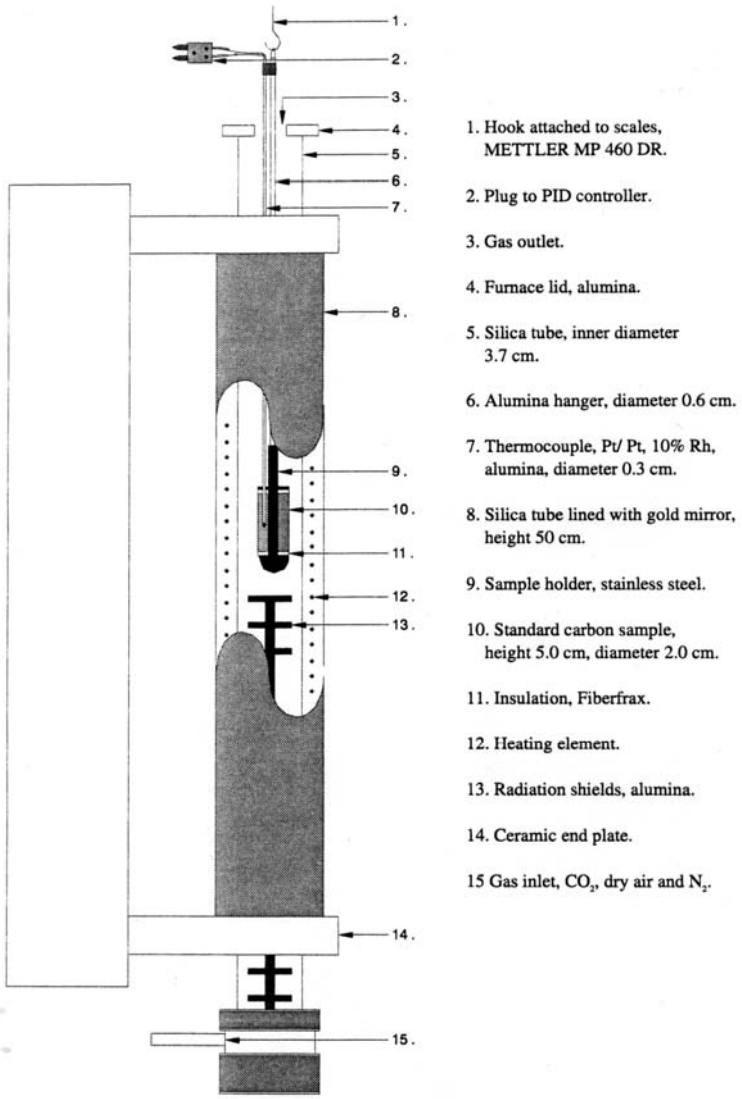

Fig. 3.8-1. Reactivity apparatus furnace with sample holder and anode sample assembled [61].

3.9 Cold crushing strength and Young's modulus

The crushing strength at ambient temperature is the capacity of a material to withstand axially directed compressive forces. When the limit of the compressive strength is reached, the materials are crushed. The cold crushing strength (CCS) is also referred to as the cold compressive strength and was measured according to ISO 18515.

The modulus of elasticity (Young's modulus) was determined experimentally from the slope of the stress-strain curve created during compression. A high Young's modulus means a high slope and therefore represents a material with low elasticity.

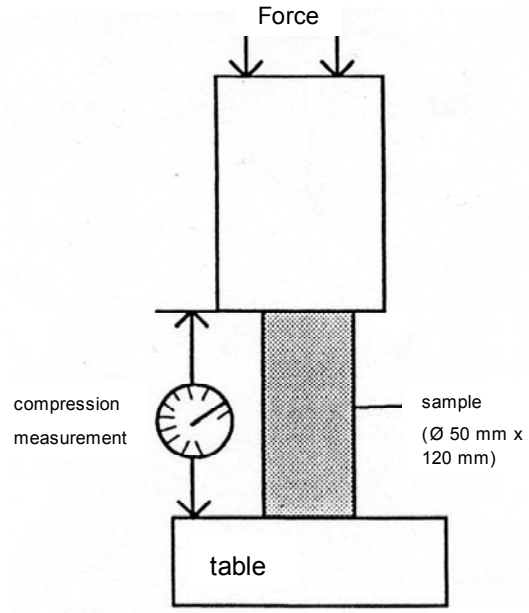

Fig. 3.9-1. Experimental setup for the measurement of cold crushing strength.

A Young's modulus within the range 7-9 GPa is favourable in order to avoid brittle behaviour, which would lead to thermal shock problems [12]. Usually pressed anodes have lower values of Young's modulus than vibrated anodes [11]. High standard deviations can be caused by inhomogeneities in the material such as micro/macrocracks and binder matrix content.

3.10 Air permeability

During baking about 40 % of the pitch matrix volatilizes and open porosity develops. The fraction of open transport pores larger than 50 μm determines the anode's gas permeability. High permeability has a great influence on air and CO_2 reactivities and leads to excess anode consumption [11].

The air permeability of the pilot scale anodes was measured according to ISO 15906 on the same samples as the specific electrical resistivity. The permeability is expressed in nanoperms (1 nPm = 1 Darcy/9.87). The permeability is calculated from the time it takes for a certain volume of air to pass through a cylindrical sample. A material has a permeability of 1 nPm when gas with a viscosity of $1 \cdot 10^{-4}$ Poise passes through a sample of 1 cm height and 1 cm^2 cross section submitted to a pressure difference of 0.1 bar, at a flow rate of 1 cm^3/s.

4 RESULTS AND DISCUSSION

4.1 Porosity of the SSA coke

Coke grains were sieved into 6 different coke fractions; 11.2-5.6 mm, 5.6-4.0 mm, 4.0-2.0 mm, 2.0-1.4 mm, 1.4-1.0 mm and 1.0-0.5 mm. These coke fractions were impregnated with resin under vacuum, polished and studied under near ultraviolet light (wavelength around 400 nm) [74].

Image analysis was found to be a useful tool also for analysing the macroporosity in the coke grains. It enables the characterization of coke porosity and pore radius within different coke fractions. Based on these findings it is possible to estimate the degree of the coke pore impregnation in bench scale anode production.

Fig. 4.1-1 shows pore size distribution curves for 6 different fractions. There is an expected increase of porosity with increasing coarseness for fractions above 2.0-4.0 mm. Fractions up to 2 mm have similar distributions at pore sizes below 80 µm. The smallest diameter peak at 40 µm is due to slit-like pores and cracks that evolve during the calcination process. For the three coarsest fractions increased porosity above 100 µm was observed, where a two peak distributions are found. This is due to the presence of large round bubble like pores (diameter several hundreds µm) created by gas entrapment in the green coke.

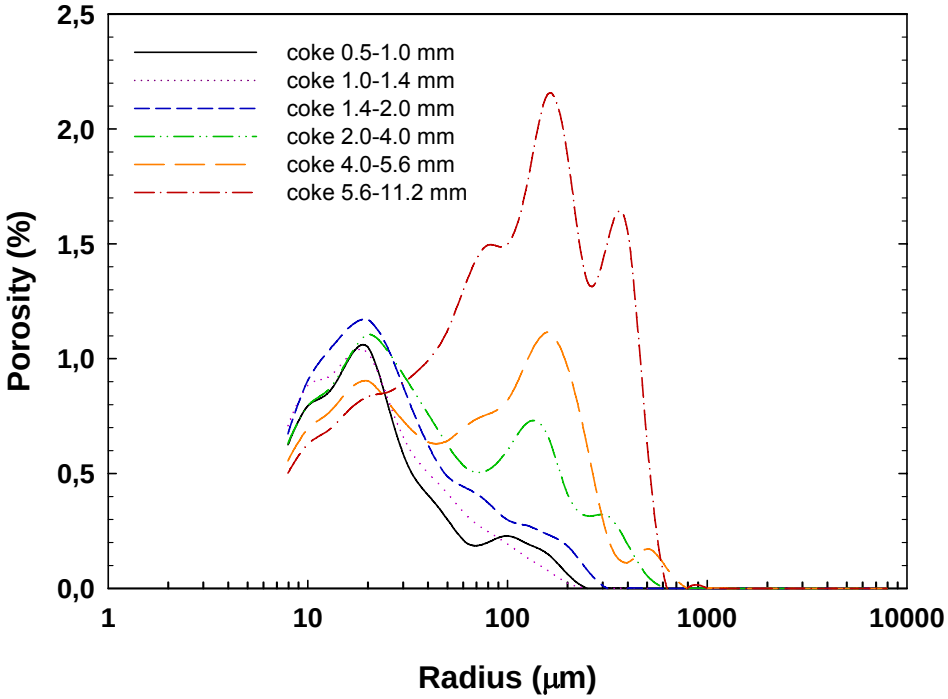

Fig. 4.1-1. Pore size distribution curves for fractions of SSA coke.

Fig. 4.1-2 to Fig. 4.1-7 shows overviews of the entire analysed areas for different coke size fractions. Just from the visual observation it is possible to observe and compare the pore types and their contribution to the total porosity. In finer fractions mostly small

pores (slit like pores) are present that contribute to a major porosity increase at 20 μm pore radius. For coarser fractions than 2.0 mm larger round pores appear

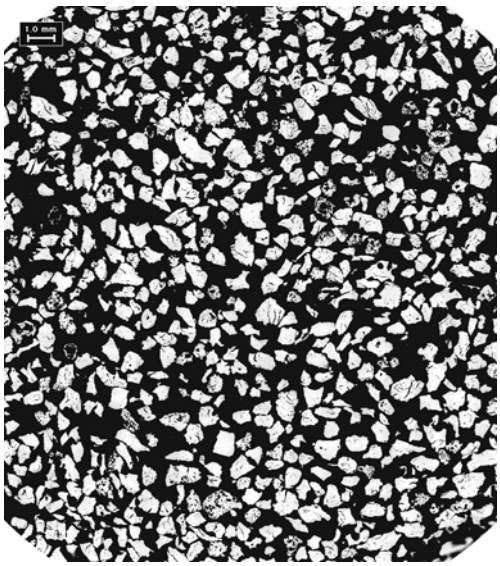

Fig. 4.1-2. Coke fraction 0.5-1.0 mm. Magnification 80 x, polarised light.

Fig. 4.1-4. Coke fraction 1.4-2.0 mm. Magnification 80 x, polarised light.

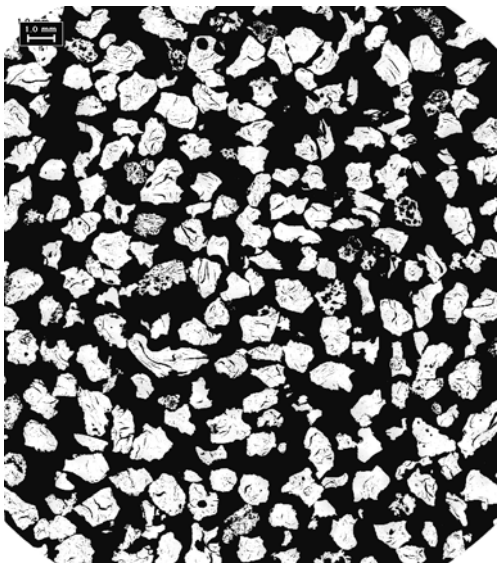

Fig. 4.1-3. Coke fraction 1.0-1.4 mm. Magnification 80 x, polarised light.

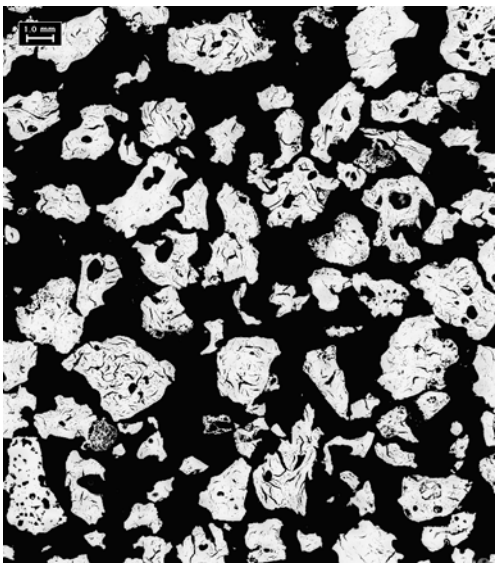

Fig. 4.1-5. Coke fraction 2.0-4.0 mm. Magnification 80 x, polarised light.

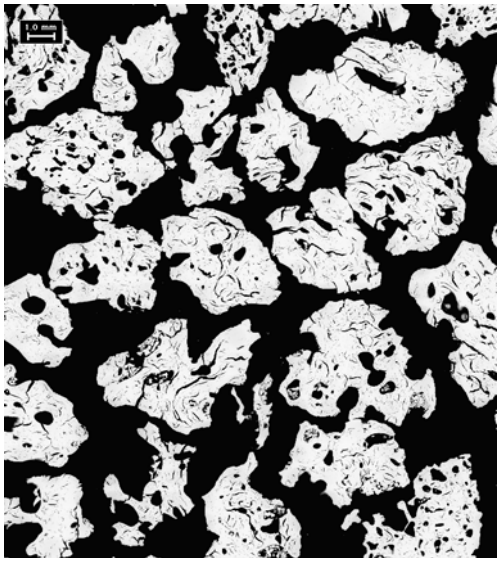

Fig. 4.1-6. Coke fraction 4.0-5.6 mm. Magnification 80 x, polarised light.

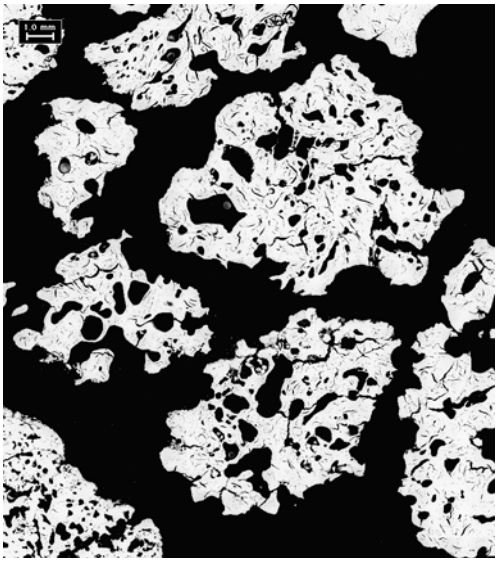

Fig. 4.1-7. Coke fraction 5.6-11.2 mm. Magnification 80 x, polarised light.

4.2 Effect of the heating rate on porosity development - laboratory pilot scale anodes from SSA coke

The influence of the various baking conditions was studied with respect to porosity development during baking. A total of 14 pilot scale anodes with identical granulometry and 18 % pitch content were produced in the anode laboratory using the sigma blade mixer. The aggregate composition was chosen according to a typical industrial recipe shown in Table 3.1-I. The medium dust size (63 % < 63 μm) was used. The dry coke aggregate was mixed for 7 minutes at 180 °C in the sigma mixer for improved homogenization and temperature distribution. Pitch (180 °C) was added and the paste was mixed for 20 minutes. Forming was done at 160 °C at 15.6 Hz vibration frequency for 3 minutes. Green and baked densities of the samples were measured by ISO 12985-1 on drilled cores with 50 mm diameter and 50 mm height.

Eight anodes were baked in two parallel series (A and B batch) using four heating rates, 10, 20, 40 and 60 °C/h up to 550 °C. The temperature 550 °C was chosen after TGA examination of the pitch, Fig. 4.2-1. After reaching 550 °C, all samples were heated at the same heating rate, 100 °C/h, to the final temperature 1100 °C. The soaking time was 5 hours. The samples were cooled by turning off the furnace. Table 4.2-I presents measured green and baked densities as well as the total porosity values.

Table 4.2-I. Density and porosity measurement results for two batches A and B.

Sample	Heating rate	Green density		Baked density		Porosity IA	
Batch A	(°C/h)	(g/cm^3)	stdev	(g/cm^3)	stdev	(%)	stdev
M4	10	1,661	0,012	1,486	0,012	22,5	0,4
M6	20	1,665	0,008	1,473	0,008	23,2	0,5
M8	40	1,618	0,008	1,427	0,008	25,0	0,3
M10	60	1,636	0,010	1,423	0,007	25,8	0,5
Batch B							
M5	10	1,663	0,001	1,489	0,008	25,8	0,6
M4N	20	1,659	0,001	1,454	0,004	24,8	1,2
M1N	40	1,624	0,001	1,422	0,016	26,8	1,0
M2N	60	1,636	0,001	1,412	0,009	27,5	1,1

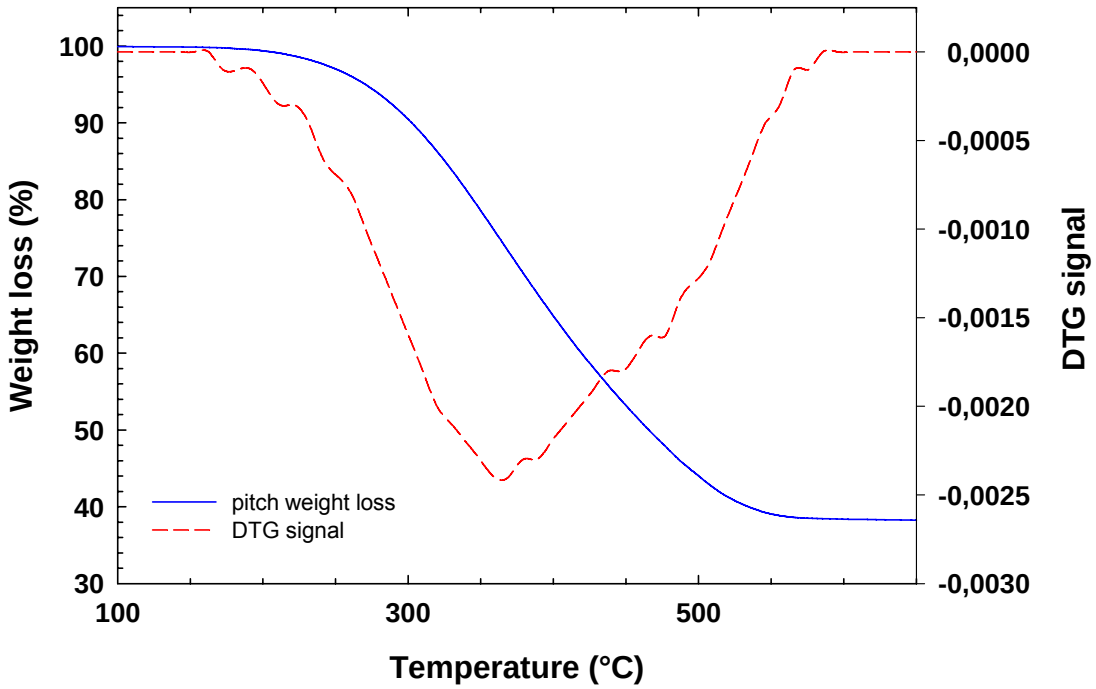

Fig. 4.2-1. TGA data for a 5 mg pitch sample. The weight loss curve and the first derivative (DTG) of the weight loss curve are shown. The first derivative of the weight loss curve has a minimum at 360 °C, which indicates maximum volatile release. At 585 °C the pitch has lost more than 98 % of the total amount of volatiles released in the entire temperature range up to 1000 °C. At this temperature the critical stages of carbonization have come to an end and a semi coke has been formed.

Extra consumption of pitch due to coke crushing during mixing makes the pitch unevenly distributed between coke particles and more pores are formed in the anode paste during mixing. The clearance between the sigma blades and trough is small to eliminate stagnant regions (Fig. 3.2-1). In some cases the overlapping sigma blade may prevent a tendency of the material to form a cylinder around the axis of each blade, which rotates without any mixing taking place. This is a problem when the aggregate contains coarser particles.

There is a slightly decreased baked density with increasing heating rate (Fig. 4.2-2). The main reason for such a density decrease would be the increasing volatiles evolution with increased heating rate. During baking, when pitch volatilization increases at higher heating rates, voids become even larger and cause increasing density reduction and porosity increase.

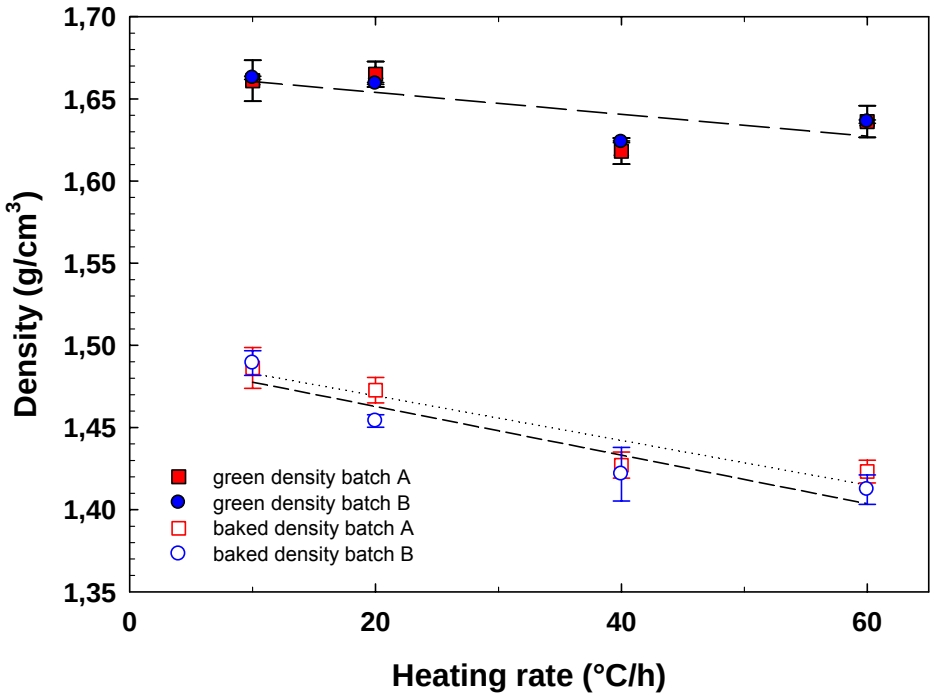

Fig. 4.2-2. Green and baked density comparison for batch A and B.

After baking, total porosity values as well as pore size distribution curves were determined. In Fig. 4.2-3 and Fig. 4.2-4 pore size distribution curves are compared for anodes that were baked at various heating rates. Each curve represents the average porosity distribution of four segments from the same pilot scale anode. All samples show similar pore size distributions with maximum porosity at pore radius 100 µm.

In both batch A and B (Fig. 4.2-3 and Fig. 4.2-4), the curves show a gradual increase in total porosity with increasing heating rate. Batch A shows a porosity development within the pore radius ranges 8-30 µm and 30-100 µm. In batch B a similar correlation is observed. The pore size distribution is almost the same for all heating rates and peaks at 100 µm. With increasing heating rate the amount of 100 µm pores increases.

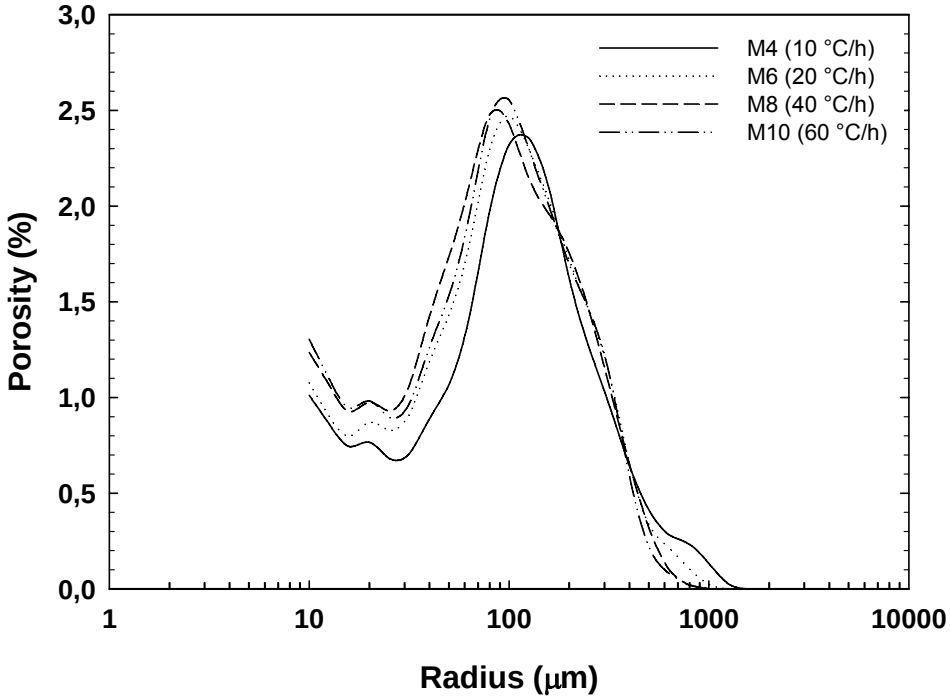

Fig. 4.2-3. Pore size distribution comparison for batch A.

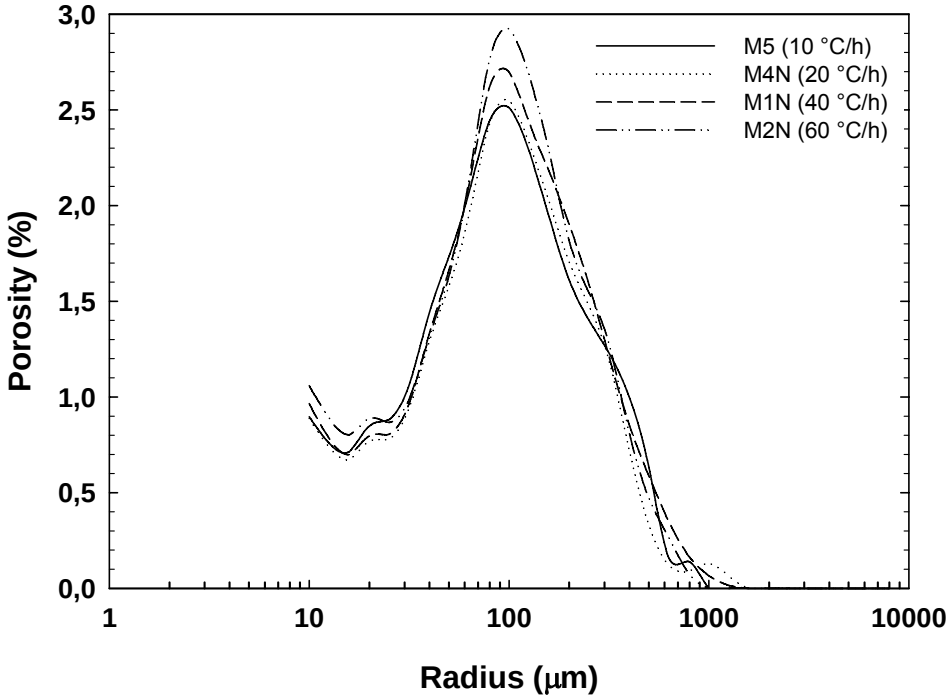

Fig. 4.2-4. Pore size distribution comparison for batch B.

Ehrburger [64] found that the porosity due to pitch volatilization takes place in a rather narrow temperature interval when the sample was slowly heated (12 °C/h). The porosity remained unchanged between 200 to 375 °C. Thereafter, a marked increase of

the porosity (up to 30 %) was found when the maximum volatile release rate culminated. In all cases the most frequently occurring pore size was in the range 100 - 200 µm, which is in good agreement with results observed in this work. This porosity increase is related to the development of baking pores.

Chmelar [80] used the same laboratory equipment and the same production procedures for pilot scale anode production as in this work. The samples were produced from various coke qualities with 15, 18 and 20 % pitch content and three levels of fines (45, 63 and 94 %, - 63 µm). The results show that the optimal pitch content for SSA coke was 18 % pitch and medium fines. However, measured maximum green densities (1.60 g/cm^3) were lower than in this study. The reason for this is different measurement methods. Chmelar [80] used the bulk dimensions and mass of the entire pilot scale anode for green density calculation, while in this work drilled cores with 50 mm diameter and 50 mm height were used.

Belitskus [87] studied the effect of heating rate on pressed pilot scale anode properties. Samples were mixed at 140 °C in a sigma blade mixer for 30 minutes. Baking was carried out at heating rates of 50, 100 and 200 °C/h. The optimum pitch content was for all aggregate compositions around 17 %. It was found that increasing heating rates over the range 200 °C/h significantly degraded the anode properties. With increasing heating rate, baked apparent density and the coke yield from the pitch decreased and the electrical resistivity increased [87]. These effects were explained as follows. Pitch coking yield was probably reduced because some cokable volatile matter is driven off from the anode before it has had sufficient time to convert to coke when the heating rate is high. The shrinkage was reduced with increasing heating rate due to increased rate of generation of gaseous products, resulting in a more porous binder coke [87]. Both the reduced shrinkage and lower coke yield contribute to the reduction in anode density with increased heating rate. Increased electrical resistivity would be expected to result from decreased density.

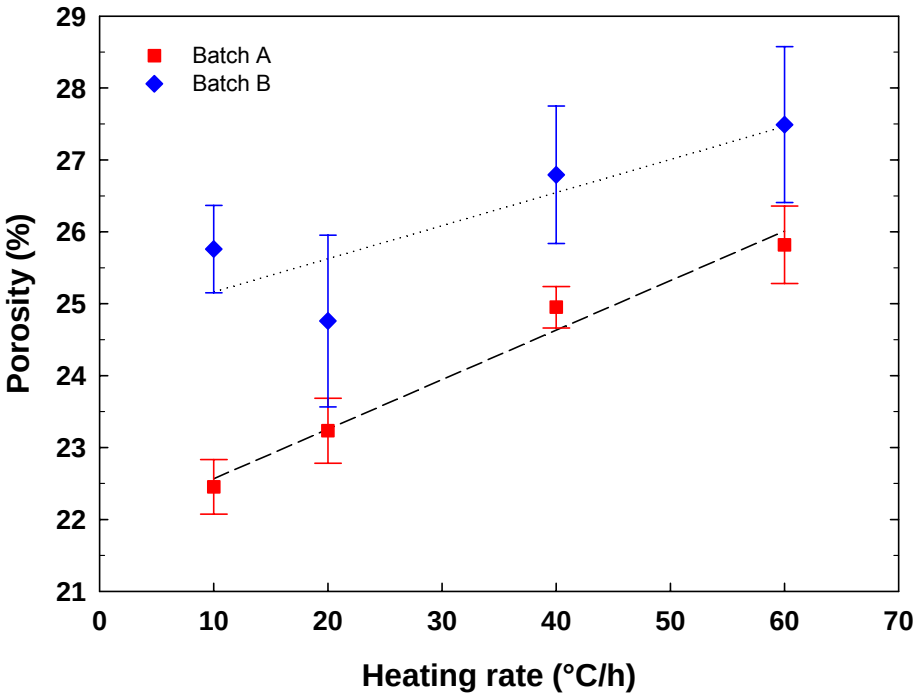

Fig. 4.2-5. Comparison of total porosity values for batch A and B.

The total porosity values are given from the areas under the distribution curves. In Fig. 4.2-5 the total porosity values of the A and B batch are compared. Increasing total porosity with increasing heating rate is observed. Different green apparent densities prior to baking (Fig. 4.2-2) are probably the reason for the deviation between the two parallel series.

4.2.1 Conclusion

The 8 anodes of identical composition were produced in two parallel batches and baked with 4 different heating rates. Correlation between the heating rate and the porosity development was found. A general increase of the total porosity with increasing heating rate was observed. In addition, all eight samples showed a similar pore distribution. Difference between total porosity values for batch A and B were probably due to random errors during sample preparation. Decreasing tendency for the baked density with increasing heating rate was observed, probably due to increased volatiles evolution.

4.3 Effect of vacuum vibroforming and vibration time on porosity development - samples from industrially prepared paste

The effect of various vibration conditions on porosity development in industrial paste was studied. A set of 20 pilot scale anodes with uniform composition were produced using industrial paste (blended coke) produced in the paste plant of Hydro Aluminium a.s. Årdal Carbon. The recipe contained 30 % butts. The aggregate was preheated and mixed with pitch in a ko-kneader at 174 °C. After cooling in the Eirich mixer to 154 °C a paste sample was taken out, transported to the laboratory and remixed in an intensive Eirich laboratory mixer (RV 08 W) for 5 minutes at 165 °C. The paste was compacted at 165 °C and 50 Hz using four different vibration times; 0.5, 1, 2 and 3 minutes. In addition, a parallel set of four 3 minute vibrated samples were produced using a vacuum of 4 kPa in the mould. The samples were baked at four different heating rates; 10, 35, 60 and 80 °C/h with 5 hour soaking time. The densities in the green and baked state as well as the open porosity were measured using the hydrostatic immersion method ISO 12985-2. Also, the specific electrical resistivity and the baking loss were measured. The experimental design and the results are shown in Table 4.3-I.

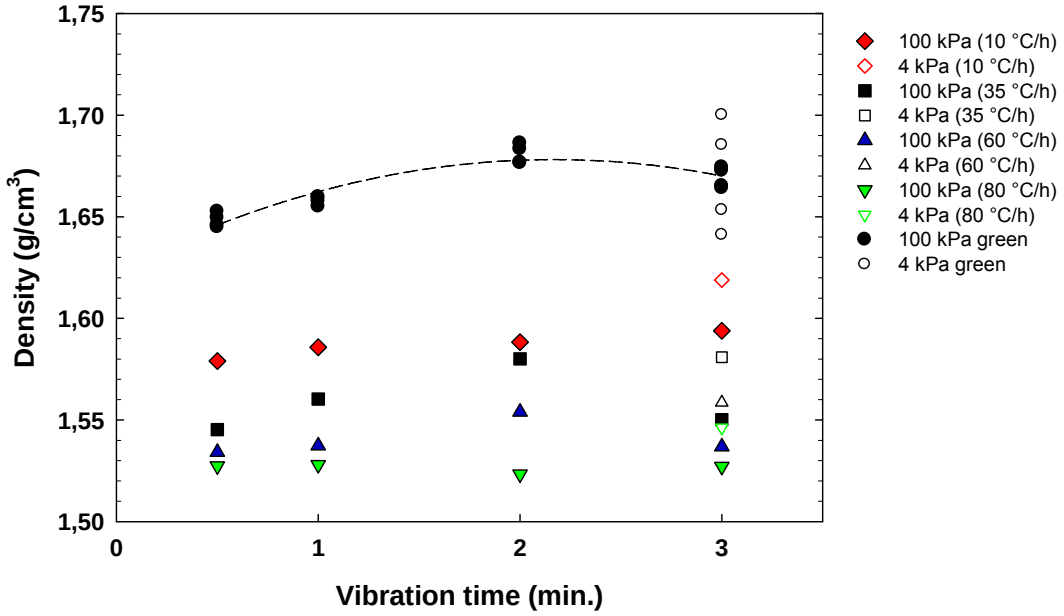

Fig. 4.3-1. Green and baked density comparison between samples from industrially prepared paste.

Fig. 4.3-1 compares green and baked densities with respect to vibration time and heating rate. There is an indication of optimal vibration time for 2 minute vibrated samples. However, there is scatter in green density for vacuum vibroformed samples. This was probably due to some irregularities during laboratory processing of paste prior to vibration. About 60 kg of paste was mixed in two batches and stored in a heating cabinet until they were vibroformed. Then the mixed paste was processed gradually and 3 kg pilot scale anodes were formed. This delay could cause a change in paste rheology that result in different green densities of the formed blocks.

Table 4.3-I. Experimental layout and measured data for pilot scale anodes prepared from industrial paste taken out from the end of mixing line.

Sample #	Vibration time (min)	Vibropressure (kPa)	Heating rate (°C/h)	Green density (kg/m^3)	Green open porosity (%)	Baked density (kg/m^3)	Baked open porosity (%)	Total porosity IA (%)	Total porosity IA stdev	SER (μΩm)	SER stdev	T eq (°E)	Baking loss (%)
2	3	4	10	1,700	0,4	1,619	17,2	8,9	0,5	51,4	0,3	1155	4,8
5	3	100	10	1,674	0,8	1,594	18,6	11,5	0,4	53,7	0,4	1149	4,6
11	2	100	10	1,686	0,7	1,588	18,6	12,2	0,5	55,6	0,9	1155	4,8
13	1	100	10	1,660	1,1	1,586	18,7	11,5	0,6	54,3	0,5	1149	4,5
19	0,5	100	10	1,653	1,1	1,579	18,8	13,1	0,6	54,5	0,4	1149	4,6
3	3	4	35	1,685	1,1	1,581	19,2	11,5	0,0	54,8	0,5	1161	5,5
7	3	100	35	1,673	0,4	1,550	20,4	14,3	0,8	58,3	0,9	1147	5,6
9	2	100	35	1,683	0,7	1,580	19,0	12,9	0,6	56,9	0,9	1161	5,4
15	1	100	35	1,659	1,0	1,560	20,0	13,9	1,1	57,9	0,7	1147	5,4
20	0,5	100	35	1,650	1,1	1,545	20,8	15,3	1,3	58,1	0,3	1147	5,6
4	3	4	60	1,653	3,5	1,559	20,0	12,3	0,0	56,8	0,3	1157	6,3
8	3	100	60	1,665	0,5	1,537	21,3	14,5	0,7	59,6	0,7	1157	5,8
10	2	100	60	1,677	0,6	1,554	20,6	14,9	0,6	59,8	0,7	1152	5,9
16	1	100	60	1,658	0,7	1,537	21,2	17,9	1,0	59,9	0,5	1152	5,8
18	0,5	100	60	1,646	2,0	1,534	21,4	19,2	2,3	59,5	0,3	1152	6,2
1	3	4	80	1,641	4,6	1,546	20,7	12,8	0,7	58,0	0,3	n/a	7,3
6	3	100	80	1,664	0,6	1,527	21,8	14,9	1,0	59,6	0,7	n/a	6,0
12	2	100	80	1,677	0,5	1,523	22,1	15,7	0,6	61,6	0,4	n/a	6,2
14	1	100	80	1,655	1,1	1,528	21,8	16,0	1,1	59,8	0,6	n/a	6,2
17	0,5	100	80	1,645	3,5	1,527	21,7	16,3	0,4	58,4	0,5	n/a	6,6

SER - specific electrical resistivity, T_{eq} – equivalent temperature

There is also an increase in baked density for 3 minutes vibration time when vacuum vibroforming is used (Fig. 4.3-1). During vacuum vibration the entrapped gas and light binder volatiles are exhausted from the paste which enables strongly reduced pore formation. This mechanism is the most probable reason for improved aggregate packing and paste densification.

Fig. 4.3-2 shows a close correlation between the baked density and the specific electrical resistivity. The specific electrical resistivity decreases as the baked density of pilot scale anodes increases. This has been observed by many authors [36, 45, 50, 52]. Increase of the aggregate packing improves the coke grain bridging and influences the electrical contacts between particles.

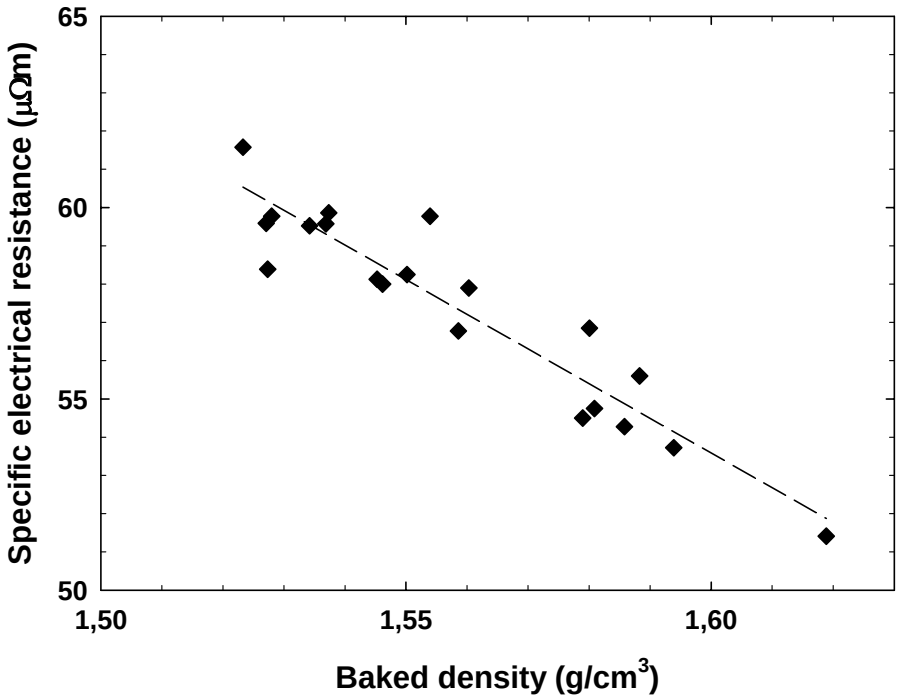

Fig. 4.3-2. Correlation between baked density and specific electrical resistivity.

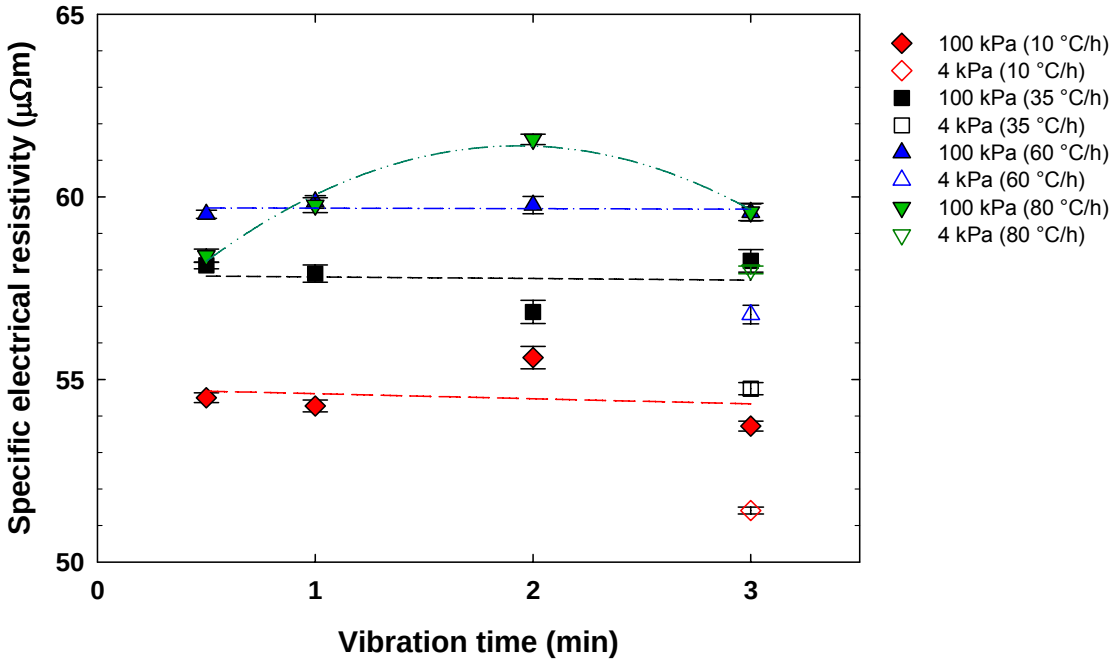

Fig. 4.3-3. Specific electrical resistivity and vibration time.

The specific electrical resistivity increases with increasing heating rate (Fig. 4.3-3). The highest resistivity values were measured for 80 °C/h baked samples. A probable reason for this is the increasing volatiles evolution during baking which causes higher porosity development in the binder phase and thus reduces the electrical conductivity. Although there is some data scatter, the effect of vacuum vibroforming is visible. Lower resistivity values were measured for the 3 minutes vibrated samples that were formed under a vacuum of 4 kPa, compared to those vibrated at 100 kPa (1 atm).

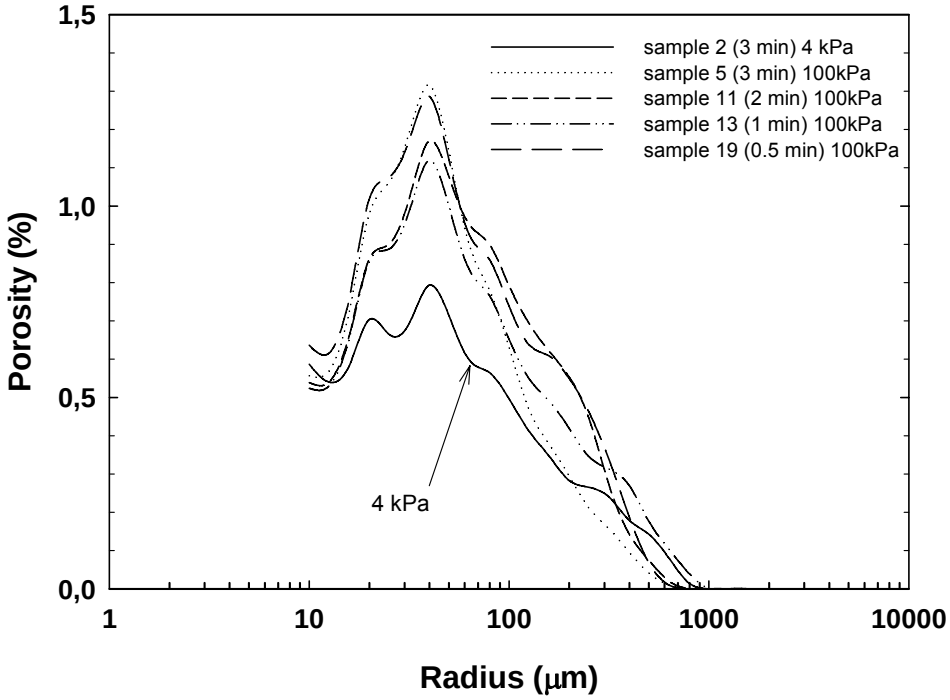

Fig. 4.3-4. Pore size distribution for anodes baked at 10 °C/h heating rate.

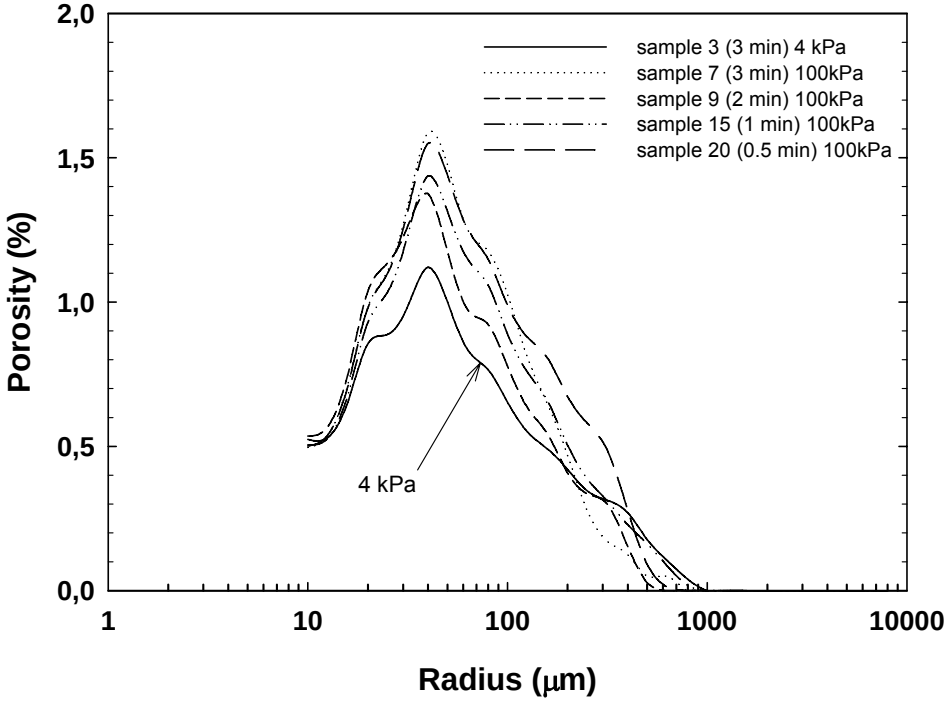

Fig. 4.3-5. Pore size distribution for anodes baked at 35 °C/h heating rate.

In Fig. 4.3-4 to Fig. 4.3-7 pore size distribution curves for anodes baked with various heating rates are presented. Similar pore distributions within the 10-20 μm radius range are observed for all heating rates. This may indicate coke pores impregnated with pitch.

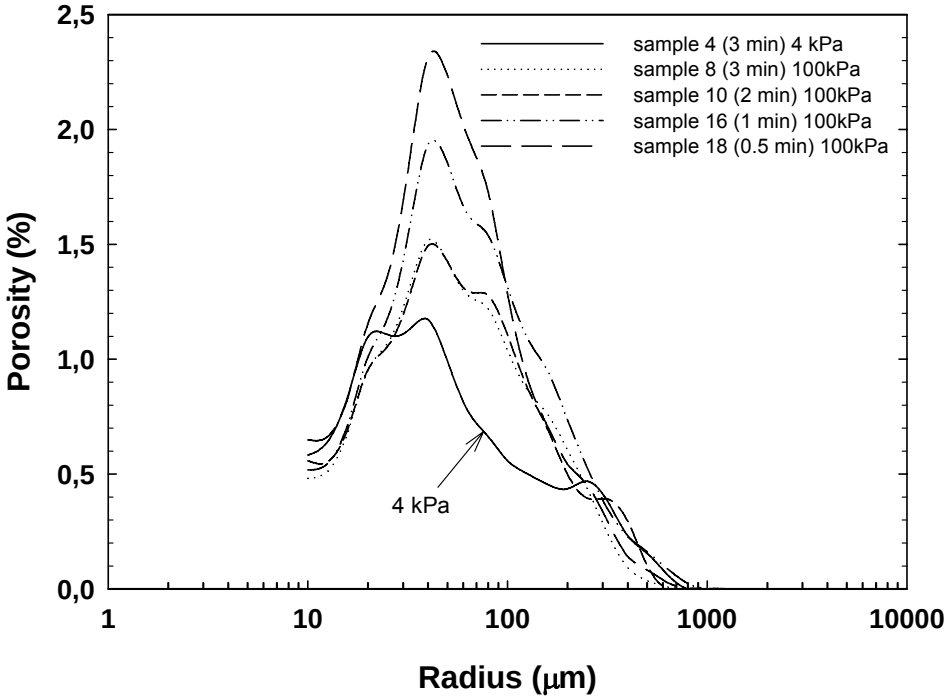

Fig. 4.3-6. Pore size distribution for anodes baked at 60 °C/h heating rate.

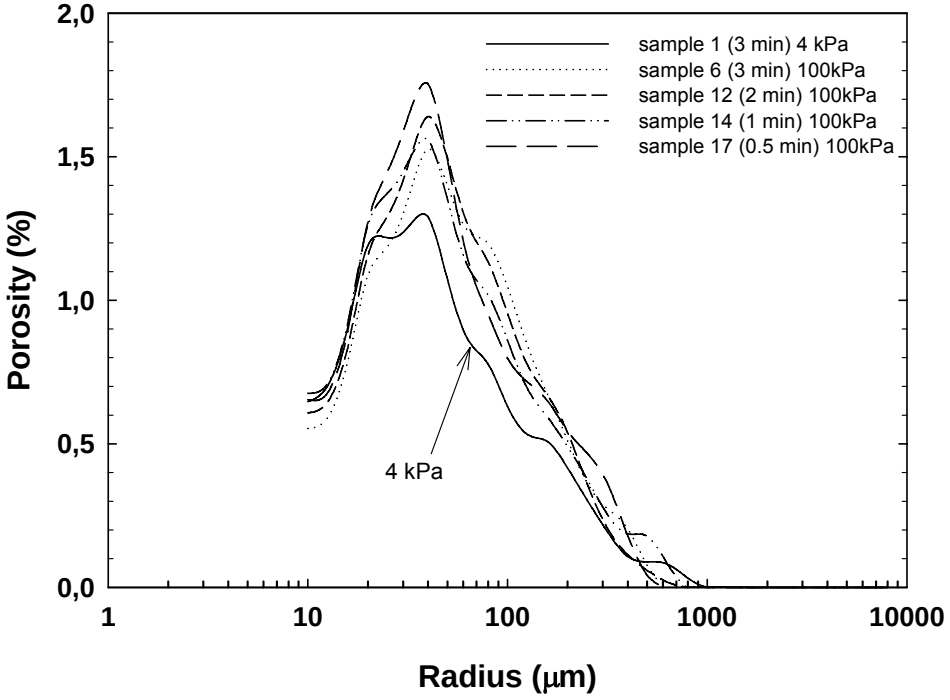

Fig. 4.3-7. Pore size distribution for anodes baked at 80 °C/h heating rate.

All the samples show the maximum porosity at 40 μm pore radius regardless of the applied heating rate. The pitch level probably determines the size and amount of volatile (baking) pores. Thus the amount of 40 μm pores decreases as the vibration time

increases and the heating rate decreases. The differences in porosity above 40 μm pore radius may indicate improved efficiency of paste densification with increasing vibration time. This effect is pronounced for samples that were vibroformed for 3 minutes under 4 kPa vacuum. The use of vacuum during vibroforming significantly reduces the porosity in the range 40-200 μm.

Fig. 4.3-8 shows a comparison of the overall analysed areas of two 50 mm segments. Each segment was drilled from 3 minute vibrated samples that were baked at 10 °C/h. The a) sample is from a vacuum vibrated anode and sample b) is from an atmospheric pressure vibrated sample. A noticeable difference of the pore structure is seen. The vacuum vibrated sample has a significantly lower amount of the pores that were formed due to gas entrapment at the forming stage.

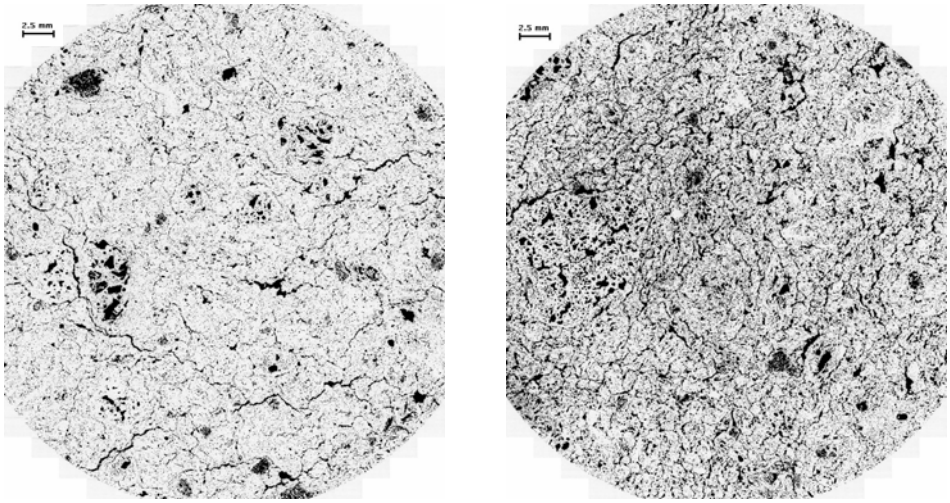

a) Sample no. 2 b) Sample no. 5

Fig. 4.3-8. Comparison of the overall analysed areas of two 50 mm segments. Sample 2 (left) was vibrated for 3 minutes under 4 kPa vacuum. Sample b) was vibrated for 3 minutes at atmospheric pressure (100 kPa). The scale bar is 2.5 mm.

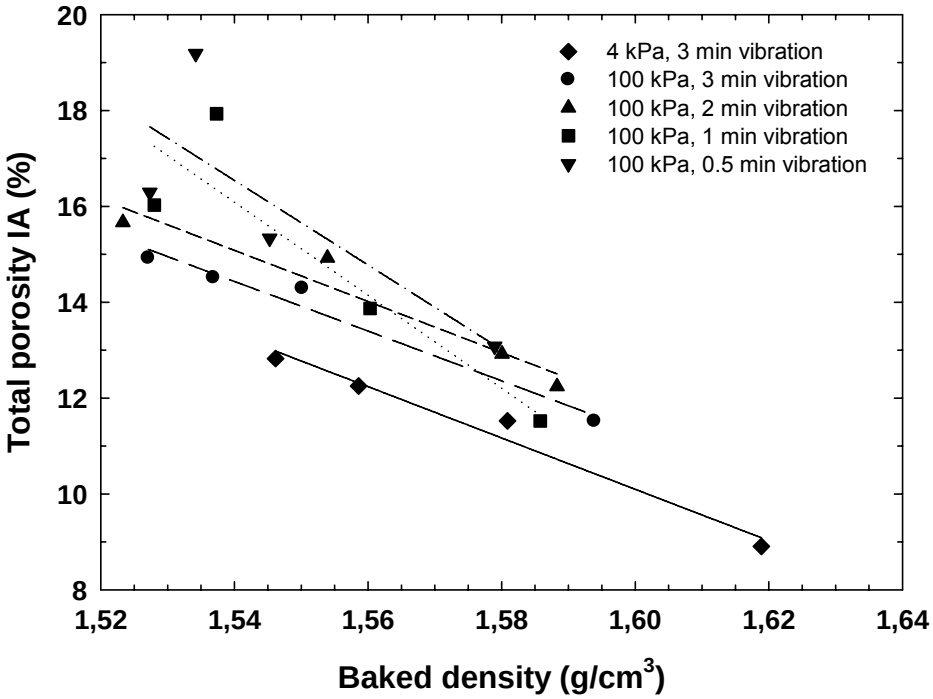

Fig. 4.3-9. Correlation between baked density and total porosity.

There is an expected linear fit between total porosity and baked density for both 3 minutes and 2 minutes vibration time (Fig. 4.3-9). Anodes vibrated for 2-3 minutes show a linear decrease in porosity with increasing baked density. However, there is scattered correlation between total porosity and baked density at low vibration times (0.5 and 1 minute) that seem to be insufficient for proper paste packing. There is a visible reduction of the porosity in the case of 3 minute vacuum vibrated samples.

Increase of the heating rate leads to increase of the total porosity values. Porosity increase may be explained by increasing amount of pores due to the escape of volatiles as the heating rate increases (Fig. 4.3-10 and Fig. 4.3-11).

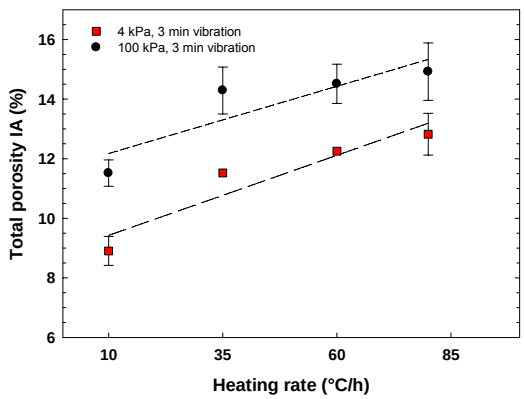

Fig. 4.3-10. Correlation plot between total porosity and heating rate for 3 minute vibrated samples.

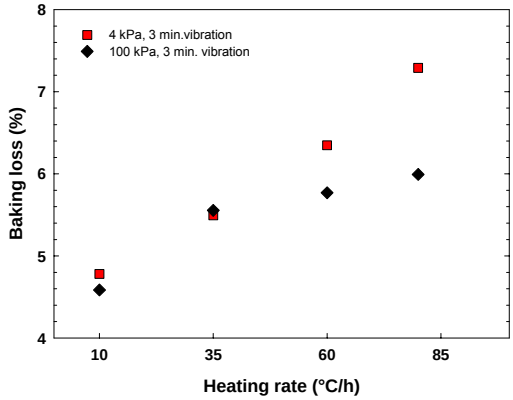

Fig. 4.3-11. Correlation plot between baking loss and heating rate for 3 minute vibrated samples.

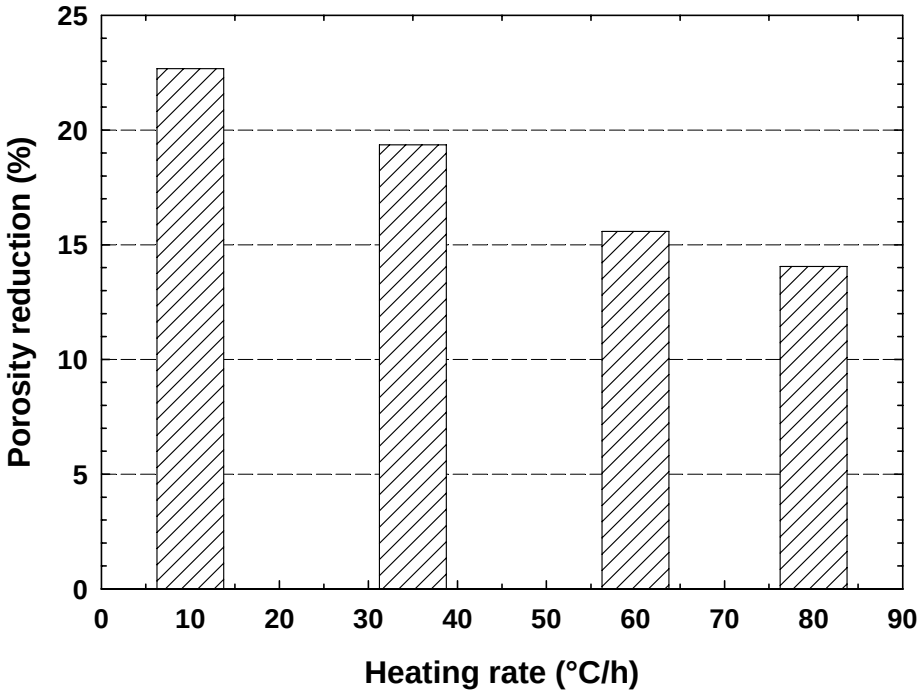

Fig. 4.3-12. Bar chart for the effect of 4 kPa vacuum vibroforming on the total porosity. Each column represents percentual porosity reduction for 3 minute vibrated samples when vacuum in mould was used.

Fig. 4.3-12 demonstrates the total porosity reduction (by %) for 3 minutes vibrated samples when lowering the vibration pressure from atmospheric (100 kPa) to vacuum (4 kPa). Vacuum vibroforming lowers the total porosity, but as the heating rate increases this effect is damped.

Fig.4.3-13 and Fig.4.3-14 show baked open porosity and baked density measured on whole pilot scale anode versus heating rate and vibration time. A general increase of the open porosity with increasing heating rate was found. The lowest open porosities were obtained for vacuum vibrated samples. Increasing heating rate caused decreasing baked density. Samples baked at 10 °C/h have the lowest open porosity. This may be due to lower development of baking pores as well as reduced probability of the expansion cracks due to excessive volatile release.

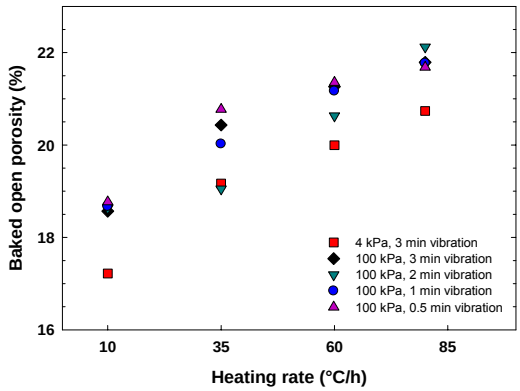

Fig.4.3-13. Baked open porosity measured by immersion method according to ISO 12985-2.

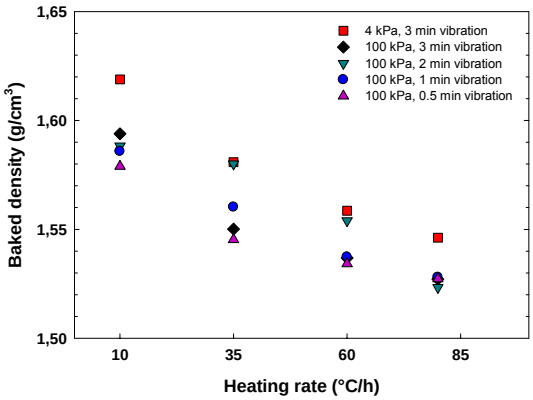

Fig.4.3-14. Baked density measured by immersion method according to ISO 12985-2.

Fig. 4.3-15 shows a detail of the bottom surface of the anode after baking at 80 °C/h. High heating rate causes excessive evolution of volatile gases and thus creates internal pressure within the anode. When this pressure is released, crack formation may occur. The effect of increasing volatile pressure has been described by many authors [22, 44]. Boenigk and Wildforster [57] observed that volatile non-carbonizing pitch compounds or pyrolysis gases exert inner pressure on the anode which causes the structural changes and porosity formation.

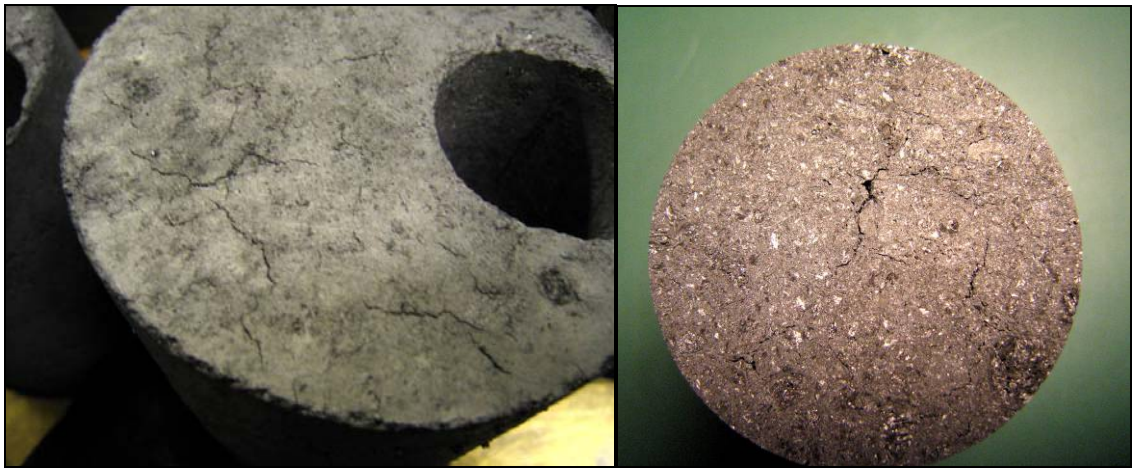

Fig. 4.3-15. The left image shows the bottom surface of a pilot scale anode baked at 80 °C/h. Cracks were formed due to excessive release of volatiles through the dense carbon body. The right image shows detail of a 50 mm segment drilled from sample 12 that was baked with 80 °C/h heating rate.

4.3.1 Conclusion

Paste with uniform composition was formed at different vibration times and mould pressure conditions. Formed blocks were baked at different heating rates in order to study the influence on porosity development.

A decrease of the baked density was found with increasing heating rate. The reason for this was probably higher mass reduction due to increasing volatiles evolution. Simultaneously there was observed an increase of the baked densities for 3 minutes vibration time when vacuum vibroforming was used. This was mainly because of closer aggregate packing due to the release of entrapped gases and light binder volatiles during vibroforming.

The specific electrical resistivity is more dependent on heating rate than on vibration time. When high heating rates are used, as in the case of 80 °C/h, excessive volatiles evolution can cause an increase of internal pressure in dense anodes. In extreme cases this may lead to crack formation (Fig. 4.3-15) that is negatively affecting the specific electrical resistivity. Therefore, slow heating rates for dense samples could minimize the potential for an anode defects.

For the total porosity, vibration at 4 kPa caused a porosity reduction regardless of the heating rate. However, at high heating rate the advantage of the vacuum vibroforming was reduced due to increased amount of the volatile (baking) pores.

4.4 Effect of mixing time and vibration time - samples from industrially prepared paste

The effect of the varying mixing time and vibration conditions were studied with respect to total porosity development and physico-mechanical properties. A set of 21 pilot scale anodes were produced in the Hydro Aluminium a.s. Årdal Carbon laboratory from industrial paste (blended coke) (Table 4.4-I). The aggregate was preheated and mixed with pitch in a ko-kneader at 174 °C. Paste was taken out at a different sampling point than described in Chapter 4.3, between the ko-kneader and the Eirich mixer. Three batches of green paste (each of 40 kg) were transported to the laboratory and mixed in an Eirich laboratory mixer (RV 08 W) at 165 °C using three different mixing times: 1, 3 and 6 minutes. Vibration was performed using a vacuum vibrocompactor (4 kPa) with constant vibrating frequency (50 Hz) and the possibility to control the vibration energy with a potentiostat by means of the vibration amplitude. From each mix 7 pilot scale anodes were produced with three different vibration times: 0.5, 1 and 2 minutes. Using normal energy input (POT 4 setting) 3 x 2 parallels were vibrated, plus one additional 2 minute high energy input (POT 10) sample. All samples were produced using a vacuum of 4 kPa. The samples were baked at a common heating rate of 20 °C/h and the soaking temperature was 1150 °C. The soaking time was 8 hours. The densities in the green and the baked state were measured using the dimensional method ISO 12985-1. In addition specific electrical resistivity, baking loss, reactivity against air and CO_2, and physical properties were measured. The results and experimental design are shown in Table 4.4-I.

Table 4.4-I. Experimental layout and measured data for pilot scale anodes prepared from industrial paste taken out from ko-kneader.

	Factors			Responses									
Sample #	Mixing time (min)	Vibration time (min)	Vibration conditions	Green density (g/cm^3)	Baking loss (%)	Total porosity IA (%)	R CO_2 (mg/cm^2h)	Dust CO_2 (%)	R air (mg/cm^2h)	Baked density (g/cm^3)	SER ($\mu\Omega m$)	YM (MPa)	CCS (MPa)	Perm (nPm)
K1	1	0.5	4 kPa, POT 4	1.612	4.50	14.5	17.7	8.0	33.2	1.528	64.7	6532	24.8	6.0
K2	1	1		1.640	4.67	12.5	13.4	7.7	33.2	1.578	54.3	8278	37.9	1.1
K3	1	2		1.656	4.80	11.2	14.4	10.0	34.4	1.584	52.1	9767	42.8	0.7
K4	1	0.5		1.605	4.47	14.9	17.1	8.6	38.4	1.559	59.3	8204	33.3	2.9
K5	1	1		1.614	4.66	14.9	14.0	11.9	37.5	1.571	55.8	8935	38.1	1.4
K6	1	2		1.658	4.76	11.6	17.3	13.4	34.5	1.591	52.6	10091	45.4	0.5
K7	1	2	4 kPa, POT10	1.636	4.82	12.2	10.6	9.3	46.1	1.578	55.0	8607	36.6	0.7
K8	3	0.5	4 kPa, POT 4	1.642	4.65	12.9	14.0	6.6	35.0	1.599	54.6	9577	41.4	1.0
K9	3	1		1.662	4.61	11.3	13.9	8.5	40.4	1.601	53.8	10115	44.3	0.6
K10	3	2		1.682	4.82	11.0	15.7	8.2	29.1	1.580	51.4	10044	43.6	0.5
K11	3	0.5		1.619	4.61	15.3	34.0	11.1	31.0	1.573	54.5	9261	39.4	1.3
K12	3	1		1.639	4.46	12.8	15.4	7.2	43.3	1.596	57.8	8596	34.3	1.5
K13	3	2		1.672	4.73	11.1	13.6	5.1	39.2	1.615	53.4	9742	44.7	0.6
K14	3	2	4 kPa, POT10	1.714	5.11	9.8	15.3	9.2	39.0	1.624	52.5	9805	44.5	0.4
K15	6	0.5	4 kPa, POT 4	1.705	4.76	8.2	15.4	8.5	38.5	1.623	49.7	10292	51.5	0.3
K16	6	1		1.707	4.63	9.7	21.0	12.7	38.9	1.621	50.6	10739	48.6	0.4
K17	6	2		1.712	4.62	8.2	23.1	13.4	33.0	1.624	50.7	10263	49.2	0.3
K18	6	0.5		1.676	4.66	11.0	16.2	8.5	33.1	1.603	52.5	9842	43.3	0.7
K19	6	1		1.658	4.68	11.0	15.2	7.0	33.6	1.608	52.8	9487	43.6	0.5
K20	6	2		1.685	4.66	10.2	16.3	11.0	42.3	1.611	52.3	10252	43.6	0.4
K21	6	2	4 kPa, POT10	1.733	4.90	8.0	14.0	7.7	39.3	1.651	49.2	11392	50.2	0.2

RCO_2 - CO_2 reactivity, R air - air reactivity, SER - specific electrical resistivity, YM - Young's modulus, CCS - cold compression strength, Perm - air permeability

4.4.1 Green density

Fig. 4.4-1 and Fig. 4.4-2 show green densities measured for pilot scale anodes. Each point, except the high energy input sample (POT10), is the average of two parallel replicates. A general increase of green density was found with increasing mixing time (Fig. 4.4-1). Increase of mixing time creates a thinner and more continuous pitch film over the coke particles that give better packing and decreased aggregate spacing [45]. Thus, the lowest densities were measured for samples with 1 minute mixing time. However, as a mixing time increases up to 6 minutes, the green densities are nearly the same. Therefore, at 6 minutes mixing time the paste demands less vibration time to achieve high green densities. This could be due to sufficient mixing time that spreads the pitch evenly and the paste is easily compacted to high density. There is a marked increase in green densities with mixing time for samples that were vibrated with high energy input (POT 10). Increase of vibration energy leads to denser aggregate packing.

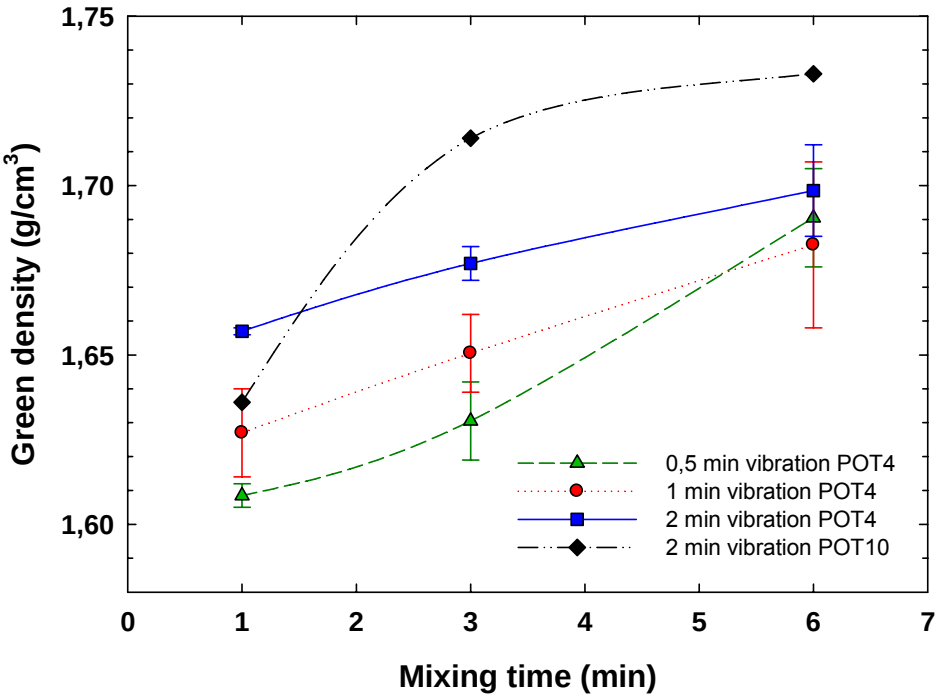

Fig. 4.4-1. Green density and mixing time.

Fig. 4.4-2 shows increasing average green densities with respect to vibration time. The lowest green densities were obtained for samples that were mixed for 1 minute and vibrated for 0.5 minutes.

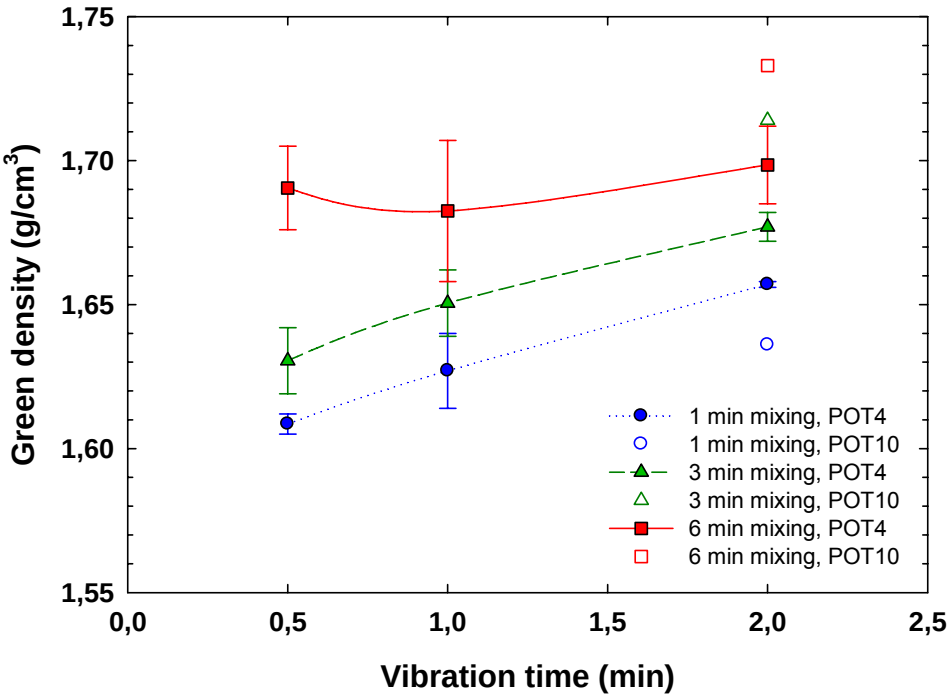

Fig. 4.4-2. Green density and vibration time.

Belitskus [45] described effects of mixing time on pilot scale anode quality, for both pressed and vibrated samples. It was observed that green and baked densities of the pressed anodes increased with increasing mixing time. Most of the density increase occurred after 30 minutes of mixing. Vibrated anode properties were optimum with 15 minute mixing time. Long mixing time was necessary because a sigma blade mixer was used. Extended mixing time highly degraded the anode properties. A probable reason for this is the increased crushing of the coke by the sigma mixer at extended mixing times. In the current experiments the samples were prepared using an intensive mixer.

4.4.2 Baking loss

The thickness of the pitch film will determine the amount of volatiles emission during baking. Mixing time and vibrating time are parameters that significantly affect the quality and continuity of the pitch film. Fig. 4.4-3 shows average baking loss for two replicates with respect to mixing and vibration time. The baking loss increases as the vibration time increases. The samples with the highest baking loss were those that were vibrated for 2 minutes with high energy input (POT10).

Extension of the mixing time will result in the development of a thinner and more homogeneous pitch fines phase around the coke particles. The binder matrix coats and bonds larger particles and partly penetrates coke pores. When vibration time increases or high energy input is used, more pitch-fines phase is expelled radially towards the outer surface of the sample. This will cause a pitch gradient in the sample making the surface richer in pitch. This can be observed visually after forming of green anodes by glossy surface where pitch has been pressed towards surface due to high energy input. The difference in surface appearance was observed also by Chmelar [80]. When such a

sample is baked the surface distributed pitch is volatilized easily causing higher baking loss.

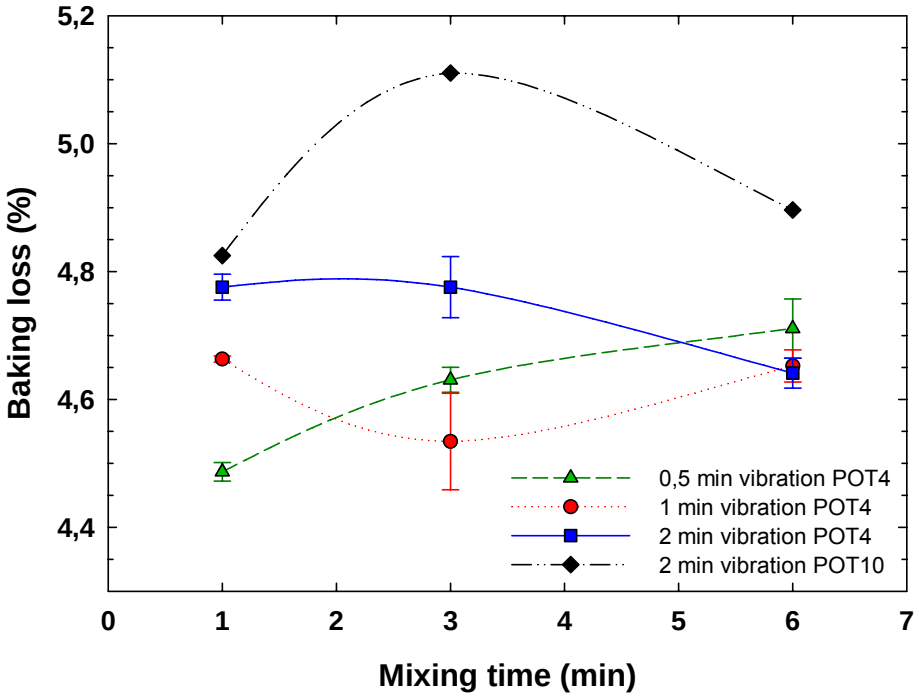

Fig. 4.4-3. Baking loss and mixing time.

4.4.3 Baked Porosity

Fig. 4.4-4 and Fig. 4.4-5 show average baked total porosity values for two replicates with respect to mixing time and vibration time.

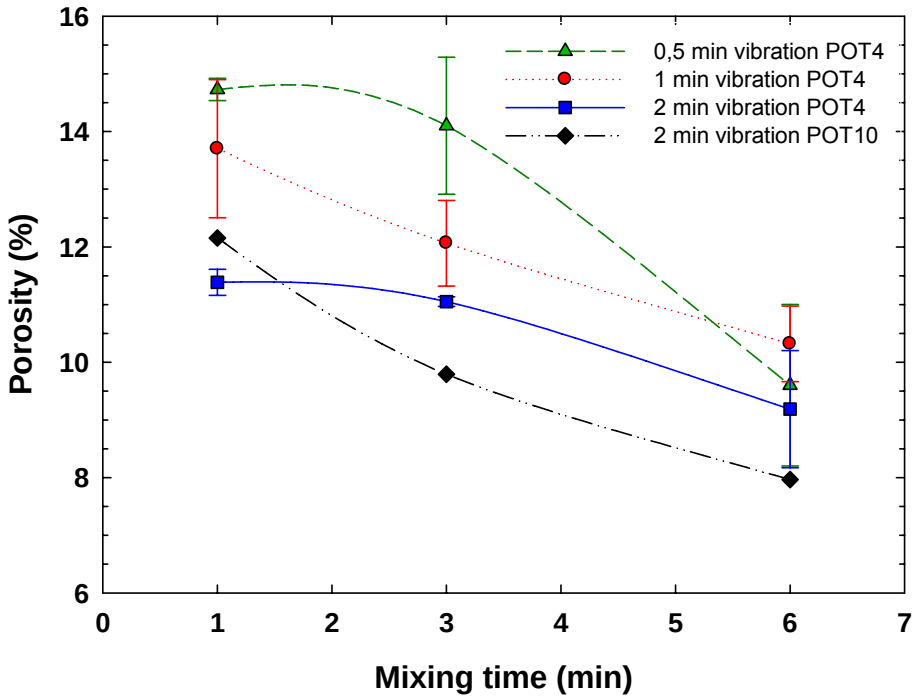

Fig. 4.4-4. Total porosity of the baked samples and mixing time.

With increasing mixing time the baked total porosity decreases. As expected, maximum porosity was measured for samples that were mixed for 1 minute and vibrated for 0.5 minutes. This is due to insufficient mixing and paste compaction. Thus, lots of intergranular voids are created in the green state and carried over to the baked state. The lowest total porosity was measured for samples mixed for 6 minutes and vibrated with high energy input (POT10).

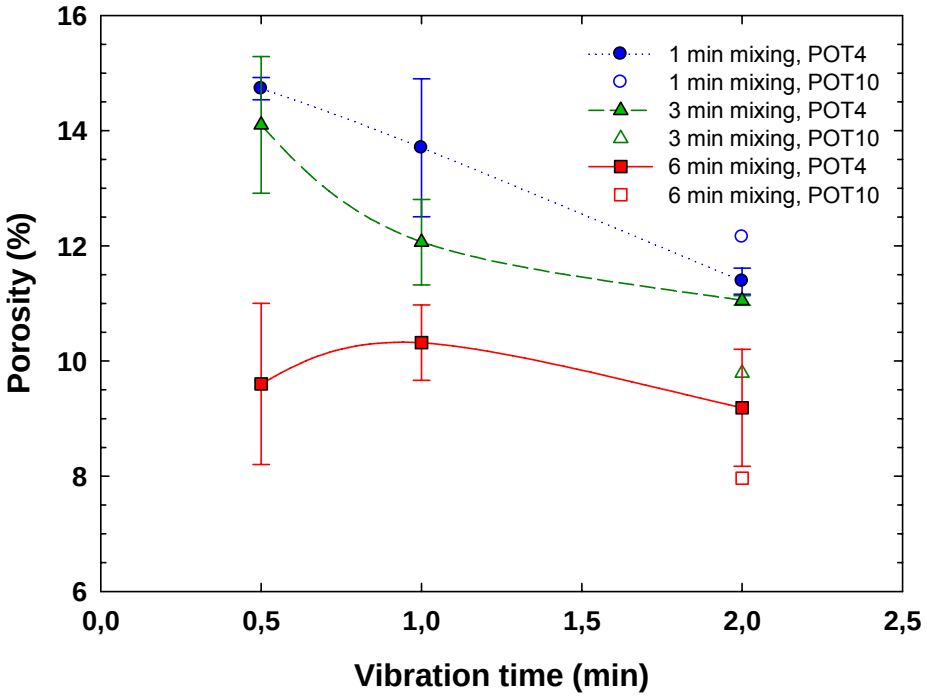

Fig. 4.4-5. Total porosity values and vibration time.

In Fig. 4.4-6-Fig. 4.4-8 a comparison of pore size distribution curves is given. Each plot compares mean values of two replicates that were mixed for 1, 3 or 6 minutes. Porosity for each replicate was determined from four analysed segments. Thus each curve in the plot represents mean value of 8 image analysis measurements (2 replicate anodes x 4 analysed segments from each).

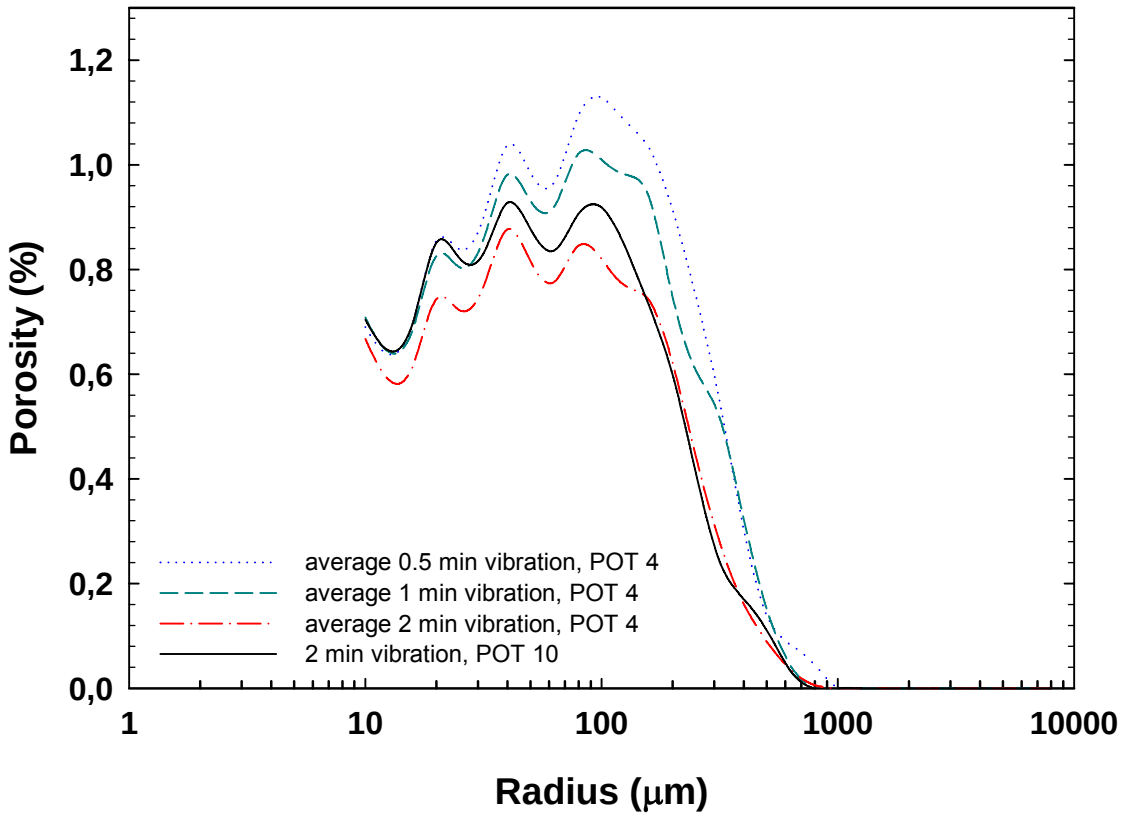

Fig. 4.4-6. Comparison of pore size distribution of mean values for 1 minute paste mixing time.

Fig. 4.4-6 shows a comparison of distribution curves for anodes that were produced from 1 minute mixed paste and vibrated for 0.5-2 minutes. As expected, the porosity decreases with increasing vibration time. The largest porosity was measured for samples with 30 seconds vibration time and lowest for those were vibrated for 2 minutes. The curves show similar pore distributions up to pore radius 100 µm. There are three common peaks at 20 µm, 40 µm and 100 µm. This peak distribution is typical for calcined coke. The largest diameter peak is probably due to void formation between coke grains due to insufficient pitch spreading. Another source for such porosity could be large round gas entrapment pores (created during the coke production process) that are not fully penetrated with pitch. The smallest diameter peaks may due to slit like pores and cracks that evolve during the calcination process. Short mixing time is not sufficient for creating the continuous binder film around the coke particles and thus coke pores are not completely impregnated with pitch. As the vibration time increases to 2 minutes the porosity is reduced.

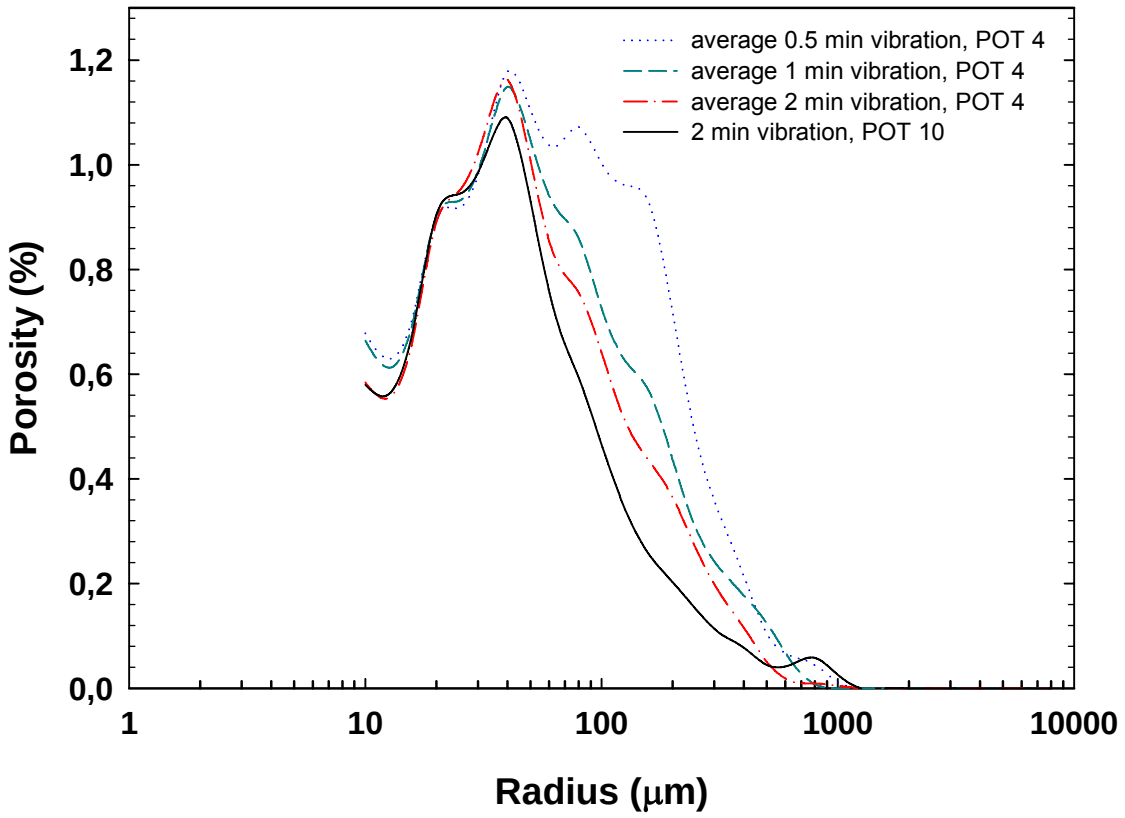

Fig. 4.4-7. Comparison of pore size distribution of mean values for 3 minutes paste mixing time.

Fig. 4.4-7 compares distribution curves for anodes produced from a 3 minutes mixed batch. The curves up to pore radius 40 µm show the same porosity distribution which indicates equal coke pore impregnation regardless of the vibration time. The porosity maximum at 40 µm was also observed in Chapter 4.3 (Fig. 4.3-4 to Fig. 4.3-7). This porosity was attributed to paste composition (which is also the same here) where the typical size of the baking pores was observed. Here the amount of 40 µm pores does not vary strongly because a uniform heating rate was used during baking. Above 40 µm the distribution curves vary. As the vibration time increases this porosity is reduced. The lowest porosity was measured for samples that were vibrated for 2 minutes with high energy input. Anodes with 0.5 minute vibration time have higher porosity above 100 µm compared to the other. The reason for such porosity reduction with increasing vibration time is probably increasing aggregate packing. It is assumed that 3 minute mixing time is sufficient to build a continuous coating over the coke particles. Additional increase of the vibration time will help to reduce porosity further by means of improved paste compactability and degassing.

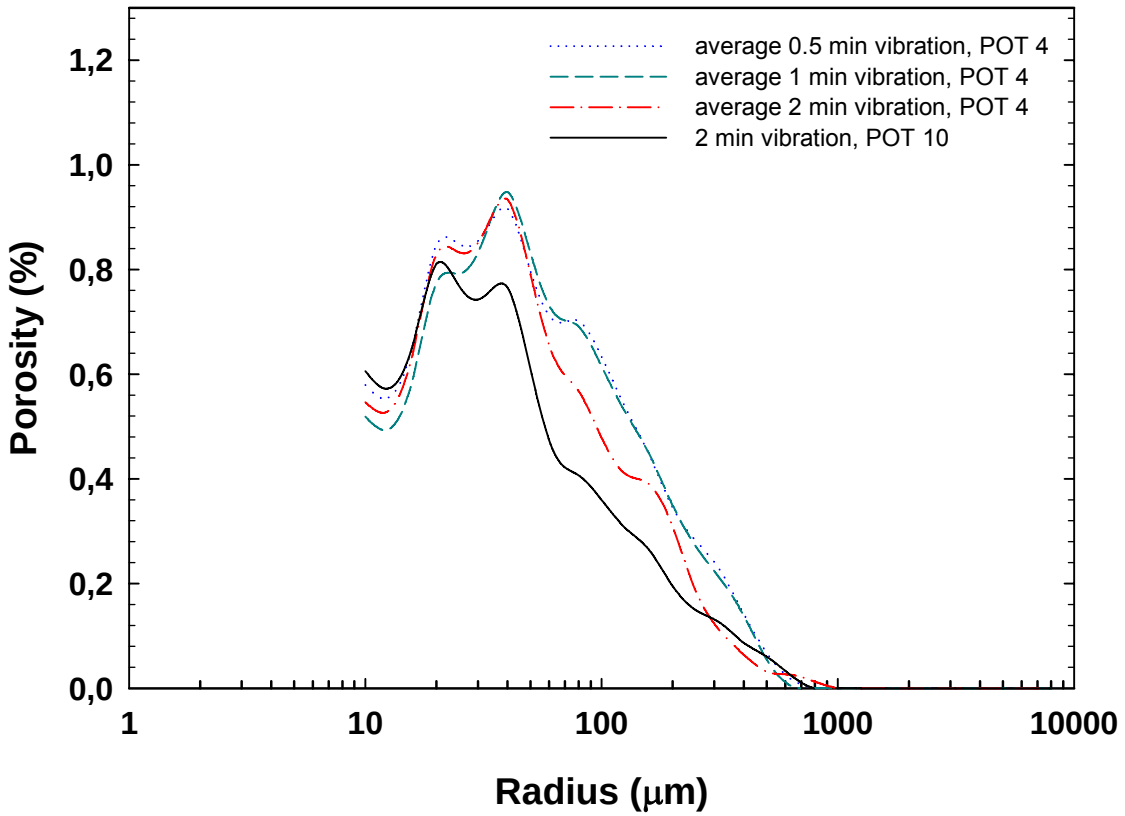

Fig. 4.4-8. Comparison of pore size distribution of mean values for 6 minutes paste mixing time.

Fig. 4.4-8 compares mean curves for anodes that were mixed for 6 minutes. Lower porosities are measured compared to the shorter mixing times shown in Fig. 4.4-6 and Fig. 4.4-7. The pore distribution curves for 0.5 and 1 minute vibration were almost identical. This small difference probably occurs because of improved uniformity and homogeneity of the paste when prolonged mixing time is used. The small differences between 6 minutes mixed samples with vibration time were also observed for green and baked density, SER, YM and CCS. However, there is a significant porosity reduction for 2 minutes high energy vibration. The results may indicate that when increasing the mixing time to 6 minutes the paste becomes more homogeneous and less demanding for longer vibration times to achieve low porosity.

0.5 minute vibration POT4

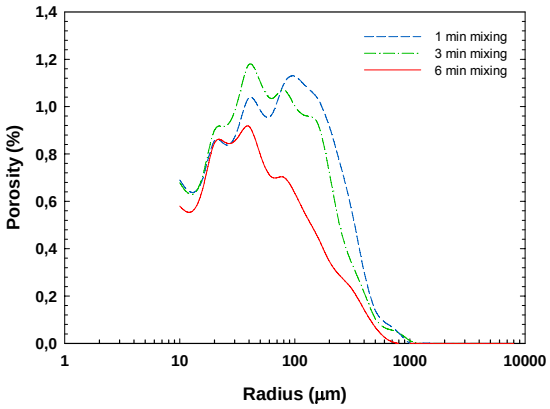

Fig. 4.4-9. Pore size distribution for anodes with various mixing times vibrated at 0.5 minute.

2 minute vibration POT4

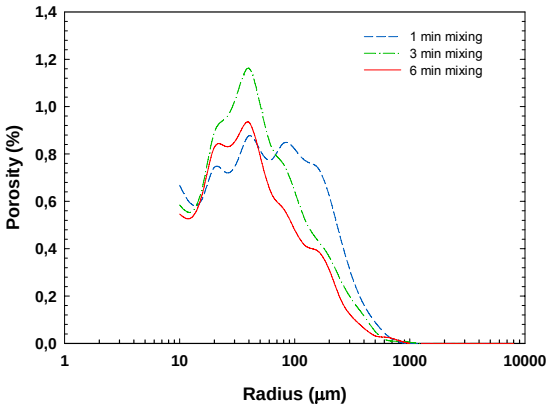

Fig. 4.4-11. Pore size distribution for anodes with various mixing times vibrated at 2 minute with POT4 energy input.

1 minute vibration POT4

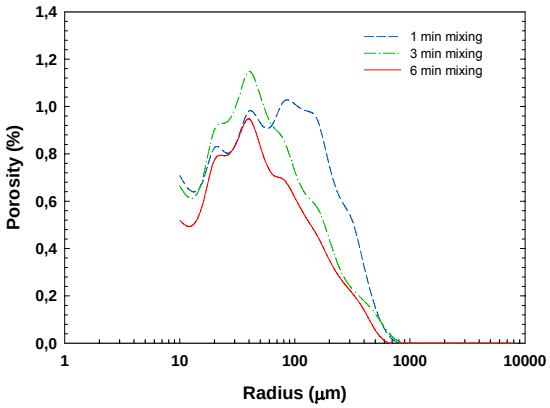

Fig. 4.4-10. Pore size distribution for anodes with various mixing times vibrated at 1 minute.

2 minute vibration POT10

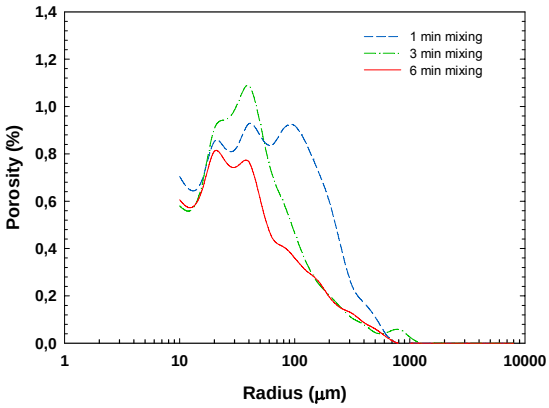

Fig. 4.4-12. Pore size distribution for anodes with various mixing times vibrated at 2 minutes with high (POT10) energy input.

Fig. 4.4-9 to Fig. 4.4-12 shows distribution curves that compare the effect of mixing time. Each plot shows distribution curves for constant vibration conditions. The porosity decreases with increasing mixing time for all vibration times. This effect is notable for pores of radius above 30 µm. For all samples mixed for 3 minutes, a maximum porosity at 40 µm is observed which may refer to baking pores. The evolution of baking pores is reduced as the binder phase is spread over the coke particles after extended mixing to 6 minutes. The increase of mixing time from 1 to 6 minutes significantly reduces the amount of pores with radius larger than 100 µm. This observation confirms the

assumption that increasing mixing time creates a homogeneous paste with a uniform binder film that enables easier reduction of intergranular porosity.

4.4.4 Reactivity measurements

Reactivity measurements were performed using the Hydro Aluminium method. In general poor correlation was found between reactivity data and other physical properties.

4.4.4.1 CO_2 and air reactivity

Fig. 4.4-13 to Fig. 4.4-18 show plots for CO_2 and air reactivities. Large scattering of the data is observed. In addition the error bars indicate large deviations for two replicates. There was also found low correlation between air reactivity and permeability.

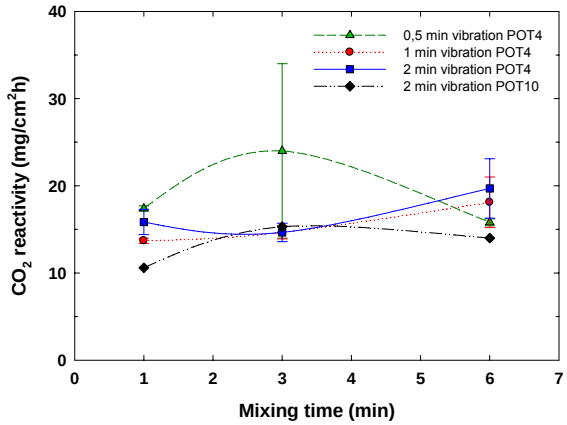

Fig. 4.4-13. CO_2 reactivity and mixing time.

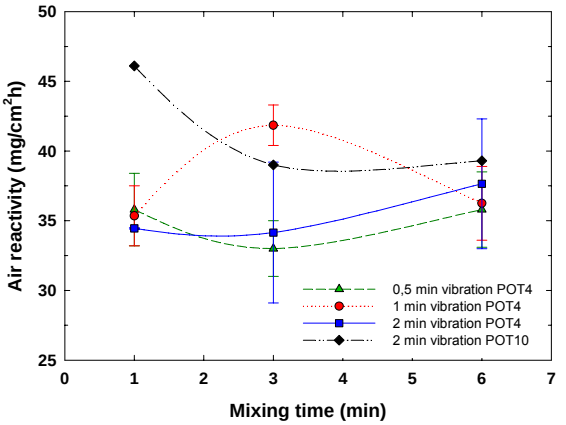

Fig. 4.4-15. Air reactivity and mixing time.

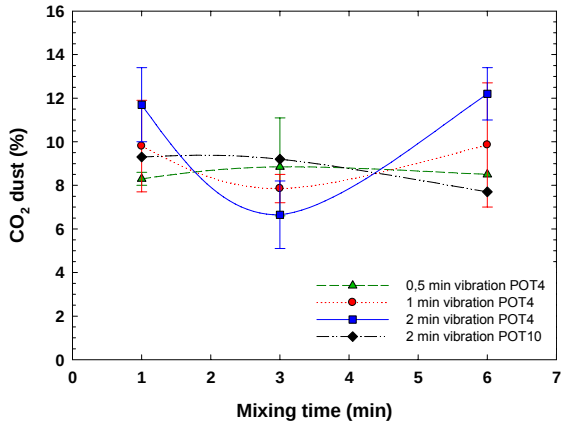

Fig. 4.4-14. CO_2 dust and mixing time.

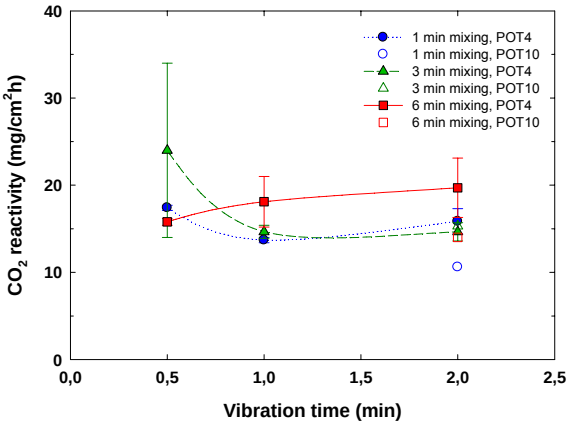

Fig. 4.4-16. CO_2 reactivity and vibration time.

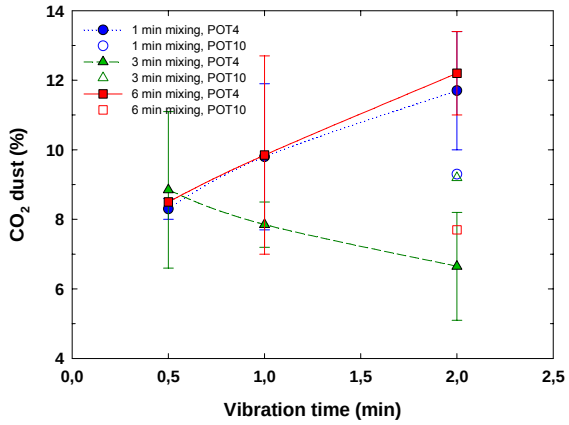

Fig. 4.4-17. CO_2 dust and vibration time.

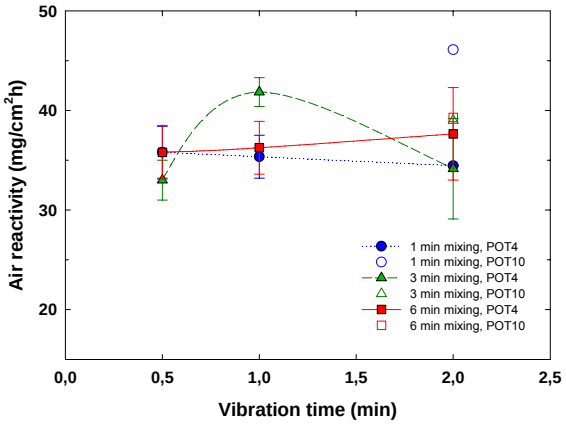

Fig. 4.4-18. Air reactivity and vibration time.

A possible reason for low correlation between reactivity properties and total porosity could be as follows. Air and CO_2 reactivity are determined by the ability of these gases to penetrate though the open pores and react with the carbon body of the anode. The total porosity determines the total amount of pores (open and closed pores together) in the sample, while for the reactivity only the open pores and their connection is important.

The way the reactivity measurement is designed does not allow the reacting gases to pass through the bulk of the sample by the connected pores (Fig. 3.8-1). The gas flows over the surface and only the large open pores can be reached. Thus the permeability may not correlate well with reactivity results.

Reactivity against CO_2 and air may then be more influenced by the presence of the catalytic elements as V, Ni, Na or S.

4.4.5 Baked density

Fig. 4.4-19 shows averaged values for two replicates of baked density with respect to mixing time. Good correlation with green density was found (Fig. 4.4-1). Increase of the mixing time gave denser anodes after baking.

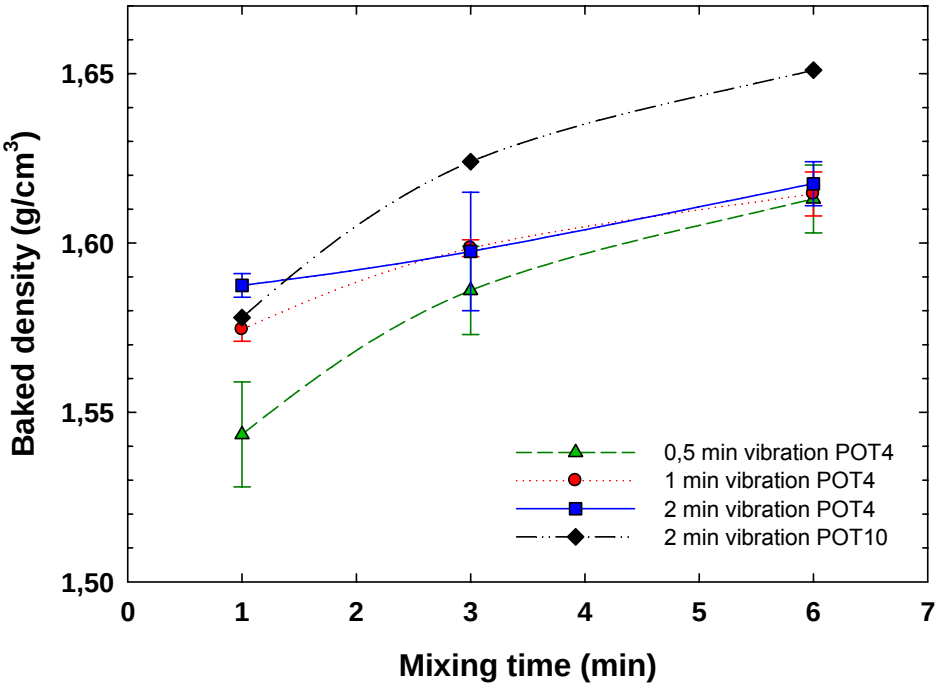

Fig. 4.4-19. Baked density and mixing time.

In Fig. 4.4-20 average baked densities are plotted vs. vibration time. Samples vibrated for longer time show higher baked densities. Maximum baked density was achieved for the samples that were vibrated for 2 minutes with high energy input (POT10). The lowest baked density was obtained for samples with the shortest mixing time (1 minute) and the shortest vibration time. There is a marked increase of baked density with increasing vibration time in the case of 1 minute mixed paste. With increasing mixing time homogenisation of the aggregate is improved and thus better packing can be achieved during vibration. In the cases of 3 and 6 minutes mixed samples a moderate density increase is found as the paste was uniform exhibiting similar compactability properties.

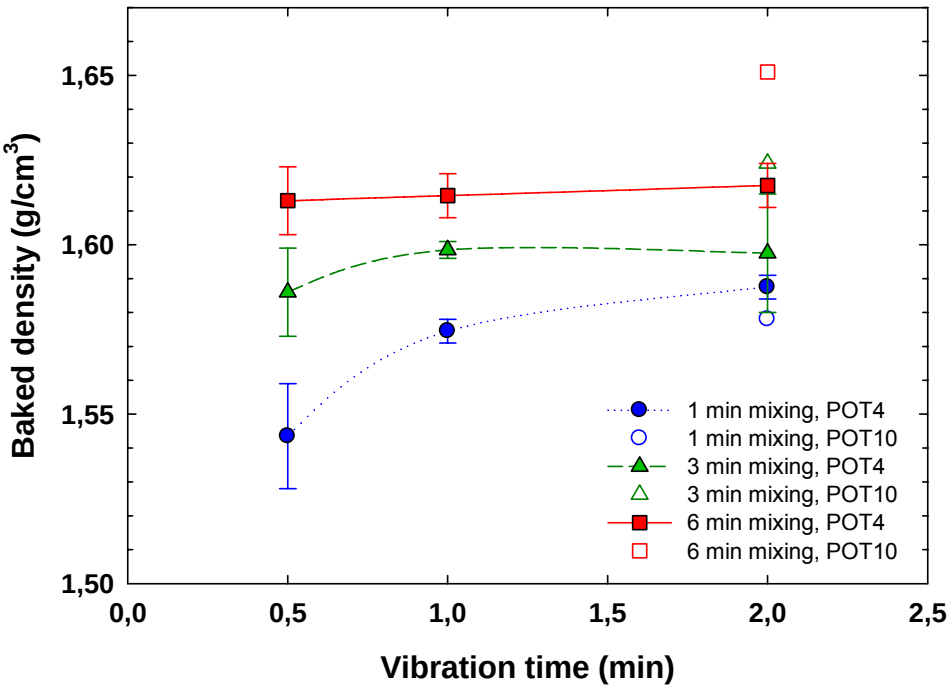

Fig. 4.4-20. Baked density and vibration time.

It will be shown later that the density in the baked state correlates well also with mechanical and electrical properties.

4.4.6 Specific electrical resistivity

Increase of the mixing time leads to a general decrease of the specific electrical resistivity values. Minimum values of SER were measured for samples with 6 minutes mixing time (Fig. 4.4-21). Taking into consideration the identical baking process for all samples, this can be explained by the interaction between two production steps; mixing and forming. Increase of the mixing time affects the amount of the bridging coke. Subsequent densification by increasing vibration time causes closer packing that enables better electrical contacts between coke grains after baking. This is seen also in Fig. 4.4-22 where the 1 minute mixed paste was affected the most by vibration time.

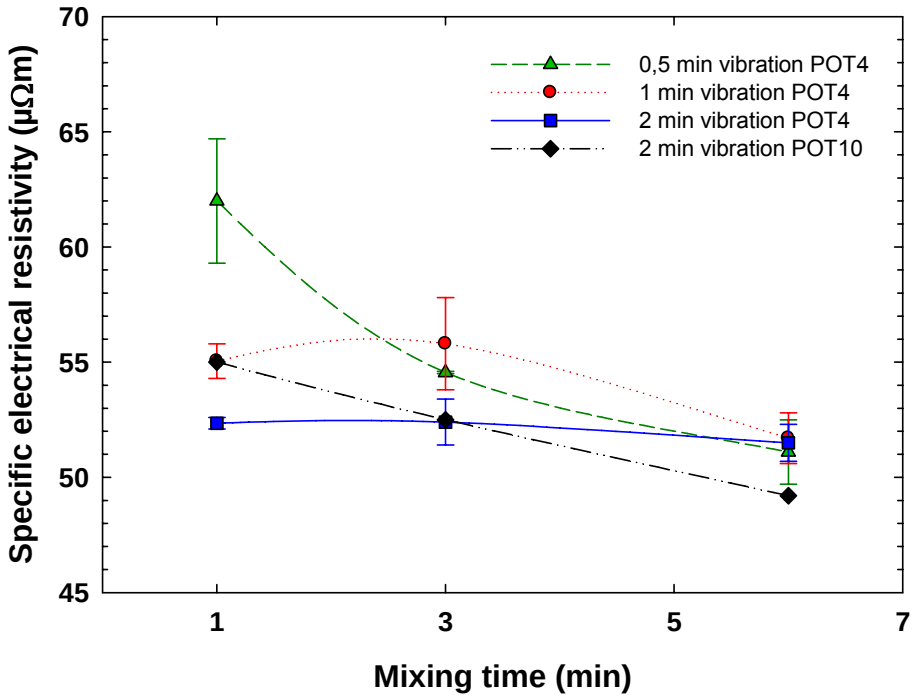

Fig. 4.4-21. Specific electrical resistivity and mixing time.

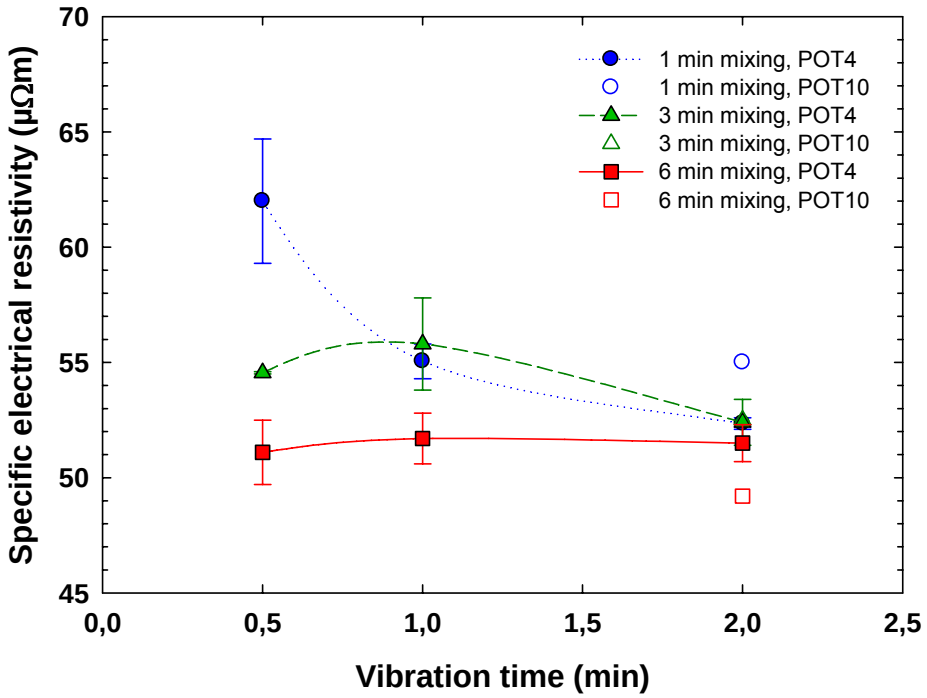

Fig. 4.4-22. Specific electrical resistivity and vibration time.

As the mixing time increases the samples become more equal regarding particle coating and vibration time will hence not play an important role for further electrical conductivity improvement.

4.4.7 Mechanical properties

4.4.7.1 Cold compression strength

Increase of the mixing time causes increase of the compression strength of the samples. The largest increase of CCS with mixing time was observed for 0.5 minute vibrated anodes and also in the case of high energy vibrated samples. The lowest strength was measured for anodes mixed for one minute and vibrated for 0.5 minutes (Fig. 4.4-23). The strength of the samples depends on the proper aggregate distribution which is affected by the mixing time. Thus, short mixing and insufficient vibration time are not favourable for obtaining mechanically strong anodes. Influence of the baking on the compression strength is difficult to define as all the anodes were baked at identical heating rate.

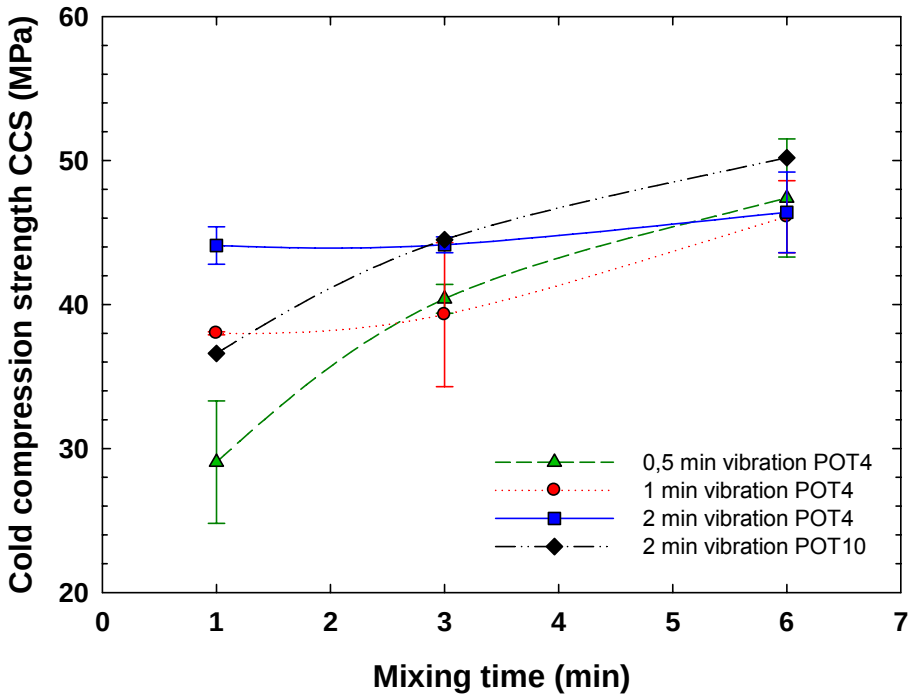

Fig. 4.4-23. Cold compression strength and mixing time.

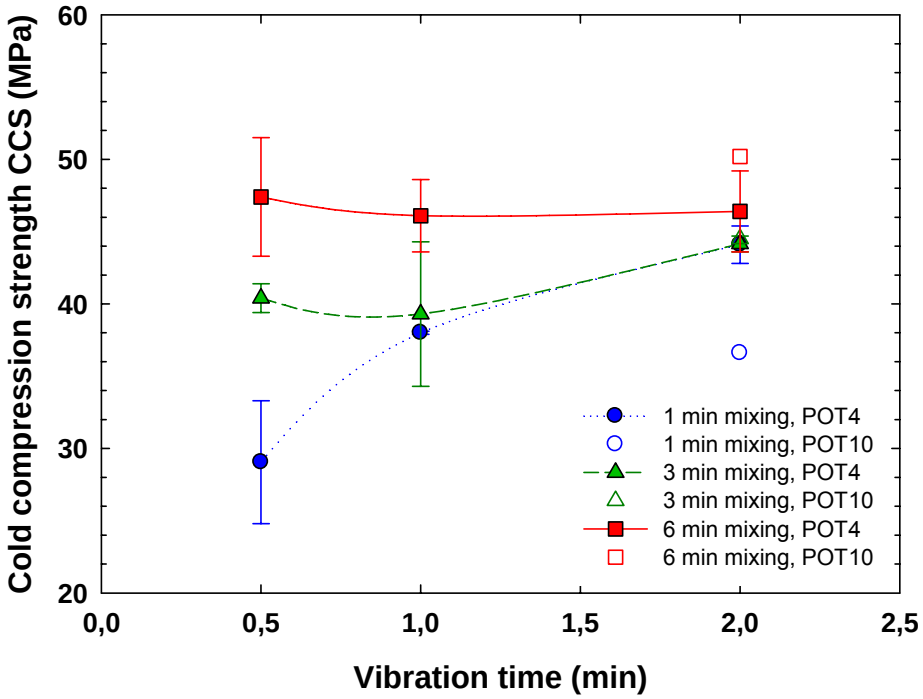

Fig. 4.4-24. Cold compression strength and vibration time.

4.4.7.2 Young's modulus

A similar trend was found for Young's modulus as for cold compression strength. Fig. 4.4-25 compares average values of two replicates for Young's modulus. In general an increase of the Young's modulus was observed when the mixing time increases. For 0.5 minute compacted samples the largest increase of Young's modulus is observed when the mixing time increased from 1 to 3 minutes. This agrees well with the baked density measurements (Fig. 4.4-19) and may probably be attributed to the development of pitch film over the coke particles. Anodes that have higher baked densities were those with higher Young's modulus.

In addition there is also good agreement between the total porosity values and Young's modulus. Anodes that were denser and less porous tend to show higher modulus values (Fig. 4.4-4).

Fig. 4.4-26 shows the same relation with respect to vibration time. With increasing vibration time YM increases most for anodes from the 1 minute mixed batch. Batches mixed for 3 and 6 minutes seem not to be significantly affected by vibration time. Coke particles are already properly coated with an even pitch film and will form denser, less elastic blocks with high YM even at shorter vibration times.

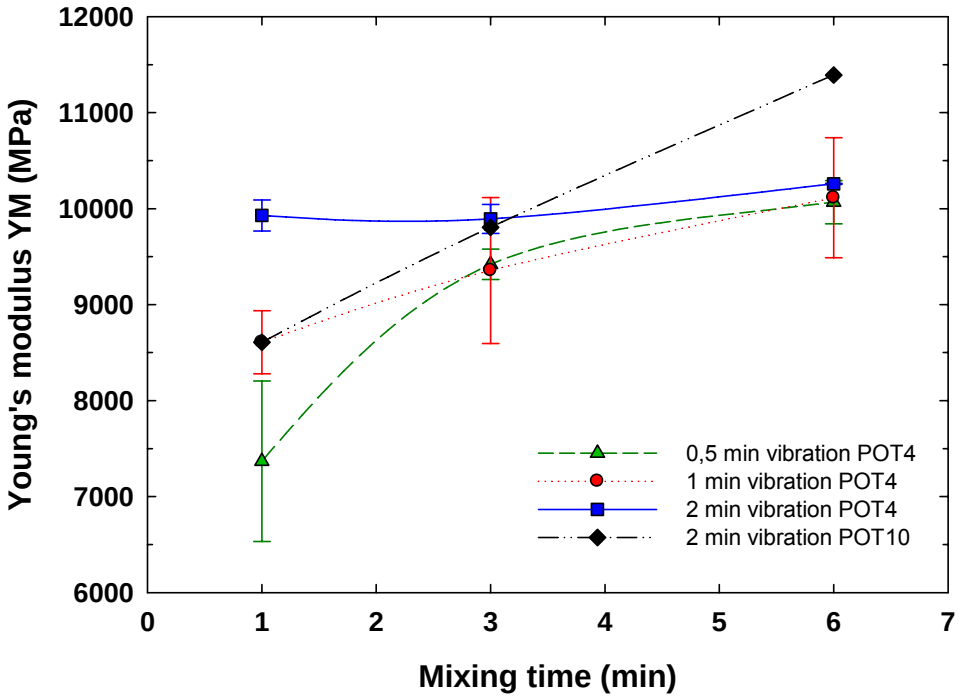

Fig. 4.4-25. Young's modulus and mixing time.

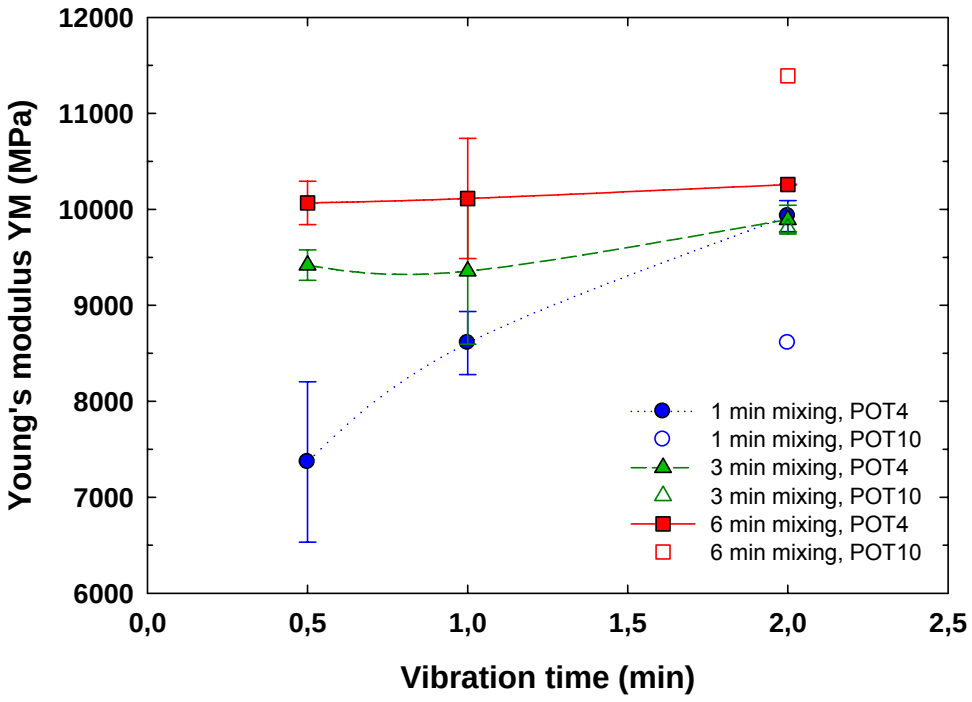

Fig. 4.4-26. Young's modulus and vibration time.

Meier [11] studied the impact of the processing parameters on mechanical properties of pilot scale anodes. The same trends for Young's modulus were observed. The influence of mixing time could be correlated to mixing energy (an increase of the torque or the

rotation frequency) that was used in Meier's study. With increasing mixing energy (in kWh/t) the elasticity modulus slightly increased. Also, increase of the mixing energy improved the flexural strength and the fracture energy.

4.4.8 Permeability

The air permeability determines the ability of air to pass through the sample and should influence the carbon consumption. Open, connected pores with more than 50 µm in diameter influences the air gas permeability [33]. This is the range that shows the largest variation in pore size distribution plots shown in Fig. 4.4-6 to Fig. 4.4-8. Thus the variations in permeability correlate well with total porosity values. Increase of the porosity above 25 µm pore radius is mostly related to presence of baking pores and intergranular voids due to production variations. This porosity also affects physical and mechanical (YM, CCS, SER) properties of the samples (Chapters 4.4.7.1, 4.4.7.1 and 4.4.6.). Permeability measurements are shown in Fig. 4.4-27 and Fig. 4.4-28. The variations in mixing and forming also influence the permeability. With increasing mixing time a moderate decrease of permeability was observed (Fig. 4.4-27). The largest decrease of permeability with vibration time was observed for 1 minute mixed samples when increasing the vibration from 0.5 to 1 minute (Fig. 4.4-28). The same effect was observed in previous measurements of physical properties for pilot scale anodes. A correlation between total porosity values and permeability is shown in Fig. 4.4-29. Samples with high porosity values are those that also exhibit high permeability.

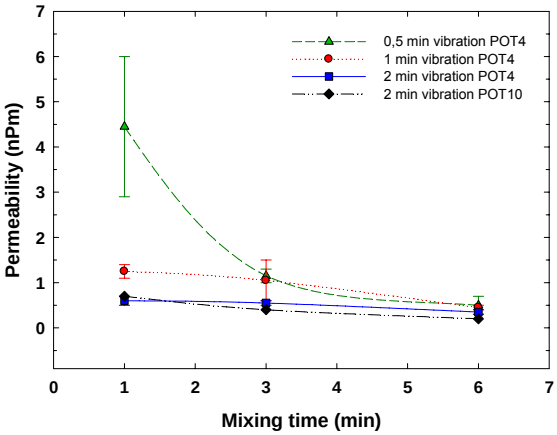

Fig. 4.4-27. Permeability and mixing time.

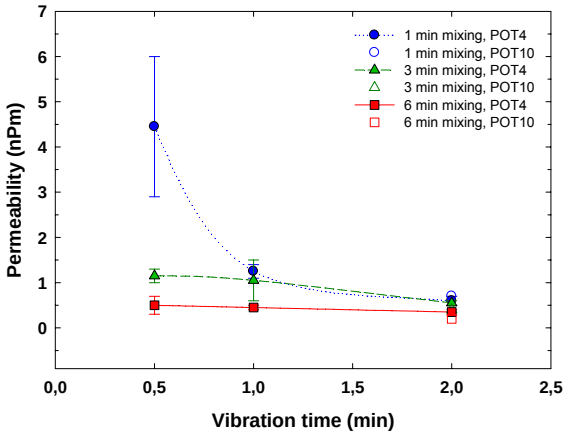

Fig. 4.4-28. Permeability and vibration time.

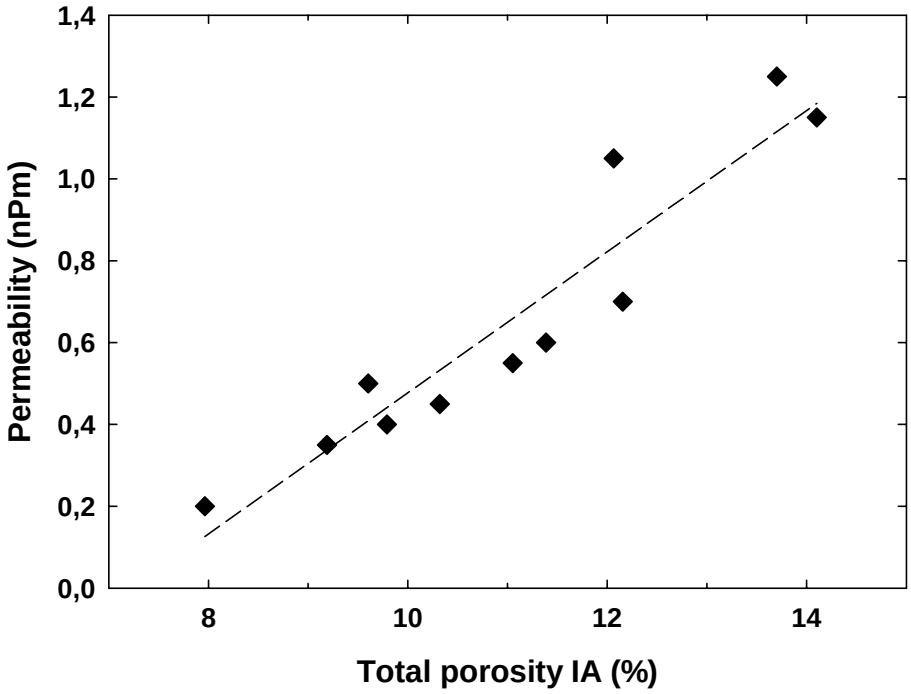

Fig. 4.4-29. Correlation between air permeability and total porosity (measured by image analysis).

4.4.9 Conclusion

Two production variables, mixing time and vibration time, were used and their influence on various anode properties was measured. When increasing the mixing and vibration time higher densities were achieved. Most marked improvement was achieved for 1 minute mixing where further increase of vibration time resulted in improved densification. The best results were observed for anodes that were vibrated for 2 minutes with high energy input. Other mechanical and electrical properties like CCS, YM, and SER were in good agreement with baked density. The lowest resistivities were measured for anodes with high baked density.

Highest baking loss was measured for anodes that were vibrated for 2 minutes with high energy input. Excessive vibration expels pitch binder radially towards sample surface. During baking, the surface pitch is volatilized easily causing larger baking loss.

Reduction of total porosity values was observed with increasing of mixing time, regardless of vibration time. The reason for this was probably improved aggregate homogenization that enables better aggregate packing. Also, with increasing mixing time the pitch spreads more uniformly over the coke particles creating an even thin film which allows denser aggregate packing. Increase of vibration time caused the largest decrease of the total porosity values for short mixing times (1 and 3 minutes mixed batches). Reduction of the total porosity value in the case of 6 minutes mixing was not so evident. This indicates that properly mixed paste (more continuous binder film) is less demanding on the duration of the vibration.

The mechanical properties (CCS and YM) were found to be closely related to the densities in the green and baked state and thus also influenced by the mixing and vibration conditions. Increase of the mixing time caused improvement of both mechanical properties. The same effect was observed for vibration time. The largest increase of the CCS and YM was observed for 1 minute mixed samples when increasing the vibration time from 0.5 to 1 minute. On the other hand the strength properties for 6 minutes batch seemed not to be influenced much by increasing vibration time.

There was observed good correlation between porosity and permeability. Samples with high porosity values were those that also exhibit high permeability. With increasing mixing time a moderate decrease of permeability was observed. The largest decrease of the permeability with vibration time was observed for 1 minute mixed samples when increasing the vibration from 0.5 to 1 minute. The same effect was observed in previous measurements of the physical properties for the pilot scale anodes.

4.5 Intensive mixer optimisation - laboratory pilot scale anodes from SSA coke

In this experimental part pilot scale anodes were produced in the anode laboratory using an intensive mixer in order to define its optimum operational conditions. A set of 24 anodes were produced in order to determine the optimum tip speed and mixing time. These parameters were needed before use of the intensive mixer (Eirich RV 02/E) in the laboratory. The applied aggregate composition was according to Table 3.1-I and medium fines were used (63 % < 63 μm). The pilot scale anodes were produced a using pitch content ranging from 14 to 21 %, two mixing times (5 and 10 minutes) and three tip speeds (10, 12 and 14 m/s) as presented in Table 4.5-I.

Table 4.5-I. Experimental layout of pilot scale anodes produced in preliminary tests of the intensive mixer.

Sample	Pitch content (%)	Tip speed (m/s)	Mixing time (min)	Green density kg/m^3	Open porosity (%)
E14/10/5	14,2	10	5	1,541	10,5
E16.5/10/5	16,7	10	5	1,634	2,5
E19/10/5	18,9	10	5	1,669	0,5
E21/10/5	21,2	10	5	1,665	0,2
E14/14/5	14,4	14	5	1,570	8,9
E16.5/14/5	16,7	14	5	1,681	1,3
E19/14/5	19,3	14	5	1,683	0,3
E21/14/5	21,2	14	5	1,677	0,3
E14/10/10	14,2	10	10	1,584	7,1
E16.5/10/10	16,5	10	10	1,655	1,9
E19/10/10	19,1	10	10	1,683	0,4
E21/10/10	21,3	10	10	1,676	0,2
E14/14/10	14,1	14	10	1,606	7,1
E16.5/14/10	16,6	14	10	1,691	1,2
E19/14/10	19,3	14	10	1,692	0,4
E21/14/10	19,9	14	10	1,684	0,2
E14/12/10	14,4	12	10	1,634	3,8
E16.5/12/10	16,6	12	10	1,676	1,1
E19/12/10	19,2	12	10	1,683	0,3
E21/12/10	21,1	12	10	1,670	0,2
E14/12/5	14,2	12	5	1,605	5,1
E16.5/12/5	17,0	12	5	1,673	1,2
E19/12/5	19,3	12	5	1,673	0,4
E21/12/5	21,1	12	5	1,670	0,3

The dry aggregate was pre-mixed at 1.8 m/s rotor tip speed at 180 °C before pitch addition in order to achieve equal starting mixing temperatures. Pitch with temperature 190 °C was added according to the recipe and the paste was mixed with the assigned rotor tip speeds for 5 or 10 minutes. The green paste was formed using the vibration compactor for 3 minutes at 15.6 Hz vibration frequency. Green density and open porosity were measured using the hydrostatic method (ISO 12985-2). Optimum tip

speed as well as mixing time was determined as those giving the highest values of the green density and the lowest open porosity values.

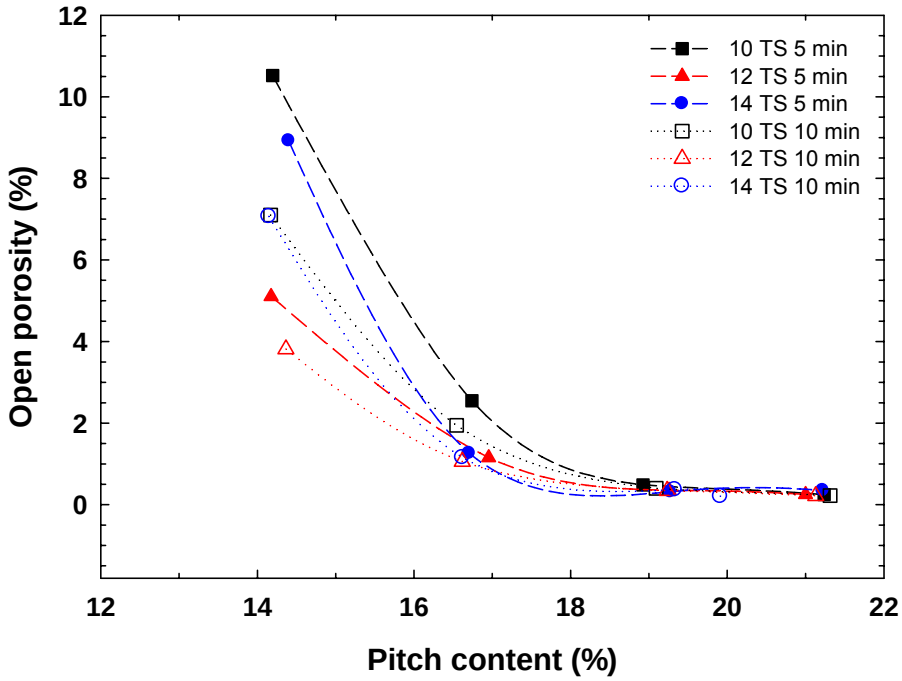

Fig. 4.5-1. Open porosity and pitch content.

In Fig. 4.5-1 open porosity values are compared with respect to pitch content, mixing time and tip speed. There is a general decrease of the open porosity with increasing pitch content. Increase of the mixing time from 5 to 10 minutes caused reduction of the porosity primarily for 14 % pitch samples. The lowest open porosity of all 14 % pitch anodes was achieved when 12 m/s rotor tip speed was used.

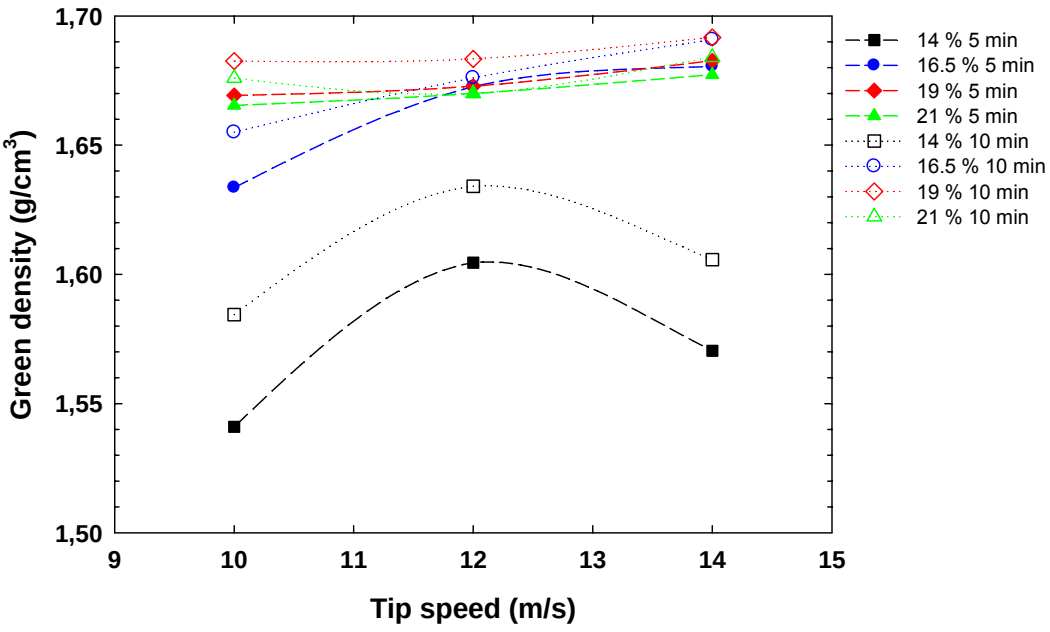

Fig. 4.5-2. Green density and tip speed.

Fig. 4.5-2 shows the variation of the green density with increasing pitch content. The highest green densities were measured for samples with 19 % pitch and 10 minutes mixing time. There is also an increase in green density as the rotor tip speed increases from 10 to 12 m/s. Further increase to 14 m/s caused decrease in green density regardless the mixing times for 14 % pitch samples. This may indicate an optimum tip speed of 12 m/s.

The three dimensional plots in Fig. 4.5-3 and Fig. 4.5-4 show comparison of all parameters in one plot. There is a general increase of green density and a decrease of open porosity as the mixing time is increased from 5 to 10 minutes. In addition an optimum tip speed of 12 m/s is indicated for 14 % pitch samples. Based on this, 12 m/s rotor tip speed was taken as the optimum for further pilot scale anode production.

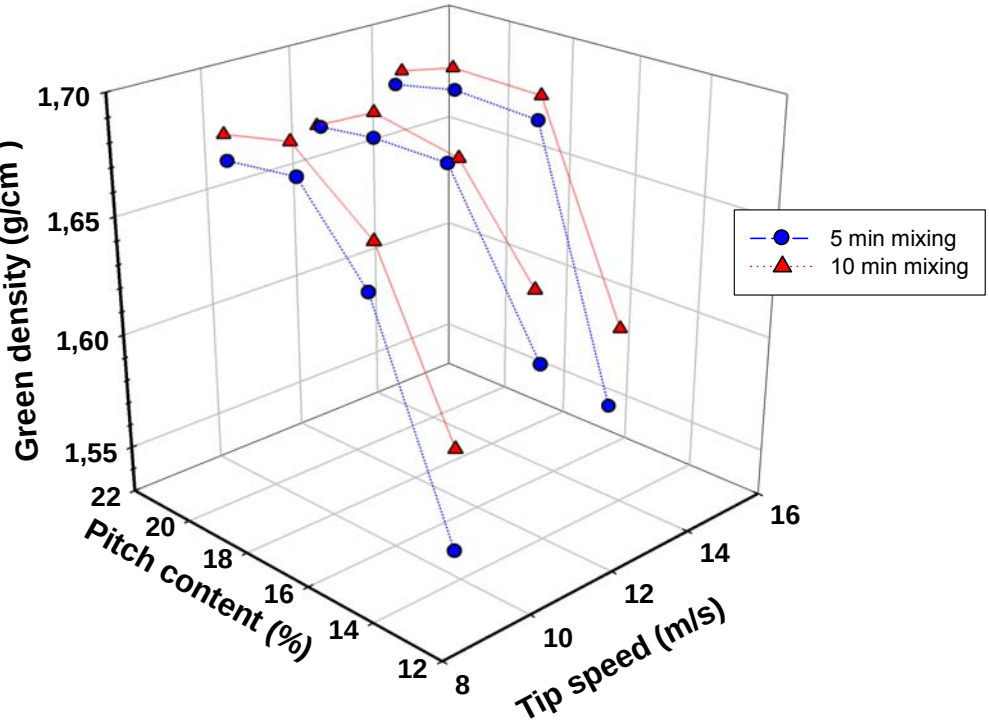

Fig. 4.5-3. 3D plot for green density measured by ISO 12985-2.

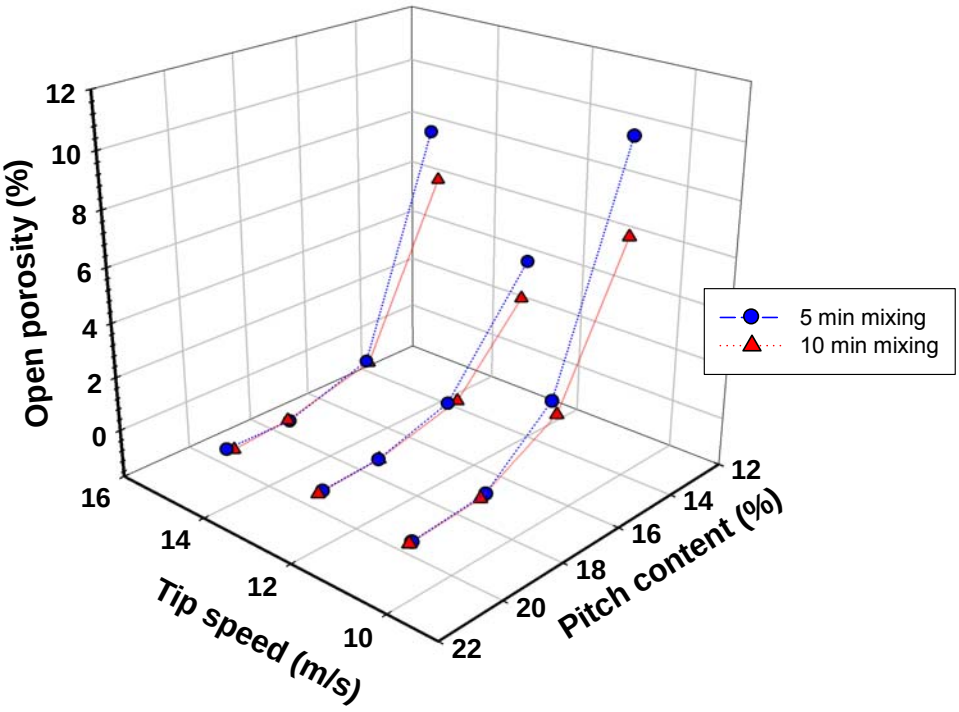

Fig. 4.5-4. 3D plot for open porosity measured by ISO 12985-2.

4.6 Effect of variation in production methods on porosity development - laboratory pilot scale anodes from SSA coke

In total 24 pilot-scale anodes were prepared from a single source petroleum coke using a typical industrial recipe. Pitch content, aggregate size distribution, mixing time, mixing techniques, and heating rate up to 550 °C were varied. The half fractional 5-factorial design that was used is presented in Table 4.6-I. The vibration time was not varied as that was found earlier to have low effect except for unrealistically short mixing time.

Table 4.6-I. Variables and levels of half fractional 5-factorial design.

Factors	***Low***	***Medium***	***High***
Fines (% < 63 μm)	45	63	94
Pitch content (%)	14	16.5	19
Eirich mixer (min)	5	7.5	10
Sigma mixer (min)	10	15	20
Heating rate (°C/h)	10	35	60

Half of the pilot scale anodes were produced using a sigma mixer and the other half was mixed in an intensive mixer (Eirich RV 02/E) with constant tip speed 12 m/s. The preheated aggregate for sigma mixed anodes was pre-mixed at 180 °C for about 5 minutes before pitch addition to obtain a uniform coke temperature and better statistical distribution of the aggregate. Pitch with temperature 190 °C was added and the paste was mixed for 10, 15 or 20 minutes. The green paste was formed on the vibration table for 3 minutes at 15.6 Hz vibration frequency to 160 mm diameter and 145 mm height blocks. The same procedure was used for manufacturing intensively mixed samples. The aggregate was preheated at 1.8 m/s rotor tip speed until 180 °C. Pitch with temperature 190 °C was added and the paste was mixed at 12 m/s tip speed for 5, 7.5 or 10 minutes. The green paste was processed in the same way as for the sigma mixed anodes.

Green densities of the anodes were determined according to ISO 12985-2. All anodes were baked under a coke bed in an electric oven. Three heating rates, 10, 35 and 60 °C/h were used up to 550 °C. Above 550 °C, all samples were heated with same heating rate, 100 °C/h, to the final temperature 1100 °C. The soaking time was 5 hours and the anodes were cooled by turning off the oven. Baked densities were measured in the same way as for the green anodes. The complete experimental layout and measured data are shown in Table 4.6-II.

Table 4.6-II. Experimental layout and measured data for laboratory prepared pilot scale anodes from SSA coke.

	Factors					Responses														
Sample #	Heating rate (°C/h)	Fines	Mixer E/S	Pitch cont. (%)	Mixing time (min)	Green density (kg/m^3)	Baking loss (%)	Total porosity IA (%)	porosity STDEV	R CO_2 (mg/cm^2h)	Dust CO_2 (%)	R air (mg/cm^2h)	Baked density (g/cm^3)	SER (µΩm)	SER STDEV	YM (MPa)	CCS (MPa)	Perm (nPm)	CTE ($*10^{-6}$ 1/K)	Teq (°E)	TSR (K/µΩm)
C1	10	low	Eirich	14	5	1,613	3,7 %	13,5	0,2	23,5	19,8	37,0	1,533	57,3	0,1	7928	35,7	0,8	4,7	1147	17,1
C17	10	high	Eirich	14	10	1,566	3,8 %	13,4	0,7	30,6	28,5	41,1	1,566	58,5	0,1	7395	35,7	0,7	4,5	1147	17,7
C5	10	low	Eirich	19	10	1,679	5,4 %	19,2	1,7	27,2	12,2	45,7	1,520	62,7	0,2	8164	31,0	13,0	4,5	1158	14,7
C24	10	high	Eirich	19	5	1,676	5,3 %	18,9	0,6	26,6	25,5	43,6	1,517	63,9	0,4	7728	33,5	11,4	4,3	1158	16,6
C9	35	medium	Eirich	16,5	7,5	1,631	5,6 %	19,8	2,4	14,0	1,7	15,3	1,517	65,6	0,3	7647	28,2	4,4	4,4	1154	13,5
C15	35	medium	Eirich	16,5	7,5	1,659	5,5 %	18,8	1,2	22,4	15,3	41,8	1,525	67,4	0,3	7204	24,8	4,6	4,5	1154	12,4
C21	35	medium	Eirich	16,5	7,5	1,661	5,5 %	17,7	0,3	23,7	17,6	34,9	1,527	62,6	0,3	7964	32,0	5,6	4,4	1162	14,5
C23	35	medium	Eirich	16,5	7,5	1,646	5,5 %	18,3	0,8	25,3	24,3	65,0	1,518	64,6	0,6	7675	27,7	5,0	4,5	1162	12,8
C10	60	low	Eirich	14	10	1,617	4,9 %	15,4	0,7	25,1	20,0	29,5	1,526	60,0	0,4	8321	35,0	1,4	4,5	1158	15,4
C14	60	high	Eirich	14	5	1,484	4,8 %	15,1	0,8	30,1	21,3	52,6	1,497	60,9	0,4	7745	33,3	1,3	4,3	1158	15,6
C11	60	high	Eirich	19	10	1,685	6,7 %	20,8	1,3	24,7	13,9	33,5	1,502	62,8	0,2	8096	33,7	18,4	4,3	1156	14,5
C12	60	low	Eirich	19	5	1,674	6,9 %	22,9	1,7	31,5	22,0	40,8	1,470	66,4	0,4	7667	31,0	16,3	4,3	1156	15,9
C4	10	high	Sigma	14	10	1,675	4,7 %	21,1	4,9	25,8	16,0	30,9	1,424	83,0	1,6	3266	18,3	20,0	4,5	n/a	13,8
C22	10	low	Sigma	14	20	1,493	4,2 %	27,7	1,7	29,9	41,5	39,1	1,411	123,8	5,9	2730	17,2	22,0	4,3	n/a	13,6
C2	10	high	Sigma	19	20	1,630	5,9 %	18,2	4,3	18,4	6,4	53,0	1,498	64,8	0,2	6897	32,6	8,9	4,2	n/a	17,6
C6	10	low	Sigma	19	10	1,675	6,1 %	17,4	0,9	30,0	10,8	43,0	1,479	67,6	0,2	6645	27,3	7,4	4,3	n/a	14,8
C7	35	medium	Sigma	16,5	15	1,674	5,2 %	22,6	3,1	18,1	4,5	25,8	1,459	65,3	0,2	6692	24,5	8,5	4,5	n/a	11,9
C18	35	medium	Sigma	16,5	15	1,579	5,4 %	20,1	3,4	19,3	10,7	39,0	1,454	65,3	0,1	7128	30,7	9,6	4,3	n/a	15,2
C19	35	medium	Sigma	16,5	15	1,570	5,3 %	20,1	1,9	24,0	15,8	32,7	1,464	64,4	0,2	7019	31,1	7,3	4,2	n/a	15,8
C20	35	medium	Sigma	16,5	15	1,570	5,5 %	23,5	3,3	24,1	16,8	44,0	1,460	64,4	0,2	7071	31,5	10,1	4,3	n/a	15,8
C3	60	low	Sigma	14	10	1,687	5,9 %	21,0	4,4	30,0	17,9	47,8	1,403	80,1	0,5	4314	17,5	14,3	4,2	n/a	11,6
C8	60	high	Sigma	14	20	1,680	5,7 %	21,6	1,0	20,8	11,2	46,9	1,421	70,6	0,6	5701	23,5	17,8	4,5	n/a	13,4
C13	60	high	Sigma	19	10	1,495	7,1 %	23,4	0,1	25,1	8,7	45,9	1,443	69,5	0,7	6292	27,9	18,7	4,2	n/a	15,1
C16	60	low	Sigma	19	20	1,661	6,9 %	23,4	4,1	10,3	2,1	12,4	1,436	70,4	0,4	6759	28,6	18,0	4,3	n/a	15

RCO_2 - CO_2 reactivity, R air - air reactivity, SER - specific electrical resistivity, YM - Young's modulus, CCS - cold compression strength, Perm - air permeability, CTE - coefficient of thermal expansion, T_{eq} - equivalent temperature TSR - thermal shock resistance

The experimental data were analyzed using the statistical software MINITAB™ [88]. Factorial design allows for the simultaneous study of the effects that several factors may have on the process. When performing an experiment, varying the levels of the factors simultaneously rather than one at a time is efficient in terms of time and cost, and also allows for the study of interactions between the factors. Without the use of factorial experiments, important interactions may remain undetected. In our case a half fractional factorial design was used in factor screening as they reduce the number of runs to a manageable size.

Results are presented in Pareto charts to compare the relative magnitude and the statistical significance of both main and interaction effects. MINITAB™ plots the effects in decreasing order of the absolute value of the standardized effects and draws a reference line on the chart. Any effect that extends past this reference line is significant.

4.6.1 Characterization of green anodes by image analysis

The image analysis of the green anodes presented in Table 4.6-II was carried out in order to characterise the differences due to composition and variations in manufacturing conditions. The common procedure [89] as described in Chapter 1.6.2 was used. The influence of mixer type, mixing time and fines in the green state were studied with regards to the green porosity and pitch thickness film around the coke particles. Detailed production parameters of the selected samples are shown in Table 4.6-II.

The Fig. 4.6-2 shows the pitch distribution curves for 14, 16.5 and 19 % pitch contents. Each curve represents the pitch distribution of one green segment drilled from the centre of a pilot scale anode. In general there was observed an increase of the pitch thickness film with increasing pitch content. Fig. 4.6-1 a) shows a pitch distribution plot for 14 % pitch anodes. The position of the maximum peak of the pitch thickness indicates that thinner film is developed when the intensive mixing technique is used. With increasing fineness of the dust fraction the pitch thickness layers become thinner. These results correlate well with measurements done by Rørvik et al. [89].

Fig. 4.6-2 b) compares samples with 16.5 % pitch content produced in the intensive and the sigma mixer. The samples had the same composition and granulometry of the dust fraction. For intensive mixing reduced pitch layer thickness was found compared with sigma mixing. This observation supports the theory that during intensive mixing there is a uniform spread of the pitch over the coke particles which results in a thinner and more continuous binder film. Slow sigma mixing results in a thicker binder film.

Fig. 4.6-2 c) compares pitch distribution curves for 19 % pitch content samples. A similar situation as in the case of 14 % pitch content was observed. The intensive mixing technique induced development of the thinner pitch layer. The pitch distribution curves show that for coarse fines the thickness of the pitch layers is greater.

a) 14 % pitch content

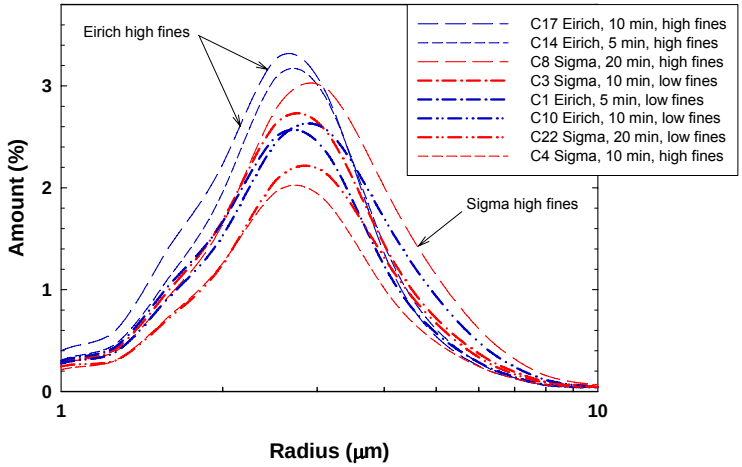

b) 16.5 % pitch content

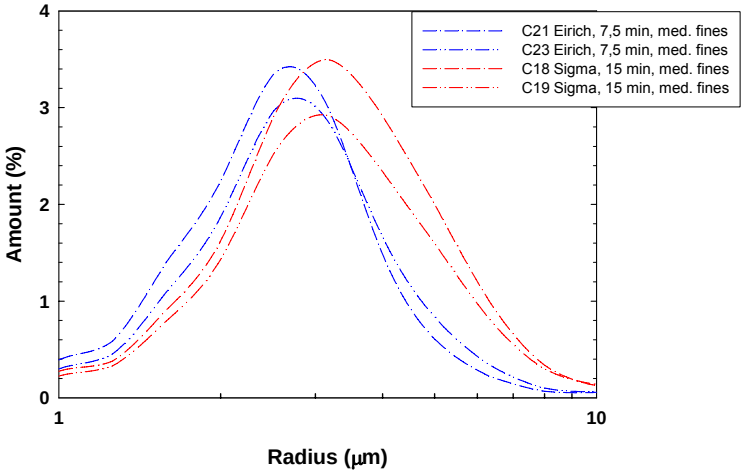

c) 19 % pitch content

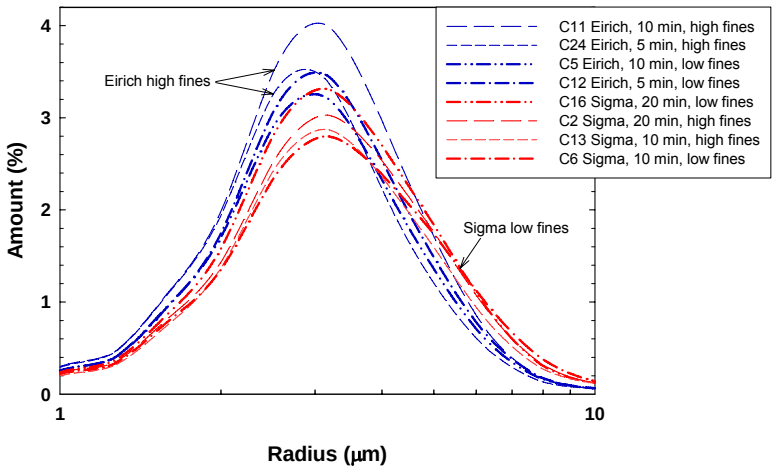

Fig. 4.6-2. Pitch thickness distribution.

In Chapter 4.6.5 (Fig. 4.6-18 to Fig. 4.6-23) the pore size distribution curves for the baked samples was presented. The largest difference was observed for 14 % pitch samples. Fig. 4.6-3 shows the porosity distribution curves for the same samples in the green state. As in baked state, there is a marked increase in process porosity (above 200 µm pore radius) for the sigma mixed samples. This porosity was present already in the green state and is due to void formation due to poor mixing. Fig. 4.6-4 shows images of two analysed areas of the samples prepared with different mixing techniques. Visual inspection of both images reveals the presence of large pores in the case of sigma mixed samples. These pores were created due to incomplete compaction of the green paste and gas entrapment during mixing.

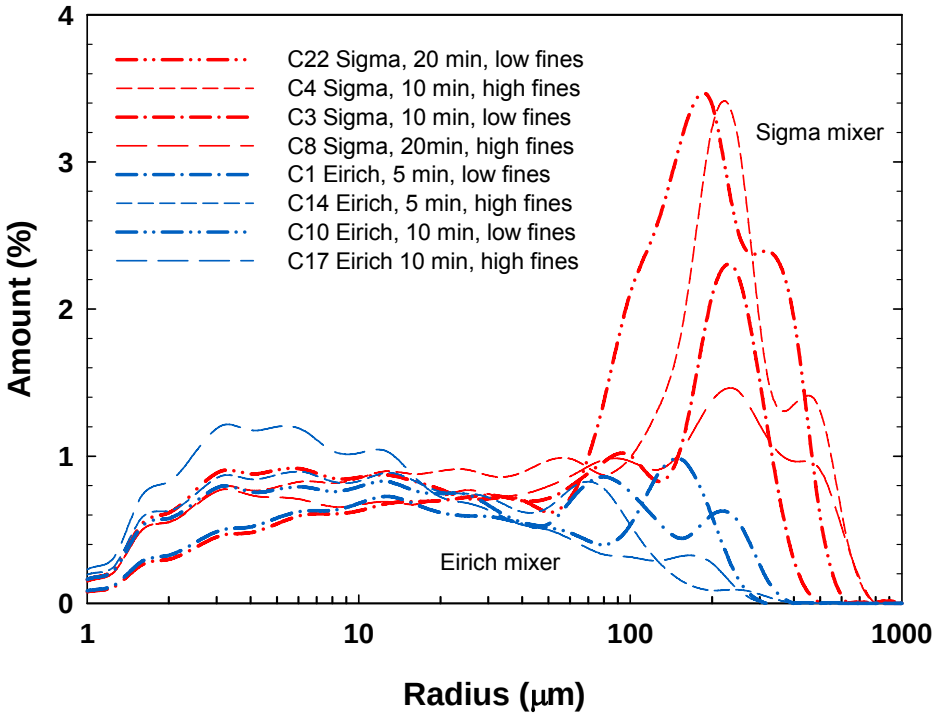

Fig. 4.6-3. Pore size distribution for green samples with 14 % pitch content.

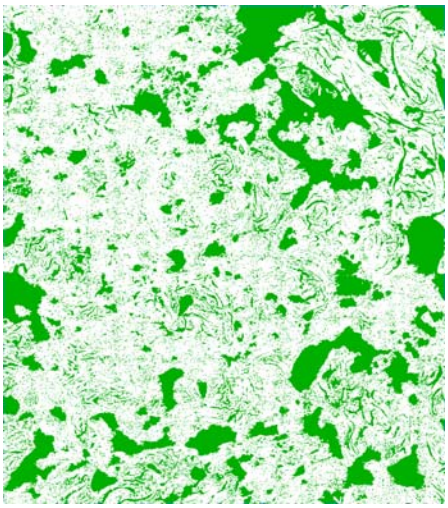

a) Sample C4, 14 % pitch content, 10 minutes sigma mixing, high fines.

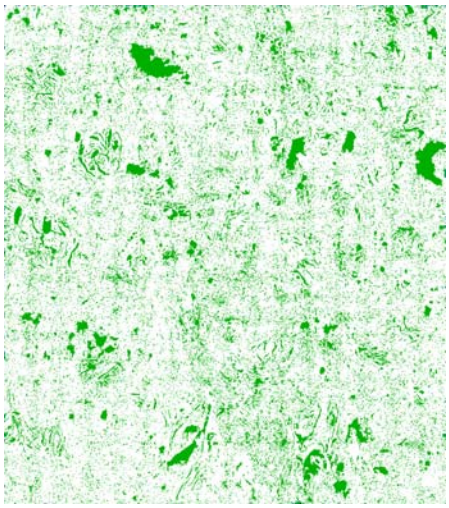

b) Sample C17, 14 % pitch content, 10 minutes intensive mixing, high fines.

Fig. 4.6-4. Overview of the green porosity for two analysed areas. In the case of sigma mixing (left) there are large voids in the intergranular space caused by poor mixing. Intensive mixing (right) has much lower porosity. Magnification 160 x.

4.6.2 Green density

There are three statistically significant effects influencing green density as seen from the Pareto chart in Fig. 4.6-5. Two main effects, pitch content (E) and mixer type (C), and one interaction effect, pitch content by mixer type (CE). The effect of pitch content is the largest. The effect of the mixing time (D) is considered statistically insignificant. The reason for his is individual setting of mixing times for each of the mixers.

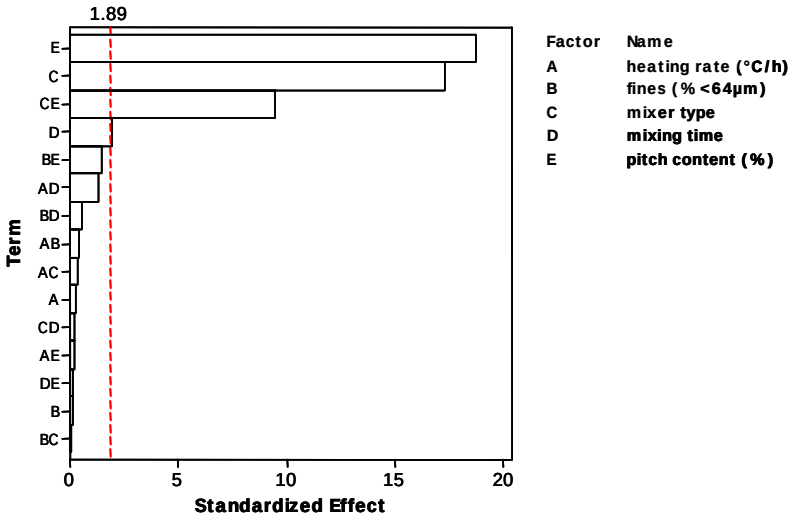

Fig. 4.6-5. Pareto chart of the standardized effects for green density.

The overall data are shown in Fig. 4.6-6. Intensive mixing gives higher green densities for anodes with the same pitch content compared to those mixed in the sigma blade mixer. The reason is probably due to better statistical distribution of grain sizes throughout the paste for intensive mixing. Also, sigma mixing may have lower possibility of filling and impregnating intergranular voids due to lower dynamic pressure gradients imposed by the mixer.

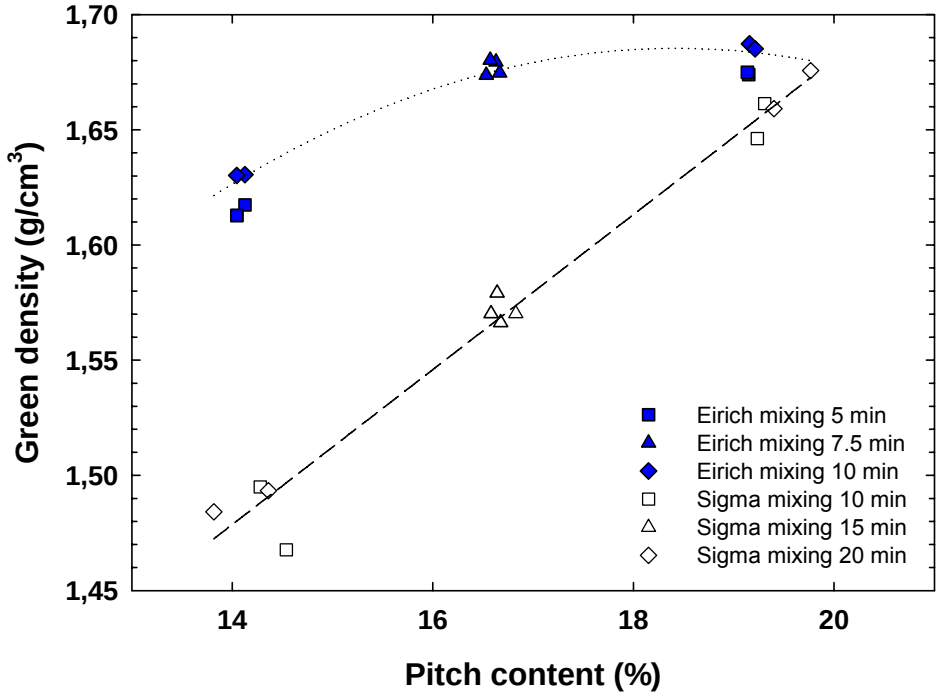

Fig. 4.6-6. Comparison of green density for intensive and sigma mixing.

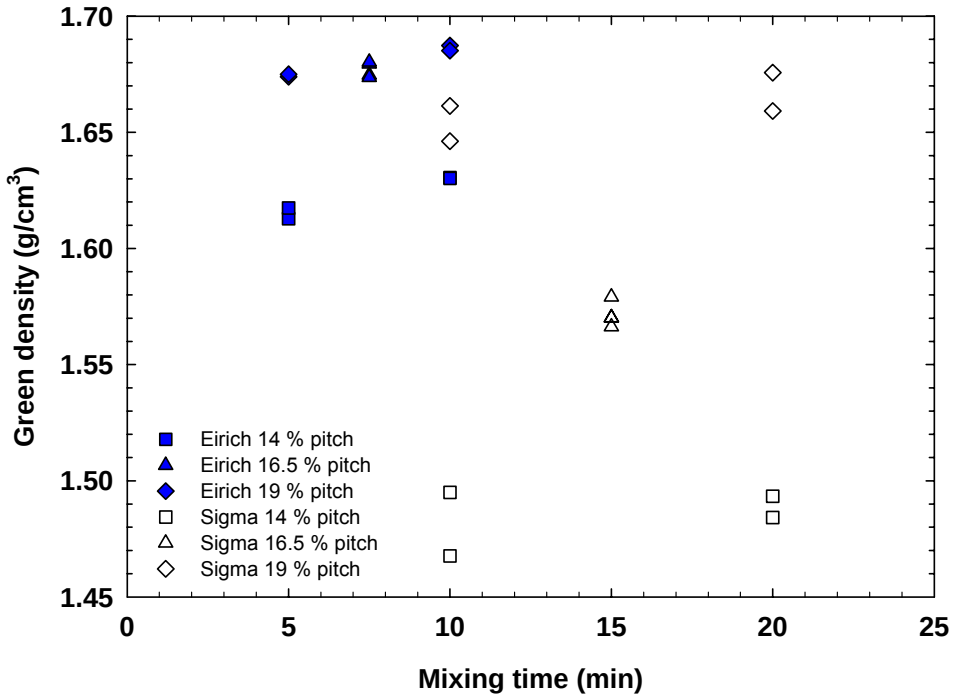

Fig. 4.6-7. Effect of mixing time for intensive and sigma mixing.

Fig. 4.6-7 compares mixing times for both mixing techniques. It shows that intensive mixing is more efficient and results in higher green densities at shorter mixing times but sigma mixer attains the same high density for 19 % pitch and 20 minutes mixing time.

4.6.3 Baked density

Fig. 4.6-8 shows the Pareto plot of the standardized effects for baked density and compares relative magnitudes and statistical significance of both main and interaction effects. There are nine statistically significant effects influencing the baked density. These include all the main effects: mixer type, heating rate, mixing time, fines and pitch content. Factor C, mixer type, has the largest effect on the baked density. The second largest effect is the interaction mixer type by pitch content (CE). The third in relative magnitude is the effect of the heating rate (A). Other effects have approximately the same influence on the baked density, but much lower in relative magnitude. These results are logical as the mixer type and pitch content strongly influences density in the green state. The amount of pitch volatiles and thus the mass and density reduction of the sample depend on the heating rate during baking. The faster heating, the more volatiles are released and the lower baked density is obtained.

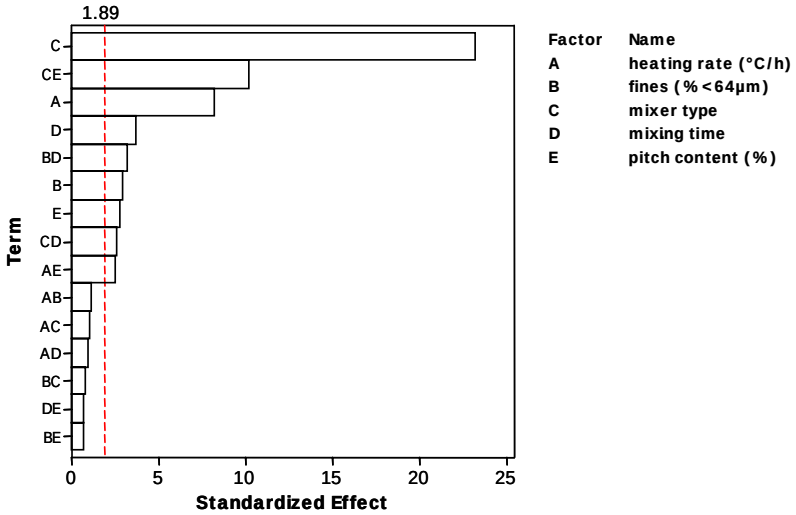

Fig. 4.6-8. Pareto chart of the standardized effects on baked density.

Another graphical display for result interpretation is the interaction plot. The interaction plot helps to assess the two-factor interactions in a design. An interaction is present when the effect of one factor depends on a second factor. Evaluating the alignment of the lines determines if there is an interaction. The greater the lines depart from being parallel, the greater the degree of interaction. If the lines are parallel, there is no interaction.

The interaction plot in Fig. 4.6-9 indicates a decrease of baked density with increasing heating rate for both mixers. The effect of the heating rate on the baked density seems to be independent of the mixer type. A strong interaction between mixer type and pitch content is demonstrated. The overall data are shown in Fig. 4.6-10. Intensive mixing results in higher baked density for samples with 14 % pitch content compared to the sigma mixer. The reason is probably again due to better statistical distribution of the aggregate and better pitch impregnation in coke particles during the intensive mixing.

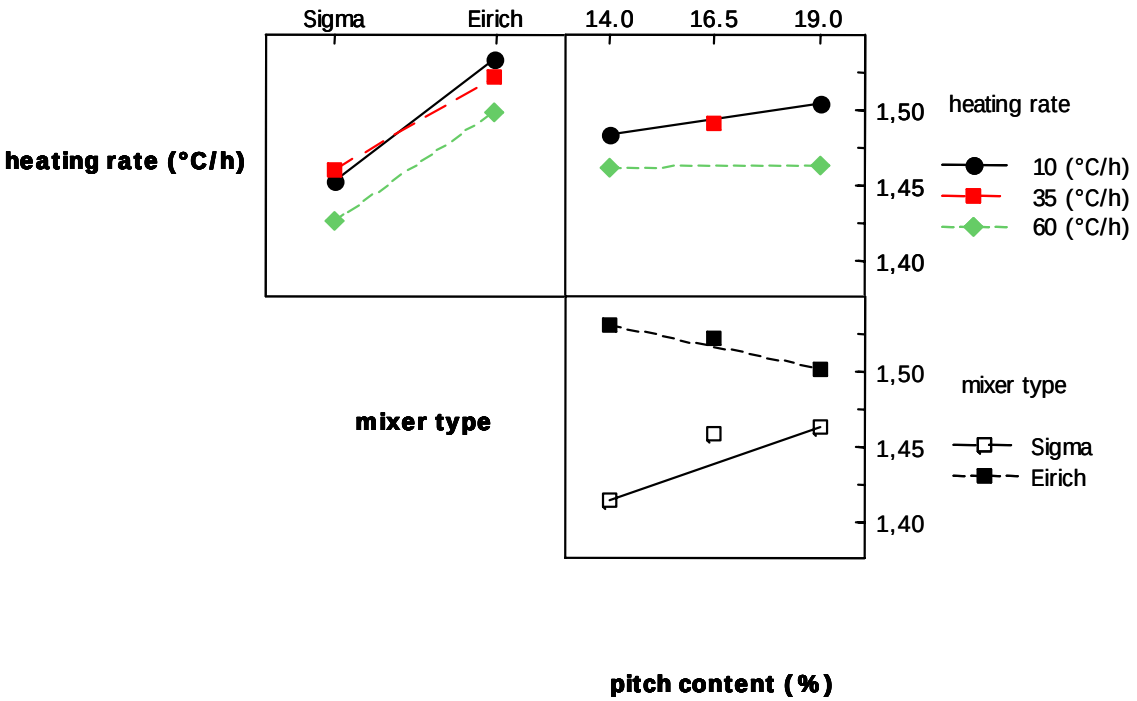

Fig. 4.6-9. Interaction plot for baked density.

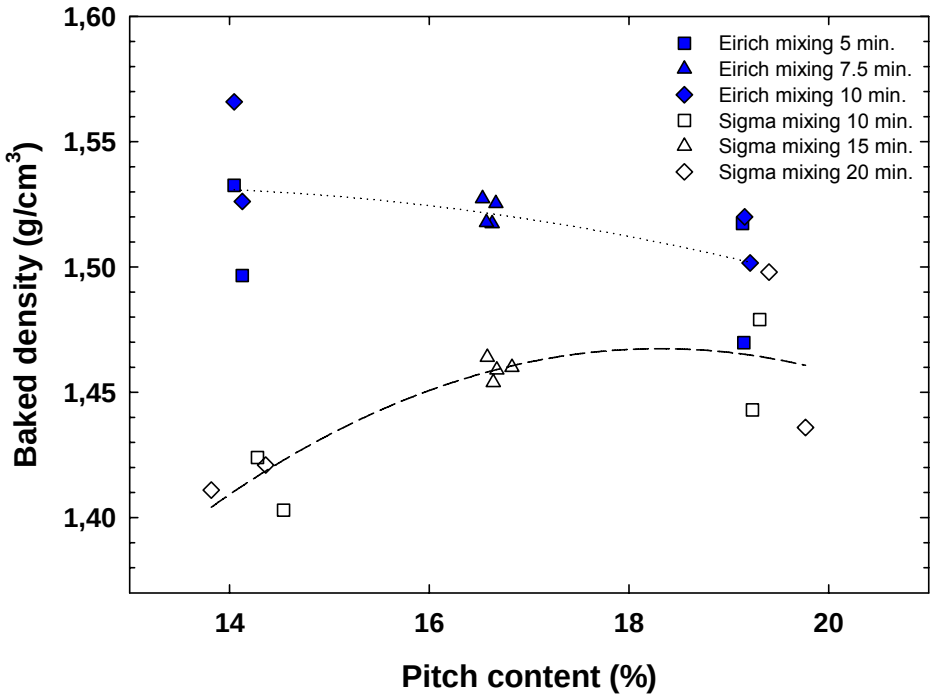

Fig. 4.6-10. Baked apparent density-effect of pitch content and mixer type.

The finest particles (dust fraction) in the sigma mixer settle at the bottom of the mixer and are not homogeneously distributed through the paste. Aggregate mixed in the intensive mixer has better statistical distribution of pitch and fines forming a continuous binder film over the coke particles (Fig.4.6-11 a, b). This may result in a more coherent

paste that will maintain the higher density after baking. There is presence of the larger pores for sigma mixed samples in green state (outlined with white colour).

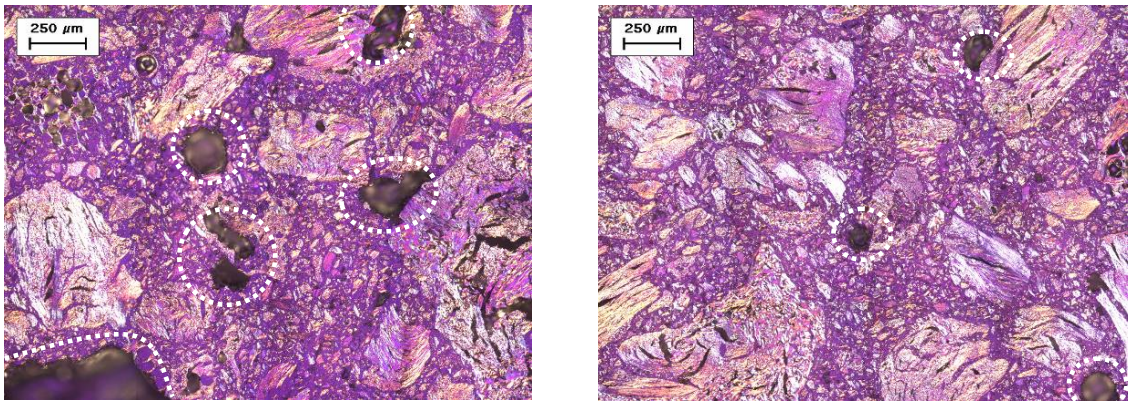

a) Sample C13, 10 min. Sigma mixing, 19 % pitch, high fines, green density 1.646 g/cm^3

b) Sample C11, 10 min. Intensive mixing, 19 % pitch, high fines, green density 1.685 g/cm^3

Fig.4.6-11. Overview of the green samples mixed with Sigma and intensive mixer. Magnification 160 x, polarized light.

4.6.4 Specific electrical resistivity

Fig. 4.6-12 shows the Pareto plot for the specific electrical resistivity. There are two statistically significant factors. One main effect is the mixer type (C) and there is an interaction effect mixer type by pitch content (CE). Other factors have no significant effect on the specific electrical resistivity.

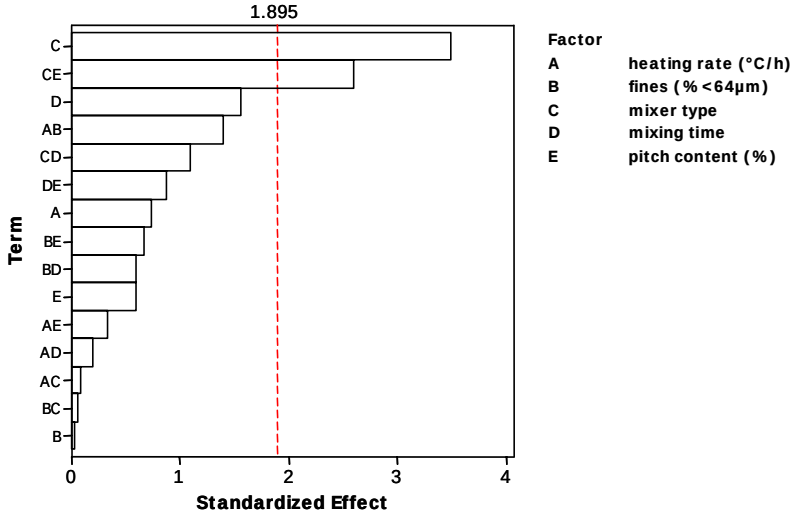

Fig. 4.6-12. Pareto chart of standardized effects on specific electrical resistivity.

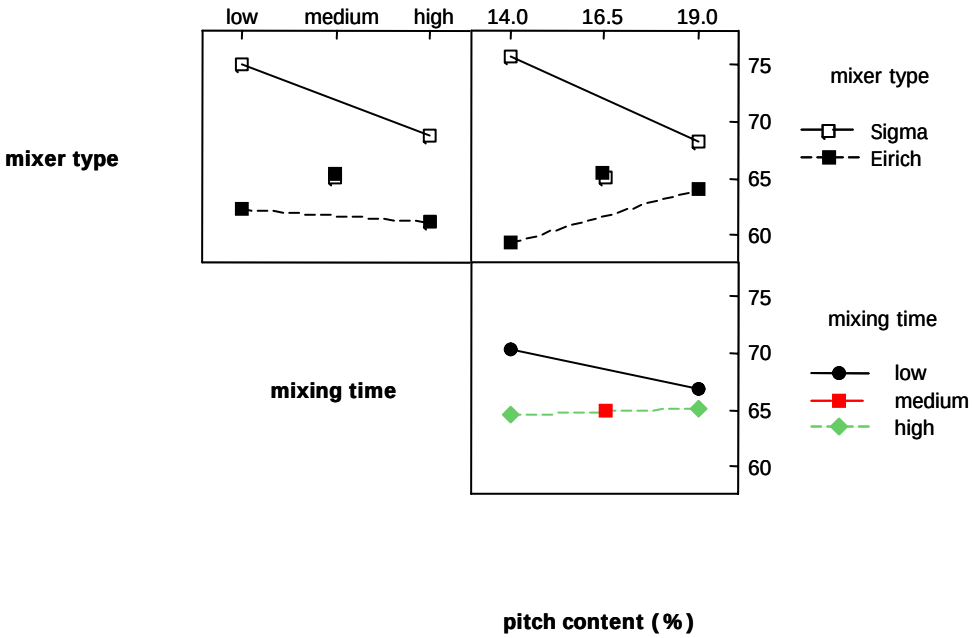

Fig. 4.6-13. Interaction plot for specific electrical resistivity.

Fig. 4.6-13 demonstrates that the largest interaction is between the pitch content and the mixer type. However, a weak interaction between mixer type and mixing time is observed. Increasing mixing time from 10 to 20 minutes for the sigma mixer will cause a reduction in resistivity while for the intensive mixer the effect of time is not so strong. The complete data set for the main effects is shown in Fig. 4.6-14.

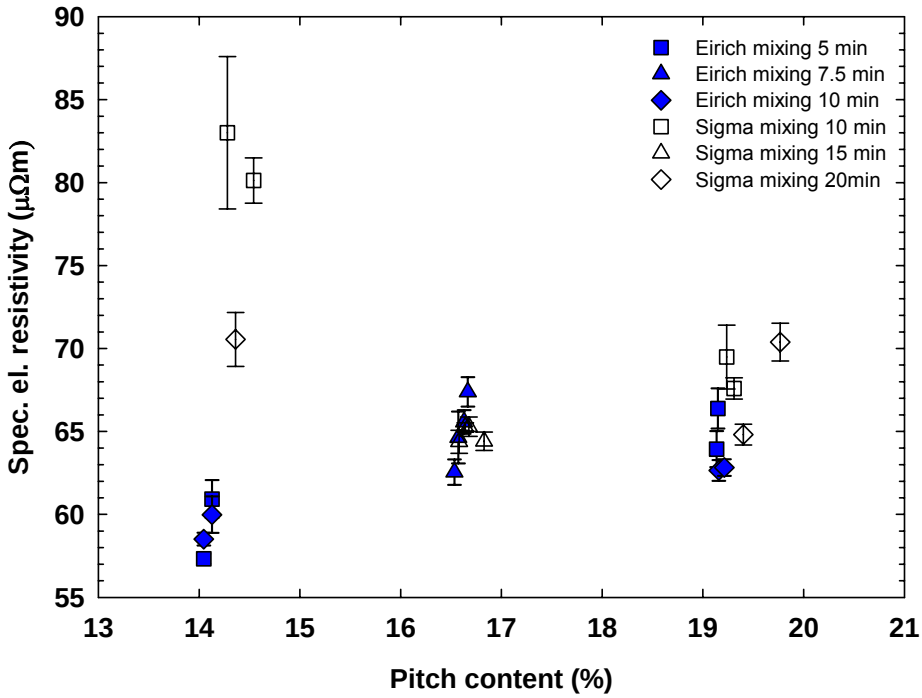

Fig. 4.6-14. Effect of pitch content and mixer type on specific electrical resistivity.

The specific electrical resistivity decreases with increasing pitch content for sigma mixing, while intensive mixing shows a moderate increase. Resistivities of the samples with 14 % pitch deviate strongly. The reason for this is the mixing technique combined with the low pitch content. In the sigma mixer crushing of particles occurs and new surface is created that has to be coated with pitch. Sigma mixing is slow and less intensive and the paste has more homogeneity defects. Thus less pitch ends in the intergranular space to create continuous binder coke around coke particles to ensure good electrical contacts. With increasing pitch content this effect is reduced as the amount of pitch in the intergranular space increases (Fig. 4.6-25, Fig. 4.6-26 and Fig. 4.6-27). The standard deviation of the resistivity values reflects the homogeneity and consistency of the paste. For sigma mixed samples there is an indication that the specific electrical resistivity passes through the minimum at 16.5 % of pitch. Similar behaviour of the pilot scale anodes was observed by several studies [36, 51, 90].

The opposite situation is observed for samples with 14 % pitch content mixed in the intensive mixer. These show the lowest values for the specific electrical resistivity of all anodes. The reason is even pitch distribution and thus better electrical contact between filler particles. There is also good correlation between baked densities (Fig. 4.6-10) and the specific electrical resistivity in Fig. 4.6-14. Samples with 14 % pitch mixed in the sigma mixer show the lowest baked densities and thus the highest resistivities.

4.6.5 Baked Porosity

There are four statistically significant factors for the total porosity. Three main effects: mixer type (C), pitch content (E) and heating rate (A). In addition there is one interaction effect between pitch content and mixer type (CE).

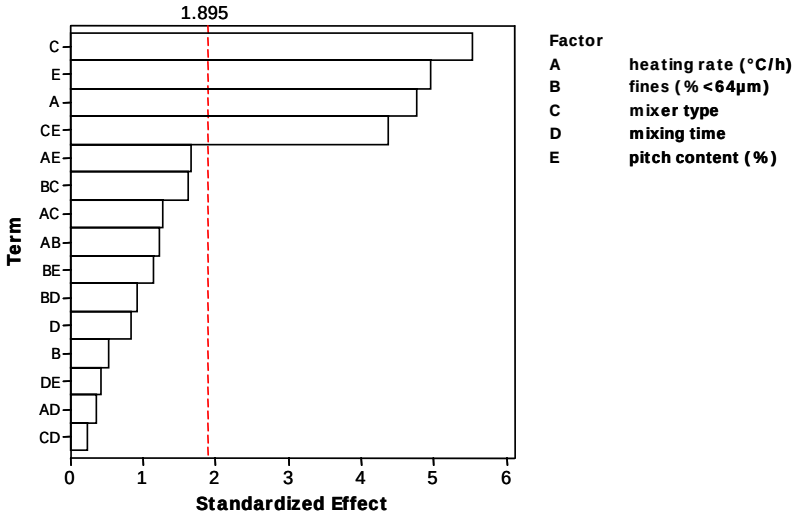

Fig. 4.6-15. Pareto chart of standardized effects on total porosity.

It is possible to estimate the interaction between two factors in Fig. 4.6-16. The strongest interaction is observed between mixer type and pitch content (CE). It is expected after previous results (Fig. 4.6-9) that mixer type and pitch content will influence the porosity as well. There is a larger porosity reduction for the intensive

mixer when lowering the pitch content to 14 % compared to the sigma mixer. Intensively mixed samples were also those with the highest baked densities and lowest specific electrical resistivities. Voids between aggregate particles and sample porosity depend strongly on pitch content and the process steps during paste production. Thus mixing plays the most important role in aggregate packing and void filling. The effect of the heating rate is also observed from the interaction plot in Fig. 4.6-16. Increase of the heating rate will cause an increase in porosity regardless of mixer type.

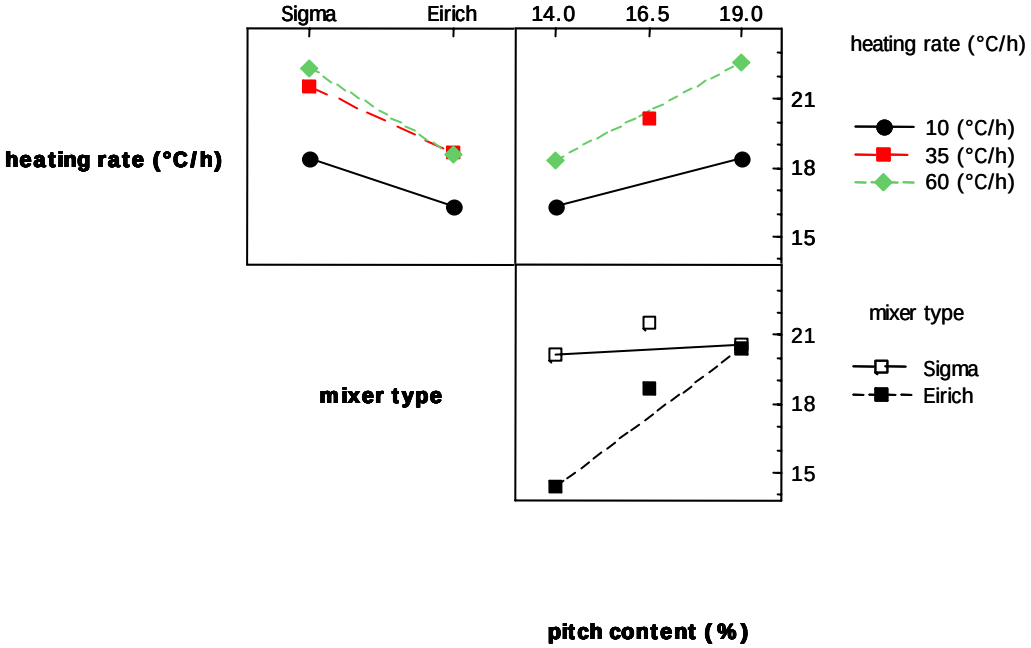

Fig. 4.6-16. Interaction plot for total porosity.

Fig. 4.6-17 compares the average total porosity values for samples from both mixers. Each column represents the average of four porosity values for pilot scale anodes with the same pitch content. The magnitudes of the standard deviation error bars reflect paste homogeneity and consistency with respect to mixer type. Sigma mixing results in more porous anodes compared to the intensive mixing. There may be several reasons for this. The intensive mixer provides more efficient mixing that result in denser and less porous samples. The second reason could be the higher shear rate of the sigma mixer that was observed also in Chapter 4.2. The coke particles are crushed more extensively during mixing of dry (14 % pitch) paste. As the pitch content increases in sigma mixed samples, more pitch is available to supply the binder demand due to crushing. In case of intensive mixing increase of porosity with increasing pitch content is related mostly to the volatile pore evolution. This fact is also indicated in Fig. 4.6-16 where samples baked with high heating rate tend to show higher porosity values.

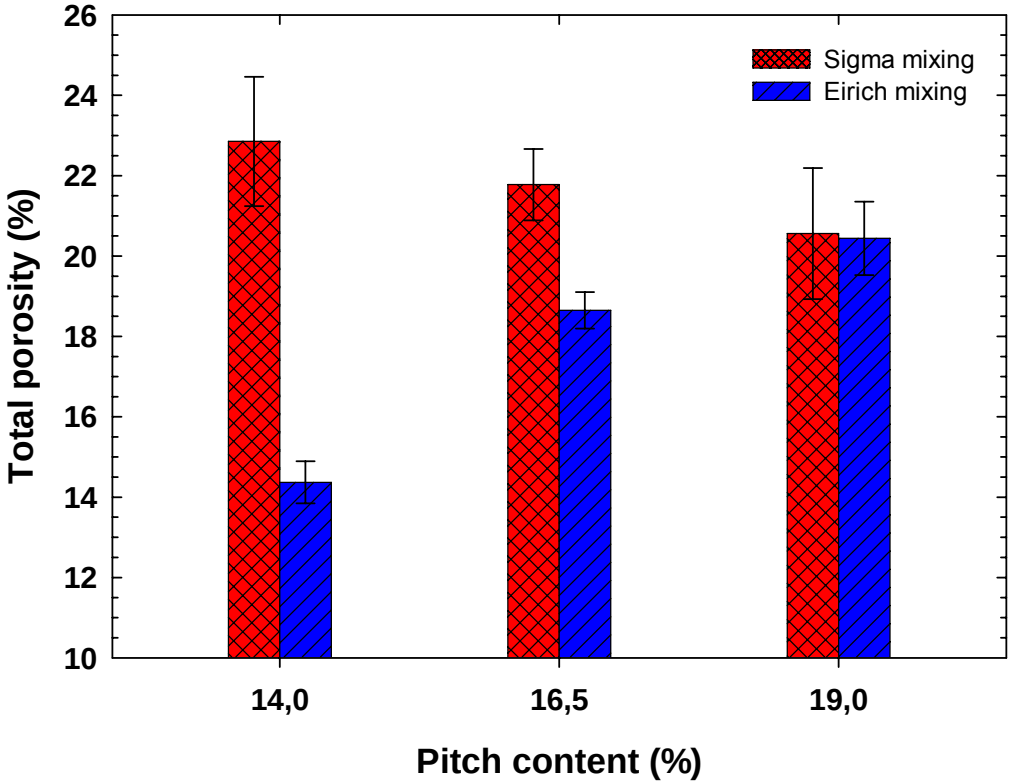

Fig. 4.6-17. Effect of pitch content and mixer type on total porosity.

Fig. 4.6-18 to Fig. 4.6-23 show pore size distribution curves for paste from the sigma and intensive mixer. Each curve represents the average porosity distribution of four segments analysed for one pilot scale anode. In the case of 14 % pitch sigma mixed samples porosity development is strongly affected by mixing time, as shown for samples mixed for 10 and 20 minutes (Fig. 4.6-18). With increasing mixing time more coke grains are crushed and thus the dry aggregate composition deviates strongly from target which results in void formation. Fig. 4.6-21 illustrates porosity distribution of the 14 % pitch anodes mixed by the intensive mixer. Compared to sigma there is a significant reduction of the porosity above 100 µm which probably refers to minimised presence of voids due to mixing pores. As the pitch content increases to 16.5 % and 19 % for both mixers, the porosity distribution is more influenced by contribution of volatile pores (pores of 100 µm radius that are created in the binder during pitch carbonization). Thus, a heating rate from 10 to 60 °C/h will cause increase of porosity for 19 % pitch samples (Fig. 4.6-20 and Fig. 4.6-23). This is clearer for intensive mixed samples, where the degree of particle crushing is far less.

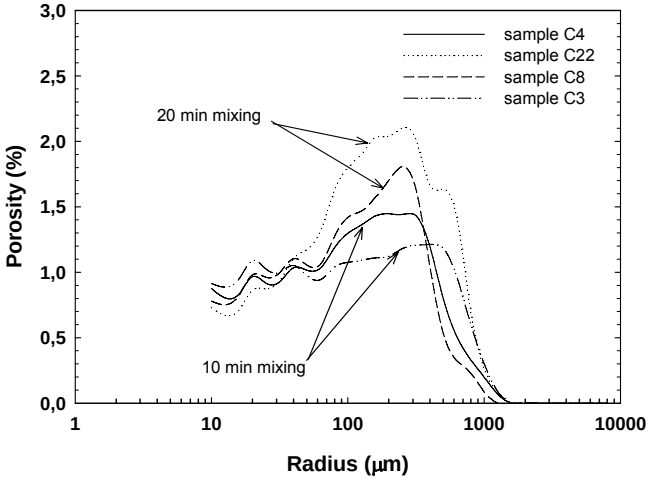

Fig. 4.6-18. Sigma mixer 14 % pitch content. The effect of mixing time.

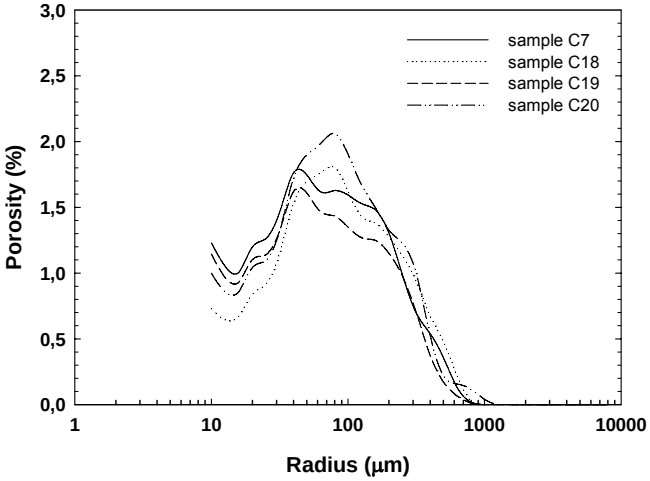

Fig. 4.6-19. Sigma mixer 16.5 % pitch content. Parallel samples with uniform composition (centre points).

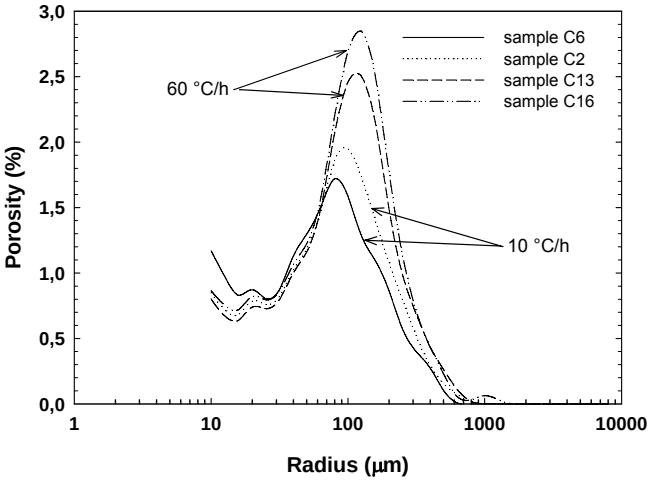

Fig. 4.6-20. Sigma mixer 19 % pitch content. The effect of heating rate.

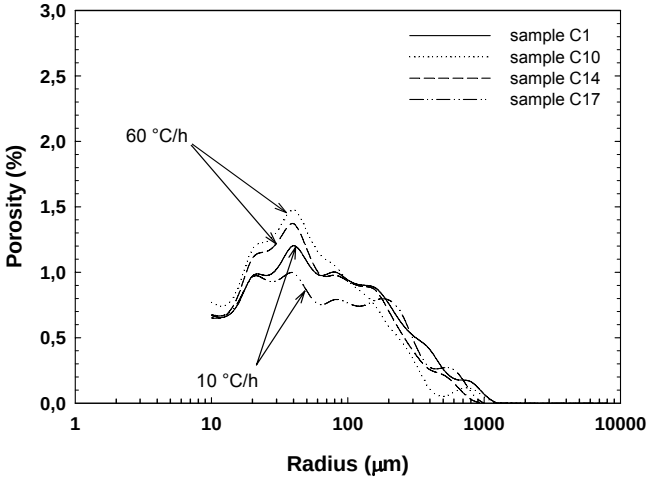

Fig. 4.6-21. Intensive mixer 14 % pitch content. Effect of heating rate.

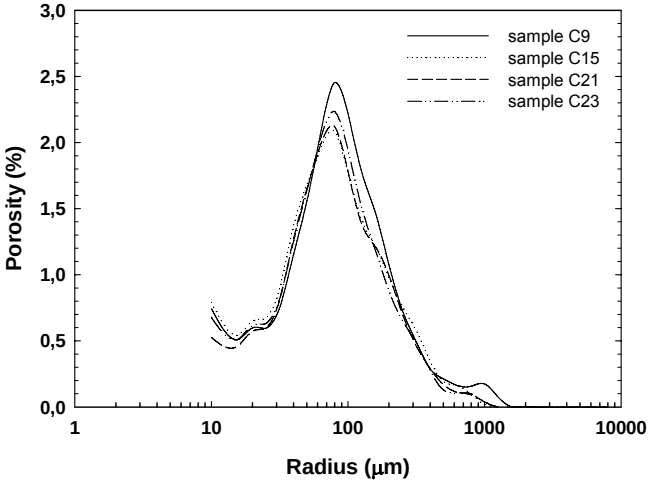

Fig. 4.6-22. Intensive mixer 16.5 % pitch content. Parallel samples with uniform composition (centre points).

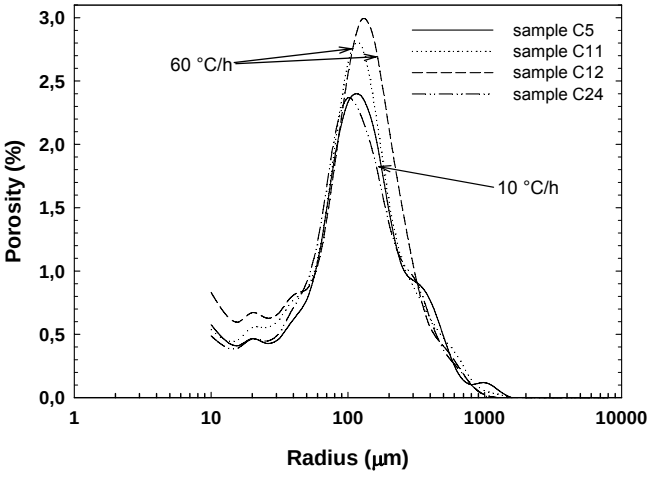

Fig. 4.6-23. Intensive mixer 19 % pitch content. Effect of heating rate.

Fig. 4.6-24 shows a summary comparison of average pore size distribution curves. Each curve represents the average pore distribution of four anodes with the same pitch content. As shown before, there is a significant difference for the samples with 14 % pitch content. Sigma mixing shows a peak around 300 µm. This indicates the presence of large pores that are caused mostly by aggregate crushing and void formation in a poorly mixed paste. Intensive mixing with 14 % pitch showed the lowest porosity of all samples. For 16.5 % pitch content samples mixed in the sigma mixer have higher amounts of pores from 10 up to 50 µm compared to those mixed in the intensive mixer. This is observed also for the 19 % pitch samples. The reason for this is probably better impregnation of coke pores within this size interval caused by high speed intensive mixing. With increasing pitch content the distribution curves tend to be more similar in shape. A peak distribution with porosity maximum at 100 µm pore radius becomes dominant with increasing pitch content. This may be due to excessive development of pitch volatile pores due to over-pitched anodes.

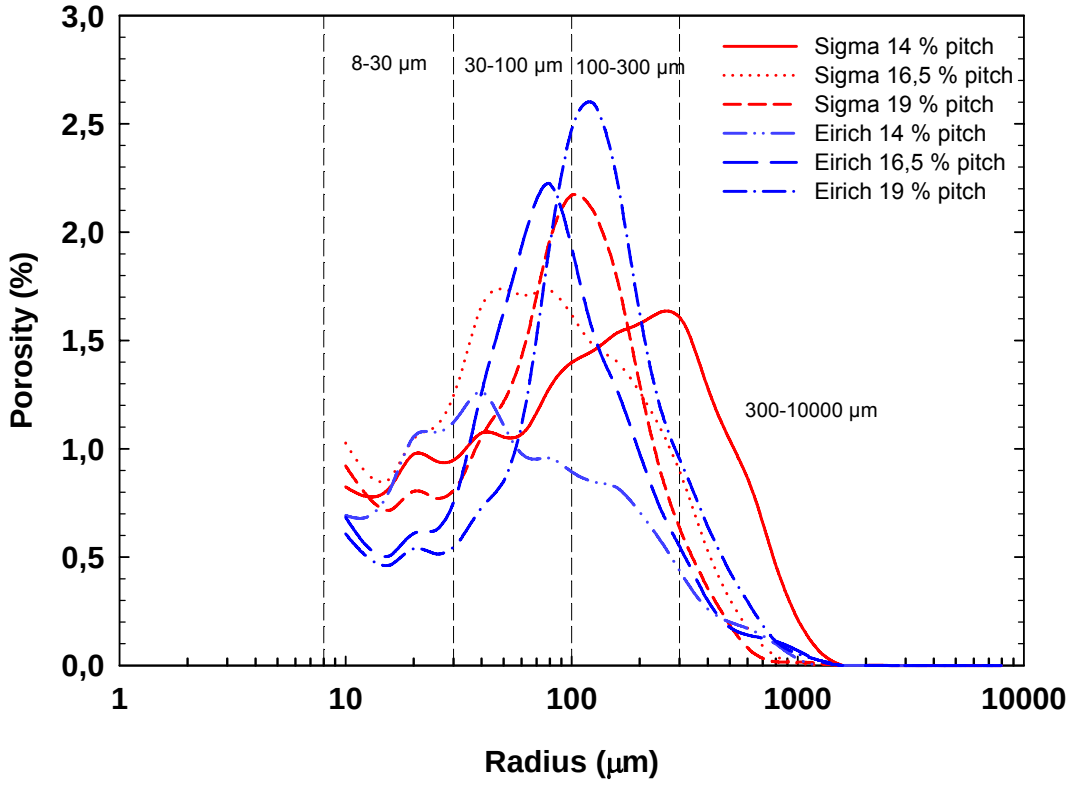

Fig. 4.6-24. Pore size distribution curves for samples with same pitch content.

Another set of plots was constructed for better comparison. Pores are grouped into four size intervals, (8-30 µm, 30-100 µm, 100-300 µm and 300-10000 µm) as indicated in Fig. 4.6-24. In Fig. 4.6-25 to Fig. 4.6-27 a comparison of pore size intervals for both mixing techniques with constant pitch content is shown. Each set of four columns represents averaged porosity values for four anodes divided into pore size intervals. Fig. 4.6-25 shows the pore size range comparison for totally eight anodes with 14 % pitch for both mixing techniques. There is an increasing porosity above 100 µm for sigma mixed samples, while other porosity intervals do not show significant difference. In

addition, for illustration there is an image of the analysed area for randomly picked segment.

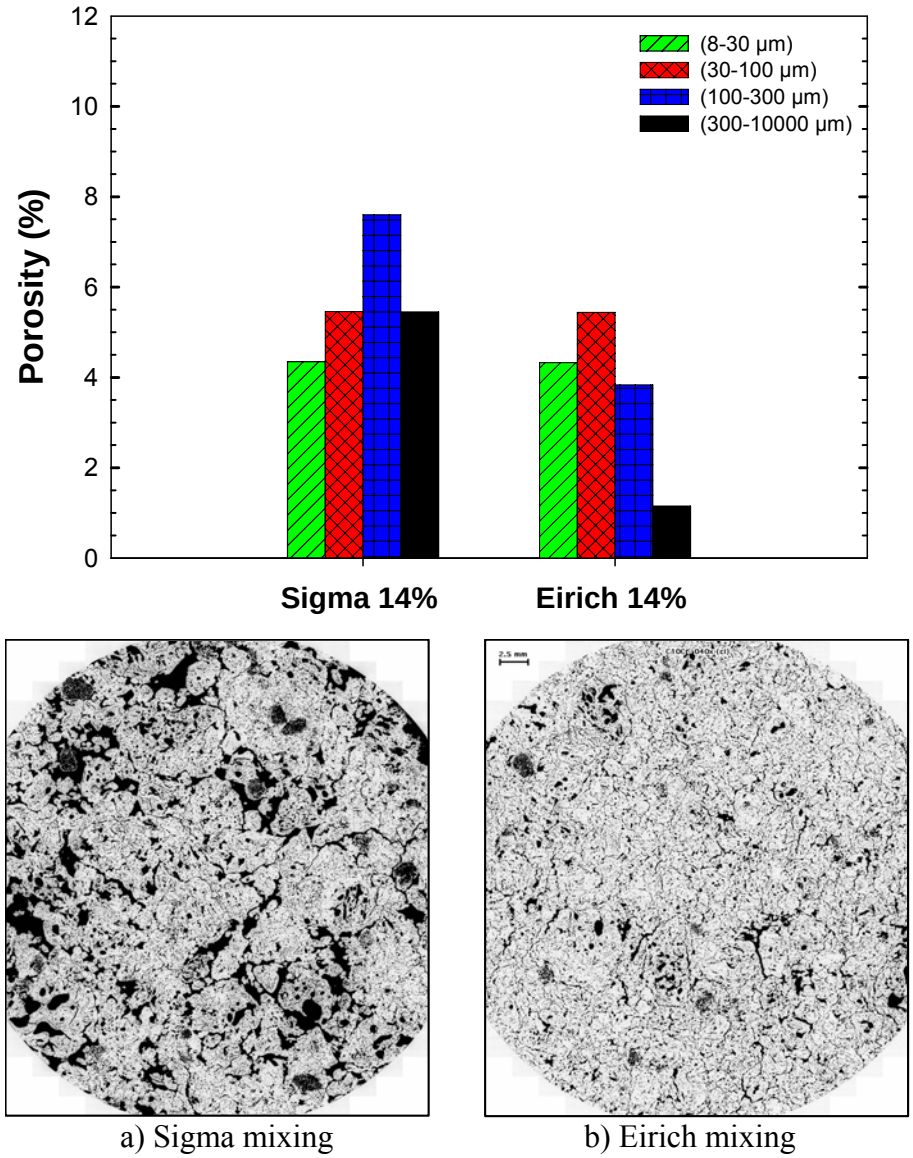

a) Sigma mixing b) Eirich mixing

Fig. 4.6-25. Pore size range comparison for samples with 14 % pitch content. The effect of mixing techniques on porosity development, scale bar 2.5 mm.

Fig. 4.6-26 compares average pore size ranges for the medium pitch level, 16.5 %. Anodes mixed in the intensive mixer indicate a lower amount of small pores and also a lower portion of the largest pores. The lowering of porosity within the interval 8-30 µm may be caused by better pitch penetration into coke particles during intensive mixing.

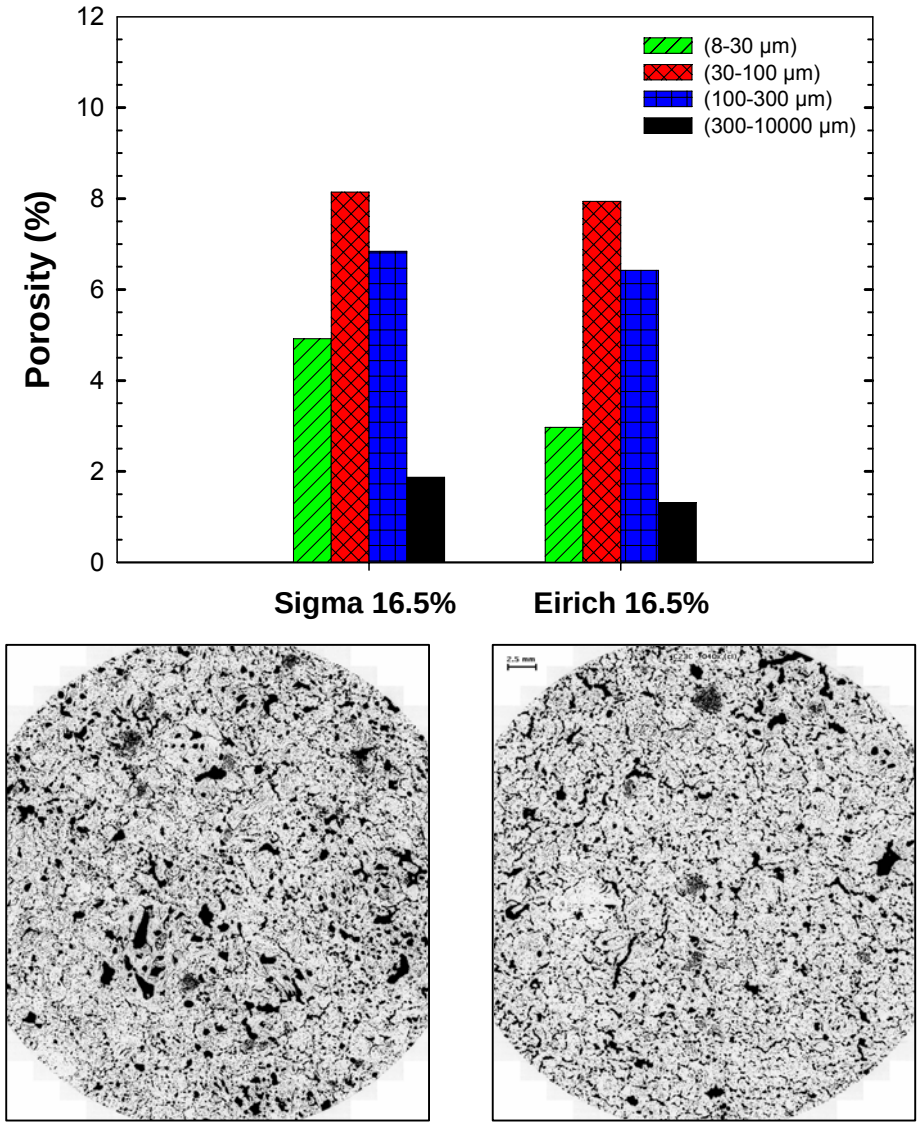

a) Sigma mixing b) Eirich mixing

Fig. 4.6-26. Pore size range comparison of the samples with 16.5 % pitch. The effect of mixing techniques on porosity development, scale bar 2.5 mm.

At 19 % pitch content differences between the mixer types are reduced. However, for the intensive mixer lowering of porosity between 8-30 µm and 30-100 µm (Fig. 4.6-27) is still maintained. This may be due to better pitch impregnation of the coke particles. An interesting observation is that the intensive mixer shows a higher porosity within the 100-300 µm range. This may indicate over-pitching of the anodes. An increased amount of pitch will cause more pitch to end up in the intergranular space. When such an anode is baked the amount of binder pores within a certain radius (around 100 µm) will increase. This effect is more probable when a high intensity and less degradable mixing technique is used. Another reason could be void formation due to gas entrapment. In sigma mixing this effect may be dampened by the creation of new surface area that has to be coated with pitch due to crushing of the aggregate.

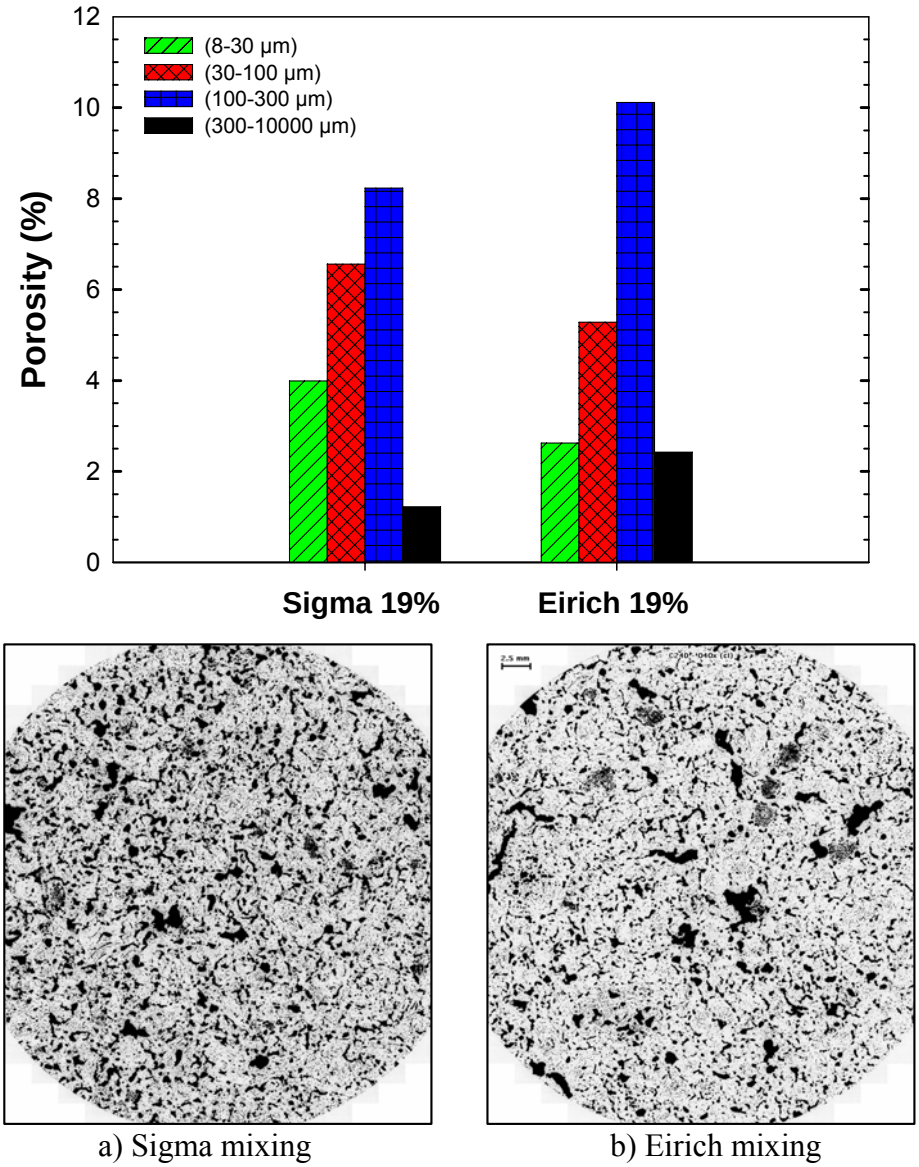

a) Sigma mixing b) Eirich mixing

Fig. 4.6-27. Pore size range comparison of the samples with 19 % pitch content. The effect of mixing techniques on porosity development, scale bar 2.5 mm.

4.6.6 Permeability

Fig. 4.6-28 shows a Pareto plot of the standardized effects on permeability. There are six statistically significant effects. Strongest influence is seen for the interaction mixer type by pitch content (CE) and mixer type (C). Next, there is also strong interaction between heating rate and pitch content. An explanation for this could be that the amount of pitch combined with heating the rate is responsible for porosity contribution from the baking pores.

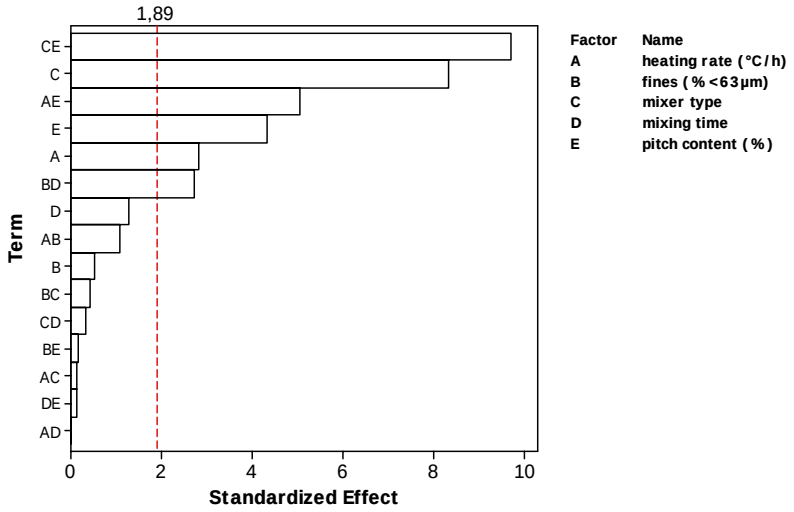

Fig. 4.6-28. Pareto chart of standardized effects on permeability.

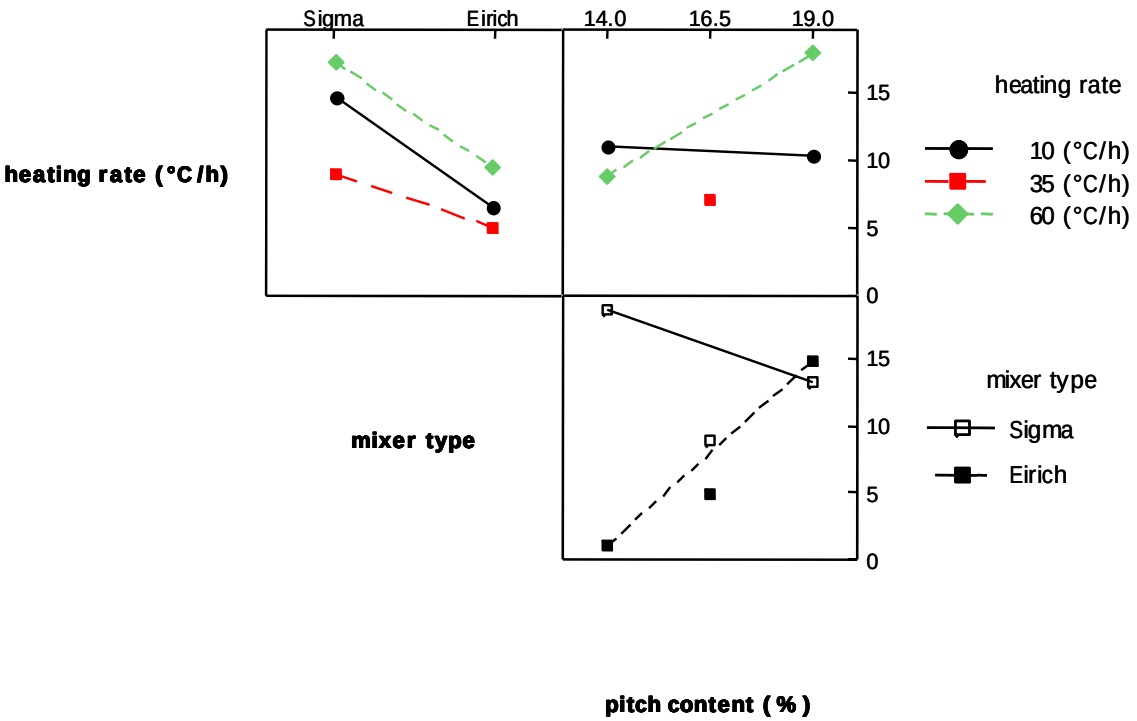

Fig. 4.6-29. Interaction plot for permeability.

The interaction plot for permeability is shown in Fig. 4.6-29. The most significant interaction, mixer type by pitch content (CE), indicates opposite results for the two mixer types. Fig. 4.6-30 shows the complete data set for permeability. Permeability for the sigma mixed samples passes through a minimum as the pitch content increases from 14 to 19 %. Optimum pitch content has been investigated by several authors [51, 91, 92]. This correlates well with the porosity distribution curves. Sigma mixed samples with 14 % had high porosity due to poor mixing. The medium pitch content (16.5 %)

seems to be optimal, and the crushing is compensated by the higher amount of pitch. Another reason for optimum permeability at this composition could be the medium fines fraction used in the production. Intensively mixed samples show increasing permeability as the pitch content increases from 14 % to 19 %. This increase of permeability is probably due to excessive development of pitch volatile pores due to over-pitched anodes. This finding also correlates well with the total porosity values in Fig. 4.6-17. The permeability increase is larger with increasing pitch content when the heating rate 60 °C/h was used compared to slow baking at 10 °C/h (AE, heating rate - pitch content interaction, Fig. 4.6-29). In the case of 10 °C/h heating rate, baking is slow and enables gradual volatile degassing of the sample without excessive development of baking pores and larger cracks. At a fast heating rate and dense anodes high internal pressure is built within the sample due to binder volatilisation. This pressure is released by escaping gases creating a porous system that is "frozen" during the following pitch solidification [57]. There is also a good correlation to the specific electrical resistivity, where similar trends were observed Fig. 4.6-14.

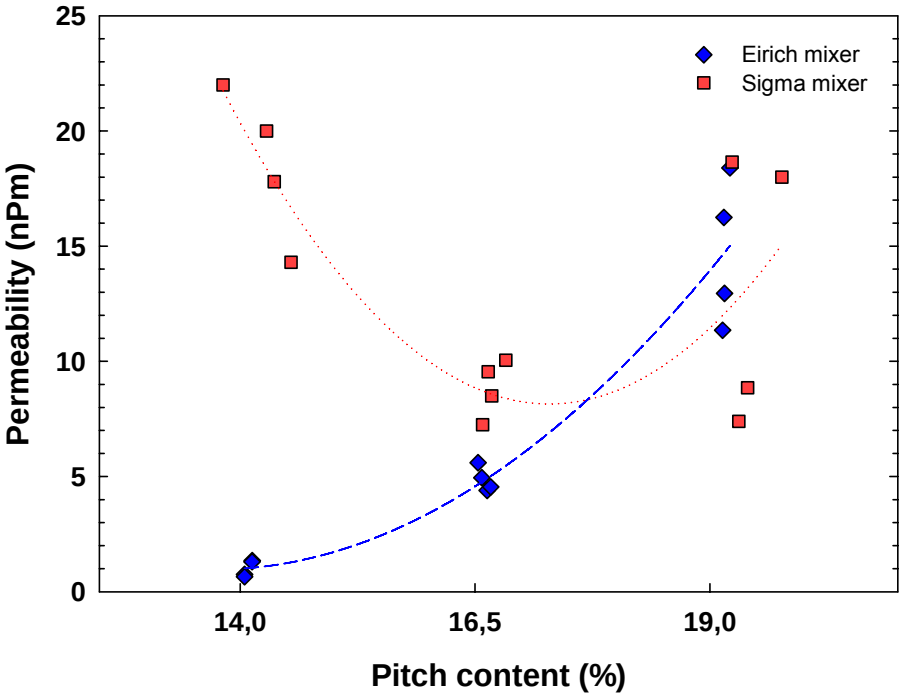

Fig. 4.6-30. Permeability. Effect of pitch content and mixer type.

4.6.7 Reactivity measurements

4.6.7.1 CO_2 reactivity

For the CO_2 reactivity there are two statistically significant effects, interaction heating rate by mixing time (AD) and main effect mixing time (D), Fig. 4.6-31. The relation between mixing time and the CO_2 reactivity with respect to mixer type is shown in Fig. 4.6-32.

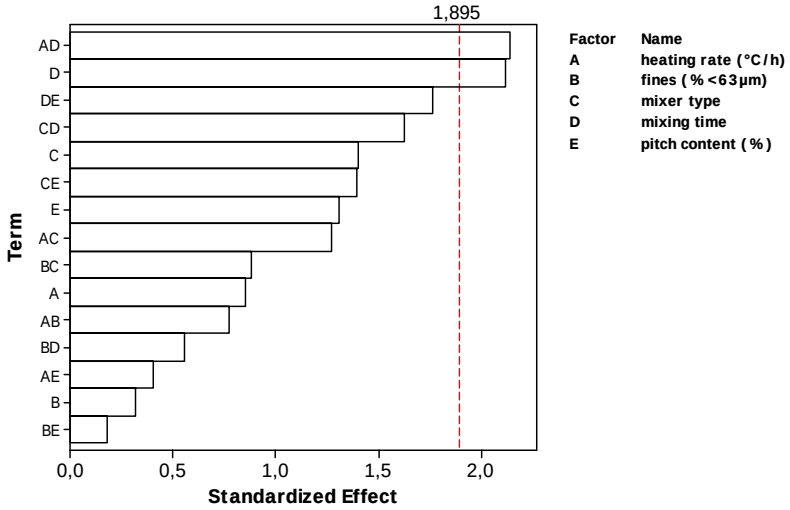

Fig. 4.6-31. Pareto chart of the standardized effects for CO_2 reactivity.

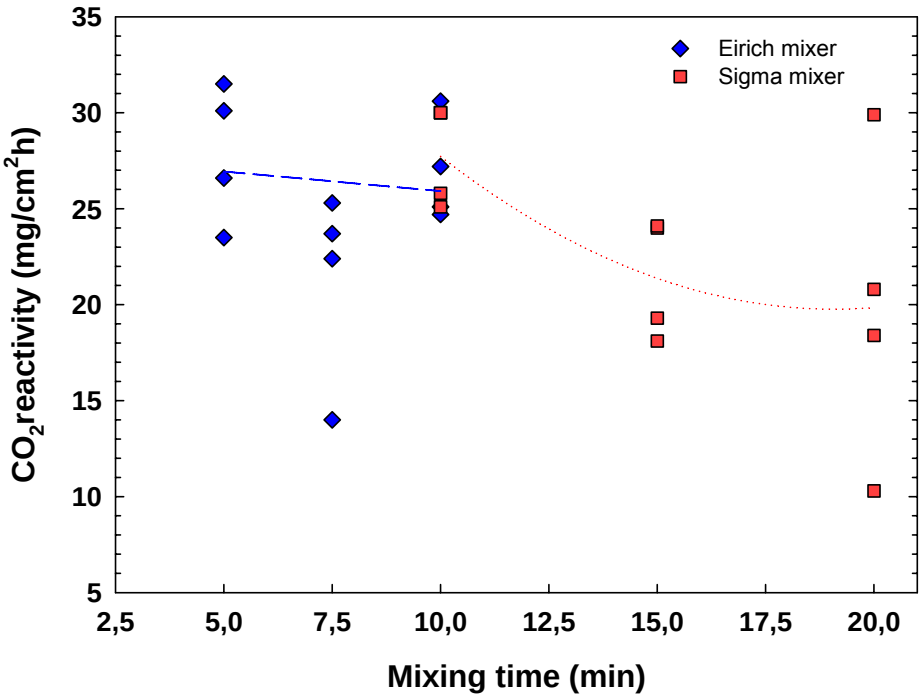

Fig. 4.6-32. CO_2 reactivity against mixing time.

Surprisingly there are lower values of CO_2 reactivities for sigma mixed samples compared to those mixed with the intensive mixer. The reason for this is uncertain and could be caused by wide scatter of the measured data. A similar situation was observed in Chapter 4.4.4 where no correlation could be found.

4.6.7.2 Air reactivity

From Fig. 4.6-33 we see that no statistically significant effects on air reactivity are found.

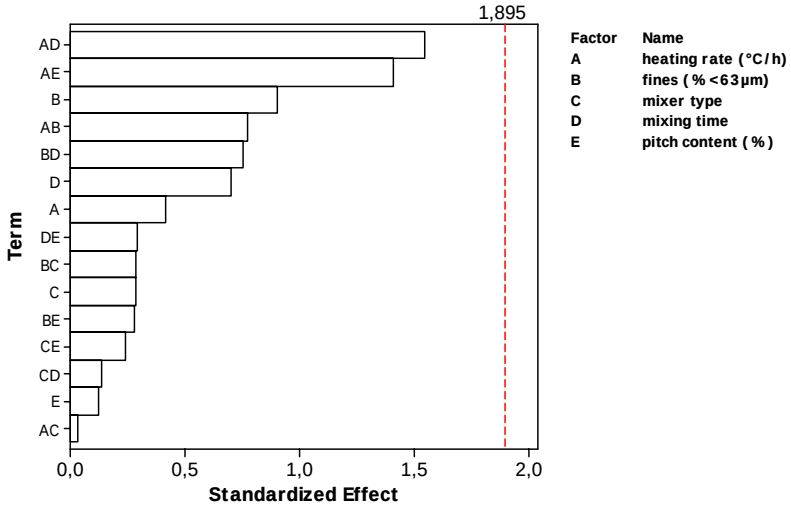

Fig. 4.6-33. Pareto chart of the standardized effects for air reactivity.

4.6.8 Mechanical properties

4.6.8.1 Cold compression strength (CCS)

There are two significant effects, mixer type (C) and interaction mixer type by pitch content (CE) (Fig. 4.6-34). The previous results show that the mixer type plays an important role for physico mechanical properties. Fig. 4.6-35 shows the interaction of pitch content and mixer type on the CCS. There are opposite trends with respect to the mixer types. In case of intensive mixing there is a reduction of the CCS for 16.5 % pitch content while sigma mixed samples reaches maximum values. Sigma mixed 14 % pitch samples were weakest in the compressive test. The reason for this is poor mixing that results in inhomogeneous pitch distribution and weak particle bonding. This was indicated also by increased porosity in the interval above 100 µm which probably causes lower strength of the samples.

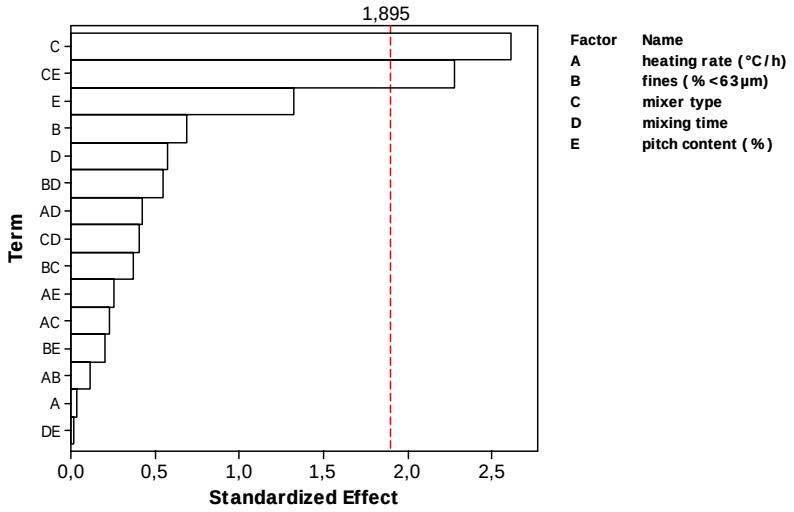

Fig. 4.6-34. Pareto chart of the standardized effects for cold compression strength.

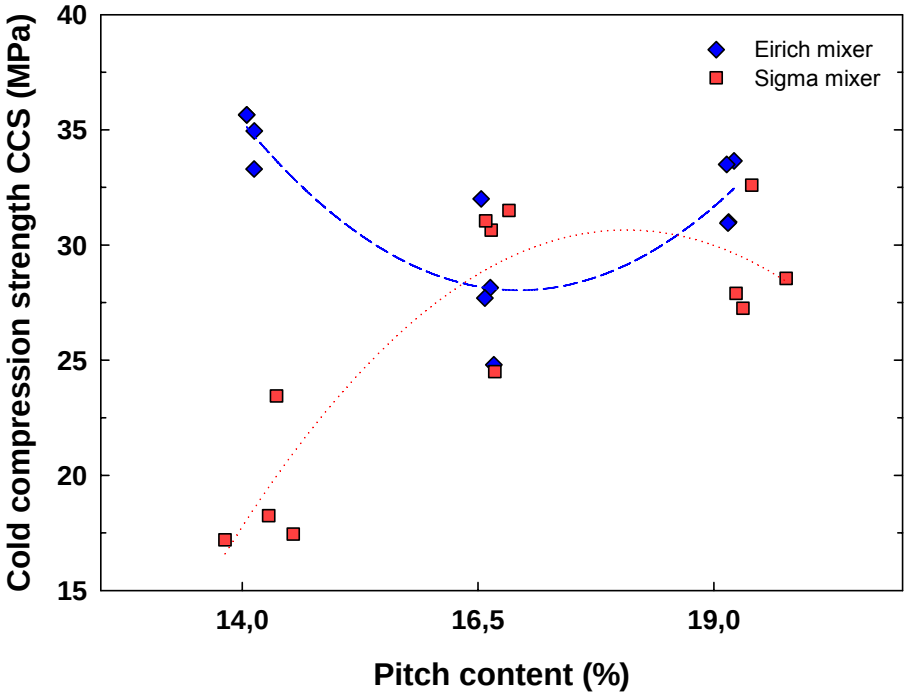

Fig. 4.6-35. Cold compression strength. The effect of pitch content and mixer type.

In the study of Brown and Rhedey [93] it was found that the properties of prebaked anodes are significantly influenced by the binder content, forming method, and baking temperature. As the binder content increased to the optimum, the cold compression strength and Young's modulus increased, and the electrical resistivity decreased.

4.6.8.2 Young's modulus (YM)

The Pareto plot in Fig. 4.6-36 shows that two main effects, mixer type (C) and pitch content (E), and their interaction (CE), have statistical significance on Young's modulus. This result seems quite logical as the amount of binder coke that determines the resulting mechanical properties may also affect the elasticity of the anode. In addition, the mixer type is also important as it determines a consistent and homogeneous distribution of binder pitch.

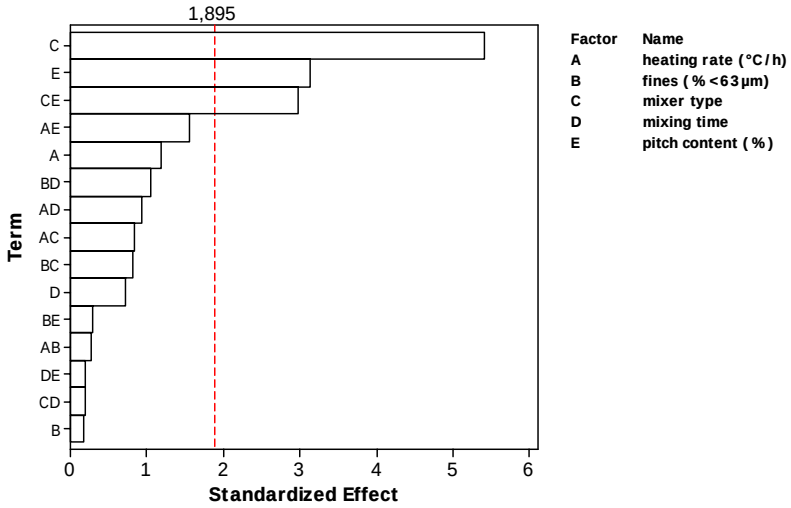

Fig. 4.6-36. Pareto chart of the standardized effects for Young's Modulus.

In Fig. 4.6-37 the statistically significant interaction pitch content by mixer type (CE) is shown. In general there are higher values for Young's modulus for intensively mixed anodes. There are uniform values of YM across the studied pitch range. Samples with 14 % pitch that were mixed in the sigma mixer show a significant decrease of YM. This correlates well with other measured properties like total porosity, baked density and specific electrical resistivity. With increasing porosity samples contain more voids and pores that may increase the elasticity of tested anode specimen. Simultaneously the baked density decreases in the case of 14 % pitch sigma mixed samples.

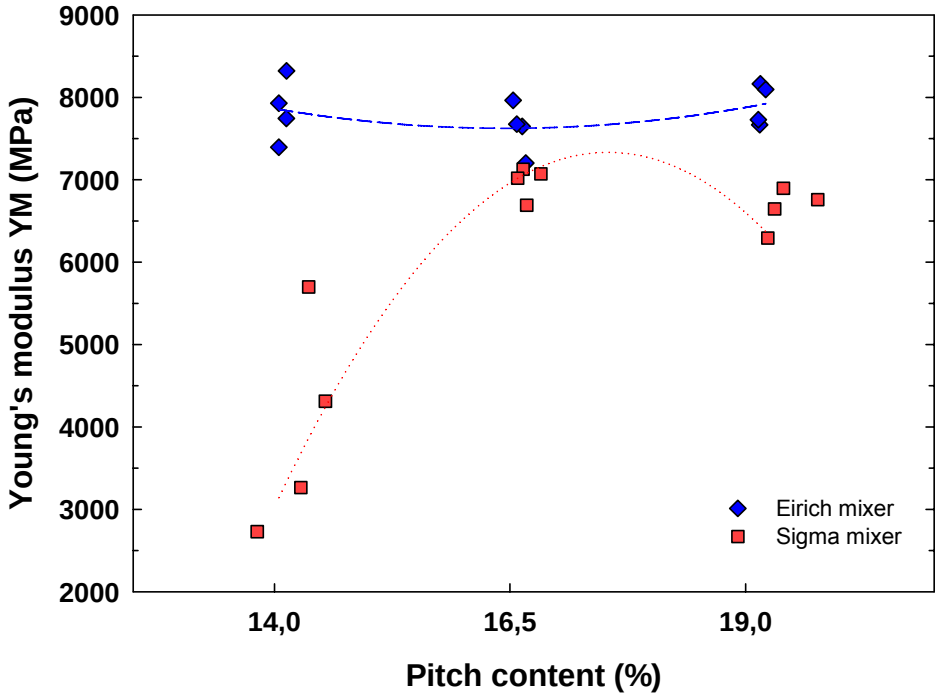

Fig. 4.6-37. Young's modulus. The effect of pitch content and mixing type.

4.6.9 Classification of pores in baked anodes

The baked samples produced in the experimental design given in Table 4.6-II were studied using a pore classification method [76]. For pore classification the central segments from the pilot scale anodes baked with 10 °C/h were picked. For medium pitch content (16.5 %, baked with 35 °C/h) only one segment for each mixing technique was chosen. Pore size distribution curves of specified classes of pores for different compositions are shown in Fig. 4.6-38 to Fig. 4.6-40.

For 14 % pitch content and sigma mixing increased porosity was observed for process pores (Fig. 4.6-38a). High amounts of process pores above 300 µm indicate void formation due to poor mixing. In addition there is an increase of porosity due to increasing mixing time from 10 to 20 minutes which may refer to increased crushing with mixing time. This process porosity for 14 % pitch sigma mixed samples was already observed in the green state (Chapter 4.6.1 in Fig. 4.6-3). For the intensively mixed samples the process porosity is far less. There is a slight porosity reduction with increasing mixing time for intensively mixed samples.

In Fig. 4.6-39 the samples with 16.5 % pitch are compared. Reduced amount of process pores is observed for intensively mixed samples (Fig. 4.6-39 a). The typical peak at 100 µm pore radius in the case of intensive mixing indicates the increased contribution of the baking pores to the process porosity.

Fig. 4.6-40 a) shows process porosity for 19 % pitch samples. The curves show similar distribution of pores with a maximum at 100 µm pore radius. The reason for this is the

same as in the case of 16.5 % pitch samples. Samples with 19 % pitch have fewer voids even though the mixing is poor. Thus the largest process porosity development is due to an increased amount of baking pores.

The porosity in the coke filler represented by the elongated and elliptic pores has in general minor contribution to the total porosity compared to the process pores. This is expected as most of the coke pores are penetrated by the pitch during the mixing stage. However, some variations that indicate improved particle penetration for intensive mixing are observed. Fig. 4.6-38 b) shows lower porosity for 14 % pitch sigma mixed samples due to elongated coke pores with 10 - 60 μm pore radius. The reason for this is unknown. Next, in Fig. 4.6-39 b, c) and Fig. 4.6-40 b, c) the intensive mixing exhibits improved filling of the elongated and elliptic pores within the 10 - 60 μm range compared to the slow and more degradable sigma mixing.

14 % pitch content

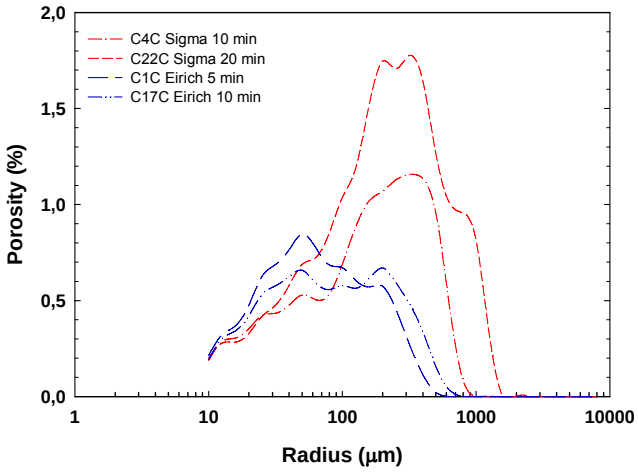

a) process pores

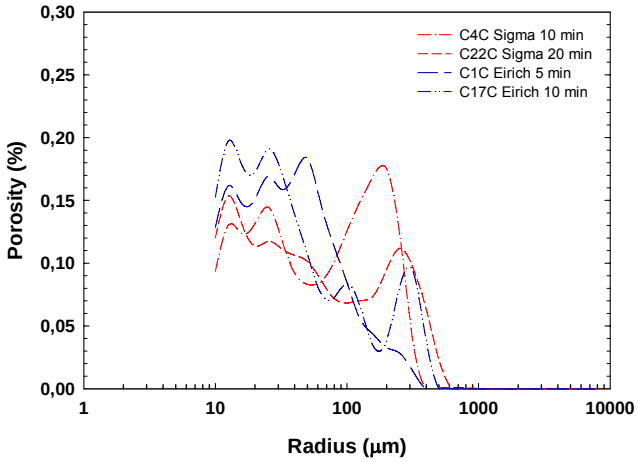

b) elongated pores

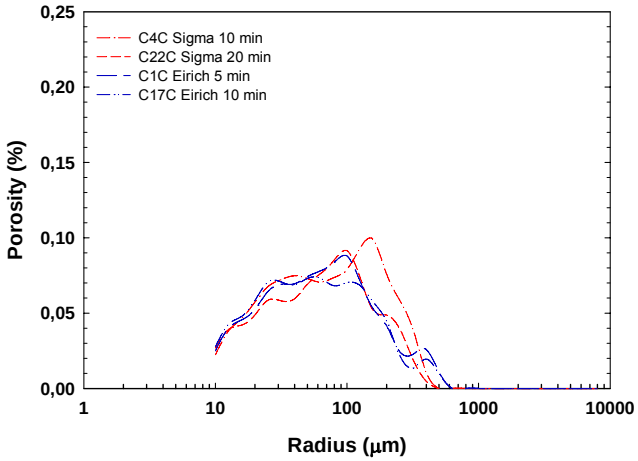

c) elliptic pores

Fig. 4.6-38. Pore classification for the samples with 14 % pitch content.

16.5 % pitch content

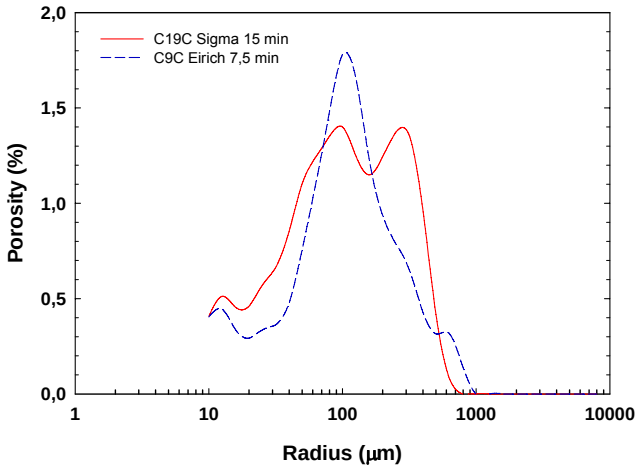

a) process pores

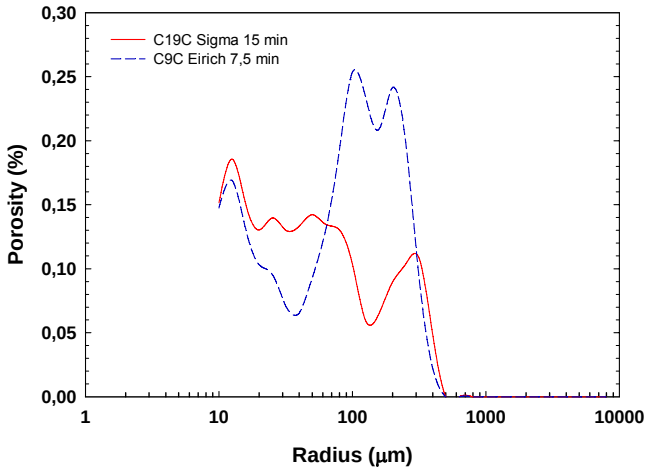

b) elongated pores

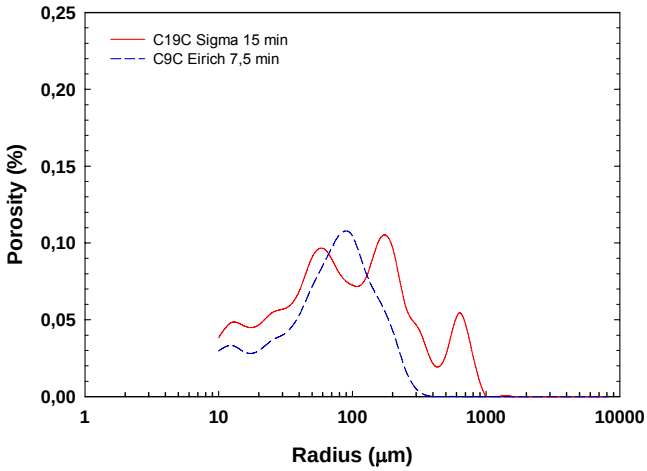

c) elliptic pores

Fig. 4.6-39. Pore classification for the samples with 16.5 % pitch content.

19 % pitch content

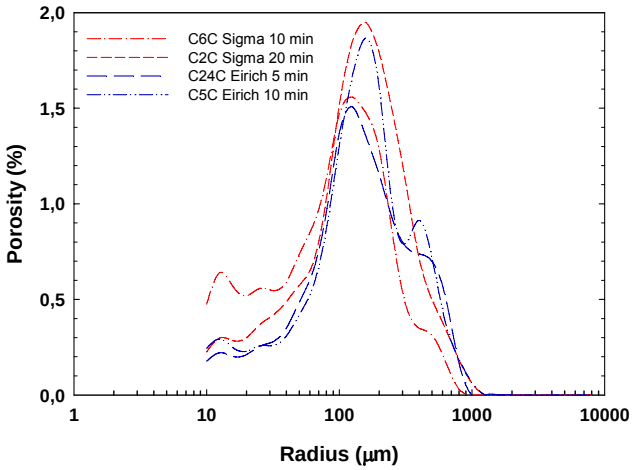

a) process pores

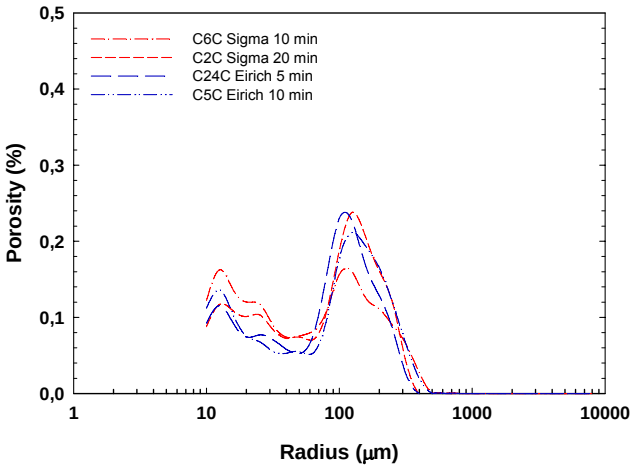

b) elongated pores

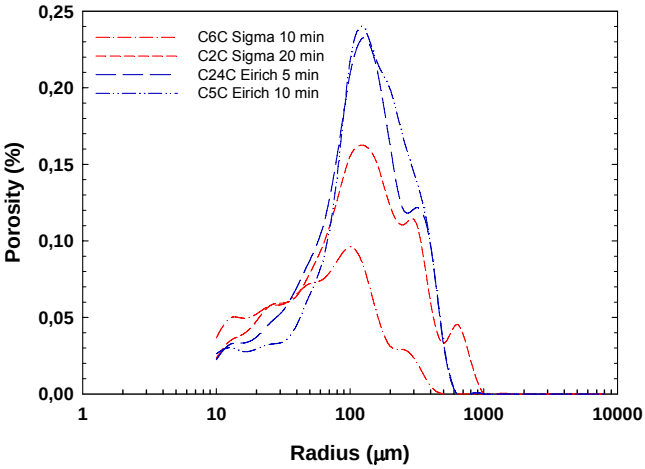

c) elliptic pores

Fig. 4.6-40. Pore classification for the samples with 19 % pitch content.

4.6.10 Conclusion

The effects of five variables during pilot scale anode production were studied. As a response to these variables, green and baked densities, specific electrical resistivity, mechanical properties and porosity were measured. The strength of the effects was statistically evaluated using the Minitab software. The mixer type was statistically the most significant factor influencing porosity, green and baked density as well as the specific electrical resistivity. Surprisingly, a low statistical effect of fines was found.

Intensive mixing was found to be more efficient and to produce samples with higher green densities compared to sigma mixed samples. One of the benefits of intensive mixing is a better statistical distribution of grain sizes throughout the paste. Sigma mixing compared to high speed intensive mixing may have lower possibility of filling and impregnating of voids by capillary effects. In addition there was a significantly higher level of aggregate crushing. During mixing, the blades in the sigma mixer crush coke particles. More surfaces are then created and more open pores need to be filled with pitch. Thus, more pitch is consumed to coat new coke particles and less pitch ends in the intergranular space as a binder.

Green density was influenced the most by pitch content (E), mixer type (C), mixer - pitch interaction (CE), and mixing time (D). Changing from the sigma mixer to the intensive mixer caused an average increase in green density by (0.087 ± 0.005 g/cm^3) or close to 6 %.

The increase of the pitch content from 14 % to 19 % gave an average increase in green density by (0.117 ± 0.006 g/cm^3) or 7.5 %.

All the investigated variables have significant impact on baked density: mixer type, mixer - pitch interaction, mixing time, pitch content, fines and heating rate.

The specific electrical resistivity was influenced by mixer type (C) and mixer - pitch interaction (CE). An average decrease of the specific electrical resistivity by (6.8 ± 1.9 μΩm), close to 10 %, was achieved when changing from the sigma to the intensive mixer.

The strongest effect on the total porosity development was due to mixer type (C), pitch content (E), heating rate (A) and mixer - pitch interaction (A). Switching from the sigma to the intensive mixer results in average a 15 % lowering of porosity (2.9 ± 0.7 %). Increasing the pitch content from 14 % to 19 % caused a close to 20 % increase of porosity by (3.2 ± 0.7 %). When changing the heating rate from 10 °C/h to 60 °C/h, an average increase of porosity by 18 % (3.1 ± 0.7 %) was obtained.

Reactivity tests against CO_2 and air were performed. Weak factorial fit of the factors, especially in case of air reactivity was found. Reactivity against CO_2 was influenced mostly by mixing time (D) and the interaction heating rate by mixing time (AD). An average decrease of the CO_2 reactivity by 16 % (4.5 ± 2.1 mg/cm^{2}h) was observed when the mixing time was increased from short to long for both mixers.

Two effects were important for the cold compression strength. Mixer type (C) and interaction pitch content by mixer type (CE). Changing the mixer type from sigma to intensive results in an average increase of cold compression strength by 23 % (5.9 ± 2.3 MPa).

Young's modulus was affected most by mixer type (C), pitch content (E) and interaction mixer type by pitch content (CE). Changing mixer type from sigma to intensive caused an average increase of 34 % for Young's modulus (1918 ± 350 MPa). An average 23 % increase of Young's modulus (1356 ± 350 MPa) was achieved when increasing the pitch content from 14 % to 19 %. The effect of pitch content was more pronounced in the case of sigma mixed samples.

There are six statistically significant effects on permeability. Changing the mixer type (C) from sigma to intensive caused an average decrease of permeability by 44 % (6.6 ± 0.8 nPm). Increase of pitch content from 14 % to 19 % results in an average increase of the permeability by 43 % (4.2 ± 1.0 nPm). In addition increase in permeability by 26 % (2.8 ± 1.0 nPm) was achieved when the heating rate was increased from 10 to 60 °C/h.

Five effects were found as statistically significant for the coefficient of thermal expansion (CTE). An average increase of CTE by 3 % (0.11 ± 0.04 · 10^{-6} 1/K) was found when changing from the sigma to the intensive mixer. Increase of pitch content from 14 % to 19 % caused an average decrease of CTE by (0.13 ± 0.04 · 10^{-6} 1/K) or 3 %.

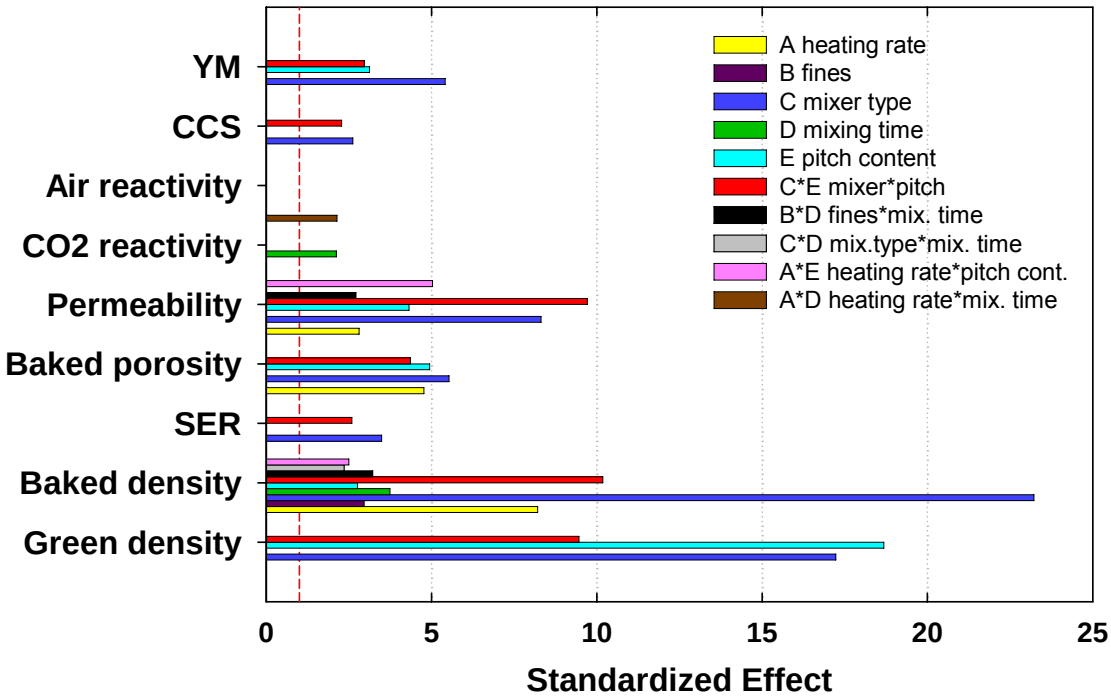

Fig. 4.6-41. Overall comparison of the standardized effects that were found statistically significant.

4.7 Effect of vacuum vibroforming on porosity development during anode baking - laboratory pilot scale anodes from SSA coke

A total of 24 pilot-scale anodes were produced in the Hydro Aluminium a.s. Årdal Carbon laboratory from single source petrol coke using a typical industrial recipe (Table 3.1-I). Similar experimental design and the same production routines were used as described in Chapter 4.6. The difference compared to the previous experimental design was that the anodes were produced with narrower pitch levels and heating rates, using exclusively the intensive mixer. In addition the compaction of the samples was performed using a vacuum vibroformer. The half fractional experimental design is presented in Table 4.7-I.

Table 4.7-I. Variables and levels of half fractional 5-factorial experimental design.

Factors	***Low***	***Medium***	***High***
Pitch content (%)	14	15	16
Mixing time (min)	5	7.5	10
Vibropressure (kPa)	4	52	100
Fines (% < 63 μm)	45	63	94
Heating rate (°C/h)	5	12.5	20

The green paste was formed on the vacuum vibration table for 30 seconds at 50 Hz vibration frequency under three mould pressure conditions, 4 kPa, 52 kPa and 100 kPa (no vacuum applied). During baking the soaking time was 8 hours. Baked densities were measured by the dimensional method as used for green anodes (ISO 12895-1). In addition there were done measurements to determine the CO_2 and air reactivities as well as the mechanical properties. The complete experimental layout and measured data are shown in Table 4.7-II. Experimental data were analyzed using the statistical software MINITAB™.

Table 4.7-II. Experimental layout and measured data for laboratory prepared pilot scale anodes from SSA coke.

	Factors					Responses										
Sample	Pitch content	Mixing time	Vibropressure	Fines	Heating rate	Green density	Baking loss	Total porosity (IA)		RCO_2	Dust CO_2	R air	Baked density	SER	YM	CCS	Perm
#	(%)	(min)	(kPa)	(% < 63 µm)	(°C/h)	(g/cm^3)	(%)	(%)	stdev	(mg/cm^2h)	(%)	(mg/cm^2h)	(g/cm^3)	(µΩm)	(MPa)	(MPa)	(nPm)
E1	14	5	4	low	20	1,572	4,1	21,8	1,1	20,4	15,9	43,4	1,512	61,0	7519	31,4	6,7
E2	16	5	4	low	5	1,699	4,1	13,5	1,2	22,4	17,5	40,7	1,634	51,1	9934	47,6	0,2
E3	14	10	4	low	5	1,663	3,4	13,1	0,9	21,1	20,8	37,4	1,625	53,5	7756	41,8	0,2
E4	16	10	4	low	20	1,722	5,5	14,2	1,6	19,9	16,5	41,8	1,622	49,2	11004	51,7	1,0
E5	14	5	100	low	5	1,500	2,3	27,5	1,3	29,9	33,0	36,4	1,436	72,4	5474	23,5	22,2
E6	16	5	100	low	20	1,634	5,0	19,6	1,1	18,0	11,3	39,0	1,540	56,4	8002	41,1	4,0
E7	14	10	100	low	20	1,537	4,1	20,8	1,4	24,5	15,6	33,8	1,508	61,2	7949	30,6	24,2
E8	16	10	100	low	5	1,665	4,0	18,6	0,9	24,9	18,3	38,1	1,584	52,0	9337	46,4	0,9
E9	14	5	4	high	5	1,562	2,8	23,6	3,2	30,7	25,9	45,5	1,505	64,0	7325	30,5	19,8
E10	16	5	4	high	20	1,663	5,1	13,7	0,5	20,5	15,8	33,2	1,567	54,0	9631	44,8	1,4
E11	14	10	4	high	20	1,646	4,4	14,8	0,2	19,1	18,7	35,6	1,587	54,0	8812	41,1	0,6
E12	16	10	4	high	5	1,687	4,0	12,8	1,3	21,6	16,2	67,0	1,621	49,8	10237	50,6	0,3
E13	14	5	100	high	20	1,501	4,5	22,7	1,3	17,0	10,8	37,1	1,449	70,3	5837	24,9	20,7
E14	16	5	100	high	5	1,627	3,9	17,3	1,3	25,0	18,4	39,0	1,559	56,4	8545	36,0	1,1
E15	14	10	100	high	5	1,551	2,6	23,5	3,7	25,8	19,2	32,5	1,455	65,3	7527	28,7	18,7
E16	16	10	100	high	20	1,647	5,1	17,0	1,7	19,1	16,7	40,8	1,562	54,1	9007	45,9	1,6
E17	15	7,5	52	medium	12,5	1,660	6,9	17,9	1,4	22,1	14,1	38,8	1,556	55,0	9415	42,9	0,9
E18	15	7,5	52	medium	12,5	1,666	6,1	18,7	0,6	19,9	13,9	39,9	1,562	54,6	9042	43,7	0,7
E19	15	7,5	52	medium	12,5	1,656	6,4	20,5	1,3	20,8	18,3	32,6	1,543	55,8	9639	41,6	1,0
E20	15	7,5	52	medium	12,5	1,667	5,5	17,4	0,5	21,0	14,9	31,6	1,568	55,0	9412	46,2	0,6
E21	15	7,5	52	medium	12,5	1,669	5,8	15,4	1,6	20,8	19,4	40,0	1,568	54,3	9361	42,2	0,7
E22	15	7,5	52	medium	12,5	1,660	6,4	16,0	1,3	24,9	18,0	37,3	1,548	55,7	8536	39,0	0,9
E23	15	7,5	52	medium	12,5	1,652	6,5	20,3	1,1	22,0	18,2	45,6	1,549	55,0	9629	40,9	0,9
E24	15	7,5	52	medium	12,5	1,670	5,7	16,9	2,0	19,7	12,9	43,9	1,564	54,8	9143	44,2	0,5

RCO_2 - CO_2 reactivity, R air - air reactivity, SER - specific electrical resistivity,
YM - Young's modulus, CCS - cold compression strength, Perm - air permeability

4.7.1 Green density

Fig. 4.7-1 shows the Pareto chart for green density. All factors except the heating rate had statistically significant effect on the green density. Four main effects were observed, pitch content, vibropressure, mixing time, fines and two interaction effects, pitch content by mixing time (AB) and pitch content by vibropressure (AC). The effect of pitch content (A) is the largest. In accordance with previous results in Chapter 4.6.1, the largest effect was observed for the pitch content. Next, the new factors vibropressure and mixing time play important roles.

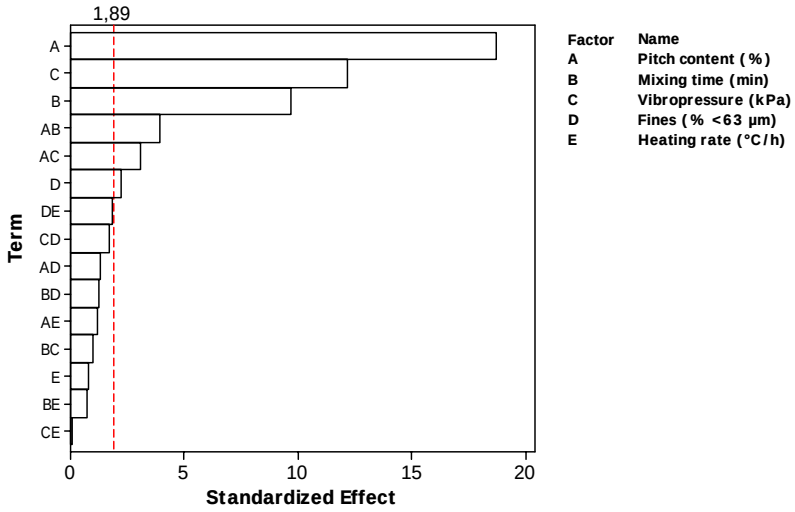

Fig. 4.7-1. Pareto chart of the standardized effects for green density.

The interaction plot in Fig. 4.7-2 shows increase in green density when pitch content and mixing time are increased. Reduction of pressure from atmospheric to 4 kPa in the mould combined with pitch content increase result in higher green densities. The effect of fines variation has very low influence on the green density.

The overall data are shown in Fig. 4.7-3. With increasing pitch content more pitch is available that penetrates the open porosity of particles and coats coke grains. Such a paste has better possibility for denser aggregate packing. Increase of mixing time causes pitch to be distributed evenly and thus creates a continuous binder film over the coke particles. Reduction of atmospheric pressure in the mould during vibration causes better paste degassing and exhaust of the light binder volatiles and entrapped air and from intergranular voids and results in even higher green density.

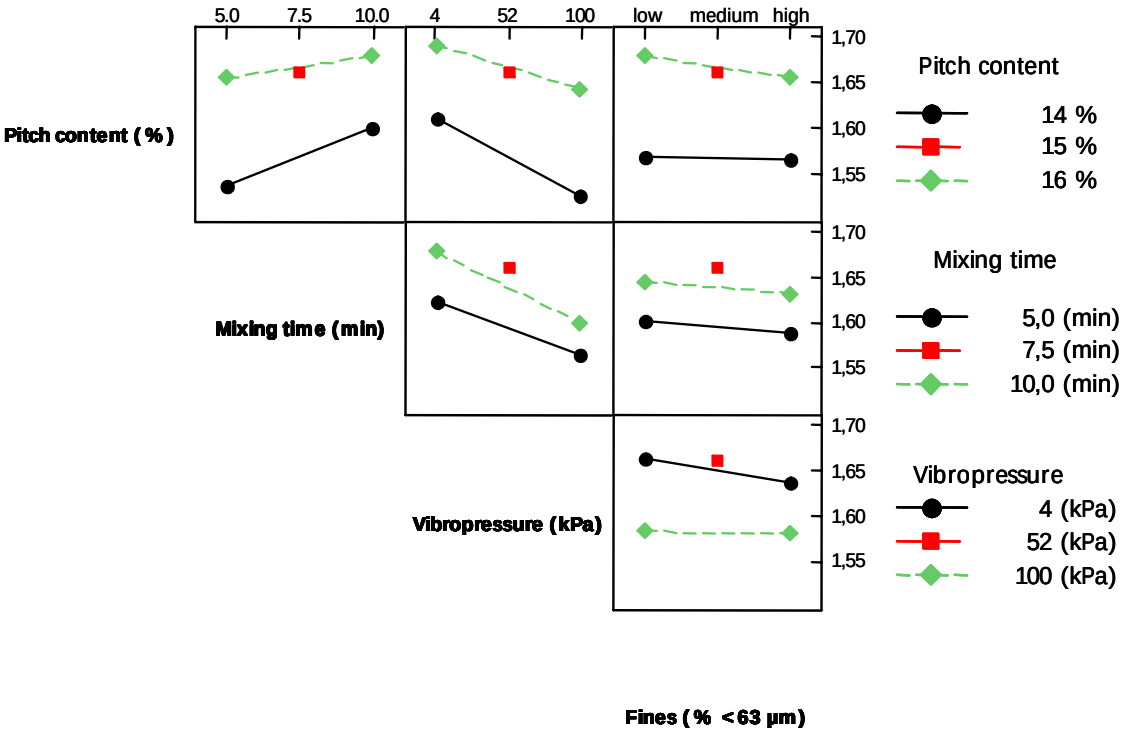

Fig. 4.7-2. Interaction plot for green density.

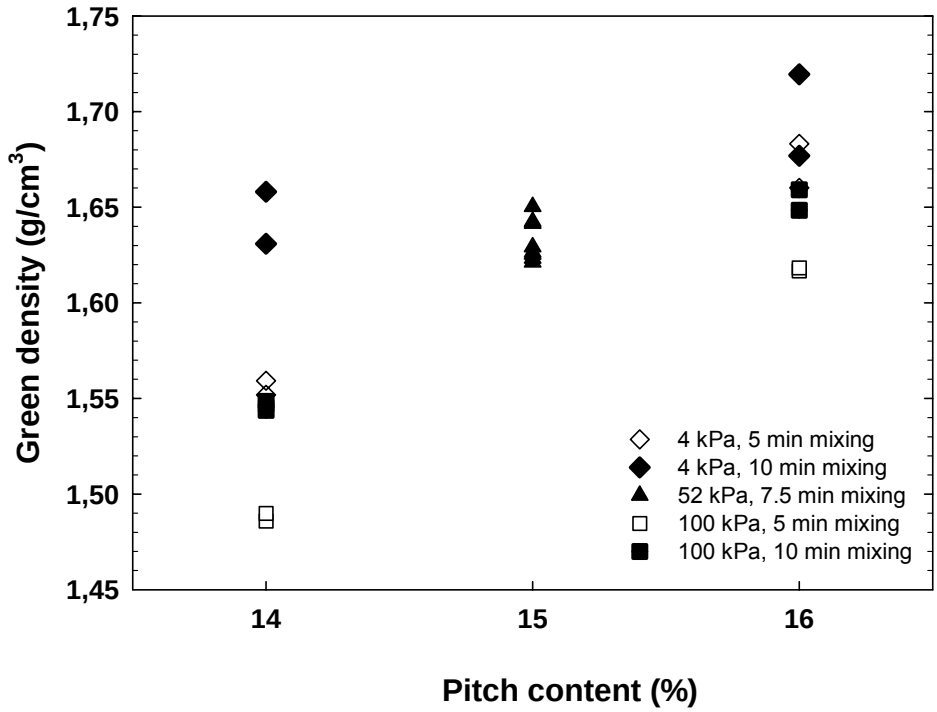

Fig. 4.7-3. Green density as function of pitch content and mixing time.

4.7.2 Green open porosity

Fig. 4.7-4 shows a comparison of the standardized effects for green open porosity. The most dominant factor is the pitch content (A). Increasing amount of the pitch causes that more pitch is pressed towards the sample periphery reducing the outer porosity. The mechanism was described in Chapter 4.4.2. Mixing time (B) and vibropressure (C) play their role in better aggregate distribution and packing due to underpressure in the forming mould. Interaction between pitch content and mixing time (AB) is presented in Fig. 4.7-5. Increase of mixing time reduces open porosity for samples that were vibrated with the same mould pressure. Based on this it is expected that anodes with the lowest green open porosity were those with 16 % pitch, mixed for 10 minutes and vibrated under maximum vacuum 4 kPa.

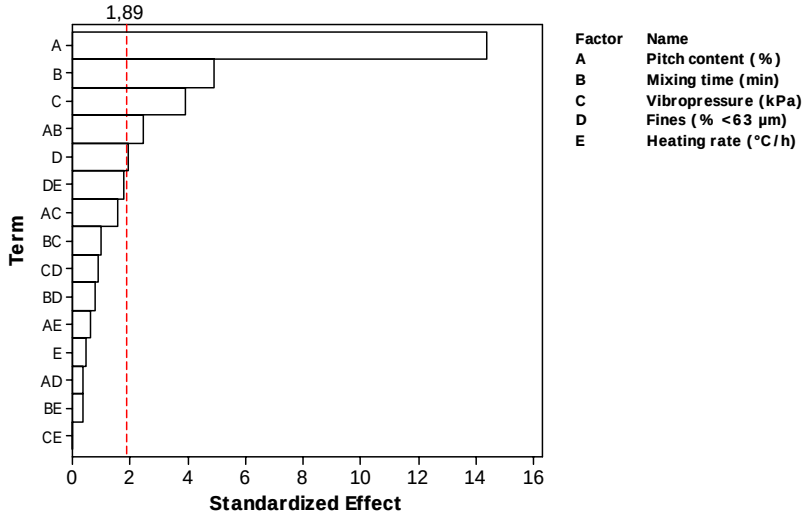

Fig. 4.7-4. Pareto chart of the standardized effects for green open porosity.

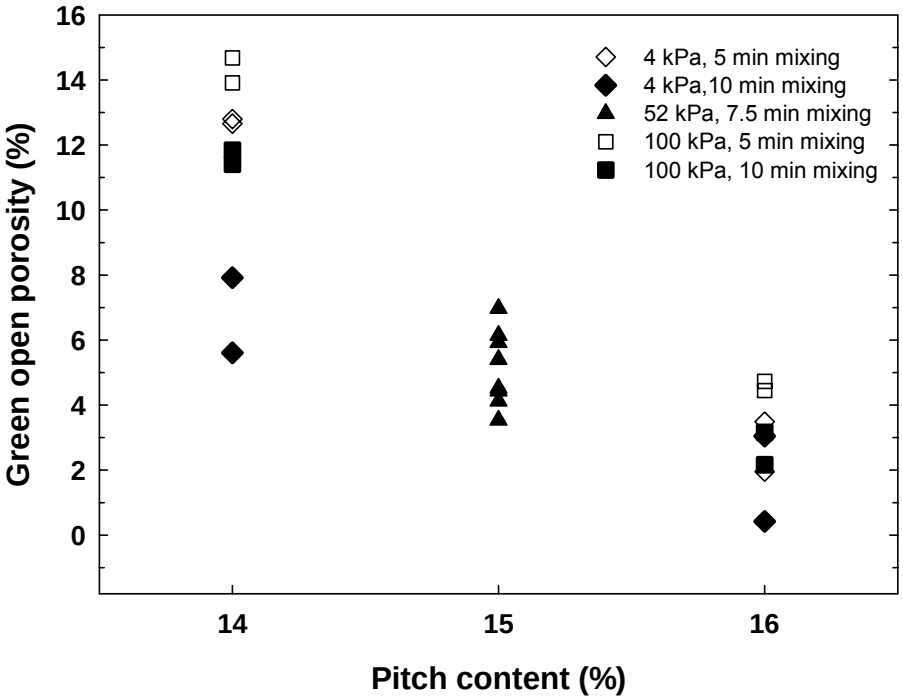

Fig. 4.7-5. Green open porosity as function of pitch content and mixing time.

4.7.3 Baking loss

It is found that the heating rate (E) and the amount of pitch (A) have the largest influence on the baking loss. This is shown in Fig. 4.7-6. All baking loss data are shown in Fig. 4.7-7. The baking loss increases for samples that are baked at higher heating rates.

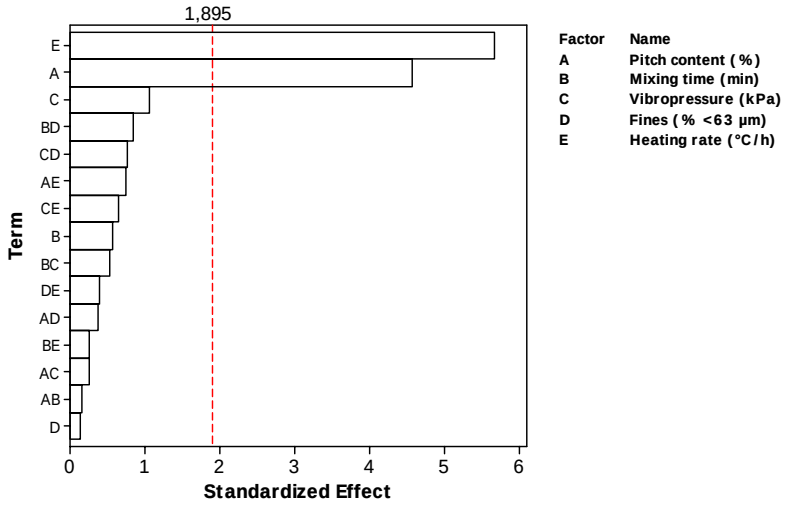

Fig. 4.7-6. Pareto chart of the standardized effects for the baking loss.

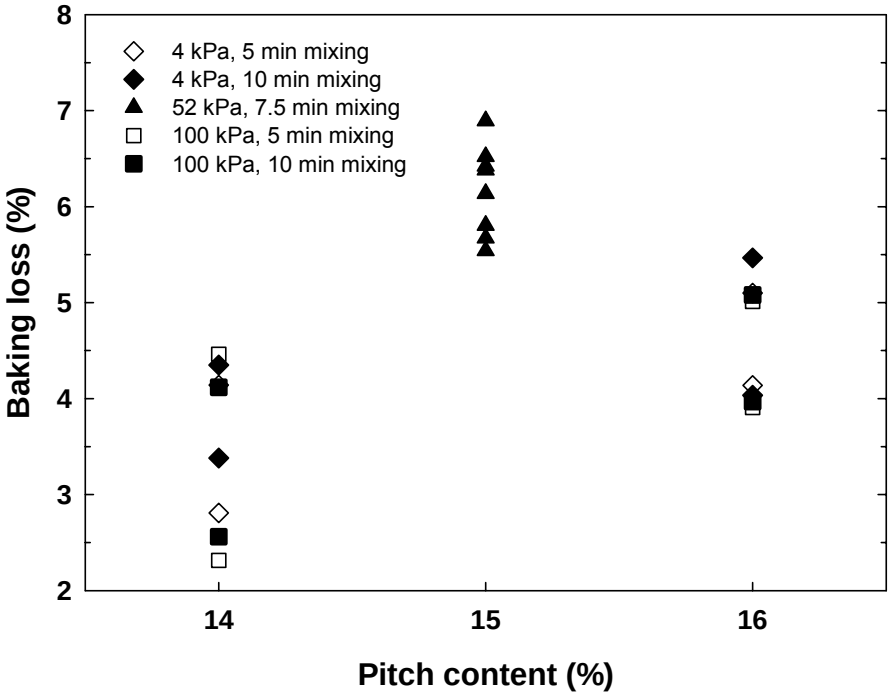

Fig. 4.7-7. Baking loss as function of pitch content and mixing time.

4.7.4 Baked density

Baked density was measured using the dimensional method according to ISO 12985-1. All the main effects except the heating rate (E) affect the baked density. Pitch content (A), mixing time (B) and vibropressure (C) have the strongest statistical influence and therefore affects baked density the most.

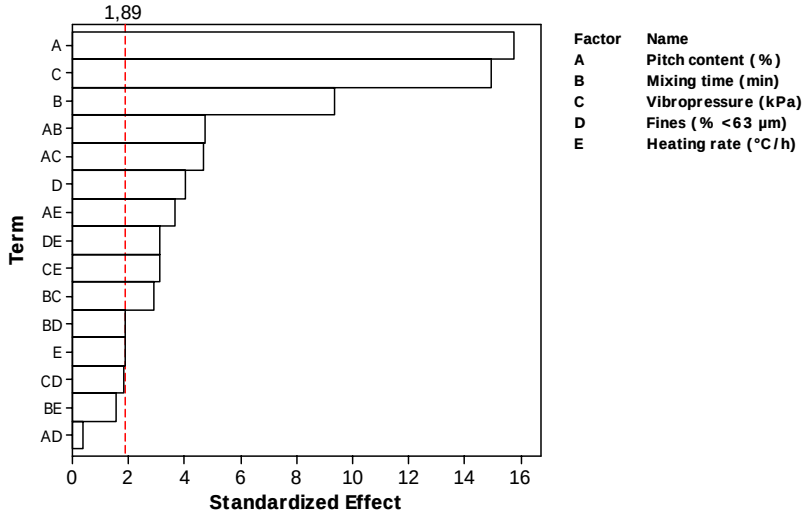

Fig. 4.7-8. Pareto chart of the standardized effects for baked density.

There are several interaction effects that are significant. Interactions between pitch content - mixing time (AB) and pitch content - vibropressure (AC) are shown in Fig. 4.7-9. The situation is similar to the case of the green density. Generally, with increasing pitch content, the baked density increases. Increasing the mixing time combined with reduced vibropressure results in higher baked densities. The difference for samples with atmospheric (100 kPa) and vacuum (4 kPa) vibration is most probably due to better paste compaction and paste densification when vacuum vibration is applied.

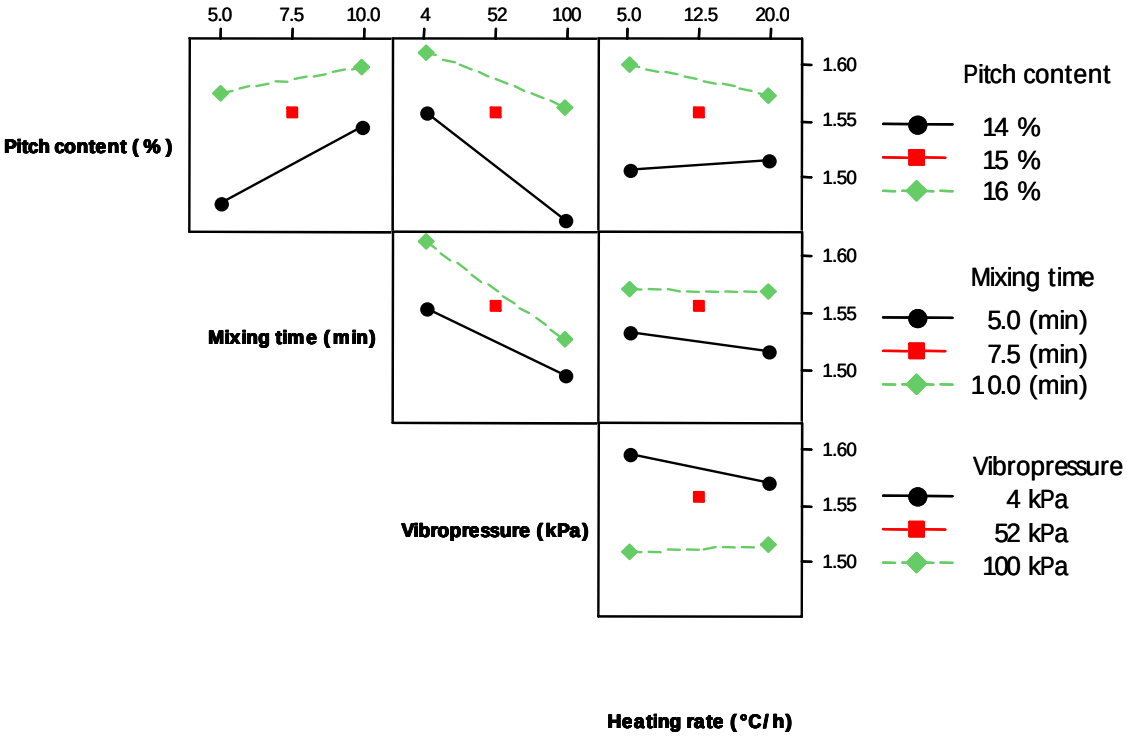

Fig. 4.7-9. Interaction plot for baked density.

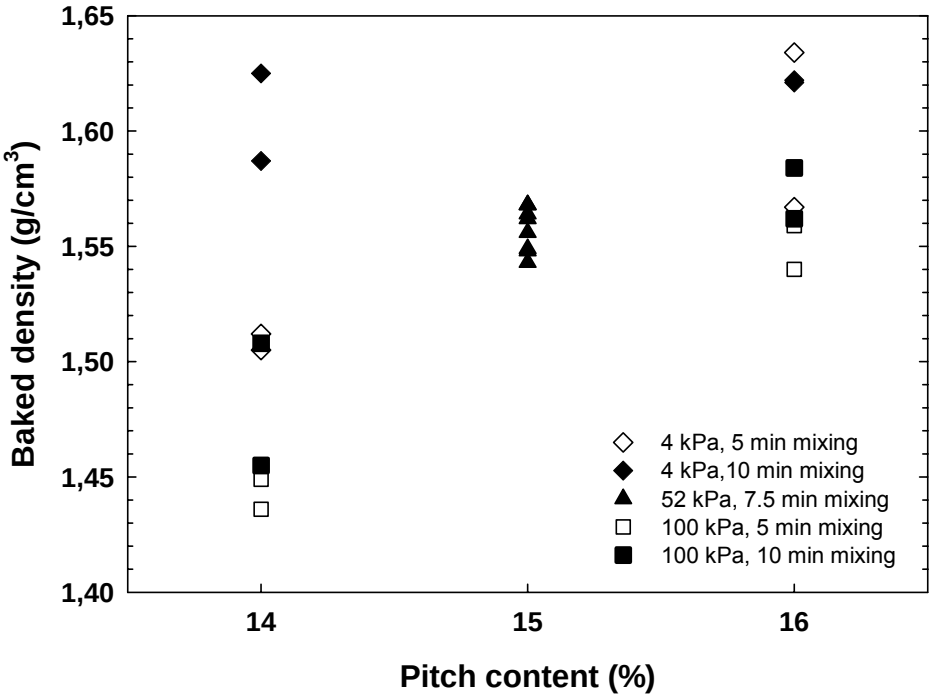

Fig. 4.7-10.Baked density as function of pitch content and mixing time.

4.7.5 Baked Porosity

According to Fig. 3.5-3 the total porosity for one pilot scale anode was determined from the average results of four analyzed segments. The relative magnitude and the statistical significance of the main and interaction effects on the total porosity are shown in Fig. 4.7-11. Compared with Chapter 4.6.5 a different order of the factors influencing the porosity was observed. The heating rate was in this case found to be insignificant. Mixing time was found to be a statistically significant factor. Overall, there are three main effects, pitch content (A), vibropressure (C) and mixing time (B). The interaction effect between pitch content and mixing time (AB) is shown on Fig. 4.7-12.

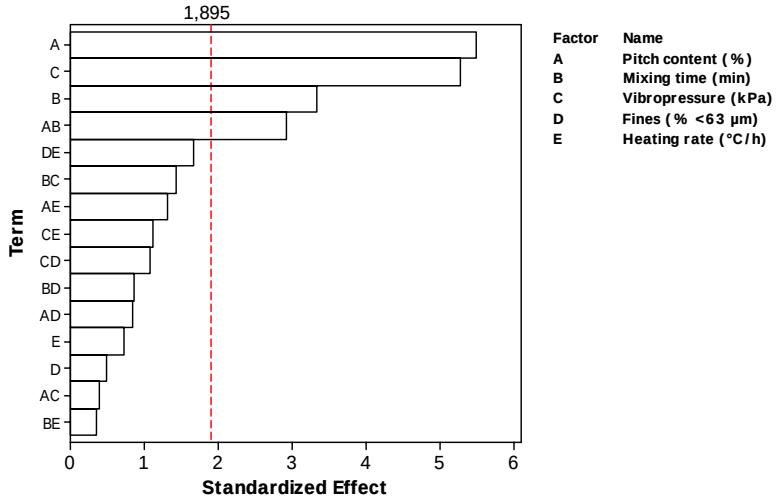

Fig. 4.7-11. Pareto chart of the standardized effects for total porosity.

There is a larger porosity reduction for 14 % pitch samples compared to 16 % pitch when the mixing time increases from 5 to 10 minutes. With increasing pitch content to 16 % porosity reduction is not so pronounced. The reason for this is that 14 % pitch paste is more sensitive to the mixing time. A 16 % pitch paste has more pitch available for aggregate bonding and void filling. Therefore even shorter mixing time is sufficient for good binder distribution resulting in low porosity. Such an effect of mixing time could not be observed in Chapter 4.6 because the mixing times were different for the applied mixing techniques (sigma/intensive).

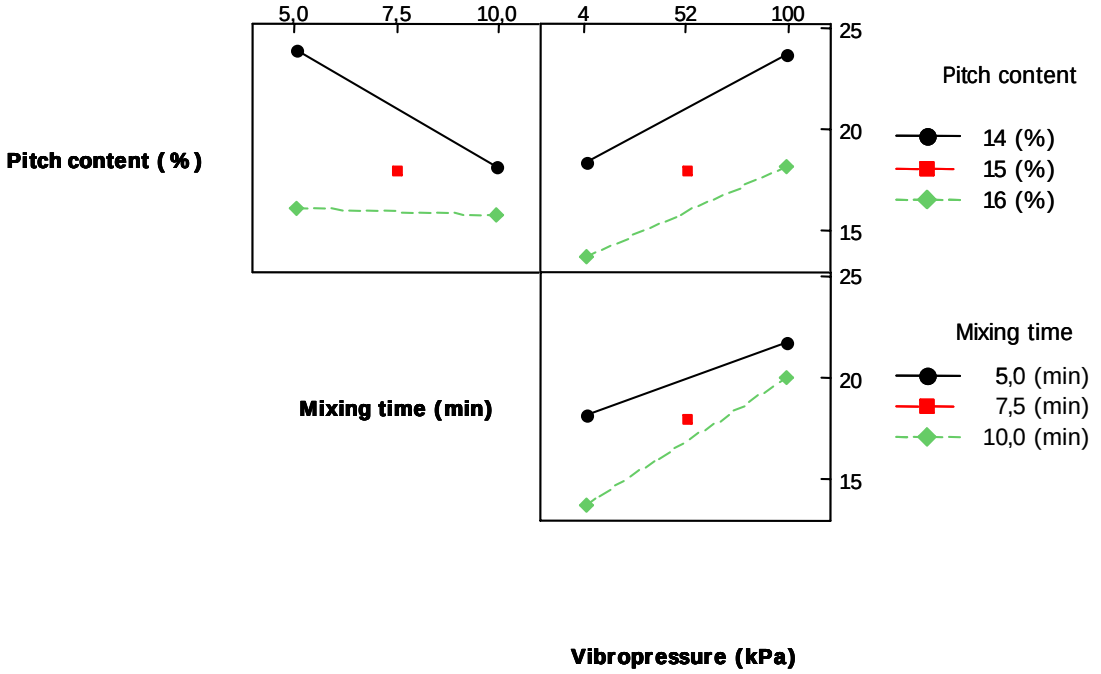

Fig. 4.7-12. Interaction plot for total porosity.

Reducing the vibropressure from 100 kPa to 4 kPa causes a uniform reduction of the total porosity regardless of pitch content. The overall data are shown in Fig. 4.7-13.

Pore size distribution curves are presented in Fig. 4.7-14 to Fig. 4.7-16. Results for 14 % pitch pilot scale anodes are shown in Fig. 4.7-14. There is a marked porosity reduction for vacuum vibrated samples (E9, E1, E11 and E3). Samples that were mixed for 10 minutes and vibroformed at 4 kPa show lower porosity compared to those mixed for 5 minutes. Increased porosity in the 100 - 10000 µm pore radius range for atmospheric vibrated samples is related to poor aggregate packing where more intergranular voids are formed.

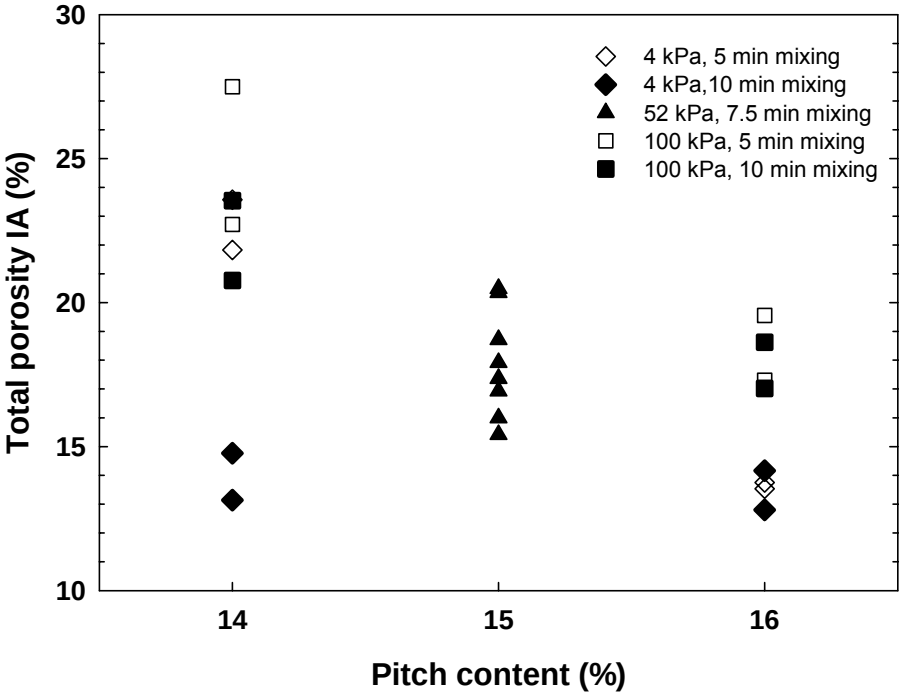

Fig. 4.7-13. Total porosity values. The effect of pitch content and mixing time.

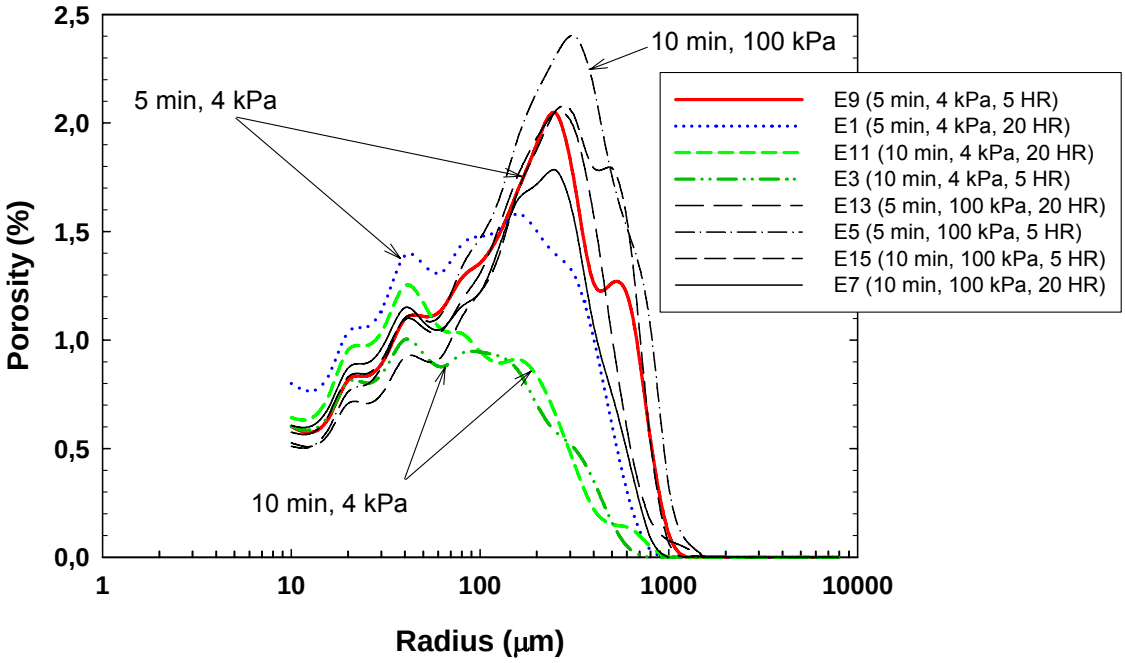

Fig. 4.7-14. Pore size distribution curves for 14 % pitch anodes. HR is heating rate in (°C/h).

In Fig. 4.7-15 the distribution curves show anodes with uniform composition (15 % pitch). All anodes were mixed for medium mixing time (7.5 min) and vibrated with a common vibropressure of 52 kPa. Samples were produced with the intention to demonstrate the reproducibility of the measurements and production methods. There are

some minor deviations between the two samples probably due to random errors during production.

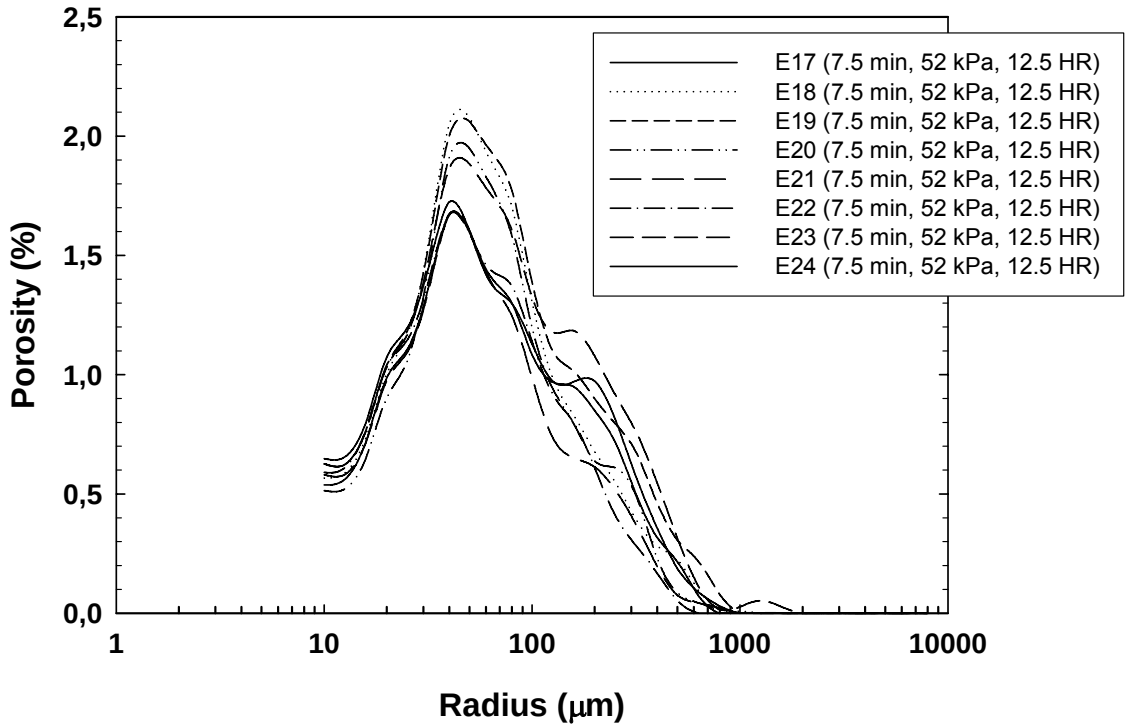

Fig. 4.7-15. Pore size distribution curves for 15 % pitch anodes. HR is heating rate in (°C/h).

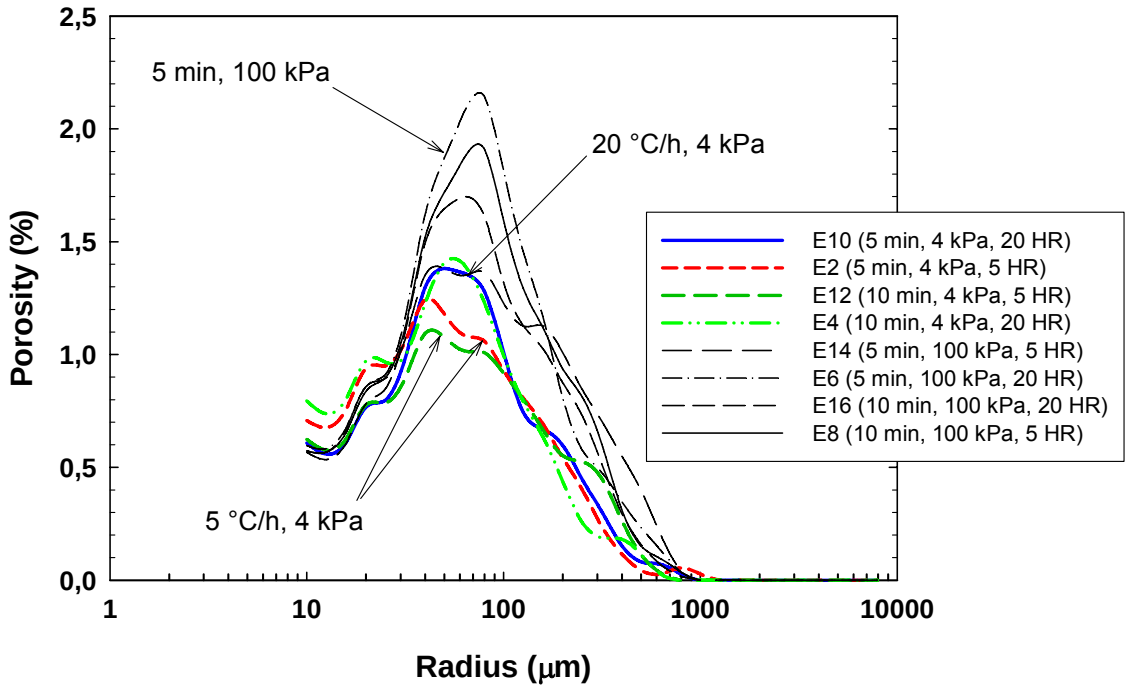

Fig. 4.7-16. Pore size distribution curves for 16 % pitch anodes. HR is heating rate in (°C/h).

Fig. 4.7-16 compares pore size distribution curves for anodes with 16 % pitch. A similar situation as in the case of 14 % pitch is observed. Lowering of mould vibropressure results in reduction of the total porosity. Increase of the heating rate from 5 to 20 °C/h for vacuum formed samples indicates increasing porosity due to increasing amount of baking pores. An overall comparison of averaged distribution curves for all pitch contents is presented in Fig. 4.7-17. Each curve represents the average pore size distribution of four anodes with the same pitch content.

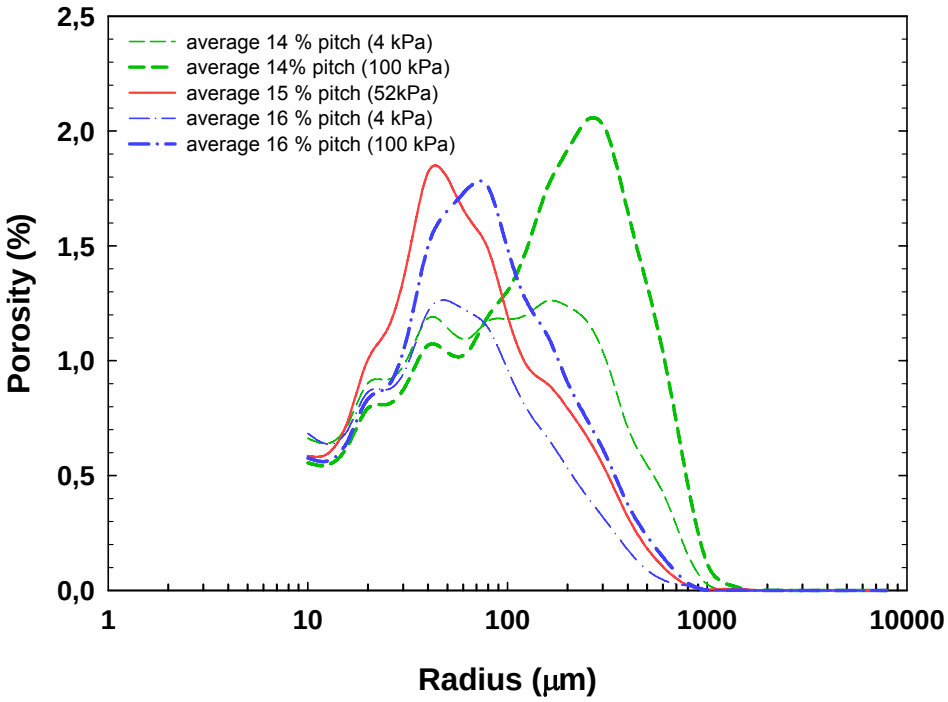

Fig. 4.7-17. Effect of vacuum vibroforming average pore size distribution curves.

Each curve presents the average pore size distribution of four anodes with the same pitch content and vibropressure. For 14 % pitch samples increasing vibration vacuum reduced the total porosity significantly above 80 μm of pore radius. This porosity is due to lower pitch content where little pitch is available in the intergranular space for complete sealing of coke pores and voids. As the pitch content increases to 16 %, distribution curves indicate even further reduction of porosity, and the effect of vacuum vibroforming is significant from 40 μm. In this case more pitch is available to penetrate coke particle pores and to coat aggregate grains with a thicker binder film. This will improve coke particle bridging. Pore size range intervals are in detail presented in the bar chart in Fig. 4.7-18. Each set of four columns represents average porosity of four anodes with the same pitch content and vibropressure conditions within the indicated pore size range.

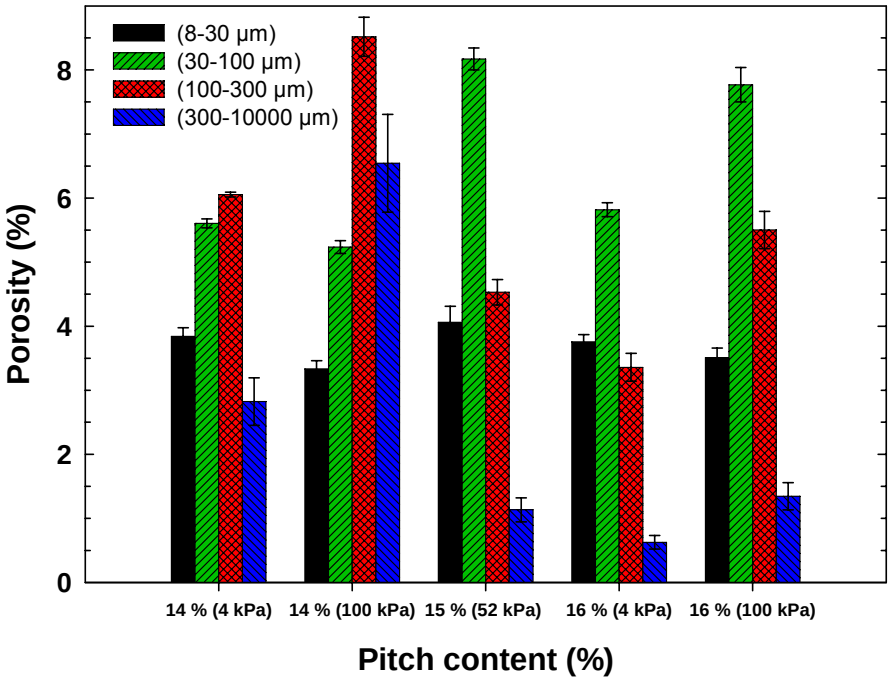

Fig. 4.7-18. Average pore size range comparison.

Pore size range interval 8-30 µm is related to the impregnation of small coke pores with pitch. The variations in porosity are small which indicate similar filling of the small pores mostly by capillary effect. Porosity of 30-100 µm pore radius represents the baking pores and partly filling of the larger coke pores. The amount of the volatile pores increases with increasing pitch content. The interval of 100-300 µm is associated with intergranular porosity due to mixing or forming, and baking pores. This porosity represents the process pores and is influenced by the mould vacuum. Samples with 16 % pitch and 4 kPa vibropressure have the lowest total porosity above 100 µm pore radius. Porosity within the interval 300-10000 µm is due to paste processing (mixing and forming). Significant reduction of porosity within this interval was observed when 4 kPa was used.

4.7.6 Permeability

Fig. 4.7-19 shows a Pareto plot of the standardized effects on permeability. All factors influencing the permeability of anodes are shown. The pitch content (A), the vibropressure (C) and the interaction pitch content by vibropressure (AC) give the strongest influence. This is expected as the pitch amount and its penetration into particles may affect both porosity and permeability. There is also a good correlation between the total porosity and the permeability. Samples with high permeability were those that had higher values of total porosity and low pitch content.

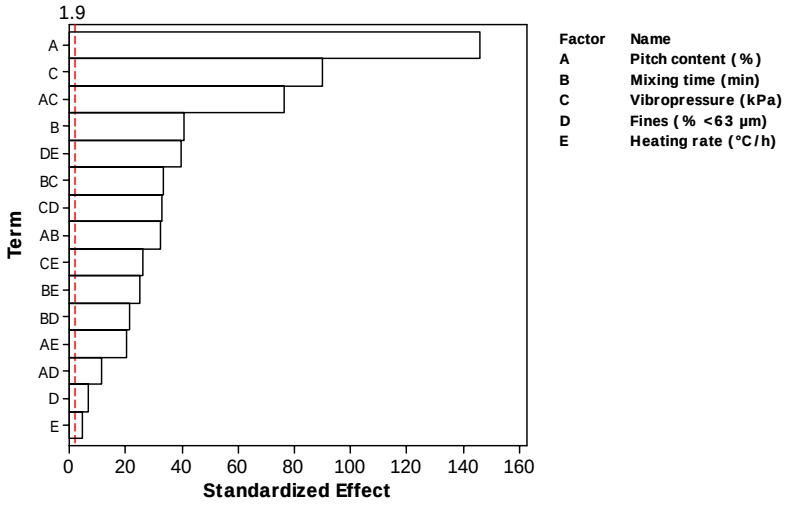

Fig. 4.7-19. Pareto chart of the standardized effects for permeability.

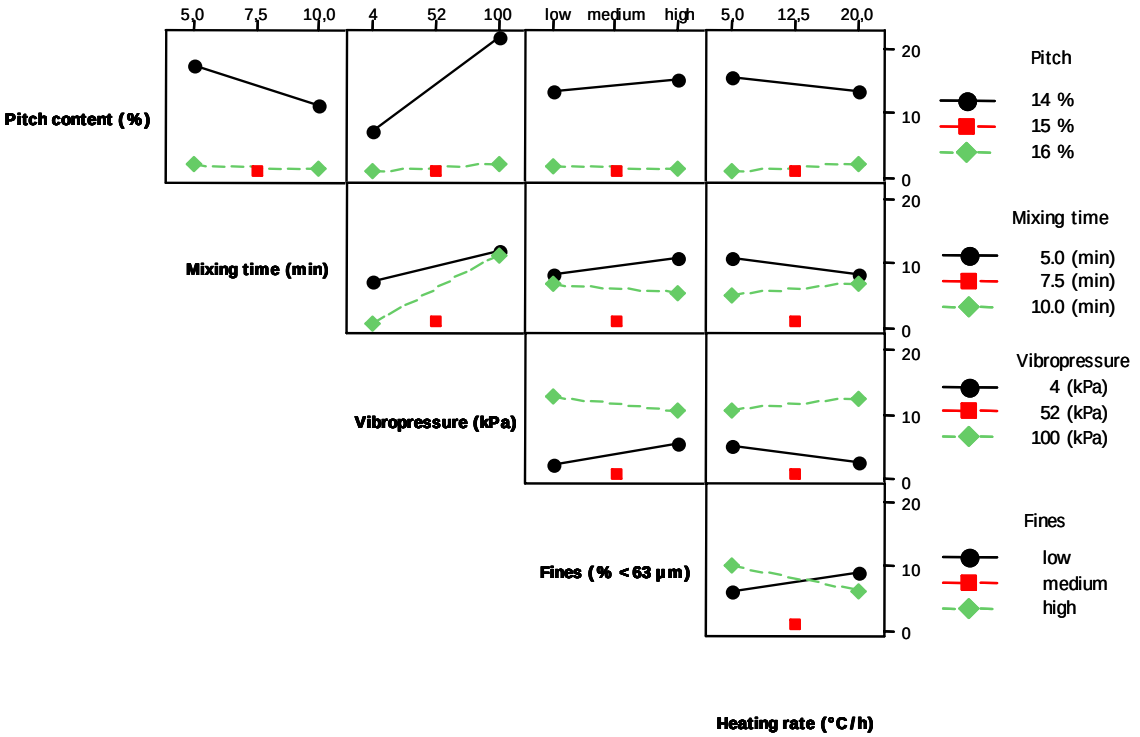

Fig. 4.7-20. Interaction plot for permeability.

Fig. 4.7-20 demonstrates the interaction of two factors on permeability. The most significant interaction, pitch content by vibropressure (AC), indicates a larger decrease of permeability with increasing vacuum during vibroforming for 14 % pitch samples compared to those with 16 % pitch. An interesting interaction also occurs when the effects of fines and the heating rate are considered (DE). There is a reduction of permeability with increasing heating rate when a high fines fraction is used. When coarser fines are used, increasing heating rate will increase the permeability of the anodes. The lowest permeabilities were achieved with medium fines (63 % < 63 μm). There is a larger reduction of permeability with increasing vacuum for anodes that were mixed for 10 minutes compared to those mixed for 5 minutes (BC). There is also a larger permeability reduction with prolonged mixing for 14 % pitch anodes compared to 16 % pitch anodes (AB).

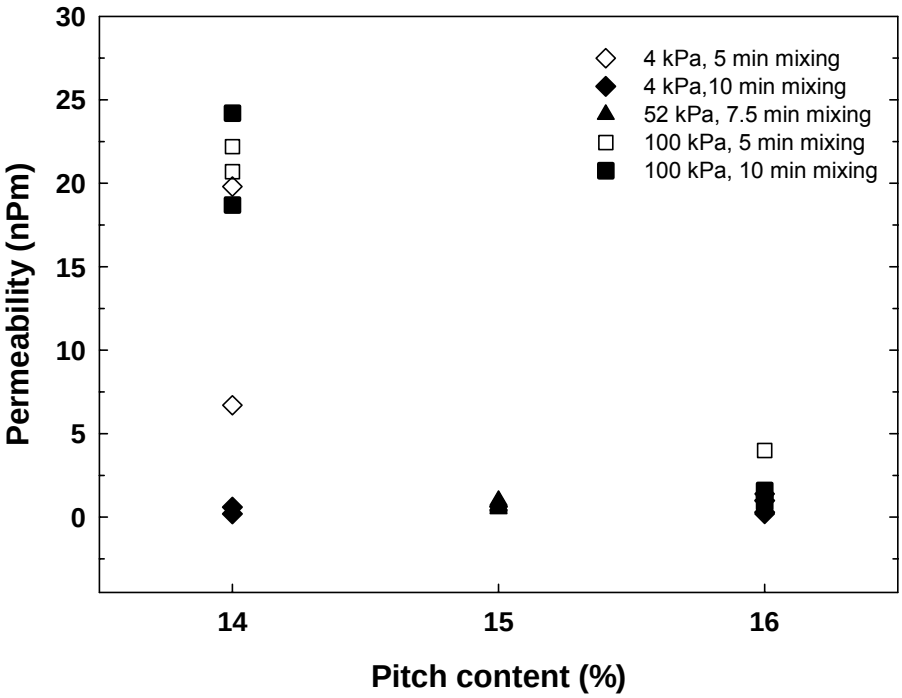

Fig. 4.7-21. Permeability, effect of pitch content, mixing time and vibropressure.

Fig. 4.7-21 demonstrates the correlation between the main effects. Excessive permeabilities were obtained for anodes with low pitch content and vibration at atmospheric pressure. A weak effect of the heating rate on the permeability was found. The reason could be that heating rate levels chosen in the experimental design were not high enough to cause individual development of transport pores that affect the permeability of the anodes.

4.7.7 Reactivity measurements

4.7.7.1 CO_2 reactivity

For the CO_2 reactivity there are five statistically significant effects. These effects include two main effects; heating rate (E) and pitch content (A), Fig. 4.7-22. There are

three interaction effects, mixing time by heating rate (BE), vibropressure by fines (CD) and mixing time by vibropressure (BC). These interactions are shown in the plot on Fig. 4.7-23 where mean values of the CO_2 reactivity are compared. The plot shows that the decrease in reactivity as we move from 5 °C/h to 20 °C/h heating rate is larger when the mixing time is 5 min than when it is 10 minutes (BE).

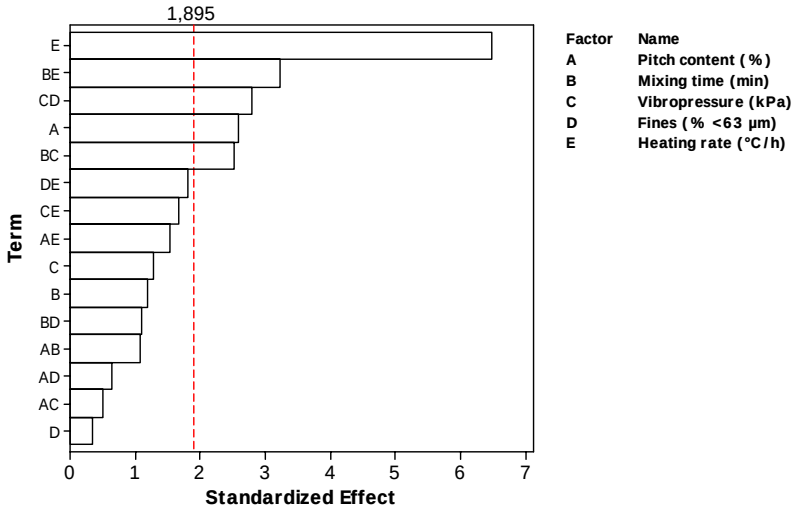

Fig. 4.7-22. Pareto chart of the standardized effects for CO_2 reactivity.

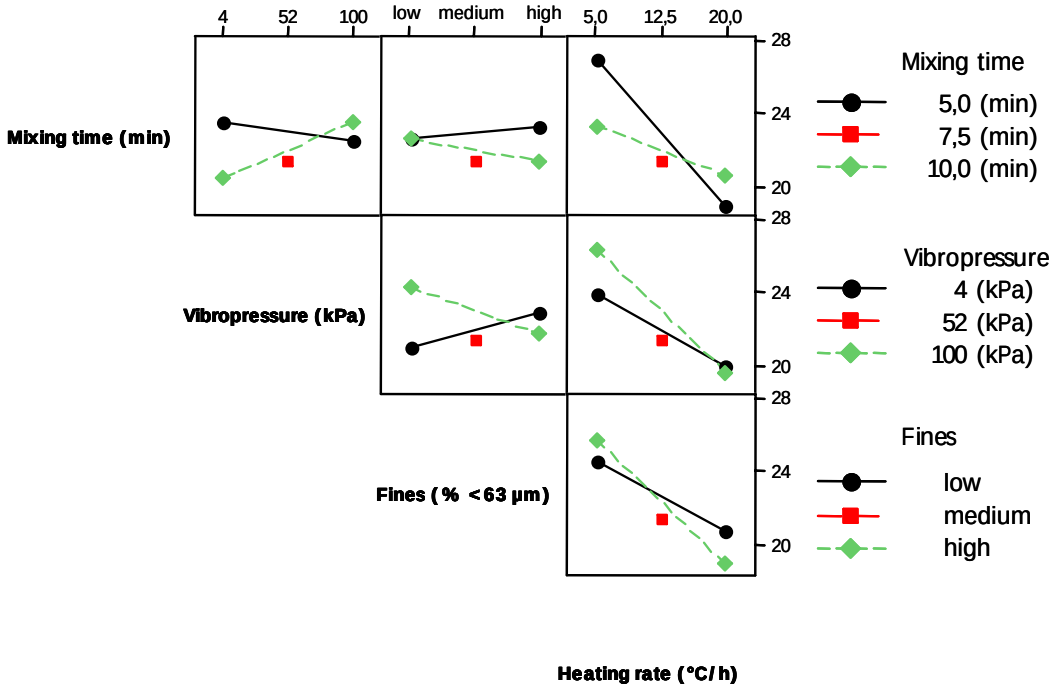

Fig. 4.7-23. Interaction plot for CO_2 reactivity.

The CO_2 reactivity is reduced with increasing fineness of dust in the case of atmospheric vibration. The increasing fineness for vacuum vibroforming caused increase of reactivity (CD). There is a larger reactivity decrease for 10 minutes mixed samples when increasing the vibration vacuum. The reactivity of 5 minutes mixed

anodes slightly increases when increasing the vacuum during vibration (BC). This may be due to insufficient mixing time and unevenly distributed pitch binder.

The heating rate (E) has statistically the strongest statistical effect on the CO_2 reactivity. The anodes were baked in three batches using three heating rates according to Table 4.7-III. For each baking cycle the equivalent temperature of the baking level was monitored [58]. Fig. 4.7-24 shows the complete data.

Table 4.7-III. Baking conditions.

Baking #	Heating rate (°C/h)	Baking level T_{eqv} (°E)
1	5	1189
2	12.5	1191
3	20	1211

The sample cores for reactivity measurements were drilled out close to the pilot scale anode surface. Therefore the open porosity of the investigated samples increased with increasing heating rate (Chapter 4.4.2). Baking # 3 has a higher baking level. We have two opposing factors; increased crystallite size will reduce the reactivity while higher porosity increases the reactivity. This indicates that the higher baking level in this case has a stronger effect than increased porosity.

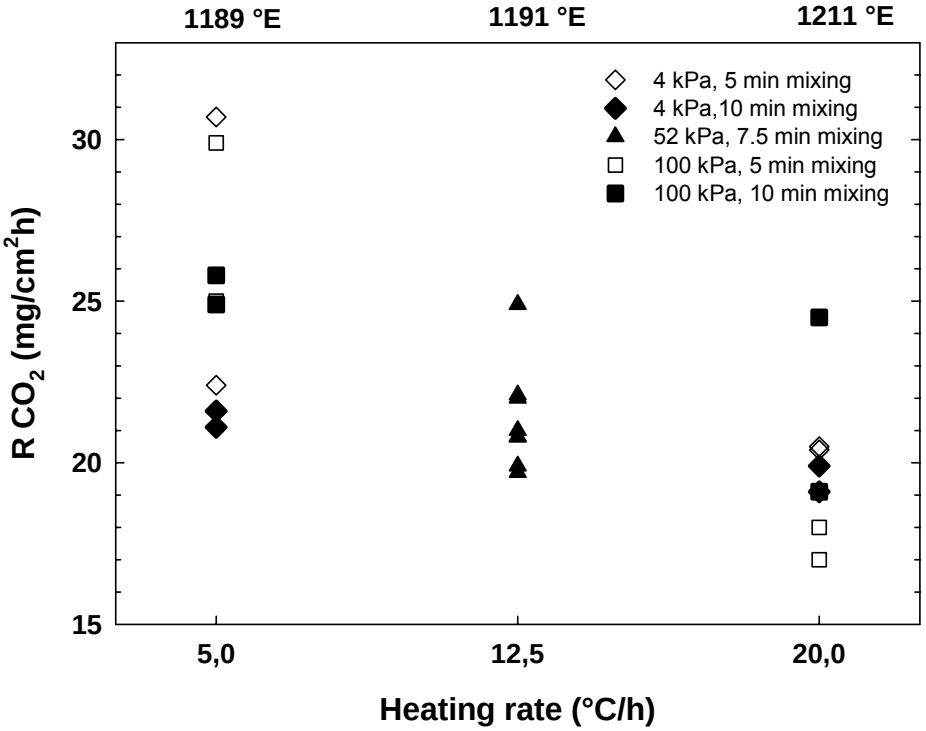

Fig. 4.7-24. CO_2 reactivity and heating rate.

4.7.7.2 Air reactivity

Fig. 4.7-25 compares the relative magnitude and statistical significance of the main and interaction effects that have influence on the air reactivity. There are five statistically significant effects, interaction pitch content by mixing time (AB), vibropressure (C), fines by heating rate (DE) and vibropressure by heating rate (CE). The effect of the pitch content (A) was weakest and is not taken into account.

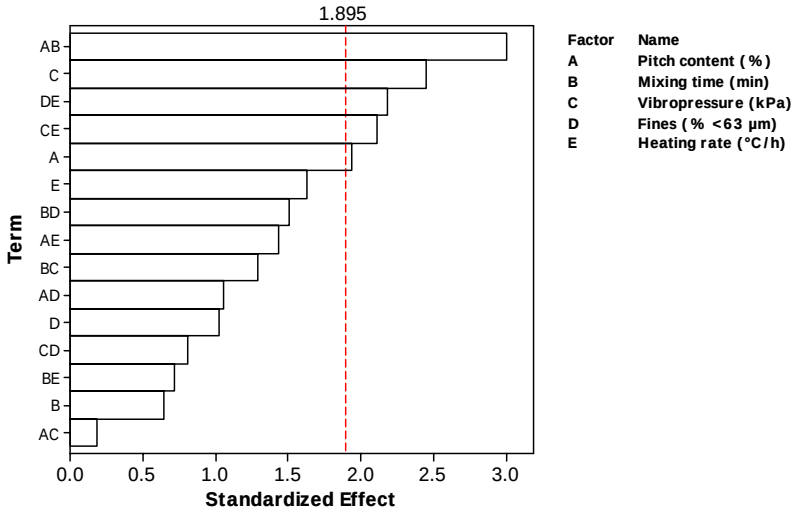

Fig. 4.7-25. Pareto chart of the standardized effects for air reactivity.

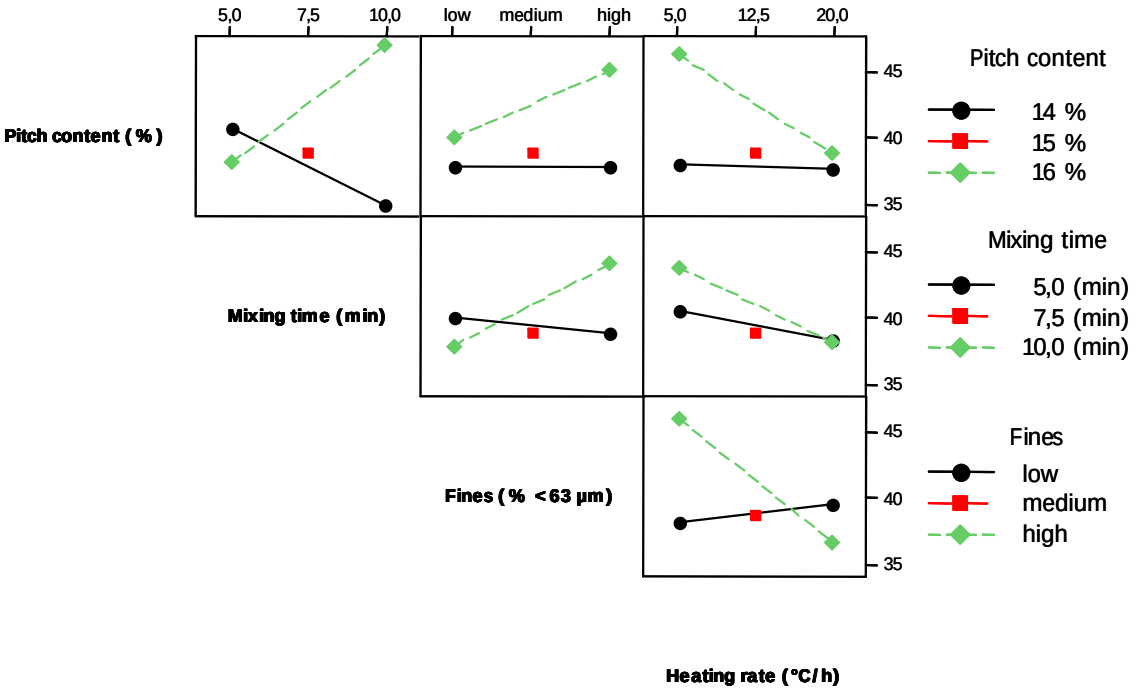

Fig. 4.7-26. Interaction plot for air reactivity.

These interactions are discussed in Fig. 4.7-26 where mean values for air reactivity are plotted. For the strongest interaction pitch content - mixing time (AB), a decrease of

reactivity is found as we increase the mixing time from 5 to 10 minutes for 14 % pitch samples. The reason for this is better continuity of binder film and homogeneity of the aggregate distribution. The opposite situation occurs for 16 % pitch samples where the air reactivity increases with increasing mixing time. This may be due to a thicker binder film over coke particles. After baking there is a higher amount of more porous binder coke that is more reactive and therefore is selectively burned.

The air reactivity for anodes with low fines (coarser particles) is not much affected by increasing the heating rate (also baking level). For the high fines (finer particles) the air reactivity increases as the heating rate (baking level) decreases (DE).

4.7.8 Specific electrical resistivity

The Pareto chart in Fig. 4.7-27 indicates that four main effects and three interaction effects have strong statistical influence on the specific electrical resistivity. The strongest main effects are pitch content (A), vibropressure (C) and mixing time (B), Fig. 4.7-28. There is a decrease of specific electrical resistivity as the pitch content increases. A decrease of the vibropressure and an increase of the mixing time caused the specific electrical resistivity to decrease.

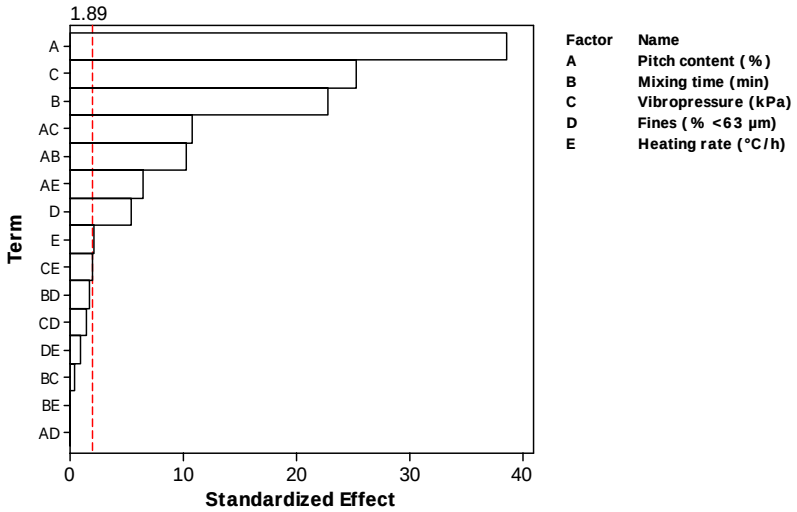

Fig. 4.7-27. Pareto chart of the standardized effects for specific electrical resistivity.

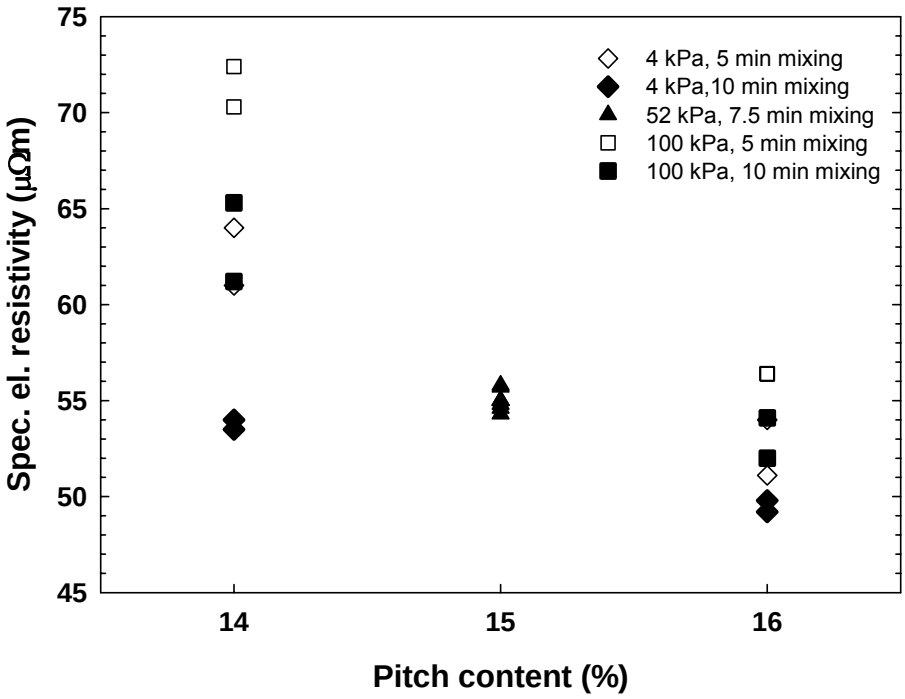

Fig. 4.7-28. Specific electrical resistivity as function of pitch content and mixing time.

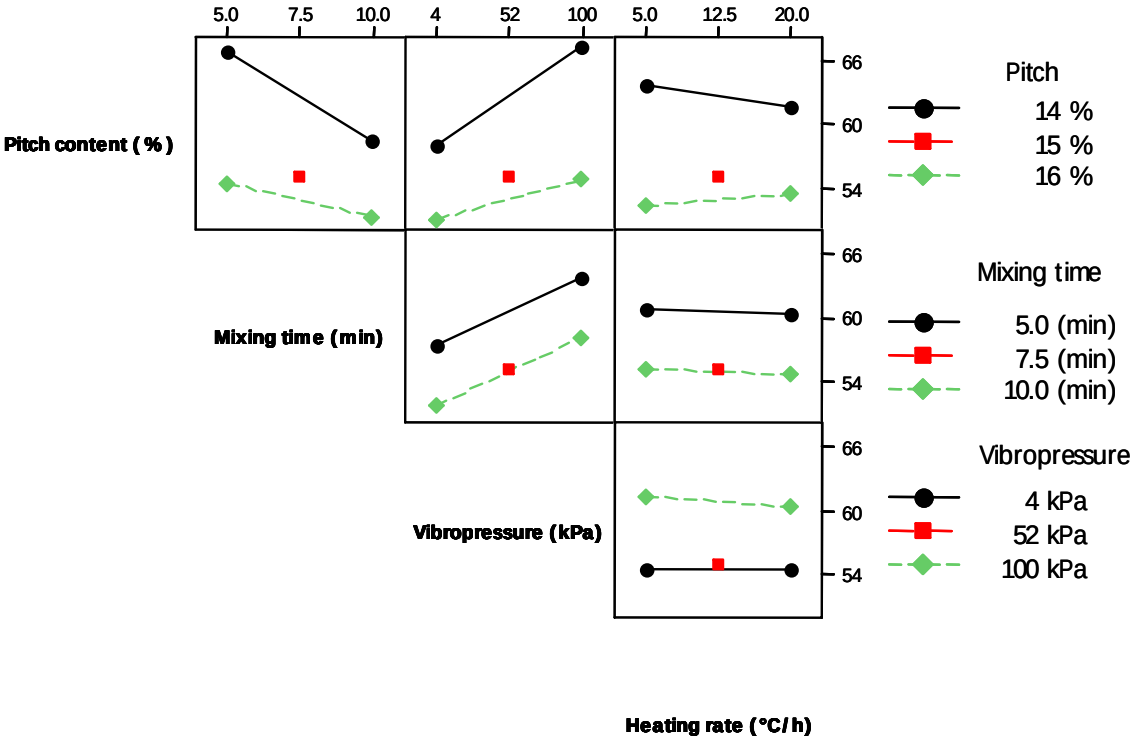

Fig. 4.7-29. Interaction plot for specific electrical resistivity.

Interactions are discussed in Fig. 4.7-29 where the average values of the specific electrical resistivity are compared. For the interaction pitch content - vibropressure (AC) the plot indicates that the specific electrical resistivity decreases for both 14 % and 16 % pitch anodes as the mixing time is prolonged from 5 to 10 minutes. When vibropressure is reduced from 100 to 4 kPa, specific electrical resistivity decreased. This is more evident in the case of 14 % pitch anodes where vacuum forming is more beneficial for denser aggregate packing. The reason for this could be that during vacuum vibration the aggregate is better packed and more binder pitch is available in the intergranular space creating better coke bridging thus enabling improved electrical contact.

4.7.9 Mechanical properties

4.7.9.1 Cold compression strength CCS

In Fig. 4.7-30 the Pareto chart demonstrates a similar situation as in the case of Young's modulus. There are three main effects that influence the cold compression strength of the anodes. These are pitch content (A), vibropressure (C) and mixing time (B).

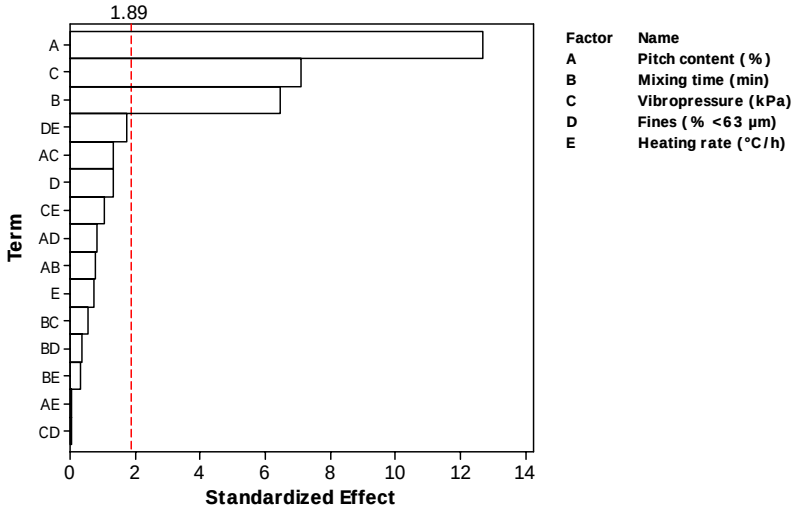

Fig. 4.7-30. Pareto chart of the standardized effects for cold compression strength.

These three factors are very important for strength properties. The amount of pitch content determines the pitch film thickness and the amount of binding pitch coke around the filler particles. The mixing time affects the continuity of the pitch film and the homogeneity of the aggregate distribution. Finally, vacuum conditions during vibration affect pitch penetration into particle pores enabling better bonding between coke grains. The resulting impact of this concurrence is indicated in Fig. 4.7-31.

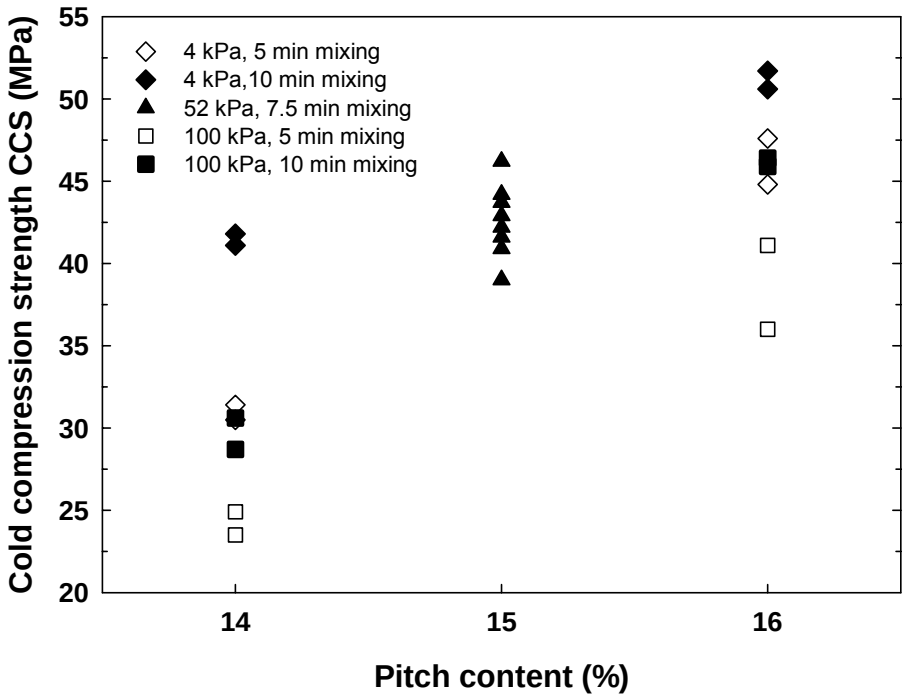

Fig. 4.7-31. Cold compression strength. Effects of pitch content, mixing time and vibropressure.

The increase of the compression strength increases with increasing pitch content. Increasing vacuum during forming and increasing mixing time leads to further increase of the cold compression strength. Porosity correlates well with the physical properties (Young's modulus, cold compression strength). Samples with low total porosity had higher cold compression strength and Young's modulus (Fig. 4.7-32).

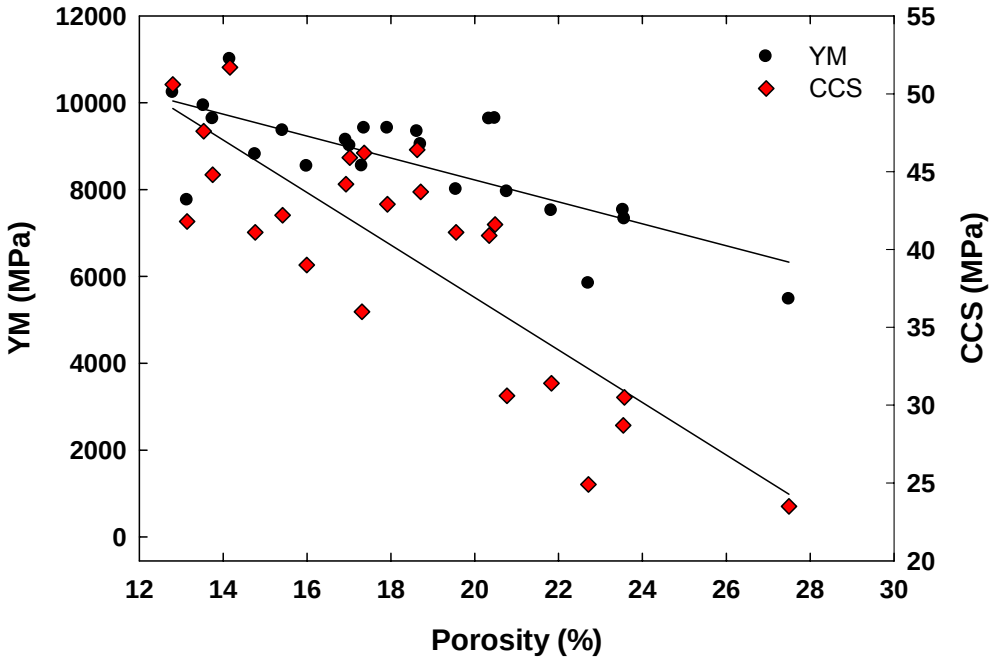

Fig. 4.7-32. Correlation of porosity and Young's modulus and cold compression strength.

4.7.9.2 Young's Modulus YM

The Pareto plot in Fig. 4.7-33 shows that three main effects, pitch content (A), mixing time (B) and vibropressure (C) have statistical significance on Young's modulus. All these factors strongly affect paste homogeneity and compactness and may have direct impact on the anode's mechanical properties. The relation between these factors is indicated in Fig. 4.7-34. There is an increase of Young's modulus for anodes with increasing pitch content. Simultaneously, increasing mixing time and reduction of pressure in the forming mould gives higher values for Young's modulus.

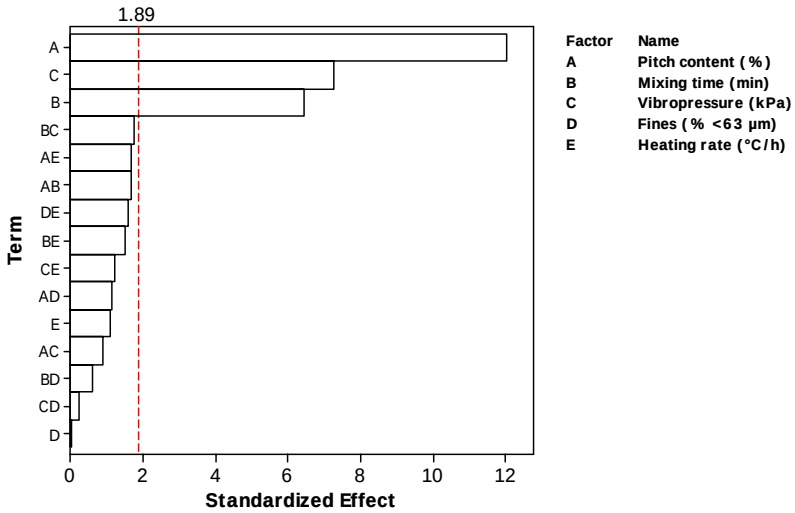

Fig. 4.7-33. Pareto chart of the standardized effects for Young's modulus.

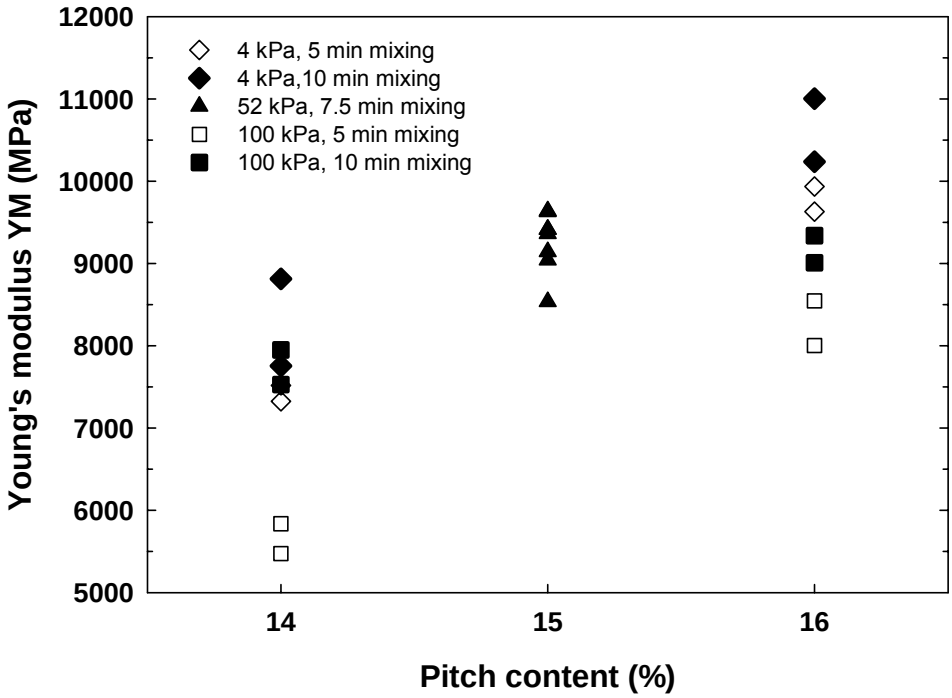

Fig. 4.7-34. Young's modulus, effect of pitch content, mixing time and vibropressure.

4.7.10 Conclusion

The effect of five variables during pilot scale anode production was studied. As a response to these production variations green and baked densities, open and total porosities, CO_2 and air reactivity and physical properties (specific electrical resistivity, Young's modulus, cold compression strength, and permeability) were measured. The statistical relevance of the effects was evaluated using the Minitab software. In most cases pitch content (A), vibropressure (C) and mixing time were factors that affect measured properties significantly.

The green density was influenced strongest by the pitch content (A), the vibropressure (C), the mixing time (B) and interactions between these three main effects. Reducing the mould pressure from atmospheric to 4 kPa caused an average increase in green density by (0,069 ± 0.003 g/cm^3) which is 4 %. Increase of pitch content from 14 % to 16 % gave in average increasing green density by 7 % (0.101 ± 0.003 g/cm^3). Extension of mixing time from 5 to 10 minutes results in an average increase in green density by 3 % or (0.045 ± 0.003 g/cm^3).

The green open porosity was influenced most by the pitch content (A), the vibropressure (C) and mixing time (B). An average decrease of green open porosity by 75 % (8.4 ± 0.6 %) was observed when changing from 14 % to 16 % pitch. Reducing the pressure in the forming mould from 100 to 4 kPa caused an average reduction in green open porosity of 30 % (2.3 ± 0.6 %). Extension of mixing time from 5 to 10 minutes reduced the open porosity by 35 % (2.9 ± 0.6 %).

The strong effect on the baking loss was due to the heating rate (E) and the pitch content (A). Increasing heating rate from 5 to 20 °C/h caused an average increasing baking loss of 39 % (1.3 ± 0.2 %). Increasing the pitch content from 14 to 16 % results in an increase in the baking loss by 30 % (1.1 ± 0.2 %).

Surprisingly, the baked density of anodes was affected by all variables except the heating rate. Pitch content (A) had the strongest statistical influence. Changing the pitch content from 14 to 16 % increased the baked density in average by 5 % (0.076 ± 0.005 g/cm^3). Increasing the mixing time from 5 to 10 minutes increased the baked density in average by 3 % or (0.045 ± 0.005 g/cm^3). Reducing the pressure in the forming mould from 100 kPa to 4 kPa caused an average increase of baked density of 5 % (0.073 ± 0.005 g/cm^3).

Four factors were important for the total anode porosity; pitch content (A), vibropressure (C), mixing time (B) and the interaction between the pitch content and the mixing time (AB). Increasing pitch content from 14 to 16 % caused an average decrease of the total porosity by 25 % (5.1 ± 1.0 %). Increasing the vacuum during vibration from 100 to 4 kPa caused an average reduction of the total porosity by 25 % (4.9 ± 1.0 %). Increasing mixing time from 5 to 10 minutes results in an average porosity value reduction by 15 % (3.1 ± 1.0 %).

The strongest influence on the CO_2 reactivity was determined by two main effects, the heating rate (E) and the pitch content (A). There are also three interaction effects that may affect the CO_2 reactivity; mixing time by heating rate (BE), vibropressure by fines (CD) and mixing time by vibropressure (BC). Increase of the heating rate from 5 to 20 °C/h reduces the reactivity in average by 20 % (5.3 ± 0.8 mg/cm^{2}h). When increasing the pitch content from 14 to 16 % an average decrease in the CO_2 reactivity of 10 % (2.1 ± 0.8 mg/cm^{2}h) was observed.

The air reactivity was mostly influenced by interaction of the pitch content by mixing time (AB), vibropressure (C), fines by heating rate (DE) and vibropressure by heating rate (CE). Increasing pitch content from 14 to 16 % caused an increase in the air reactivity of 12 % (7.4 ± 2.4 mg/cm^{2}h). Decreasing reactivity in average by 15 % (6.0 ± 2.4 mg/cm^{2}h) was observed when vibroforming at 100 kPa was used.

Changing the pitch content from 14 to 16 % caused an average reduction in the specific electrical resistivity of 15 % (9.8 ± 0.3 μΩm). Increasing vacuum during vibration from 100 to 4 kPa results in an average decrease of the specific electrical resistivity by 10 % (6.4 ± 0.3 μΩm). Extension of the mixing time from 5 to 10 minutes caused an average decrease of specific electrical resistivity by 10 % (5.8 ± 0.3 μΩm).

For both Young's modulus and the cold compression strength the same factors were found that have significant statistical influence: pitch content (A), vibropressure (C) and mixing time (B). An average increase of the Young's modulus by 30 % (2187 ±180 MPa) was obtained by increasing of pitch content from 14 to 16 %. Also, increasing mixing time from 5 to 10 minutes increased the average value of the Young's modulus by 15 % (1170 ± 180 MPa). Compaction at 4 kPa gave an average increase of the

Young's modulus by 17 % (1317 ±180 MPa). When increasing the pitch content from 14 to 16 % an average increase of the cold compression strength by 45 % (13.9 ± 1.1 MPa) was achieved. An average increase in the cold compression strength of 20 % (7.8 ± 1.1 MPa) was observed when vacuum of 4 kPa was used. Prolonging the mixing time from 5 to 10 minutes results in an average increase in the cold compression strength of 20 % (7.1 ± 1.1 MPa).

All factors influence the permeability of the anodes. Strongest influence has the pitch content (A), the vibropressure (C) and the interaction of pitch content by vibropressure (AC). Increase of pitch content from 14 to 16 % results in an average permeability reduction by 90 % (12.8 ± 0.1 nPm). An average decrease of the permeability by 70 % (7.9 ± 0.1 nPm) was measured when a vacuum of 4 kPa was used.

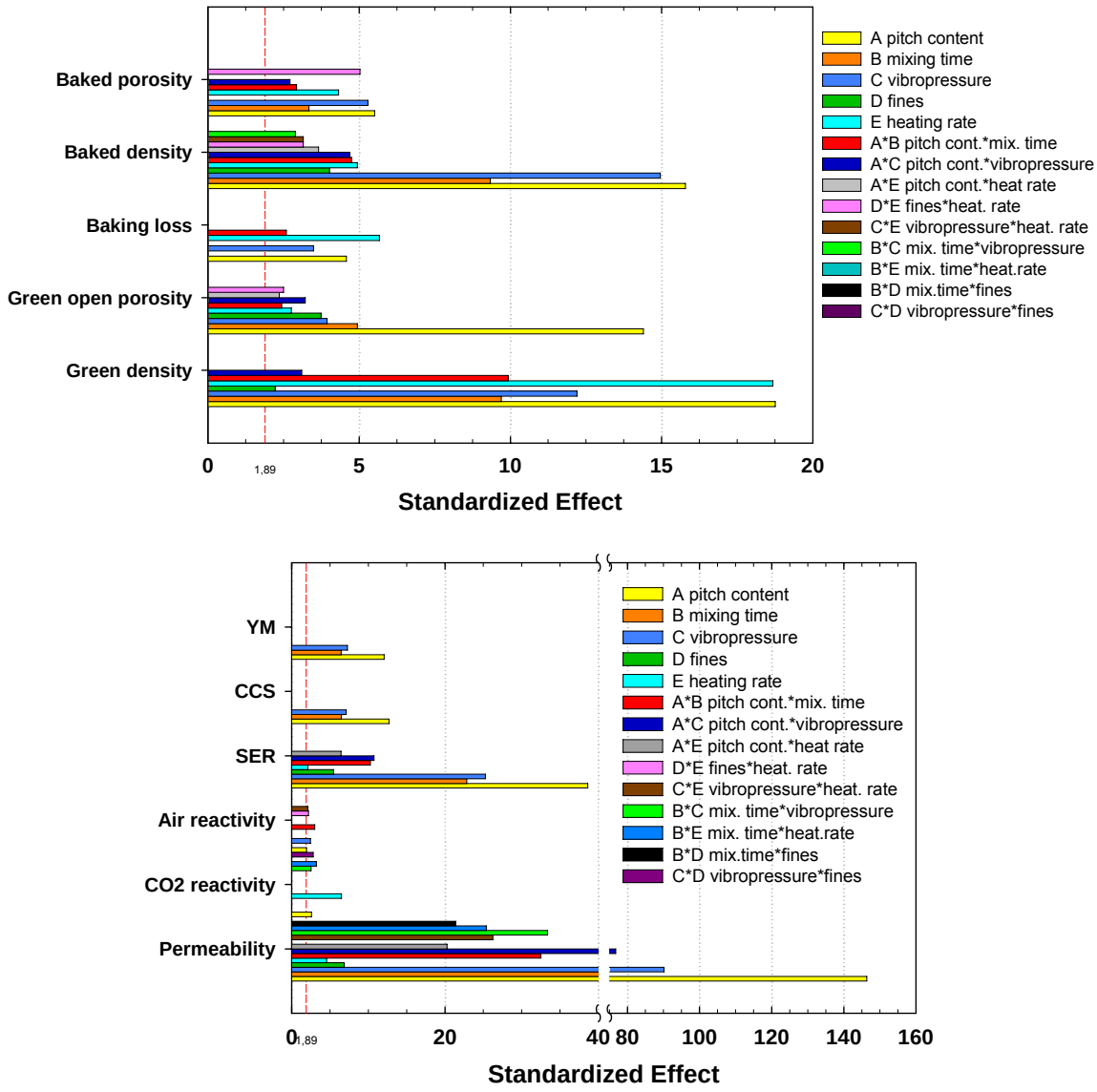

Fig. 4.7-35. Overall comparison of the standardized effects that were found statistically significant.

5 CONCLUDING REMARKS

The pilot scale work was done in order to study the effect of various production parameters on anode properties. The samples were produced both from industrial paste and from single source petrol coke.

In Chapter 4.2 the influence of the heating rate on the porosity development was described for samples prepared from laboratory mixed paste. It was shown that the high heating rate results to increased porosity development and reduction of baked densities. Slow heating rates are therefore recommended for baking.

Chapter 4.3 deals with anodes prepared from industrial paste sampled from the end of the production line. Increasing vibration time increased densities in green and baked state. Additional vacuum during vibration improved the aggregate packing. The increasing heating rate increased the specific electrical resistivity. The lowest porosities were observed for vacuum vibrated samples. With too fast baking cracks were observed in the samples.

Chapter 4.4 describes a more developed experimental design than Chapter 4.3. Samples were prepared from 3 different mixes with different vacuum compaction. The largest improvement of anode properties was observed for samples with short mixing times. The sufficiently mixed paste did not require long vibration times. Samples with a higher porosity showed poorer electrical and mechanical properties. In general, porosities measured on the industrial paste were lower compared to those prepared in the laboratory.

Chapter 4.5 was dedicated to the optimisation and preliminary testing of the intensive mixer. A set of pilot scale anodes was produced and optimal conditions were found.

It was described in Chapter 4.6 that two different mixing techniques had the largest effect on porosity development. The intensive mixing was found to be more suitable and efficient for the laboratory preparation of the pilot scale anodes. When the slow sigma mixer was used, a significant crushing of the aggregate was observed and it caused a degradation of measured anode properties.

Chapter 4.7 discussed the influence of five factors on the porosity development as well as other important anode properties. A significant lowering of the porosity for vacuum vibrated samples was observed. Improvement of electrical and mechanical properties was observed with increasing pitch content and reduced vibropressure in the forming mould.

REFERENCES

1. Grjotheim, K., Kvande, H., *Introduction*, in *Introduction to aluminium electrolysis*, Grjotheim, K., Kvande, H., 2nd edition, 1993, Aluminium Verlag, Dusseldorf, p. 1-34, ISBN 3-87017-233-9.
2. Fischer, W. K., Keller, F., and Perruchoud, R. C., "*Interdependence between anode net consumption and pot design, pot operating parameters and anode properties"*, Light Metals (Warrendale, PA, United States), 1991, p. 681-686.
3. Rhedey, P. J., "*Carbon reactivity and aluminum reduction cell anodes"*, Light Metals (Warrendale, PA, United States), 1982, p. 713-725.
4. Houston, G. J. and Øye, H. A., "*Reactivity testing of anode carbon materials"*, Light Metals (Warrendale, PA, United States), 1985, p. 885-899.
5. Hume, S. M., Influence of raw material properties, PhD thesis, 1999, School of Engineering, University of Auckland, New Zeland, p. 433, ISBN 3-9521028-2-2.
6. Sverdlin, V. A., Dyblin, B. S., and Vetyukov, M. M., "*Porous structure of a carbon anode"*, Tsvetnye Metally, 1976 (11), p. 37-40.
7. Belitskus, D. and Danka, D. J., "*A comprehensive determination of effects of calcined petroleum coke properties on aluminum reduction cell anode properties"*, Light Metals (Warrendale, PA, United States), 1989, p. 429-442.
8. Tkac, M., Foosnaes, T., Øye, H. A., and Ausland, G., "*Effects of variation in production methods on porosity development during anode baking"*, Proceedings of the 12th Arab International Aluminium Conference (Arabal - 2006), 2006, p. 93-113.
9. Tkac, M., Foosnaes, T., and Øye, H. A., "*Effect of Vacuum Vibroforming on Porosity Development during Anode Baking"*, Light Metals, 2007, p. 885-890.
10. Fischer, W. K. and Perruchoud, R., "*Influence of coke-calcining parameters on petroleum-coke quality"*, Light Metals (Warrendale, PA, United States), 1985, p. 811-826.
11. Meier, M. W., Cracking behaviour of anodes, PhD thesis, 1996, Federal Institute of Technology, Zurich, p. 364, ISBN 3-9521028-1-4.
12. Foosnæs, T. and Naterstad, T., *Carbon: Basics and principles*, in *Introduction to Aluminium Electrolysis*, Grjotheim, K. and Kvande, H., 2nd edition, 1993, Aluminium Verlag, Dusseldorf, p. 87-138, ISBN 3-87017-233-9.
13. Madshus, S., Thermal reactivity and structure of carbonized binder pitches, Dr. Ing. thesis, 2005, Department of Materials Technology, Norwegian University of Science and Technology, Trondheim, p. 133, ISBN 82-471-7041-8.
14. Zander, M., *Pitch Characterization for Industrial Applications*, in *Introduction to carbon technologies*, Harry Marsh, Edward A. Heintz, and Rodriguez-Reinoso, F., 1997, University of Alicante, p. 425-465, ISBN 84-7908-317-4.
15. Fischer, W. K. and Perruchoud, R., "*Determining prebaked anode properties for aluminum production"*, Journal of Metals, 1987, 39 (11), p. 43-45.
16. Vanvoren, C. and Kuijpers, J., "*Major parameters for anode manufacturing application to paste plant design"*, Proc Conversazione \"Prod Liq Alum\", 25th Annu Conf Metall, 1986, p. 109-121.

17. Clery, P., "*Green paste density as an indicator of mixing efficiency*", Light Metals (Warrendale, Pennsylvania), 1998, p. 625-626.
18. Grjotheim, K. and Welch, B. J., *Aluminium smelter technology*, 1988, Aluminium Verlag, Dusseldorf, p. 146, ISBN 3-87017-132-4.
19. Hohl, B. and Gocnik, L., "*Installation of an anode paste cooling system at Slovalco*", Light Metals (Warrendale, PA, United States), 2002, p. 583-586.
20. Hohl, B. and Bühler, U., "*New technology for continuous preparation of anode paste*", Light Metals (Warrendale, PA, United States), 1994, p. 719-22.
21. Kuang, Z., On the consumption of carbon anodes in aluminium electrolysis, PhD thesis, 1994, Department of Electrochemistry, Norwegian University of Science and Technology, Trondheim, p. 109,
22. Fischer, W. K., Keller, F., Perruchoud, R. C., and Oderbolz, S., "*Baking parameters and the resulting anode quality*", Light Metals (Warrendale, PA, United States), 1993, p. 683-689.
23. *Baking furnaces for manufacturing carbon*, Riedhammer GmbH Industrial kiln plants, [PDF file], Available from: http://www.sacmi.com/FilePdf/82/17/0.632794025465781250.pdf.
24. McEnaney, B. and Mays, T. J., *Porosity in Carbons and Graphites*, in *Introduction to carbon science*, Marsh, H., 1989, Butterworths, London, p. 154-196, ISBN 0-408-03837-3.
25. Sing, K. S. W. J., Everett, D. H., and Haul, R. A., "*Reporting physisorption data for gas solid systems with special reference to the Determination of surface-area and porosity*", Pure and applied chemistry, 1985, 57 (4), p. 603-619.
26. Rand, B., Hosty, A. J., and West, S., *Physical Properties of Pitch relevant to the Fabrication of Carbon Materials*, in *Introduction to carbon science*, Marsh, H., 1989, Butterworths, London, p. 76-106, ISBN 0-408-03837-3.
27. Belitskus, D., "*Standardization of a calcined coke bulk density test*", Light Metals (Warrendale, PA, United States), 1982, p. 673-689.
28. Belitskus, D., "*Evaluating calcined coke for aluminum smelting by bulk density*", Aluminium (Isernhagen, Germany), 1975, 51 (2), p. 170-173.
29. Jones, S. S., "*Variation of anode performance with coke quality*", Journal of Metals, 1976, 28 (12), p. A67.
30. Rhedey, P., "*Review of Factors Affecting Carbon Anode Consumption in Electrolytic Production of Aluminum*", Journal of Metals, 1970, 22 (12), p. A20.
31. Ragan, S. and Marsh, H., "*Science and Technology of Graphite Manufacture*", Journal of materials science, 1983, 18 (11), p. 3161-3176.
32. Wallouch, R. W. and Fair, F. V., "*Kinetics of the coke shrinkage process during calcination*", Carbon, 1980, 18 (2), p. 147-153.
33. Keller, F. and Fischer, W. K., "*Development of anode quality criteria by statistical evaluation of operational results in the electrolysis*", Light Metals (Warrendale, PA, United States), 1982, p. 729-740.
34. Fischer, W. K. and Perruchoud, R. C., *Practical applications of binder matrix torque measurement using a plastograph laboratory mixer*, in *Anodes for aluminium industry*, 1st edition, 1995, R&D Carbon Ltd., Sierre, p. 183-192,
35. Gehlbach, R. E. and Grindstaff, L. I., "*Effect of Calcination Temperature on Real Density of High Sulfur Coke*", Journal of Metals, 1976, 28 (12), p. A31.

36. Dreyer, C., Samanos, B., and Vogt, F., "*Coke calcination levels and aluminum anode quality*", Light Metals (Warrendale, Pennsylvania), 1996, p. 535-542.
37. Garbarino, R. M. and Tonti, R. T., "*Desulfurization and its effect on calcined coke properties*", Light Metals (Warrendale, PA, United States), 1993, p. 517-20.
38. Kakuta, M., Tanaka, H., Sato, J., and Noguchi, K., "*A new calcining technology for manufacturing of coke with lower thermal expansion coefficient*", Carbon, 1981, 19 (5), p. 347-352.
39. Letizia, I. and Padeletti, G., "*Correlation between CTE and Pore Shape Factor and Crystallinity in Petroleum Coke*", Light Metals, 1988, p. 455-460.
40. Medek, J., Weishauptova, Z., and Vaverkova, Z., "*Effect of porosity on the properties of needle coke and graphite electrodes*", Izvestiya po Khimiya, 1990, 23 (2), p. 222-8.
41. Yanko, E. A., Lazarev, V. D., Potapova, V. I., and Anokhin, Y. M., "*Physicochemical Properties of Some Electrode Cokes*", Coke & chemistry U.S.S.R, 1973 (6), p. 34-38.
42. Stokka, P., "*Green paste porosity as an indicator of mixing efficiency*", Light Metals (Warrendale, Pennsylvania), 1997, p. 565-568.
43. Vanvoren, C., "*Recent improvement in paste plant design industrial application and results*", Light Metals (Warrendale, PA, United States), 1987, p. 525-531.
44. Martirena, H., "*Laboratory studies on mixing, forming and calcining carbon bodies*", Light Metals (Warrendale, PA, United States), 1983, p. 749-64.
45. Belitskus, D., "*Effects of mixing variables and mold temperature on prebaked anode quality*", Light Metals (Warrendale, PA, United States), 1985, p. 915-924.
46. Couderc, P., Hyvernat, P., and Lemarchand, J. L., "*Correlations between Ability of Pitch to Penetrate Coke and the Physical Characteristics of Prebaked Anodes for the Aluminum-Industry*", Fuel, 1986, 65 (2), p. 281-287.
47. Lahaye, J. and Ehrburger, P., "*Pitch-coke interactions*", Fuel, 1985, 64 (9), p. 1187-1191.
48. Rocha, V. G., Blanco, C., Santamaria, R., Diestre, E. I., Menendez, R., and Granda, M., "*Pitch/coke wetting behaviour*", Fuel, 2005, 84 (12-13), p. 1550-1556.
49. Adams, A. N. and Schobert, H. H., "*Characterization of the surface properties of anode raw materials*", Light Metals (Warrendale, PA, United States), 2004, p. 495-498.
50. Belitskus, D. L., Peterson, R. W., Krupinski, K. C., and Osterholm, R. J., "*Designed experiment for effects of normal QI, carry-over QI, and beta resin in pitch on prebaked anode properties part I - preparation and testing of experimental pitches and bench-scale anodes*", Light Metals (Warrendale, Pennsylvania), 1995, p. 583-588.
51. Proulx, A. L., "*Optimum binder content for prebaked anodes*", Light Metals (Warrendale, PA, United States), 1993, p. 657-61.
52. Wright, K. B. and Peterson, R. W., "*Pitch content optimization model for anode mixes*", Light Metals (Warrendale, PA, United States), 1989, p. 479-488.
53. Benton, M., "*Anode mix pitch demand*", Light Metals (Warrendale, PA, United States), 1990, p. 657-9.

54. Castonguay, L. and Rhedey, P. J., "*Effect of raw material properties and processing methods on electrode behavior"*, Proc Int Symp Qual Process Control Reduct Cast Alum Other Light Met, 1987, p. 67-84.
55. Auguie, D., Oberlin, M., Oberlin, A., and Hyvernat, P., "*Formation of thin mesophase layers at the interface between filler and binder in prebaked anodes. Effect of mixing on mesophase"*, Carbon, 1981, 19 (4), p. 277-284.
56. Mannweiler, U., *Anode manufacturing: An introduction*, in *Anodes for the Aluminium Industry*, 1994, R&D Carbon Ltd., Sierre, p. 197-202,
57. Boenigk, W. and Wildforster, R., "*Weight-Loss of Green Anodes During the Baking Process"*, Journal of Metals, 1988, 40 (11), p. 18.
58. Foosnæs, T., Kulset, N., Linga, H., Naeumann, G. R., and Werge-Olsen, A., "*Measurement and control of the calcining level in anode baking furnaces"*, Light Metals (Warrendale, Pennsylvania), 1995, p. 649-652.
59. Cutshall, E. R., "*Influence of anode baking temperature and current density upon carbon sloughing"*, Light Metals (Warrendale, PA, United States), 1986, p. 629-637.
60. Kuang, Z.-l., Thonstad, J., and Sorlie, M., "*Effect of baking temperature and anode current density on anode carbon consumption"*, Light Metals (Warrendale, PA, United States), 1994, p. 667-75.
61. Eidet, T., Reactions on carbon anodes in aluminium electrolysis, Dr. Ing. thesis, 1997, Norwegian University of Science and Technology, Trondheim, p. 91,
62. Sverdlin, V. A., "*Effect of baking time on properties of prebaked anodes"*, Tsvetnye Metally, 1979, 9 (65), p. 45-53.
63. Lossius, L. P., Eie, M., Rørvik, S., and Øye, H. A., "*Mass loss, fume and porosity studies of pitch + dust binder matrix for anodes"*, Light Metals (Warrendale, Pennsylvania), 1996, p. 515-520.
64. Ehrburger, P., Sanseigne, E., and Tahon, B., "*Formation of porosity and change in binder pitch properties during thermal treatment of green carbon materials"*, Carbon, 1996, 34 (12), p. 1493-1499.
65. Alford, H. E. and Marsh, E. N., 1979, Desulfurization of petroleum coke, Application: US, Standard Oil Company (Cleveland, OH), US 1976-684344, 05/684,344, 5pp.
66. Paul, C. A. and Herrington, L. E., "*Desulfurization of petroleum coke beyond 1600 °C"*, Light Metals (Warrendale, PA, United States), 2001, p. 597-601.
67. Akhmetov, M. M., Stekhun, A. I., and Borzilova, V. V., "*Thermal desulfurization of high-sulfur cokes"*, Tsvetnye Metally (Moscow, Russian Federation), 1990 (7), p. 74-5.
68. Vogt, F., Ries, K., and Smith, M., "*Anode desulfurization on baking"*, Light Metals (Warrendale, Pennsylvania), 1995, p. 691-700.
69. Xue, J., Aune, F., Rørvik, S., and Øye, H. A., "*X-ray and microscopy investigations on the catalytic carbonization of coal tar pitch-petroleum coke bench-scale anodes"*, Light Metals (Warrendale, Pennsylvania), 1997, p. 535-541.
70. Xue, J., Sørlie, M., and Øye, H. A., "*Kinetic study of the catalytic carbonization of coal tar pitch - petroleum coke mixtures"*, Light Metals, 1996, p. 551-557.

71. Byrne, J. F. and Marsh, H., *Introductory overview*, in *Porosity in Carbons*, Patrick, J., 1995, Edward Arnold, Suffolk and Hartnolls Ltd., Bodmin, Cornwall, London, p. 1-48, ISBN 0 340 544732.
72. Rørvik, S. and Øye, H. A., "*A method for characterization of anode pore structure by image analysis*", Light Metals, 1996, p. 561-568.
73. Adams, A. N., Karacan, O., Grader, A., Mathews, J. P., Halleck, P. M., and Schobert, H. H., "*The non-destructive 3-D characterization of pre-baked carbon anodes using X-ray computerized tomography*", Light Metals (Warrendale, PA, United States), 2002, p. 535-539.
74. Rørvik, S. and Øye, H. A., "*Characterization of porosity in cokes by image analysis*", Light Metals (Warrendale, PA.), 2001, p. 603-609.
75. Rasband, W., U.S. National Institute of Health, NIH Image 1.63, available at: http://rsb.info.nih.gov/nih-image/download.html
76. Rørvik, S. and Øye, H. A., "*Classification of pores in prebake anodes using automated optical microscopy*", Light Metals (Warrendale, PA.), 2003, p. 531-534.
77. Certificate of Quality, Hydro Aluminium Metal, Technology & Operational Support, Årdalstangen, 2003, reference number H03-1821
78. Certificate of Analysis of Calcined Delayed Petroleum Coke, Hydro Aluminium Metal, Technology & Operational Support, Årdalstangen, 2003, Order number: 101799
79. Raw material analysis, Hydro Aluminium Metal, Technology & Operational Support, Årdalstangen, 2002, Document number: KA331
80. Chmelar, J., Size reduction and specification of granular petrol coke with respect to chemical and physical properties, Dr. Ing. thesis, 2006, Department of Geology and Mineral Resources Engineering, Norwegian University of Science and Technology, Trondheim, p. 134, ISBN 82-471-7899-0.
81. Certificate of Analysis, Hydro Aluminium Metal, Technology & Operational Support, Årdalstangen, 2006, No. 11000738
82. Aune, F., Rørvik, S., and Støre, A., Pilot anodes: Optimum pitch content and mixing study, NTNU, Trondheim, 1996, Technical report, IUK-96-25
83. Uhl, V. W. and Gray, J. B., "*Mixing, theory and practise*", Vol. 2, 1967, Academic press, London, p. 340, ISBN 0127066020.
84. Lossius, L. P., Vibration press manual with description and test results, NTNU report, Trondheim, 1995, IUK-95-50
85. National Instruments, LabView 6.1, 2004, Available from internet: http://www.ni.com,
86. RDC-150 Specific electrical resistance apparatus: User's manual, Sierre, 1997, R&D Carbon Ltd.,
87. Belitskus, D., "*Effects of formulation and heating rate on changes occurring during baking of bench-scale Hall cell anodes*", Light Metals (Warrendale, PA, United States), 1983, p. 741-7.
88. Minitab Inc., Release 14 for Windows, State College, Pennsylvania, MiniTab Statistical Software, 2003, MINITAB is a registered trademark of Minitab Inc.,
89. Rørvik, S., Ratvik, A. P., and Foosnaes, T., "*Characterization of green anode materials by image analysis*", Light Metals, 2006, p. 553-558.

90. Belitskus, D., "*Evaluation of volumetric anode mix formulation"*, Light Metals (Warrendale, PA, United States), 1984, p. 923-932.
91. Fischer, W. K. and Perruchoud, R. C., *Pitch evaluation*, in *Anodes for the aluminium industry*, 1995, R&D Carbon, Sierre, p. 141-148,
92. Perruchoud, R. C. and Fischer, W. K., *Bench scale evaluation of the mechanical and chemical behaviour of coke in anode manufacturing*, in *Anodes for the aluminium industry*, 1995, R&D Carbon, Sierre, p. 93-101,
93. Brown, J. A. and Rhedey, P. J., "*Characterization of prebaked anode carbon by mechanical and thermal properties"*, Light Metals (Warrendale, PA, United States), 1975, p. 253-269.